

Institut für Strukturmechanik Institute of Structural Mechanics

Bauhaus-

Bauhaus-Universität Weimar

Weimar

ISM-Bericht 1/2011
Maik Brehm

Vibration-based model updating:
Reduction and quantification of uncertainties

Herausgeber

Carsten Könke

Timon Rabczuk

ISM-Bericht 1/2011

ISSN: 1610-7381

Institut für Strukturmechanik
Fakultät Bauingenieurwesen
Bauhaus-Universität Weimar
Marienstraße 15
D-99421 Weimar
Germany

Tel. +49(0)3643/584504

Fax. +49(0)3643/584514

<http://www.uni-weimar.de/Bauing/ism>

Vibration-based model updating: Reduction and quantification of uncertainties

Modellkalibrierung basierend auf Schwingungsversuchen:
Reduzierung und Quantifizierung von Unsicherheiten

– DISSERTATION –

zur Erlangung des akademischen Grades
Doktor-Ingenieur (Dr.-Ing.)
an der Fakultät Bauingenieurwesen
der Bauhaus-Universität Weimar

vorgelegt von
Dipl.-Ing. Maik Brehm
geboren am 11. April 1979 in Sonneberg, Deutschland

Weimar, März 2011

Gutachter:

Univ.-Prof. Dr.-Ing. habil. Carsten Könke, Bauhaus-Universität Weimar
Univ. Prof. Dipl.-Ing. Dr. techn. Christian Bucher, Technische Universität Wien
Prof. dr. ir. Guido De Roeck, Katholieke Universiteit Leuven

Disputation am 23. Juni 2011

Danksagung

Die vorliegende Promotionsschrift entstand während meiner Anstellung als wissenschaftlicher Mitarbeiter und Doktorand am Institut für Strukturmechanik. Die thematische Ausrichtung der Arbeit steht im engen Zusammenhang mit meiner aktiven Mitarbeit als Organisator und Wissenschaftler in den europäischen Projekten SAFERELNET (Safety and reliability of industrial products, systems and structures), DETAILS (Design for optimal performance of high-speed railway bridges by enhanced monitoring systems) und FADLESS (Fatigue damage control and assessment for railway bridges). Der enge und frühe Kontakt zu international führenden Forschern und Forschergruppen förderte maßgeblich den Innovationscharakter und die Qualität der vorliegenden Arbeit.

Mein besonderer Dank richtet sich an meine Mentoren Prof. Carsten Könke und Prof. Christian Bucher, welche mir nicht nur die finanzielle Grundlage für die Erstellung der Arbeit ermöglichten, sondern auch aktiv zum Problemlösungsprozess wissenschaftlicher Fragestellungen beitrugen. Das von ihnen geförderte, unabhängige und kreative Handeln, spiegelt sich in meiner Dissertation wieder. Ein recht herzlicher Dank gilt auch Herrn Prof. Guido De Roeck für die Begutachtung der Arbeit. Er war insbesondere durch die gemeinsamen Projekte DETAILS und FADLESS in einem sehr frühen Stadium an der Ausrichtung der Arbeit beteiligt. Ein weiterer sehr vertrauter Förderer meiner wissenschaftlichen Aktivitäten war Dr. Volkmar Zabel, der sich immer Zeit für ausführliche wissenschaftliche Diskussionen nahm und die strategische Ausrichtung der Arbeit prägte. Er weihte mich weiterhin in die Geheimnisse der experimentellen Schwingungsanalyse ein und befähigte mich zur eigenständigen Planung und Durchführung von Schwingungsversuchen. Fachkundige Hilfe bei der praktischen Umsetzung von Versuchen erhielt ich ebenfalls von der versuchstechnischen Einrichtung der Bauhaus-Universität Weimar unter der Leitung von Herrn Wolf-Dieter Vogler, dem hiermit herzlichst gedankt sei.

Weitere wertvolle fachliche Unterstützung durfte ich von Prof. Michael Link, Dr. Reto Cantieni, Dr. Klaus Markwardt, Dr. Thomas Most und Dr. Tom Lahmer erfahren. Eine Bereicherung meiner wissenschaftlichen Arbeit war ebenfalls der mehrmonatige Gastaufenthalt von Diogo Ribeiro, welcher seinerzeit Doktorand an der Universität FEUP in Portugal unter der Anleitung von Prof. Rui Calçada war. Zahlreiche anregende Diskussion mit ihm beeinflussten nachhaltig die Schwerpunkte meiner Arbeit. Weiterer Dank

geht an meine Freunde, die mir insbesondere in der Endphase der Promotion hilfreich zur Seite standen und tatkräftig zur Qualitätssicherung der Arbeit beitrugen.

Bedanken möchte ich mich auch bei Prof. Carsten Könke, Prof. Timon Rabczuk und Dr. Volkmar Zabel für die Möglichkeit der eigenverantwortlichen Leitung von diversen Seminaren, Vorlesungen und Projekten, wobei mir Frau Dr. Dagmar Hintze oftmals hilfreich zur Seite stand.

Sehr stark werde ich meine langjährigen Kollegen und Freunde am Institut für Strukturmechanik vermissen. Ohne Benjamin, Torsten, und Ingmar wäre die Zeit nicht annähernd so angenehm gewesen. Einen besonderen Dank an alle, die mir in der Endphase ihre Rechenkapazitäten für meine aufwendigen Berechnungen zur Verfügung stellten. In diesem Zusammenhang ein großes Lob an die erstklassigen Administratoren des Instituts, Heiko und Michael. Nicht wegzudenken ist natürlich Frau Terber, unsere gute Seele des Instituts, die oftmals meine Dienstreiseaufträge fertig hatte, bevor ich wusste wohin die Reise geht.

Auch mein Leben außerhalb der wissenschaftlichen Arbeit wurde stark durch die vom Institut für Strukturmechanik initiierten Aktivitäten bereichert. Die zahlreichen sportlichen Veranstaltungen waren ein perfekter Ausgleich für die herausfordernde wissenschaftliche Arbeit. Herauszuheben sind hierbei die Organisatoren und Trainingspartner Torsten, Benjamin, Ingmar, Michael und Heiko.

Neben den Aktivitäten am Institut für Strukturmechanik konnte ich ebenfalls einen tiefen Einblick in die industrienaher Forschung gewinnen. Die während meiner Arbeit als Entwickler bei der Dynardo GmbH gewonnenen Kenntnisse in Strukturmechanik und Optimierungsmethoden bereicherten exzellent meine Doktorarbeit. An dieser Stelle möchte ich Dr. Johannes Will, Dr. Dirk Roos, Dr. David Schneider, Daniel Arnold, Heiko Beinersdorf, Ulrike Adam und Andreas Grosche stellvertretend für das gesamte Team danken.

Den wichtigsten Anteil am Erfolg meiner Arbeit hatte meine Familie, deren stetiger Zuwachs an Mitgliedern mein Leben zunehmend bereicherte. Einen großen Dank an meine Partnerin Anne, die nicht nur einen großen Anteil an der Betreuung unserer Kinder besteuerte, sondern auch liebevoll mit meinen Eigenheiten umzugehen wusste. Weiterhin hatte sie fundamental zur Verbesserung der anglistischen Herausforderungen dieser Promotionsschrift und zahlreicher Veröffentlichungen beigetragen. Auch meinen Kindern Aaron und Leander gilt ein außerordentlicher Dank. Sie verstanden es mich in meinen Fähigkeiten zu fordern und zu fördern und ermöglichten mir einen alternativen Blick auf die Welt und unser Dasein. Natürlich möchte ich auch meinen Eltern für die wohlbehütete Kindheit danken. Insbesondere meine Mutter ermögliche mir eine exzellente Bildung und die notwendigen Freiheiten für ein selbstständiges und weltoffenes Leben.

Maik Brehm

Weimar, 23. Juni 2011

Abstract

Numerical models and their combination with advanced solution strategies are standard tools for many engineering disciplines to design or redesign structures and to optimize designs with the purpose to improve specific requirements. As the successful application of numerical models depends on their suitability to represent the behavior related to the intended use, they should be validated by experimentally obtained results. If the discrepancy between numerically derived and experimentally obtained results is not acceptable, a model revision or a revision of the experiment need to be considered. Model revision is divided into two classes, the model updating and the basic revision of the numerical model.

The presented thesis is related to a special branch of model updating, the vibration-based model updating. Vibration-based model updating is a tool to improve the correlation of the numerical model by adjusting uncertain model input parameters by means of results extracted from vibration tests. Evidently, uncertainties related to the experiment, the numerical model, or the applied numerical solving strategies can influence the correctness of the identified model input parameters. The reduction of uncertainties for two critical problems and the quantification of uncertainties related to the investigation of several nominally identical structures are the main emphases of this thesis.

First, the reduction of uncertainties by optimizing reference sensor positions is considered. The presented approach relies on predicted power spectral amplitudes and an initial finite element model as a basis to define the assessment criterion for predefined sensor positions. In combination with geometry-based design variables, which represent the sensor positions, genetic and particle swarm optimization algorithms are applied. The applicability of the proposed approach is demonstrated on a numerical benchmark study of a simply supported beam and a case study of a real test specimen. Furthermore, the theory of determining the predicted power spectral amplitudes is validated with results from vibration tests.

Second, the possibility to reduce uncertainties related to an inappropriate assignment for numerically derived and experimentally obtained modes is investigated. In the context of vibration-based model updating, the correct pairing is essential. The most common criterion for indicating corresponding mode shapes is the modal assurance criterion. Un-

fortunately, this criterion fails in certain cases and is not reliable for automatic approaches. Hence, an alternative criterion, the energy-based modal assurance criterion, is proposed. This criterion combines the mathematical characteristic of orthogonality with the physical properties of the structure by modal strain energies. A numerical example and a case study with experimental data are presented to show the advantages of the proposed energy-based modal assurance criterion in comparison to the traditional modal assurance criterion.

Third, the application of optimization strategies combined with information theory based objective functions is analyzed for the purpose of stochastic model updating. This approach serves as an alternative to the common sensitivity-based stochastic model updating strategies. Their success depends strongly on the defined initial model input parameters. In contrast, approaches based on optimization strategies can be more flexible. It can be demonstrated, that the investigated nature inspired optimization strategies in combination with Bhattacharyya distance and Kullback-Leibler divergence are appropriate. The obtained accuracies and the respective computational effort are comparable with sensitivity-based stochastic model updating strategies.

The application of model updating procedures to improve the quality and suitability of a numerical model is always related to additional costs. The presented innovative approaches will contribute to reduce and quantify uncertainties within a vibration-based model updating process. Therefore, the increased benefit can compensate the additional effort, which is necessary to apply model updating procedures.

Kurzfassung

Eine typische Anwendung von numerischen Modellen und den damit verbundenen numerischen Lösungsstrategien ist das Entwerfen oder Ertüchtigen von Strukturen und das Optimieren von Entwürfen zur Verbesserung spezifischer Eigenschaften. Der erfolgreiche Einsatz von numerischen Modellen ist abhängig von der Eignung des Modells bezüglich der vorgesehenen Anwendung. Deshalb ist eine Validierung mit experimentellen Ergebnissen sinnvoll. Zeigt die Validierung inakzeptable Unterschiede zwischen den Ergebnissen des numerischen Modells und des Experiments, sollte das numerische Modell oder das experimentelle Vorgehen verbessert werden. Für die Modellverbesserung gibt es zwei verschiedene Möglichkeiten, zum einen die Kalibrierung des Modells und zum anderen die grundsätzliche Änderung von Modellannahmen.

Die vorliegende Dissertation befasst sich mit der Kalibrierung von numerischen Modellen auf der Grundlage von Schwingungsversuchen. Modellkalibrierung ist eine Methode zur Verbesserung der Korrelation zwischen einem numerischen Modell und einer realen Struktur durch Anpassung von Modelleingangsparametern unter Verwendung von experimentell ermittelten Daten. Unsicherheiten bezüglich des numerischen Modells, des Experiments und der angewandten numerischen Lösungsstrategie beeinflussen entscheidend die erzielbare Qualität der identifizierten Modelleingangsparameter. Die Schwerpunkte dieser Dissertation sind die Reduzierung von Unsicherheiten für zwei kritische Probleme und die Quantifizierung von Unsicherheiten extrahiert aus Experimenten nominal gleicher Strukturen.

Der erste Schwerpunkt beschäftigt sich mit der Reduzierung von Unsicherheiten durch die Optimierung von Referenzsensorpositionen. Das Bewertungskriterium für vordefinierte Sensorpositionen basiert auf einer theoretischen Abschätzung von Amplituden der Spektraldichtefunktion und einem dazugehörigen Finite Elemente Modell. Die Bestimmung der optimalen Konfiguration erfolgt durch eine Anwendung von Optimierungsmethoden basierend auf genetischen Algorithmen und Schwarmintelligenzen. Die Anwendbarkeit dieser Methoden wurde anhand einer numerischen Studie an einem einfach gelagerten Balken und einem real existierenden komplexen Versuchskörper nachgewiesen. Mit Hilfe einer experimentellen Untersuchung wird die Abschätzung der statistischen Eigenschaften der Antwortspektraldichtefunktionen an diesem Versuchskörper validiert.

Im zweiten Schwerpunkt konzentrieren sich die Untersuchungen auf die Reduzierung von Unsicherheiten, hervorgerufen durch ungeeignete Kriterien zur Eigenschwingformzuordnung. Diese Zuordnung ist entscheidend für Modellkalibrierungen basierend auf Schwingungsversuchen. Das am Häufigsten verwendete Kriterium zur Zuordnung ist das *modal assurance criterion*. In manchen Anwendungsfällen ist dieses Kriterium jedoch kein zuverlässiger Indikator. Das entwickelte alternative Kriterium, das *energy-based modal assurance criterion*, kombiniert das mathematische Merkmal der Orthogonalität mit den physikalischen Eigenschaften der untersuchten Struktur mit Hilfe von modalen Formänderungsarbeiten. Ein numerisches Beispiel und eine Sensitivitätsstudie mit experimentellen Daten zeigen die Vorteile des vorgeschlagenen energiebasierten Kriteriums im Vergleich zum traditionellen *modal assurance criterion*.

Die Anwendung von Optimierungsstrategien auf stochastische Modellkalibrierungsverfahren wird im dritten Schwerpunkt analysiert. Dabei werden Verschiedenheitsmaße der Informationstheorie zur Definition von Zielfunktionen herangezogen. Dieser Ansatz stellt eine Alternative zu herkömmlichen Verfahren dar, welche auf gradientenbasierten Sensitivitätsmatrizen zwischen Eingangs- und Ausgangsgrößen beruhen. Deren erfolgreicher Einsatz ist abhängig von den Anfangswerten der Eingangsgrößen, wobei die vorgeschlagenen Optimierungsstrategien weniger störanfällig sind. Der Bhattacharyya Abstand und die Kullback-Leibler Divergenz als Zielfunktion, kombiniert mit stochastischen Optimierungsverfahren, erwiesen sich als geeignet. Bei vergleichbarem Rechenaufwand konnten ähnliche Genauigkeiten wie bei den Modellkalibrierungsverfahren, die auf Sensitivitätsmatrizen basieren, erzielt werden.

Die Anwendung von Modellkalibrierungsverfahren zur Verbesserung der Eignung eines numerischen Modells für einen bestimmten Zweck ist mit einem Mehraufwand verbunden. Die präsentierten innovativen Verfahren tragen zu einer Reduzierung und Quantifizierung von Unsicherheiten innerhalb eines Modellkalibrierungsprozesses basierend auf Schwingungsversuchen bei. Mit dem zusätzlich generierten Nutzen kann der Mehraufwand, der für eine Modellkalibrierung notwendig ist, nachvollziehbar begründet werden.

List of figures

1.1	General overview of the framework for model verification and model validation.	4
1.2	General overview of the framework for model updating.	5
2.1	Statistical properties of the Fourier transform of a random multiple impulse excitation time history.	25
2.2	Comparison of predicted spectral amplitudes using eigenvectors and power spectral amplitudes. The spectral response based on the first three bending modes of a simply supported beam are shown separately. The modal damping varies by 1%, 5%, and 20%.	30
2.3	Workflow for optimal reference sensor placement.	33
2.4	Simply supported beam with rectangular cross-section.	34
2.5	Normalized spectral amplitudes of the simply supported beam in case of ambient excitation. (only left half span is considered due to symmetry)	35
2.6	Objective functions assuming one reference sensor detecting a certain number of vertical modes of a simply supported beam. \oplus indicates the optimal position with respect to the number of modes of interest.	35
2.7	Objective function using two reference sensors to detect a certain number of vertical modes of a simply supported beam assuming ambient excitation. \oplus indicates the optimal position.	36
2.8	Objective function using two reference sensors to detect a certain number of vertical modes of a simply supported beam assuming ambient excitation. \oplus indicates the optimal position.	37
2.9	Objective function value at the optimum for different numbers of available reference sensors and modes to be detected assuming white noise	38
2.10	Variance of the real and imaginary part of the Fourier spectrum of random multiple impulse excitation. Vertical lines indicate the position of circular eigenfrequencies corresponding to vertical bending modes of the simply supported beam.	39

2.11	Normalized spectral amplitudes expecting random multiple impulse excitation on a simply supported beam.	40
2.12	Objective functions assuming one reference sensor detecting a certain number of vertical modes of a simply supported beam assuming random multiple impulse excitation. \oplus indicates the optimal position with respect to the number of modes of interest.	40
2.13	Objective function using two reference sensors to detect a certain number of vertical modes of a simply supported beam assuming random multiple impulse excitation. \oplus indicates the optimal position.	41
2.14	Objective function using two reference sensors to detect a certain number of vertical modes of a simply supported beam assuming random multiple impulse excitation. \oplus indicates the optimal position.	42
2.15	Objective function value at optimum for different numbers of available reference sensors and modes to be detected assuming random multiple impulse excitation.	43
2.16	First 11 non-local, non-rigid body modes obtained by numerical modal analysis.	45
2.17	Left: Test specimen with free-free support conditions. Right: Accelerometers PCB338B35 mounted with magnets at lower flange.	45
2.18	Finite element model. The measurement points and excitation points are indicated with MP and F, respectively.	46
2.19	Example of a time history of the force signal at position F1.	47
2.20	First impulse of the force time history given in Figure 2.19.	47
2.21	Example of an averaged power spectral density of the force signal at position F1 using 180 statistically independent blocks of a 180s time history.	47
2.22	Example of a time history of the response signal at position MP12.	48
2.23	Example of an averaged power spectral density of the response signal at position MP12 using 180 statistically independent blocks of a 180s time history.	48
2.24	Sample mean values and sample variances of the Fourier transform of the force signal at position 1 with respect to the multiple impulse excitation. The smoothed curves for the variances are based on a moving least squares algorithm. The sample means are approximated by a constant value zero.	50
2.25	Comparison of mean values of auto power spectral amplitudes of the responses at MP1 to MP6 using different approaches.	52
2.26	Comparison of mean values of auto power spectral amplitudes of the responses at MP7 to MP12 using different approaches.	53

2.27	Objective function value of each measurement position according to Equation (2.48). black: calculation based on measured data; red: prediction based on structural model; The dotted line is related to a signal to noise ratio of 100 derived from the spectral density of measurement noise.	55
2.28	Objective function value of each measurement position depending on the distribution and size of modal damping ratios.	55
2.29	Objective function for the placement of one reference sensor for the detection of the first 11 global modes of the structure. The symbol \oplus indicates the optimal position with an objective value of 0.99781.	56
2.30	Subdomains of preselected degrees of freedom.	58
2.31	Original and random degree of freedom (DOF) numbering for subdomains 1 and 7.	60
2.32	Position of best four suboptima. The first suboptimum is the global optimum. The red dots mark the reference sensor positions.	61
2.33	Results of search strategy (i) with geometry-based design variables and genetic algorithm.	63
2.34	Results of search strategy (ii) with geometry-based design variables and particle swarm optimization.	63
2.35	Results of search strategy (iii) with design variables based on a modified degree of freedom numbering and genetic algorithm.	64
2.36	Results of search strategy (iv) with design variables based on a modified degree of freedom numbering and particle swarm optimization.	64
2.37	Results of search strategy (v) with design variables based on a randomly reordered degree of freedom numbering and genetic algorithm.	65
2.38	Results of search strategy (vi) with design variables based on a randomly reordered degree of freedom numbering and particle swarm optimization.	65
2.39	Results of search strategy (vii) based on Monte Carlo sampling.	66
3.1	Workflow for mode pairing using the energy-based modal assurance criterion.	75
3.2	Geometrical description of the cantilever truss system.	76
3.3	First four experimental mode shapes of the system obtained by simulation. Only the vertical modal displacements of the marked positions (\bullet) are assumed to be available from tests.	77
3.4	First nine mode shapes of the modified numerical model.	78
3.5	Modal assurance criterion (MAC) – numerical vs. experimental modes.	79
3.6	Modal assurance criterion (MAC) – identified numerical vs. experimental modes.	79
3.7	Identified mode shapes from numerical modal analysis using MAC.	80
3.8	Relative modal strain energies for vertical and horizontal degrees of freedom.	80

3.9	Energy-based modal assurance criterion (EMAC) for vertical degrees of freedom – numerical vs. experimental modes.	81
3.10	Energy-based modal assurance criterion (EMAC) for vertical degrees of freedom – identified numerical vs. experimental modes.	81
3.11	Modal assurance criterion (MAC) – identified numerical vs. experimental modes. Numerical modes are previously selected by the energy-based modal assurance criterion (EMAC).	82
3.12	Identified mode shapes from numerical modal analysis using the energy-based modal assurance criterion (EMAC).	82
3.13	Objective function using MAC-based mode pairing strategy. The minimum is obtained at $(k_2, k_4) = (0.70182, 0.70768)$ and marked by the white dot. Diagram (b) shows a detail of diagram (a).	85
3.14	Objective function using EMAC-based mode pairing strategy. The minimum is obtained at $(k_2, k_4) = (1.00010, 0.99994)$ and is marked by the white dot.	85
3.15	Longitudinal section of the simplified bridge model.	87
3.16	Cross section of the simplified bridge model.	87
3.17	Finite element model of the bridge.	87
3.18	Modal assurance criterion (MAC) – (a) all numerical vs. experimental modes of the Erfittal bridge; (b) identified numerical vs. experimental modes of the Erfittal bridge.	88
3.19	Energy-based modal assurance criterion (EMAC) for vertical degrees of freedom of the slab – (a) all numerical vs. experimental modes of the Erfittal bridge; (b) identified numerical vs. experimental modes of the Erfittal bridge.	89
3.20	Modal assurance criterion – identified numerical vs. experimental modes of the Erfittal bridge. The numerical modes are selected previously by the energy-based modal assurance criterion.	90
3.21	Modulus of the linear Spearman correlation coefficient based on 750 sample sets. Coefficients smaller than 0.3 are set to 0. (a) using the modal assurance criterion (MAC) for mode assignment (b) using the energy-based modal assurance criterion (EMAC) for mode assignment.	93
4.1	Definition of discrete points based on a full factorial design for a two-dimensional parameter space.	118
4.2	Example of a slice l of the objective function using four points per slice.	118
4.3	Definition of discrete points $(\mathbf{X})_{k,l}$ for a three-dimensional parameter space with two points per slice.	119
4.4	Three degree of freedom mass-spring system	121

4.5	Probability density functions of the nominal stiffness and corresponding natural frequencies. The histograms are density estimations based on 1,000,000 Latin hypercube samples.	122
4.6	Averaged objective function properties of the three degree of freedom benchmark study using 10 Latin hypercube samples. The acronyms are defined in Table 4.2.	123
4.7	Averaged objective function properties of the three degree of freedom benchmark study using 100 Latin hypercube samples. The acronyms are defined in Table 4.2.	124
4.8	Averaged objective function properties of the three degree of freedom benchmark study using 1,000 Latin hypercube samples. The acronyms are defined in Table 4.2.	125
4.9	Slices of one representative objective function evaluation. The stochastic structural analysis of the three degree of freedom system is based on 1,000 Latin hypercube samples.	127
4.10	Slices of one representative objective function evaluation. The stochastic structural analysis of the three degree of freedom system is based on 1,000 Latin hypercube samples. (continued from Figure 4.9)	128
4.11	Statistics of the error norm ε_1 according to Equation (4.64) using genetic algorithm (GA). The statistics are based on 20 independent optimization runs. To evaluate one objective function value, 100 and 10,000 Latin hypercube samples are applied.	131
4.12	Statistics of the error norm ε_1 according to Equation (4.64) using particle swarm optimization (PSO). The statistics are based on 20 independent optimization runs. To evaluate one objective function value, 100 and 10,000 Latin hypercube samples are applied.	132
4.13	Statistics of the error norm ε_1 according to Equation (4.64) using adaptive response surface optimization methods (ARSM). The statistics are based on 20 independent optimization runs. To evaluate one objective function value, 100 Latin hypercube samples are applied.	133
4.14	Convergence of the solution indicated by the best objective function value depending on the generation or iteration number.	133
4.15	Truss system with indicated measurement points (MP) and directions. . . .	137
4.16	First four vertical mode shapes of the system related to the nominal mean values of the stiffnesses. Only the vertical modal displacements of the marked positions (\bullet) are assumed to be available for the artificial experiment.	138
4.17	Examples of probability density functions of target features. The histogram is a density estimation related to 1,000,000 Latin hypercube samples. The best fit based on a normal distribution is indicated by the red line.	138

4.18	Objective function properties for the truss system. The indicators are averaged over 10 identical runs using 100 Latin hypercube samples for each objective function evaluation.	140
4.19	Objective function properties for the truss system. The indicators are averaged over 10 identical runs using 1,000 Latin hypercube samples for each objective function evaluation.	141
4.20	Representative slices of objective functions. 1,000 Latin hypercube samples are utilized for the stochastic structural analysis of the truss system.	142
4.21	Representative slices of objective functions. 1,000 Latin hypercube samples are utilized for the stochastic structural analysis of the truss system. (continued from Figure 4.20)	143
4.22	Statistics of the error ε_1 according to Equation (4.64) using genetic algorithm (GA) for the truss benchmark study. The statistics are based on 20 independent optimization runs. To evaluate one objective function value, 100 and 10,000 Latin hypercube samples are applied.	146
4.23	Statistics of the error norm ε_1 according to Equation (4.64) using particle swarm optimization (PSO) for the truss benchmark study. The statistics are based on 20 independent optimization runs. To evaluate one objective function value, 100 and 10,000 Latin hypercube samples are applied.	146

List of tables

2.1	Statistical properties of random input parameters used for simulation, whereas $p_0^{(i)} = p_0^{(i_s)} p_0^{(i_m)}$ and $t_0^{(i)} = \sum_{j=0}^i \Delta t_0^{(j)}$	25
2.2	Objective function value and respective optimal positions assuming ambient excitation. The positions are related to the distance of the sensor to the left support.	38
2.3	Objective value and respective optimal positions assuming random multiple impulse excitation.	43
2.4	Comparison of numerically derived and experimentally obtained modal properties. The statistics rely on 507 stochastic subspace identification (SSI) evaluations of data sets with time duration of 27s. The modal assurance criterion is calculated between the mode shapes obtained from the SSI algorithm and numerical mode shapes.	49
2.5	Most important configuration parameters of the genetic algorithm (GA) depending on a total number of design evaluations b	58
2.6	Most important configuration parameters of the particle swarm optimization (PSO) depending on a total number of design evaluations b	58
2.7	Averaged calculation time to evaluate one design sample set.	62
3.1	Original modal displacements.	77
3.2	Perturbations of modal displacements.	77
3.3	Dependency of successful mode assignment on the degree of noise.	83
3.4	Comparison of identified numerical mode shapes with the mode shapes obtained from measurements.	91
3.5	Notation, lower bounds, and upper bounds for all input variables.	92
4.1	Adjustments applied during the calculation of the dissimilarity measures to avoid unrepresentable numerical values.	115
4.2	Abbreviations and respective formula applied in the diagrams of the benchmark studies in Sections 4.5 and 4.6.	116

4.3	Configuration parameters of the genetic algorithm (GA) applied to the three degree of freedom benchmark study.	130
4.4	Configuration parameters of the particle swarm optimization (PSO) applied to the three degree of freedom benchmark study.	130
4.5	Configuration parameters of the adaptive response surface method (ARSM) applied to the three degree of freedom benchmark study.	130
4.6	Comparison between genetic algorithm and particle swarm optimization. The statistical values of identified input parameters are based on 20 independent optimization runs.	135
4.7	Results derived from the adaptive response surface method (ARSM) and a variation in configuration parameters of the genetic algorithm (GA). The statistical values of identified input parameters are based on 20 independent optimization runs.	135
4.8	Comparison of different updating methods with similar computational expense. The statistical values of identified input parameters are based on 20 independent optimization runs.	135
4.9	Covariance matrix properties of the random feature vector.	141
4.10	Most important configuration parameters of the genetic algorithm (GA) applied to the truss system.	144
4.11	Most important configuration parameters of the particle swarm optimization (PSO) applied to the truss system.	144
4.12	Comparison of different updating methods for the truss system. The statistical values of identified input parameters are based on 20 independent optimization runs.	147
B.1	Standard configuration parameters of the genetic algorithm (GA).	163
B.2	Standard configuration parameters of the particle swarm optimization (PSO).	164
B.3	Standard configuration parameters of the adaptive response surface method (ARSM).	165

Nomenclature

Most important abbreviations and symbols are presented in the following.

General abbreviations

ARSM	adaptive response surface method
ASME	American society of mechanical engineers
DOE	design-of-experiments
DOF	degree of freedom
DOFs	degrees of freedom
EFDD	enhanced frequency domain decomposition
EMAC	energy-based modal assurance criterion
EÜ	Eisenbahnüberführung (railway bridge crossing a traffic line)
GA	genetic algorithm
LHS	Latin hypercube sampling, Latin hypercube samples
MAC	modal assurance criterion
MP	measurement point
p-LSCF	poly-reference least squares complex frequency
PSO	particle swarm optimization
SNR	signal to noise ratio
SQP	sequential quadratic programming
SSI	stochastic subspace identification

General notations

a	scalar value
argmax	argument of the maximum
argmin	argument of the minimum
$\exp(a)$	exponential function of a

$\text{Im}(a)$	imaginary part of complex value a
\lim	limit operator
$\ln(a)$	natural logarithm of a
\max	maximum operator
\min	minimum operator
$\text{Re}(a)$	real part of complex value a
\mathbf{A}	matrix or vector
$\text{tr}(\mathbf{A})$	trace of matrix \mathbf{A}
$\text{diag}(a_1, \dots, a_n)$	diagonal matrix with entries (a_1, \dots, a_n) at the diagonal
$(\mathbf{A})_i$	row i of vector \mathbf{A}
$(\mathbf{A})_{i,j}$	entry i, j of matrix \mathbf{A}
$\{\mathbf{A}\}_j$	column i of matrix \mathbf{A}
\mathbf{A}^*	complex conjugate of matrix \mathbf{A}
\mathbf{A}^+	generalized inverse of matrix \mathbf{A}
\mathbf{A}^{-1}	inverse of matrix \mathbf{A}
\mathbf{A}^T	transpose of \mathbf{A}
$ \mathbf{A} $	determinant of matrix or vector
$\ \mathbf{A}\ _B^2$	squared weighted L_2 norm $\mathbf{A}^T \mathbf{B} \mathbf{A}$
$\ \mathbf{A}\ ^F$	Frobenius norm of matrix
$\ \mathbf{A}\ ^{L_2}$	L_2 norm of matrix or vector
$\mathbf{A} \circ \mathbf{B}$	Schur product between \mathbf{A} and \mathbf{B}
$\mathbf{A} \otimes \mathbf{B}$	Kronecker product
$\mathbb{C}^{a \times b}$	space of complex matrices with size $a \times b$
\mathbb{C}^a	space of complex vectors with size a
$\mathbb{R}^{a \times b}$	space of real matrices with size $a \times b$
\mathbb{R}^a	space of real vectors with size a
\mathbf{C}	covariance matrix
\mathbf{E}	mean value of random vector
\mathbf{V}	variance of random vector

Optimal reference sensor positions

MLS	moving least squares
-----	----------------------

$(\mathbf{A})_j$	maximum of normalized spectral amplitudes of the least represented mode within a sensor position set j
$(\mathbf{B})_{j,i}$	maximum of normalized spectral amplitudes of a sensor position set j and mode i
\mathbf{C}	combinatoric matrix of possible sensor positions
$\mathbf{D}(\omega)$	complex diagonal matrix
$\mathcal{F}_f(\omega, T)$	finite Fourier transformation of excitation
$\tilde{\mathcal{F}}_f(\omega)$	finite Fourier transformation of excitation, short form of $\mathcal{F}_f(\omega, T)$
$\tilde{\mathcal{F}}_{f,\mathbf{G}}(\omega)$	finite Fourier transformation of excitation with respect to global coordinate system
$\tilde{\mathcal{F}}_{f,\mathbf{L}}(\omega)$	finite Fourier transformation of excitation with respect to local coordinate system
$(\mathbf{F}_k)_{j,i}$	normalized spectral amplitude of sensor position k and mode i in the sensor position set j
$\{\tilde{\mathcal{F}}_{\mathbf{p}}\}_k$	discrete Fourier transformation of discrete signal \mathbf{p} at frequency step k
$\{\tilde{\mathcal{F}}_{\mathbf{p}}^{(i)}\}_{k_t}$	power spectral density of discrete signal \mathbf{p} and block i at frequency step k_t
$\mathbf{f}(t)$	excitation vector
$\mathcal{F}_x(\omega, T)$	finite Fourier transformation of response
$\tilde{\mathcal{F}}_x(\omega)$	finite Fourier transformation of response, short form of $\mathcal{F}_x(\omega, T)$
$\tilde{\mathcal{F}}_{x,\mathbf{G}}(\omega)$	finite Fourier transformation of response with respect to global coordinate system
$\tilde{\mathcal{F}}_{x,\mathbf{L}}(\omega)$	finite Fourier transformation of response with respect to local coordinate system
$\mathbf{H}_{\mathbf{x}\mathbf{f}}(\omega)$	frequency response function
$\mathbf{H}_{\mathbf{x}\mathbf{f},\mathbf{G}}(\omega)$	frequency response function with respect to global coordinate system
$\mathbf{H}_{\mathbf{x}\mathbf{f},\mathbf{L}}(\omega)$	frequency response function with respect to local coordinate system
λ	vector of classical undamped eigenvalues
$(\mathbf{N})_{j,i}$	Euclidean norm of normalized spectral amplitudes for sensor position set j and mode i
ω	vector of circular eigenfrequencies
Φ	matrix of eigenvectors
$\overset{\Delta}{\Phi}$	modulus of eigenvector matrix Φ
Φ_f	mode shape matrices of excitation degrees of freedom
$\Phi_{f,\mathbf{G}}$	mode shape matrices of excitation degrees of freedom with respect to global coordinate system
$\Phi_{f,\mathbf{L}}$	mode shape matrices of excitation degrees of freedom with respect to local coordinate system

$\Phi_{\mathbf{x}}$	mode shape matrices of response degrees of freedom
$\Phi_{\mathbf{x},\mathbf{G}}$	mode shape matrices of response degrees of freedom with respect to global coordinate system
$\Phi_{\mathbf{x},\mathbf{L}}$	mode shape matrices of response degrees of freedom with respect to local coordinate system
$\{\mathbf{p}\}_n$	vector of discrete signals at time step n
$\mathbf{R}_{\mathbf{ff}}(\tau)$	autocorrelation function of excitation
$\mathbf{R}_{\mathbf{xx}}(\tau)$	autocorrelation function of response
$\mathbf{S}_{\mathbf{ff}}(\omega, T)$	estimation of power spectral density of excitation
$\mathbf{S}_{\mathbf{ff}}(\omega)$	power spectral density of excitation
$\tilde{\mathbf{S}}_{\mathbf{ff}}(\omega)$	estimation of power spectral density of excitation, short form of $\mathbf{S}_{\mathbf{ff}}(\omega, T)$
$\{\tilde{\mathbf{S}}_{\mathbf{p}}\}_k$	power spectral density of discrete signal \mathbf{p} at frequency step k
$\{\tilde{\mathbf{S}}_{\mathbf{p}}^{\Delta}\}_{k_t}$	averaged power spectral density of discrete signal \mathbf{p} at frequency step k_t
$\{\tilde{\mathbf{S}}_{\mathbf{p}}^{(i)}\}_{k_t}$	power spectral density of discrete signal \mathbf{p} and block i at frequency step k_t
$\mathbf{S}_{\mathbf{xx}}(\omega, T)$	estimation of power spectral density of response
$\mathbf{S}_{\mathbf{xx}}(\omega)$	power spectral density of response
$\tilde{\mathbf{S}}_{\mathbf{xx}}(\omega)$	estimation of power spectral density of response, short form of $\mathbf{S}_{\mathbf{xx}}(\omega, T)$
$\tilde{\mathbf{S}}_{\mathbf{x}}(\omega)$	estimation of power spectral density of response
θ_p	location vector of optimum
$\mathbf{T}_{\mathbf{x}}$	transformation matrix
Υ	column-wise arrangement of spectral amplitudes
$\bar{\Upsilon}$	normalized matrix of Υ
$\mathbf{x}(t)$	response vector
ζ	vector of modal damping ratios
α	complex scalar value to define the frequency response function
b_1, b_2, b_3, b_4, b_5	parameters for regression function
$\Delta\omega$	discrete circular frequency step
Δt	discrete time step
d_p	minimal distance to optimum
ι	imaginary unit
J	objective function
\tilde{J}	minimal expected objective function value
m_f	number of considered excitation degree of freedom
m_{λ}	number of eigenvalues

m_p	number of considered response degree of freedom for the discrete signal vector \mathbf{p}
m_x	number of considered response degree of freedom
ω	circular frequency
\bar{p}	suboptimum number
R	influence radius
S_0	power spectral density related to noise
σ^2	variance of white noise excitation
T	time or period of time history
t	time
w_1, w_2	weightings of weighted objective function

Energy-based modal assurance criterion

COMAC	coordinate modal assurance criterion
ECOMAC	enhanced coordinate modal assurance criterion
ELMAC	energy-based linearized modal assurance criterion
LMAC	linearized modal assurance criterion
LNCO	linearized normalized cross orthogonality
ModMAC	modified modal assurance criterion
MSF	modal scale factor
NCO	normalized cross orthogonality
NMD	normalized modal differences
SCO	SEREP cross orthogonality
SEREP	system equivalent reduction and expansion process
WMAC	weighted modal assurance criterion
ELMAC	matrix of energy-based linearized modal assurance criterion
$(\text{ELMAC})_{i,j}^{(k)}$	entry (i, j) of the energy-based linearized modal assurance criterion matrix with respect to cluster k
$(\text{EMAC})_{i,j}^{(k)}$	entry (i, j) of the energy-based modal assurance criterion matrix with respect to cluster k
\mathbf{f}_m	known measured natural frequencies
\mathbf{f}_p	numerically derived natural frequencies regarding updating step p
\mathbf{I}	identity matrix
$(\bar{\mathbf{j}})_i$	assigned numerical modes number with respect to measured mode i
$(\bar{\mathbf{j}})_i^{(k)}$	assigned numerical modes number with respect to measured mode i and cluster k

K	stiffness matrix of model
\mathbf{K}_a^S	condensed stiffness matrix
$\mathbf{K}^{(k,l)}$	stiffness matrix of model with respect to clusters k and l
L	left singular vectors
LMAC	matrix of linearized modal assurance criterion
LNCO	matrix of linearized normalized cross orthogonality
M	mass matrix of model
MAC	matrix of modal assurance criterion
\mathbf{MAC}_p	matrix of modal assurance criterion regarding updating step p
\mathbf{M}_a^S	condensed mass matrix
MSE	matrix of modal strain energy regarding clusters and modes
$(\mathbf{MSE})_j^{(k)}$	modal strain energy of mode j with respect to cluster k
NCO	matrix of normalized cross orthogonality
$\boldsymbol{\omega}$	vector of circular frequencies
$\boldsymbol{\Phi}$	column-wise arrangement of eigenvectors in the eigenvector matrix
$\hat{\boldsymbol{\Phi}}$	column-wise arrangement of reduced eigenvector in a matrix
$\{\boldsymbol{\Phi}\}_i$	eigenvector corresponding to mode i
$\{\hat{\boldsymbol{\Phi}}\}_i$	reduced eigenvector corresponding to mode i
$\{\boldsymbol{\Phi}\}_i^{(k)}$	mode shape vector corresponding to mode i and cluster k
$(\boldsymbol{\Pi})_j^{(k)}$	relative modal strain energy with respect to mode j and cluster k
R	right singular vectors
S	diagonal matrix with singular values
T	transformation matrix
$\boldsymbol{\theta}_0$	initial values of unknown model input parameters
$\boldsymbol{\theta}_p$	unknown model input parameters regarding updating step p
W	weighting matrix
\mathbf{z}_m	vector of experimentally obtained target output parameters
\mathbf{z}_p	numerically derived output parameters regarding updating step p
J	objective function
k_1, k_2, k_3, k_4, k_5	spring stiffnesses
m_1, m_2, m_3	point masses

Stochastic model updating

α	Rényi α -divergence
β	β -divergence

βS	symmetrized β -divergence
BH	Bhattacharyya distance
CH	Chernoff distance
χ^2	χ^2 divergence
$\chi^2 S$	symmetrized χ^2 divergence
$E2L$	weighted Euclidean norm of first two L moments
$E2S$	weighted Euclidean norm of first two statistical moments
$E2SC$	weighted Euclidean norm of first two statistical moments including correlation coefficients
$E4L$	weighted Euclidean norm of first four L moments
$E4S$	weighted Euclidean norm of first four statistical moments
$E4SC$	weighted Euclidean norm of first four statistical moments including correlation coefficients
EF	Euclidean Frobenius norm
HC	Hellinger coefficient
HD	Hellinger distance
HI	Hellinger integral
KL	Kullback-Leibler divergence
KLS	symmetrized Kullback-Leibler divergence
MF	Mahalanobis Frobenius norm
PF	Patrick-Fisher distance
rKL	reversed χ^2 divergence
rKL	reversed Kullback-Leibler divergence
SHD	squared Hellinger distance
SPF	squared Patrick-Fisher
WEF	weighted Euclidean Frobenius norm
K	kurtosis of random vector
L₁	L_1 moment random vector
L₂	L_2 moment random vector
L₃	L_3 moment random vector
L₄	L_4 moment random vector
r	matrix of correlation coefficients
S	skewness of random vector
I_t	identity matrix of size $t \times t$
O_c	convexity indicator

\mathbf{O}_g	gradient indicator
\mathbf{O}_m	monotonicity indicator
$(\Phi)_{i,j}$	modal displacement of mode j and position i
θ	random vector of model parameters
$\hat{\theta}$	nominal random vector of model parameters
$\tilde{\theta}$	best identified random vector of model parameters
θ_0	initial random vector of model parameters
\mathbf{u}	random vector
$(\mathbf{X})_{i,j}$	discrete design point of objective function
\mathbf{x}	input parameter vector
$\hat{\mathbf{x}}$	nominal input parameter vector
$\tilde{\mathbf{x}}$	best identified input parameter vector
\mathbf{x}_0	initial input parameter vector
ξ	vector of normalized coordinates
\mathbf{y}	output parameter vector
\mathbf{y}_m	output parameter vector of experimentally obtained features
\mathbf{z}	random vector of model response
\mathbf{z}_m	random vector of experimentally obtained features
$D(P, Q)$	dissimilarity between distribution P and Q based on probability density functions
$D(P\ Q)$	dissimilarity of distribution P with respect to distribution Q based on probability density functions
$D^{\mathcal{N}}(P\ Q)$	explicit formula for dissimilarity of normal distribution P with respect to normal distribution Q based on probability density functions
$D^S(P\ Q)$	dissimilarity of normal distribution P with respect to normal distribution Q based on statistical moments
$\varepsilon_1, \varepsilon_2, \varepsilon_{3E}, \varepsilon_{3\sigma}$	measures of errors
J	objective function
m_x	number of input parameters
\mathcal{LN}	Lognormal distribution
\mathcal{N}	Normal distribution
P, Q	distributions
$p(\cdot), q(\cdot)$	probability density function of distributions P and Q , respectively
s	parameter of dissimilarity measures
$S(P\ Q)$	similarity of distribution P with respect to distribution Q
$S^{\mathcal{N}}(P\ Q)$	similarity of normal distribution P with respect to normal distribution Q
w_1, w_2	scalar weighting parameters

Contents

Danksagung	iii
Abstract	v
Kurzfassung	vii
List of figures	xii
List of tables	xiv
Nomenclature	xv
1 Introduction	1
1.1 Motivation	1
1.2 Framework for model updating	3
1.3 Scope and novelty of the presented thesis	9
2 Optimal placement of reference sensors	13
2.1 Problem overview	13
2.1.1 Motivation	13
2.1.2 Literature review	14
2.1.3 Proposed approach	16
2.2 Determination of random responses due to random excitation	17
2.2.1 Fundamental equations	17
2.2.2 Amendment for discrete signals	20
2.2.3 Transformation to local coordinate systems	21
2.2.4 White noise excitation	22
2.2.5 Multiple impulse excitation	23
2.3 Determination of optimal reference sensor positions	26
2.4 Possible simplifications for ambient excitation	29
2.5 Search strategy	31
2.6 Benchmark study: Simply supported beam	34

2.6.1	System description	34
2.6.2	Ambient excitation	34
2.6.3	Multiple impulse excitation	39
2.7	Case study: Test specimen	44
2.7.1	System description	44
2.7.2	Description of finite element model	44
2.7.3	Validation of spectral response amplitudes	46
2.7.4	Determination of optimal reference sensor positions	54
2.8	Discussion	66
3	The energy-based modal assurance criterion	69
3.1	Problem overview	69
3.2	Most important existing mode pairing criteria	72
3.2.1	Modal assurance criterion (MAC)	72
3.2.2	Normalized cross orthogonality (NCO)	72
3.3	Mode assignment using the energy-based modal assurance criterion	73
3.4	Benchmark study: Cantilever truss	76
3.4.1	Description of the system	76
3.4.2	Application of mode assignment	78
3.4.3	Optimization	83
3.5	Case study: High-speed railway bridge EÜ Erfttalstraße	86
3.5.1	Description of the system	86
3.5.2	Application of mode assignment	86
3.5.3	Global sensitivity analysis	90
3.6	Discussion	94
4	Objective functions for stochastic model updating	97
4.1	Problem overview	97
4.1.1	Motivation	97
4.1.2	Literature review	98
4.1.3	Proposed methodology	101
4.2	Optimization-based stochastic model updating	102
4.3	Dissimilarity measures	104
4.3.1	Definitions	104
4.3.2	Similarity measures based on probability density functions	106
4.3.3	Dissimilarity measures based on probability density functions	107
4.3.4	Dissimilarity measures based on statistical moments	113
4.3.5	Numerical and computational aspects	115
4.4	Numerical evaluation of objective function properties	117
4.5	Benchmark study: Three degree of freedom mass-spring system	120

4.5.1	Description	120
4.5.2	Numerically derived properties of the objective functions	123
4.5.3	Dissimilarity measures applied as objective functions	129
4.6	Benchmark study: Truss system	136
4.6.1	Description	136
4.6.2	Numerically derived properties of the objective functions	139
4.6.3	Dissimilarity measures applied as objective functions	144
4.7	Discussion	148
5	Summary and conclusions	151
6	Recommendations for future research	155
6.1	Pretest phase	155
6.1.1	Robust optimal reference sensor positions	155
6.1.2	Optimal roving sensor positions	156
6.2	Model updating	156
6.2.1	Multivariate non-normal distributions	156
6.2.2	Sequential parameter optimization	157
6.2.3	Surrogate modeling	158
A	Statistical values	161
A.1	Statistical measures of distributions	161
A.2	L moments of marginal distributions	162
B	Optimization methods	163
B.1	Genetic algorithm	163
B.2	Particle swarm optimization	163
B.3	Adaptive response surface method	164
	Bibliography	184

1.1 Motivation

The typical challenge in civil, mechanical, and aerospace engineering's practice is the design or redesign of structures (e.g., bridge, automobile, airplane) by minimizing total costs, while ensuring all requirements on performance, safety, and reliability. In addition, structures become more and more complex, new designs will be created, and innovative materials will be implemented, about which little experience of their behavior is available. Hence, the application of numerical models in combination with advanced solving strategies is standard in current practice. The systematic optimization of designs with the purpose to improve specific requirements (e.g., robustness, weight reduction, reduction of costs, or increase of comfort) is a wide field of applied and fundamental research. Consequently, numerical models are very important for design optimization and predictive calculations. A numerical model is always based on certain simplifications, and will usually not be able to consider all physical phenomena, like structural resistance, heat transfer, or electro magnetic behaviors at the same time. Therefore, each numerical model is strongly related to its intended use, which is in general a predictive calculation of a certain physical behavior.

The successful application of numerical models depends on the quality or suitability of the model itself. The suitability of the model covers questions regarding the possibility to represent a respective required physical behavior or the ability of the model to converge at least asymptotically to the true solution, assuming that all model parameters are correct. The choice of constitutive law, numerical method for time integration, and applied simplifications need to be approved by experience or validated by experiments, for example.

Once the numerical model has been established and its basic suitability has been confirmed at least based on engineering experience, it is required to define model specific input parameters. Such input parameters are, for instance, material parameters (e.g.,

Young's modulus), geometry parameters (e.g., width of plates), loading conditions (e.g., size and direction of excitation loads), or boundary conditions. Typically, the specific input parameter values are uncertain due to the involved manufacturing, construction, and production processes, but they can be described by random variables. For simplifications, codes and standards can provide typical distributions or deterministic values associated with specific safety concepts. However, the confidence on predictive results derived by the numerical model relies on the chosen numerical model and its usually uncertain model input parameters. If the confidence in the chosen numerical model or the defined model input parameters is not sufficient, validation or calibration experiments need to be conducted, respectively. A model revision or revision of the experiment needs to be applied, if the discrepancy between numerically derived and experimentally obtained results is not acceptable. The numerical model revision can be divided into two classes: the model updating (i.e., adjustment of model input parameters) and the basic revision of the numerical model (i.e., change of basic assumptions to improve the suitability of the model). Obviously, also experimentally obtained results can be effected by inaccurate and unsuitable experiments. Therefore, also a revision of the experiment needs to be considered. A general concept of model verification and validation is presented in [ASME V&V 10 2006].

In this PhD thesis, the reduction and quantification of uncertainties in vibration-based model updating is the main emphasis. Model updating is a method to improve the correlation between the numerical model and a realistic structure using measured data by adjusting previously selected uncertain model input parameters (e.g., [Steenackers et al. 2006]). If the numerical model is a finite element model, the term finite element model updating is very common ([Friswell et al. 1995]). Vibration-based model updating is a type of model updating, in which the measured data is obtained by vibration experiments. The measured quantities are typically, time histories of accelerations, velocities, displacements, or strains. Based on these time histories, features like natural frequencies, modal damping ratios, mode shapes, or frequency response functions can be derived. Suitable modal parameter identification methods are stochastic subspace identification (SSI) (e.g., [Peeters et al. 1999], [Peeters et al. 2001]), enhanced frequency domain decomposition (EFDD) (e.g., [Brincker et al. 2000]), or poly-reference least squares complex frequency domain (p-LSCF) algorithm (e.g., [Cauberghe 2004]).

Assuming that the numerical model is suitable to cover the required principle physical behavior, the reliability of the identified model input parameters depends on the accuracy of the experimentally obtained features and numerically derived model responses. Hence, it is important to determine and reduce uncertainties in the experiments and the numerical calculation. Numerical uncertainties are, for instance, unreliable mode pairing strategies, numerical noise, inaccuracies due to ill-conditioned matrices, convergence problems, or discretization. In general, numerical uncertainties need to be reduced to

a minimum and should be determined or approximated by error estimators or repeated numerical calculations. Uncertainties related to experiments are, for example, electronic noise generated by the measurement instruments, sensitivity of sensor locations with respect to the kind of measured quantity, random or systematic errors introduced by external excitation sources, unrecognized additional masses of the instrumentation, or signal processing errors. Such uncertainties are difficult to separate and to quantify. Frequently, they can only be determined by repeating several identical experiments with one identical structure under identical environmental conditions. Experimental campaigns to quantify experimental uncertainties were described in [Adhikari et al. 2009], [Govers et al. 2010b], and [Govers et al. 2006]. Based on assumptions about these uncertainties, the most likely set of input parameters can be identified and the model accuracy of the input parameters can be expressed, for example, by confidence intervals or a certain variance. Obviously, the obtained variation cannot be interpreted as a true physical variation of the identified model input parameters.

Of course, assuming an experimental campaign investigating several nominally identical test structures or one test structure under different experimental conditions (e.g., uncertain loading conditions), a variation of the experimental results can be expressed as a physical variation of model input parameters. If the variation of the identified model input parameters can be interpreted as a property of a real physical quantity, the model updating is denoted by stochastic model updating. In the case that the variations of model input parameters are not determined, uncertainties are not considered in general, or variations cannot be directly related to a physical variation of the identified model parameters, the model updating strategy is a deterministic model updating.

Another very common possibility to distinguish uncertainties is the separation in aleatory (i.e., inherent, irreducible) and epistemic (i.e., reducible) uncertainties (e.g., [ASME V&V 10 2006]). However, this separation is not appropriate to distinguish deterministic and stochastic model updating.

1.2 Framework for model updating

Model updating algorithms are numerical tools to calibrate or to adjust uncertain model input parameters to increase the correlation between numerically derived model responses and experimentally obtained features. Several investigations and calculations are required to provide all necessary information for model updating, such as, number and kind of input parameters, the experimentally obtained features, or the initial numerical model. Hence, a general framework for updating a numerical model is presented in the current section. The framework does not only link the different analyses, it also provides the main terminology used in this thesis. This is important, as the main methods have been developed independently by many researchers within the last 20 years. A commonly

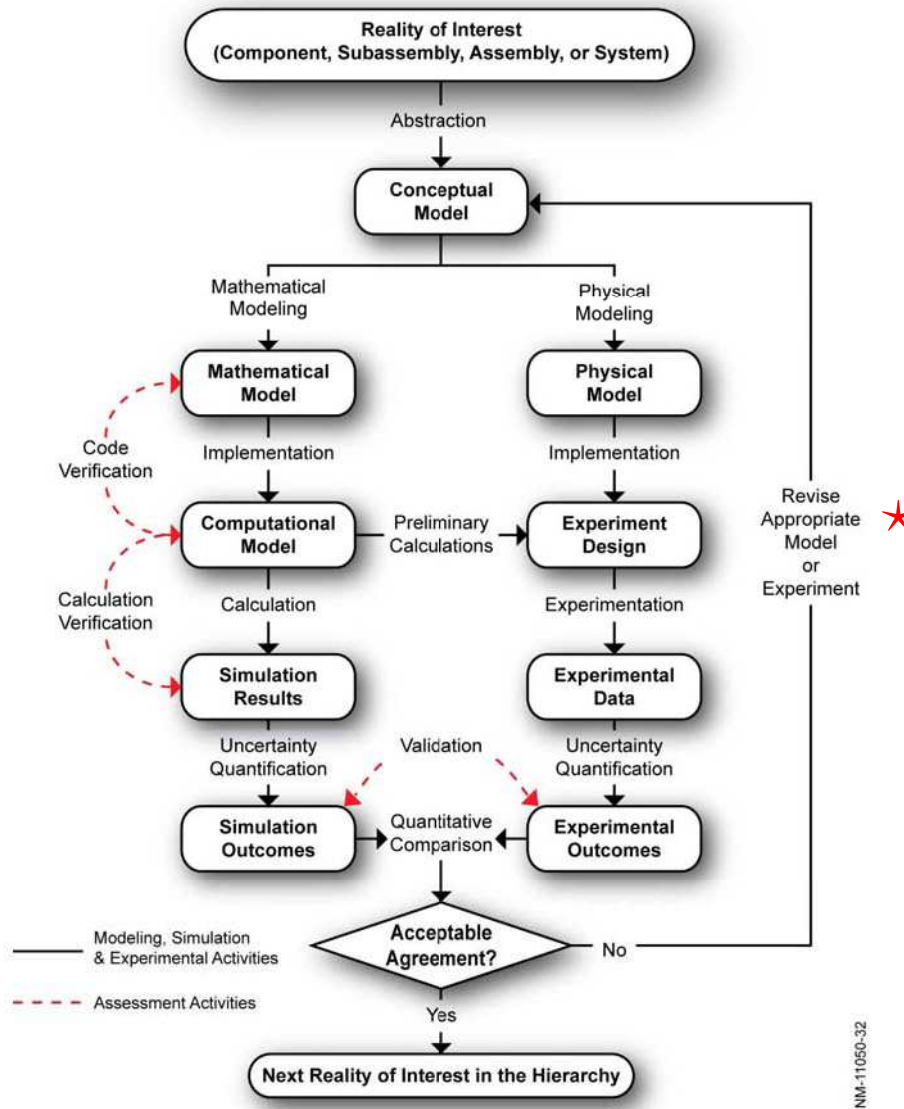


Figure 1.1: General overview of the framework for model verification and model validation [Schwer 2006]. The symbol \star indicates the link to the framework for model updating.

agreed terminology does not exist.

The American society of mechanical engineers (ASME) is one organization, who tried to unify the concept of model verification, validation, and updating. An overview of this guideline is given in Figure 1.1. For an exhaustive description, it is referred to the guideline [ASME V&V 10 2006] itself. Unfortunately, the current guide for verification and validation in computational solid mechanics [ASME V&V 10 2006] is rather concentrated on verification and validation of models than on model updating and necessary pretest analysis.

The framework for model updating, presented in Figure 1.2, can be considered as an extension to the general concept given in [ASME V&V 10 2006]. Assuming the discrepancy between numerical model outputs and validation experiment outputs cannot be

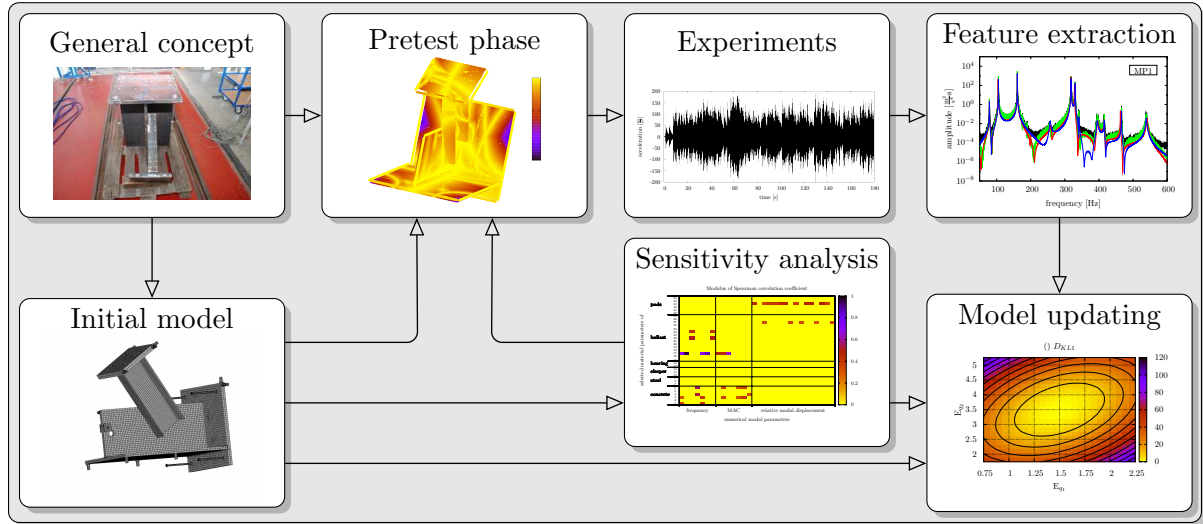


Figure 1.2: General overview of the framework for model updating.

accepted and a numerical model revision in form of adjusting model input parameters is decided, the framework for model updating can be applied. The star in Figure 1.1 indicates the position, where the framework for model updating can be included into the framework for model verification and validation.

General concept: At the beginning of the framework, a general concept has to be prepared, which includes some conditions for the planned model updating procedure. For example, time schedule, accessibility of the structure on site, a preselection of most uncertain model input parameters, and a preselection of possible features to be extracted from experimental results are important. Of course, the size of uncertainty has to be estimated, for instance, by defining some reasonable upper and lower bounds for the uncertain model input parameters.

Initial model: The initial numerical model was already designed and verified in previous stages of the model verification and validation procedure. However, it is possible that some parts need to be modified or some algorithms need to be added or replaced to fit the requirements defined in the general concept of model updating. At least, the possible model outputs should be harmonized with the desired experimentally obtained features.

Sensitivity analysis: Using the initial model, a sensitivity analysis can be performed to investigate the influence of changes in the preselected uncertain model input parameters on changes in the preselected assortment of possible features. These sensitivities support the decision in the pretest phase to select appropriate features to be extracted from the measured data. In addition, the sensitivity is used to select the most sensitive parameters to be later included in the model updating. The final selection of uncertain model input

parameters is very important, as only sensitive model input parameters can be identified with sufficient accuracy. The sensitivity analysis can be performed globally or locally.

The global sensitivity analysis is typically a correlation analysis using the Pearson correlation coefficient or Spearman correlation coefficient. The obtained correlation matrices can be postprocessed, for example, by principle component analysis or calculating the coefficients of determination to identify the most sensitive model input parameters.

Whereas the global sensitivity analysis determines an averaged sensitivity for the whole design space, the local sensitivity analysis is related to the first derivatives calculated for example by finite differences in the vicinity of a certain set of model input parameters.

Sometimes it is difficult to obtain meaningful results, as the sensitivity analysis is related to certain assumptions, for example, to the degree of regression polynomial (e.g., linear, quadratic). Furthermore, it is difficult to recognize global sensitivities, if the output data tends to cluster in certain regions of the output space. A comprehensive overview about sensitivity analysis methods is given in [Saltelli et al. 2004], [Saltelli et al. 2008], [Fellin et al. 2006], and [Obergguggenberger et al. 2009]. Applications can be found in [Brehm et al. 2010], [Keitel et al. 2010], and [Zabel et al. 2008c].

Pretest phase: The planning of experiments is conducted in the pretest phase. Several aspects need to be considered in parallel to obtain a design, which optimally suits predefined conditions.

Once the features are selected according to the previous sensitivity analysis, the measurement quantity, such as accelerations, velocities, displacements, or strains, needs to be defined. The expected or applied excitation with certain characteristics and spatial distribution can influence the results obtained from measurements. The selection of sensors with respect to the required accuracy, measurement range, and resolution is fundamental. Furthermore, the number of test setups, the number of sensors, their spatial distribution, and their mounting on the structure need to be defined. Technical parameters of the data acquisition system, such as, trigger possibilities, number of available channels, and resolution of the analog digital converter (bit rate) are important, as well. Also the recording duration per setup and the sampling rate are essential parameters, which strongly depend on the properties of the given structural system. Moreover, the number of repeated experiments to evaluate the uncertainty is relevant.

In practice, the available measurement equipment, as well as, the available time for experiments restrict possible options. Most of the decisions are based on the experience of the engineer. Information extracted from the initial numerical model, like the range of natural frequencies of interest and the mode shapes, can support the decision process. Moreover, the accessibility to the structure may reduce the available sensor positions. Restrictions to the accessibility are, for instance, traffic below or on an investigated bridge or high-voltage cables at train bridges. Because the numerical model is not calibrated at

the time of pretest analysis, most extracted information is very uncertain. Therefore, the robustness (i.e., the sensitivity to small changes) of the final experimental setup should be considered.

Recommendations about measurement setups, measurement equipment, and the choice of sensors were collected in [Wenzel et al. 2005] and [Kuendig et al. 2009]. [Franchi et al. 1995] and [Brehm et al. 2011] gave an introduction regarding optimal sensor placement.

Experiments: The experiment itself needs to be conducted as accurate as possible based on the results of pretest analysis. All changes to the initial configuration of the experiment should be documented. Typically, many individuals with widely spread professional background, such as technicians, managers, engineers, and scientists, need to interact in a team. This requires a well organized time schedule for the experiments. Experiments with the aim to update a model are called calibration experiments. Validation experiments are conducted to proof the numerical model's capability regarding predictive calculations. In contrast, the calibration experiment is designed to provide features to be used to adjust uncertain model input parameters. Both experiments should be performed independently from each other.

Practical realizations of vibration experiments were described, for example, in [Cantieni 2009], [Liu et al. 2009], [Chellini et al. 2009], [Ribeiro et al. 2009], [Cantieni et al. 2008a], [Link et al. 2008], [Reynders et al. 2008], [Zabel et al. 2008b], and [Zabel et al. 2008a] and moreover in [Cunha et al. 2006], [Maeck et al. 2003], [Brincker et al. 2003], and [Krämer et al. 1999].

Feature extraction: Common features, extracted from vibration test data, are natural frequencies, modal damping ratios, and modal displacements. Of course, power spectral densities, frequency response functions, or wavelet transforms can also be of interest. Alternative features are statistical values of time histories, such as maximal amplitudes or signal energy contents. The most frequently applied modal parameter identification methods are stochastic subspace identification (SSI) (e.g., [Peeters et al. 1999], [Peeters et al. 2001]), enhanced frequency domain decomposition (EFDD) (e.g., [Brincker et al. 2000]), or poly-reference least squares complex frequency domain (p-LSCF) algorithm (e.g., [Cauberghe 2004]), which were summarized in [Reynders 2009] and [Zabel et al. 2009b]. [Reynders et al. 2008] proposed a theoretical uncertainty quantification for the stochastic subspace identification algorithm. General theoretical descriptions about modal testing, especially for experimentally derived frequency response functions, were provided by [Ewins 2000b].

Experimental investigations on uncertainties of extracted features were conducted by [Adhikari et al. 2009], [Govers et al. 2010b], and [Govers et al. 2006].

Model updating: A model updating algorithm adjusts the most sensitive uncertain model input parameters, identified by the sensitivity analysis, with the aim to minimize the discrepancy between model responses and the experimentally obtained features. Depending on the applied algorithm, objective functions need to be defined to evaluate the discrepancy. Model updating is also known as model calibration, parameter estimation, or physical parameter identification. A good overview about model updating techniques with respect to vibration test data was given in [Mottershead et al. 1993] and more recently in [Marwala 2010].

The deterministic model updating techniques can be subdivided in direct methods and indirect methods. The direct methods are trying to modify entries of system matrices, like stiffness, mass, or damping matrix. In many cases, the updating leads to a good agreement with the features extracted from measured data. Unfortunately, the process can produce updated matrices, which are ill-conditioned and non-sparse. Some direct methods were explained in [Friswell et al. 1995]. Wavelet-based direct algorithms were proposed by [Zabel 2003], [Brehm et al. 2005], and [Brehm 2006].

The indirect methods are based on a design variable description using material properties, geometrical measures, support conditions, or loading definition. Therefore, unreasonable system matrices can be avoided and the models are more suitable for predictions. A large class of model updating strategies is related to the partial derivative of the input parameters with respect to the output parameters and is therefore denoted by sensitivity-based model updating. Examples were given in [Brownjohn et al. 2001], [Jaishi et al. 2007], [Bakir et al. 2007], [Adhikari et al. 2010], and [Mottershead et al. 2010]. Other researchers, for example, [Levin et al. 1998] and [Brehm et al. 2009a], used standard optimization techniques, such as, simulated annealing and genetic algorithms. The updating can rely on forced [Lin et al. 2006] or ambient vibration data [Jaishi et al. 2005]. Due to considerable dynamic effects, railway bridges are frequently in the focus of research (e.g., [Chellini et al. 2007], [Teughels et al. 2003], [Brehm et al. 2009a]). [Chellini et al. 2010] applied model updating on a steel concrete composite frame.

One possibility how to implement measurement uncertainties of a single test structure is proposed by [Friswell et al. 1995] and applied by [Steenackers et al. 2006]. In this approach, the variances were used to assemble a weighting matrix for a squared weighted Euclidean norm. This norm was applied to determine the discrepancy between numerically derived and experimentally extracted features. Hence, the squared weighted Euclidean norm accentuated more reliable features. A more sophisticated weighting function is the inverse of the covariance matrix, which leads to the squared Mahalanobis distance as, for example, applied in [Doebbling et al. 2000]. However, the adjusted parameters are still deterministic. The first approach to obtain a measure of confidence for the identified parameters was presented by [Collins et al. 1974]. He considered the updating of a single test structure, perturbed by some known measurement noise. Furthermore, the uncertainty of

the unknown parameters was estimated at the initial step. Within an iteration procedure, the unknown parameters were updated together with their confidences indicated by the covariance matrix of the unknown parameters. A similar minimum variance method was proposed by [Friswell 1989]. [Mares et al. 2002] tried to reduce the uncertainties applying a robust estimation technique.

Sensitivity-based stochastic model updating techniques were proposed by [Mares et al. 2006], [Mottershead et al. 2006], [Khodaparast et al. 2008b], and [Govers et al. 2010a]. [Doebling et al. 2000] and [Zabel et al. 2009a] presented first applications of standard optimization techniques for the purpose of stochastic model updating.

1.3 Scope and novelty of the presented thesis

The previous description of the framework for model updating demonstrates the large field of different calculations and methods necessary to be considered to guarantee a successful updated model suitable for predictive calculations. Of course, in every substep uncertainties are present and need to be determined, reduced, and quantified. Due to the variety of different analyses in various substeps, the contributions of this thesis are restricted to three main tasks:

- (i) optimal placement of reference sensors within roving setup configurations,
- (ii) pairing of numerically derived and experimentally obtained mode shapes, and
- (iii) suitability of objective functions for optimization-based stochastic model updating.

Based on the author's practical experience by planning and conducting several measurement campaigns and subsequent updating of models, deficits of current theory and its limited applicability for particular cases have been identified. Such deficits are the main reasons for current unsatisfying results obtained from available deterministic or stochastic model updating procedures.

Even though the identified problems arise frequently, they are hardly covered in literature or the available methods are insufficient. Hence, the combination of all three proposed approaches will improve essentially the reliability of results obtained by predictive calculations using updated models. The three major contributions, their innovative novel approaches, and advantages for applications are summarized in the following.

Optimal reference sensor placement: This part is strongly related to the pretest phase, in which sensor locations need to be defined. Assuming a wide sense stationary process, the proposed approach is strongly connected to power spectral densities of estimated model responses.

Generally, two main sensor setup configurations are possible to generate vibration data. First, all sensors are fixed at certain positions during all measurements. This configuration is appropriate, if the access to the sensor locations on the structure is difficult and if the number of sensors is sufficiently large to obtain a certain spatial resolution of information at the structure. Second, at least one sensor is fixed during all measurements and at least one sensor is roved across the structure. This roving sensor setup configuration is applied, if the number of sensors is not sufficient to get the necessary resolution of information in space at the structure. The fixed sensors are denoted by reference sensors and they will be used to merge the information of different setups. It is obvious that the success of this merging approach strongly depends on the signal quality and frequency content of the reference sensors.

In contrast to available methods, which are reviewed exhaustively in Chapter 2, the proposed approach will be able to determine optimal reference sensor positions with respect to different signal quantities, like accelerations, velocities, or displacements and different damping values of each mode. While most approaches rely on a white noise excitation, the presented approach will be able to consider all excitation types, as long as, a wide sense stationary process can be assumed. Moreover, the number of modes to be considered does not restrict the number of reference sensors. Furthermore, an innovative geometry-based search strategy is proposed to support the convergence of the applied, nature inspired optimization strategies. Details about the methodology and its application to numerical benchmark studies and an experimental case study are presented in Chapter 2.

Pairing of numerically derived and experimentally obtained mode shapes:

Once the mode shapes, together with their natural frequencies, are extracted from the experimental data, they need to be assigned to the most likely numerically derived modes.

This task can be challenging, as mode switches are possible due to the variation of model input parameters. In addition, the numerical model can represent modes, for instance, local modes, which cannot be obtained from experimental data. The classical criterion to pair modes is the modal assurance criterion (MAC). However, this criterion tends to fail for certain typical applications as only the mathematical property of orthogonality is considered. A reliable mode pairing is required for sensitivity analysis and model updating.

Therefore, an enhanced modal assurance criterion based on modal strain energies is proposed to guarantee a reliable mode assignment for the process of sensitivity analysis or model updating. This novel criterion is termed energy-based modal assurance criterion (EMAC), which is described in Chapter 3. The related studies using artificially generated and measured test data show the effects of a wrong mode assignment and the successful application of the energy-based modal assurance criterion. Hence, uncertainties from a

wrong mode assignment can be reduced.

Objective functions for optimization-based stochastic model updating: The current sensitivity-based methods for stochastic model updating problems are limited in their applications. For a successful updating, the initial input parameters need to be close to the optimum that cannot be ensured in real applications. Furthermore, the approaches determine only the first two statistical moments of the target distribution. This restricts the applicability to a few distribution types.

Therefore, an alternative approach, the optimization-based stochastic model updating, using standard optimization techniques, like genetic algorithm or particle swarm optimization is proposed. Even if it is advantageous, the input parameter values do not need to be close to the optimum. The presented methodology is not restricted to certain distribution types. In contrast to deterministic model updating, where optimization methods were already successfully applied, the definition of a suitable objective function to compare two distributions is not straightforward for stochastic model updating. The innovative contribution of this thesis is the application of dissimilarity measures, usually applied to information theory problems, as objective functions to compare the distributions of target features and numerical model responses. As various dissimilarity measures are existing, the properties of such objective functions will be numerically investigated by means of two benchmark studies. It can be derived that certain dissimilarity measures are suitable to be applied as objective functions in the context of optimization-based stochastic model updating. The approach and the subsequent benchmark studies are explained in Chapter 4.

The thesis will be closed by a general conclusion and recommendations for future research.

Optimal placement of reference sensors

2.1 Problem overview

2.1.1 Motivation

The success of vibration-based model updating depends on the applied theoretical methods, their numerical realization, computational efficiency, and the quality of measured values. Applying the framework for model updating introduced in Section 1.2, a pretest analysis needs to be performed to optimize the measurement configuration. The pretest analysis will ensure suitable and reliable features used for model updating. Those features are extracted from measured time series at certain positions of the structure. As not all positions of a structure can be instrumented, a preselection is usually conducted.

Accordingly, one of the main tasks of a pretest analysis in the field of experimental modal analysis is the optimal placement of sensors. Two main sensor setup configurations are possible. First, all sensors are fixed at certain positions during all measurements. This one-setup configuration is appropriate, if the positions at the structure are difficult to reach and if the number of sensors is sufficient to obtain a certain spatial resolution of information about the structure. Second, at least one sensor is fixed during all measurements and at least one sensor is moved across the structure. This roving sensor setup configuration is applied, if the number of available sensors or channels is not sufficient to get the necessary resolution of information in space at the structure. The fixed sensors are called reference sensors, which will be used to merge the different setups. It is obvious that the success of this merging approach strongly depends on the signal quality and frequency content of the reference sensors.

This contribution is focused on the determination of optimal reference sensor positions within a roving sensor vibration test conducted to provide experimentally obtained features for updating an initial finite element model. An output-only vibration measurement with random excitation is assumed that can be interpreted as a weakly stationary process.

As this specific topic is hardly addressed in literature, pretest approaches with respect to one-setup configurations are reviewed, as well.

2.1.2 Literature review

Assessment criteria are reviewed regarding one-setup and roving setup configurations. Then, the search strategies available in literature will be discussed. The reviewed criteria are based on mode shapes of a numerical model in the pretest phase.

One common measure to judge the suitability of sensor positions in one-setup configurations is the Fisher information matrix, which leads to the D-optimal design criterion. By maximizing the determinant of the Fisher information matrix (e.g., [Kammer 1991], [Yao et al. 1993], [Kammer et al. 1994], [Kammer 1996], [Li et al. 2009], [Kincaid et al. 2002], [Tongco et al. 1994], [Tongco et al. 1996], [Bayard et al. 1988]), maximizing the smallest eigenvalue of the Fisher information matrix (e.g., [Reynier et al. 1999]), minimizing the trace of inverse of the Fisher information matrix (e.g., [Heredia-Zavoni et al. 1998]), or minimizing the condition number of the Fisher information matrix (e.g., [Kim et al. 2001]), it is assumed that the correlation between the reduced mode shape vectors can be minimized. Of course, these approaches assume that the number of sensors is at least as big as the number of target modes that should be identified [Li et al. 2007a]. Otherwise, the independency of modes cannot be guaranteed. Garvey [Garvey et al. 1996] enhanced the original criterion by a Guyan reduced mass weighting scheme.

Another criterion to judge combinations of sensor positions within one-setup configurations is the modal kinetic energy, proposed by [Kammer 1991] and applied by [Papadopoulos et al. 1998] and [Li et al. 2007a]. It is assumed that large response amplitudes at a certain position are related to high modal kinetic energy. With this criterion, it should be possible to increase the signal to noise ratio. This is essential, if notable measurement noise is expected. The drawback of this method is the high dependency on the element mesh size [Papadopoulos et al. 1998]. Therefore, the method tends to choose regions with large element sizes where the mass is concentrated. This can lead to unsatisfying results. As the kinetic energy is only a mass weighted version of the Fisher information matrix, the connection to the effective independence method is obvious. This has been investigated in detail by [Li et al. 2007a]. [Tuttle et al. 2005] proposed a subsequent application of the iterative residual kinetic energy method and the mass weighted effective independence method. These methods are modifications of the modal kinetic energy method and the effective independence method, respectively.

Several other objectives and assessment criteria for optimal sensor positions within one-setup configurations have been proposed. One set of criteria is derived from the modal assurance criterion originally introduced by [Allemang et al. 1982], whereas the off-diagonal terms of the MAC matrix need to be minimized (e.g., [Liu et al. 2008]).

This typically leads to uncorrelated modes shapes. The MAC and the mass weighted MAC were proposed as assessment criterion, for example, by [Penny et al. 1994]. Modal strain energy based criteria were proposed by [Liu et al. 2008] and [Reynier et al. 1999]. An information entropy based criterion was introduced in [Papadimitriou et al. 2000] and applied in [Papadimitriou 2004]. However, [Papadimitriou 2005] concluded that the information entropy is related to the determinant of the Fisher information matrix.

In [Schwarz et al. 2002], a comprehensive overview about criteria to assess reference sensor positions within a roving sensor setup configuration was presented. For example, the shape product was suggested, which is the multiplication of a certain degree of freedom of all modes of interest. This method aims to visualize the nodal points of target modes in one plot. Those nodal points should be generally avoided as reference sensor positions. Another possibility to avoid nodal points of target modes is the use of driving point frequency response functions (e.g., [Schwarz et al. 2002]). Reference sensor positions should be preferably located at positions with a high driving point frequency response function value. If several reference positions are of interest, the complex mode indicator function or the multivariate mode indicator function can be relevant, which was explained in [Schwarz et al. 2002]. [Avitabile et al. 1996] proposed a method based on the singular value decomposition of the frequency response function matrix. Herein, the contribution of each possible position to the singular values indicates the suitability of a certain position to be used as reference sensor position. This idea leads to an enhanced algorithm termed test reference identification procedure as presented in [Chandler et al. 2001] and [Avitabile et al. 2002]. It is worthy to note that the complex mode indicator function is defined by the eigenvalues deduced from the frequency response function [Chandler et al. 2001].

So far, only the criteria to rank possible sensor positions are reviewed. The search strategies to find the best sensor positions can be classified into three groups. The first group simply calculates all possible combinations. This leads to the global optimum, but is only possible for a small number of combinations. With an increasing number of possible sensor locations and available sensors, the computational effort becomes too high. A second group uses sequential schemes within the effective independence approaches proposed by [Kammer 1991]. [Papadimitriou 2004] suggested sequential schemes in combination with the information entropy criterion. However, those schemes mostly lead to a near-optimal sensor placement, as a strong monotonic behavior of the process cannot be guaranteed.

The most frequently proposed search algorithms are based on optimization strategies, which are arranged in a third group. In most cases, a discrete combinatoric optimization problem needs to be solved. As predefined algorithms are available, the application of such methods can be easily realized. However, the success of such methods strongly depends on the definition of design variables.

Most researchers, for example, [Papadimitriou 2004], [Papadimitriou 2005], and [Liu

et al. 2008], proposed discrete design variables based on the possible degrees of freedom for sensor locations. This approach leads to a minimal number of design variables, but destroys in many cases the spatial connection of proximate sensor positions. [Swann et al. 2004] and [Maghami et al. 1993] suggested a design variable definition based on the spatial location of sensor positions. [Swann et al. 2004] used the design variables to describe a regular mesh of sensors. Maghami [Maghami et al. 1993] approximated the output measurements with spatially continuous functions. As optimization strategies prefer continuous design variables, [Pape 1994] proposed to approximate the discrete mode shapes by a function based on Chebyshev polynomials. In many studies, a genetic algorithm was applied as optimization strategy for this kind of problems (e.g., [Stabb et al. 1995], [Swann et al. 2004], [Papadimitriou 2004], [Papadimitriou 2005], [Liu et al. 2008], [Cruz et al. 2009], [Franchi et al. 1995]). Alternatives are, for example, the specific branch-and-bound technique developed by [Fijany et al. 2005] and the gradient-based algorithm proposed by [Al-Shehabi et al. 2002]. A comparison of several search strategies was given in [Bedrossian 1998].

Comprehensive comparisons of several methods by means of numerical (e.g., [Penny et al. 1994]) and real size examples (e.g., [Meo et al. 2005], [Larson et al. 1994b], [Larson et al. 1994a], [Papadopoulos et al. 1998]) were presented in literature. However, most methods lead to similar and reasonable results.

Even though the results are reasonable, the methods are based on certain limiting assumptions. First, the methods optimize the sensor placement with respect to a white noise excitation. The general case of random excitation at certain degrees of freedom of the structure is not covered in the analytical approaches. Second, most approaches neglect the effect of damping, which is important, if the modal damping ratios are not equal for all modes. The only exception are methods that rely on frequency response functions. Third, the applied mass normalized eigenvectors of the initial numerical model are only related to accelerations, which is unfortunately not always mentioned in the references. If the measured quantities are velocities or displacements, the optimal sensor configurations may differ from the proposed acceleration-based optimal sensor placements.

2.1.3 Proposed approach

The forcing idea of the proposed approach is based on the idea of maximizing the signal to noise ratio of reference sensors. The signal energy should be as high as possible for all frequencies of interest. In contrast to other methods, the expected power spectral densities of responses at the frequencies corresponding to the modes of interest are calculated by using a random spectral description of the excitation. The highest spectral response amplitudes with respect to all positions and modes of interest will be the optimal ones. This idea is implemented into a mathematically formulated objective function. Moreover,

a search algorithm is proposed, which is based on nature inspired optimization strategies, where the design variables are related to a geometrical description of possible sensor positions.

Consequently, the proposed approach is able to consider all types of random excitation as long as the requirements for a weakly stationary process are fulfilled. Furthermore, the number of reference sensors and the number of target mode shapes are not restricted. The quantity of vibration measure, namely accelerations, velocities, and displacements, are taken into account. Different measurement noise levels, as well as, different modal damping ratios can be considered.

The presented approach is assessed by means of a numerical benchmark study of a simply supported beam assuming white noise and multiple impulse excitation at several points on the structure. In addition, a case study of a test specimen is provided, which is supposed to be investigated within an experimental modal analysis using a roving sensor vibration test. The excitation for this test is applied at two predefined positions on the structure. Reference sensor locations are determined by the proposed approach. Furthermore, the analytically derived predictive power spectral amplitudes are compared with experimentally obtained power spectral amplitudes. The experimental data rely on 507 time histories of time length 27 seconds with identical testing conditions. This procedure allows a sufficient statistical analysis.

2.2 Determination of random responses due to random excitation

2.2.1 Fundamental equations

Almost all reference-based output-only experimental modal analysis procedures assume that the reference signals cover all modes of interest with a certain intensity. This can be easily assessed by the power spectral density of the measured response signal. The following approach assumes that the system response and excitation can be interpreted as a random wide sense stationary process. Therefore, the first and second statistical moments are time invariant [Norton et al. 2003]. The signals of excitation do not need to be measured. It is sufficient to know their basic stochastic characteristics. Based on these statistics, the response spectral densities can be predicted.

Assuming a structural response in space and time due to a random excitation, which is independent with respect to all discrete spatial points m_f and regarding time, equation [Natke 1992]

$$\mathbf{S}_{\mathbf{xx}}(\omega) = \mathbf{H}_{\mathbf{xf}}(\omega)^* \mathbf{S}_{\mathbf{ff}}(\omega) \mathbf{H}_{\mathbf{xf}}(\omega)^T \quad (2.1)$$

holds for all circular frequencies ω . $\mathbf{S}_{\mathbf{xx}}(\omega) \in \mathbb{C}^{m_x \times m_x}$ and $\mathbf{S}_{\mathbf{ff}}(\omega) \in \mathbb{C}^{m_f \times m_f}$ are the auto

power spectral density matrices of the response $\mathbf{x}(t) \in \mathbb{R}^{m_x}$ and the excitation $\mathbf{f}(t) \in \mathbb{R}^{m_f}$, respectively. The frequency response function between response and excitation is denoted by $\mathbf{H}_{\mathbf{x}\mathbf{f}}(\omega) \in \mathbb{C}^{m_x \times m_f}$. The superscripts $*$ and T indicate the complex conjugate and the transpose of a matrix, respectively.

According to the Wiener-Khintchine theorem (e.g., [Papoulis et al. 2002]), the spectral densities

$$\mathbf{S}_{\mathbf{xx}}(\omega) = \int_{-\infty}^{+\infty} \mathbf{R}_{\mathbf{xx}}(\tau) \exp(-i\omega\tau) d\tau \quad \text{and} \quad \mathbf{S}_{\mathbf{ff}}(\omega) = \int_{-\infty}^{+\infty} \mathbf{R}_{\mathbf{ff}}(\tau) \exp(-i\omega\tau) d\tau \quad (2.2)$$

are defined by the Fourier transform of the belonging autocorrelation functions $\mathbf{R}_{\mathbf{xx}}(\tau)$ and $\mathbf{R}_{\mathbf{ff}}(\tau)$ (e.g., [Bucher 2009]). The value $i = \sqrt{-1}$ is the imaginary unit.

However, for real finite continuous signals $\mathbf{x}(t) \in \mathbb{R}^{m_x}$ and $\mathbf{f}(t) \in \mathbb{R}^{m_f}$ defined within a time interval $[0, T]$, the power spectral densities can be approximated [Natke 1992] by

$$\begin{aligned} \tilde{\mathbf{S}}_{\mathbf{xx}}(\omega) = \mathbf{S}_{\mathbf{xx}}(\omega, T) &= \frac{1}{T} \mathcal{F}_{\mathbf{x}}(\omega, T)^* \mathcal{F}_{\mathbf{x}}(\omega, T)^T \quad \text{and} \\ \tilde{\mathbf{S}}_{\mathbf{ff}}(\omega) = \mathbf{S}_{\mathbf{ff}}(\omega, T) &= \frac{1}{T} \mathcal{F}_{\mathbf{f}}(\omega, T)^* \mathcal{F}_{\mathbf{f}}(\omega, T)^T \end{aligned} \quad (2.3)$$

with

$$\lim_{T \rightarrow \infty} \mathbf{E}(\mathbf{S}_{\mathbf{xx}}(\omega, T)) = \mathbf{S}_{\mathbf{xx}}(\omega) \quad \text{and} \quad \lim_{T \rightarrow \infty} \mathbf{E}(\mathbf{S}_{\mathbf{ff}}(\omega, T)) = \mathbf{S}_{\mathbf{ff}}(\omega) \quad (2.4)$$

using the finite Fourier transform of the excitation

$$\tilde{\mathcal{F}}_{\mathbf{f}}(\omega) = \mathcal{F}_{\mathbf{f}}(\omega, T) = \int_0^T \mathbf{f}(t) \exp(-i\omega t) dt \quad (2.5)$$

and the finite Fourier transform of the response

$$\tilde{\mathcal{F}}_{\mathbf{x}}(\omega) = \mathcal{F}_{\mathbf{x}}(\omega, T) = \int_0^T \mathbf{x}(t) \exp(-i\omega t) dt \quad (2.6)$$

with $\tilde{\mathcal{F}}_{\mathbf{f}}(\omega) \in \mathbb{C}^{m_f}$ and $\tilde{\mathcal{F}}_{\mathbf{x}}(\omega) \in \mathbb{C}^{m_x}$. Hence, Equation (2.1) can be reformulated.

$$\tilde{\mathbf{S}}_{\mathbf{xx}}(\omega) = \frac{1}{T} \mathbf{H}_{\mathbf{x}\mathbf{f}}(\omega)^* \tilde{\mathcal{F}}_{\mathbf{f}}(\omega)^* \tilde{\mathcal{F}}_{\mathbf{f}}(\omega)^T \mathbf{H}_{\mathbf{x}\mathbf{f}}(\omega)^T \quad (2.7)$$

Combining Equations (2.3), (2.6), and (2.7), the finite Fourier transformation of the response derives

$$\tilde{\mathcal{F}}_{\mathbf{x}}(\omega) = \mathbf{H}_{\mathbf{x}\mathbf{f}}(\omega) \tilde{\mathcal{F}}_{\mathbf{f}}(\omega). \quad (2.8)$$

Assuming proportional viscous damping, the complex frequency response function matrix $\mathbf{H}_{\mathbf{x}\mathbf{f}}(\omega)$ can be analytically determined by using the classical undamped eigenvalues $\boldsymbol{\lambda} \in \mathbb{R}^{m_\lambda}$ and the classical undamped mass normalized eigenvector matrix $\boldsymbol{\Phi}$ of the structure

and corresponding modal damping ratios $\zeta \in \mathbb{R}^{m_\lambda}$. The mode shape matrices of response degrees of freedom $\Phi_{\mathbf{x}} \in \mathbb{R}^{m_x \times m_\lambda}$ and of excitation degrees of freedom $\Phi_{\mathbf{f}} \in \mathbb{R}^{m_f \times m_\lambda}$ are assembled from the eigenvector matrix Φ . An initial estimate of eigenvalues and eigenvectors can be extracted, for example, by conducting an analytical modal analysis using a finite element model. If no other information is available, the damping values need to be estimated based on experience. [Ewins 2000a, p. 64] and [Lin et al. 2006] showed a simple approach to evaluate the complex frequency response function matrix

$$\mathbf{H}_{\mathbf{x}\mathbf{f}}(\omega) = \alpha \Phi_{\mathbf{x}} \mathbf{D}(\omega) \Phi_{\mathbf{f}}^T. \quad (2.9)$$

In this context, $\mathbf{D}(\omega) \in \mathbb{C}^{m_\lambda \times m_\lambda}$ represents a complex diagonal matrix. Its diagonal elements depend on the circular frequency ω .

$$(\mathbf{D}(\omega))_{l,l} = \frac{(\lambda)_l - \omega^2 - \iota \left(2\omega \sqrt{(\lambda)_l} (\zeta)_l \right)}{(\lambda)_l^2 - 2\omega^2 (\lambda)_l + \omega^4 + 4\omega^2 (\lambda)_l (\zeta)_l^2} \quad (2.10)$$

The scaling factor α depends on the physical interpretation of the response and can be set to 1, $\iota\omega$, and $-\omega^2$ for displacements, velocities, and accelerations, respectively. [Lin et al. 2006] derived frequency response functions for proportional structural damping and general proportional damping.

The diagonal elements of the auto power spectral density of the responses $(\tilde{\mathbf{S}}_{\mathbf{xx}}(\omega))_{k,k} \forall k \in \mathbb{Z}$ and $k = 1, \dots, m_x$ are arranged in a vector $\tilde{\mathbf{S}}_{\mathbf{x}}(\omega) \in \mathbb{R}^{m_x}$. According to Equation (2.3), the vector of diagonal elements yields

$$\tilde{\mathbf{S}}_{\mathbf{x}}(\omega) = \frac{1}{T} \tilde{\mathcal{F}}_{\mathbf{x}}(\omega)^* \circ \tilde{\mathcal{F}}_{\mathbf{x}}(\omega). \quad (2.11)$$

The symbol \circ denotes the Schur product. Assuming random excitation, the respective mean value is given by

$$\begin{aligned} \mathbf{E} \left(\tilde{\mathbf{S}}_{\mathbf{x}}(\omega) \right) &= \frac{1}{T} \left(\mathbf{E} \left(\operatorname{Re} \left(\tilde{\mathcal{F}}_{\mathbf{x}}(\omega) \right) \right) \circ \mathbf{E} \left(\operatorname{Re} \left(\tilde{\mathcal{F}}_{\mathbf{x}}(\omega) \right) \right) \right. \\ &\quad + \mathbf{E} \left(\operatorname{Im} \left(\tilde{\mathcal{F}}_{\mathbf{x}}(\omega) \right) \right) \circ \mathbf{E} \left(\operatorname{Im} \left(\tilde{\mathcal{F}}_{\mathbf{x}}(\omega) \right) \right) \\ &\quad \left. + \mathbf{V} \left(\operatorname{Re} \left(\tilde{\mathcal{F}}_{\mathbf{x}}(\omega) \right) \right) + \mathbf{V} \left(\operatorname{Im} \left(\tilde{\mathcal{F}}_{\mathbf{x}}(\omega) \right) \right) \right). \end{aligned} \quad (2.12)$$

If the real and imaginary parts of the finite Fourier transform of excitation are independent in space and regarding each other, the mean value

$$\mathbf{E} \left(\tilde{\mathcal{F}}_{\mathbf{x}}(\omega) \right) = \mathbf{H}_{\mathbf{x}\mathbf{f}}(\omega) \mathbf{E} \left(\tilde{\mathcal{F}}_{\mathbf{f}}(\omega) \right) \quad (2.13)$$

and variance

$$\begin{aligned} \mathbf{V} \left(\operatorname{Re} \left(\tilde{\mathcal{F}}_{\mathbf{x}}(\omega) \right) \right) &= \\ &\quad \left(\operatorname{Re} \left(\mathbf{H}_{\mathbf{x}\mathbf{f}}(\omega) \right) \circ \operatorname{Re} \left(\mathbf{H}_{\mathbf{x}\mathbf{f}}(\omega) \right) \right) \mathbf{V} \left(\operatorname{Re} \left(\tilde{\mathcal{F}}_{\mathbf{f}}(\omega) \right) \right) + \\ &\quad \left(\operatorname{Im} \left(\mathbf{H}_{\mathbf{x}\mathbf{f}}(\omega) \right) \circ \operatorname{Im} \left(\mathbf{H}_{\mathbf{x}\mathbf{f}}(\omega) \right) \right) \mathbf{V} \left(\operatorname{Im} \left(\tilde{\mathcal{F}}_{\mathbf{f}}(\omega) \right) \right) \end{aligned} \quad (2.14)$$

$$\begin{aligned} \mathbf{V} \left(\text{Im} \left(\tilde{\mathcal{F}}_{\mathbf{x}}(\omega) \right) \right) = & \\ & \left(\text{Im} \left(\mathbf{H}_{\mathbf{x}\mathbf{f}}(\omega) \right) \circ \text{Im} \left(\mathbf{H}_{\mathbf{x}\mathbf{f}}(\omega) \right) \right) \mathbf{V} \left(\text{Re} \left(\tilde{\mathcal{F}}_{\mathbf{f}}(\omega) \right) \right) + \\ & \left(\text{Re} \left(\mathbf{H}_{\mathbf{x}\mathbf{f}}(\omega) \right) \circ \text{Re} \left(\mathbf{H}_{\mathbf{x}\mathbf{f}}(\omega) \right) \right) \mathbf{V} \left(\text{Im} \left(\tilde{\mathcal{F}}_{\mathbf{f}}(\omega) \right) \right) \end{aligned} \quad (2.15)$$

of $\tilde{\mathcal{F}}_{\mathbf{x}}(\omega)$ can be derived from Equation (2.8). $\text{Re}(\cdot)$ and $\text{Im}(\cdot)$ denote the real and imaginary part of a complex number, complex vector, or complex matrix.

Consequently, Equations (2.12)-(2.15) can be applied to predict the expected value of the response power spectral density, assuming that the statistics of the finite Fourier transform of excitation are known. The predicted power spectral densities are fundamental for the definition of the objective function that indicates the best reference sensor positions. The objective function is introduced in Section 2.3. Note that Equation (2.12) can be derived directly using an approximation of the power spectral density matrix of excitation $\tilde{\mathbf{S}}_{\mathbf{ff}}(\omega)$ in Equation (2.1). As only the diagonal elements of the spectral density matrix are of interest, the proposed approach is computationally more efficient.

2.2.2 Amendment for discrete signals

For reasons of completeness and consistency, the discrete Fourier transformation is discussed, as well. The discrete Fourier transformation is mainly applied to measured signals. Assuming a set of discrete signals $\{\mathbf{p}\}_n \in \mathbb{R}^{m_p}$, defined in equidistant time steps $\Delta t \forall n \in \mathbb{Z}$ and $n = 0, \dots, N-1$ with even $N \in \mathbb{Z}$, the discrete finite Fourier transformation (e.g., [Natke 1992])

$$\begin{aligned} \left\{ \tilde{\mathcal{F}}_{\mathbf{p}} \right\}_k &= \Delta t \sum_{n=0}^{N-1} \{\mathbf{p}\}_n \exp \left(-\iota \frac{2\pi}{N} kn \right) \\ &= \Delta t \sum_{n=0}^{N-1} \{\mathbf{p}\}_n \left(\cos \left(-\frac{2\pi}{N} kn \right) + \iota \sin \left(-\frac{2\pi}{N} kn \right) \right) \end{aligned} \quad (2.16)$$

can be derived. Then, the rectangular rule can be applied to the continuous formulation of the finite Fourier transformation analogously to Equation (2.5). $\left\{ \tilde{\mathcal{F}}_{\mathbf{p}} \right\}_k \in \mathbb{C}^{m_p}$ is subsequently defined for equidistant circular frequency steps $\Delta\omega = \frac{2\pi}{T} \forall k \in \mathbb{Z}$ and $k = 0, \dots, \frac{N}{2}$. The unit of the Fourier transform is the basis unit of the signal multiplied by the time unit.

Consequently, the discrete power spectral density is defined as

$$\left\{ \tilde{\mathbf{S}}_{\mathbf{p}} \right\}_k = \frac{1}{T} \left\{ \tilde{\mathcal{F}}_{\mathbf{p}} \right\}_k^* \circ \left\{ \tilde{\mathcal{F}}_{\mathbf{p}} \right\}_k. \quad (2.17)$$

Hence, the unit of spectral densities is the square of the basis unit of the signal multiplied by the time unit. For example, if the signal is a force time series with unit [N] and discrete time steps declared in seconds, the Fourier transform and the power spectral densities are given in units [Ns] and [N²s], respectively.

[Natke 1992] proposed an averaging algorithm to reduce the variance of the spectra obtained from a measured signal. By splitting a given signal of duration $T = n_t T_t$ into n_t statistically independent blocks with constant time length T_t , an averaging can be performed based on the finite discrete spectral densities of blocks $\left\{ \tilde{\mathbf{S}}_{\mathbf{P}}^{(i)} \right\}_{k_t}$. The averaged power spectral density yields

$$\left\{ \overset{\Delta}{\mathbf{S}}_{\mathbf{P}} \right\}_{k_t} = \frac{1}{n_t} \sum_{i=1}^{n_t} \left\{ \tilde{\mathbf{S}}_{\mathbf{P}}^{(i)} \right\}_{k_t} = \frac{1}{T} \sum_{i=1}^{n_t} \left\{ \tilde{\mathcal{F}}_{\mathbf{P}}^{(i)} \right\}_{k_t}^* \circ \left\{ \tilde{\mathcal{F}}_{\mathbf{P}}^{(i)} \right\}_{k_t}, \quad (2.18)$$

whereas the frequency resolution is reduced to $\Delta\omega_t = \frac{2\pi}{T_t}$. The averaged power spectral density corresponds to the sample mean value of the power spectral density. The Fourier transform of the i th block is indicated by $\left\{ \tilde{\mathcal{F}}_{\mathbf{P}}^{(i)} \right\}_{k_t}$.

2.2.3 Transformation to local coordinate systems

In some applications, it is very difficult to measure the response and the excitation in global coordinate directions. Therefore, it is appropriate to define several local coordinate systems for the excitations and the responses.

Based on Equation (2.8), the transformations

$$\tilde{\mathcal{F}}_{\mathbf{x},\mathbf{L}}(\omega) = \mathbf{T}_{\mathbf{x}} \tilde{\mathcal{F}}_{\mathbf{x},\mathbf{G}}(\omega) = \mathbf{T}_{\mathbf{x}} \mathbf{H}_{\mathbf{x}\mathbf{f},\mathbf{G}}(\omega) \tilde{\mathcal{F}}_{\mathbf{f},\mathbf{G}}(\omega) \quad (2.19)$$

and

$$\tilde{\mathcal{F}}_{\mathbf{f},\mathbf{L}}(\omega) = \mathbf{T}_{\mathbf{f}} \tilde{\mathcal{F}}_{\mathbf{f},\mathbf{G}}(\omega) \quad (2.20)$$

can be performed by using transformation matrices $\mathbf{T}_{\mathbf{x}} \in \mathbb{R}^{m_x \times m_x}$ and $\mathbf{T}_{\mathbf{f}} \in \mathbb{R}^{m_f \times m_f}$. The subscripts \mathbf{L} and \mathbf{G} indicate whether a matrix or a vector is defined in the local or global coordinate system. Assuming that the transformation matrices $\mathbf{T}_{\mathbf{x}}$ and $\mathbf{T}_{\mathbf{f}}$ are orthogonal matrices with the properties $\mathbf{T}_{\mathbf{x}}^T = \mathbf{T}_{\mathbf{x}}^{-1}$ and $\mathbf{T}_{\mathbf{f}}^T = \mathbf{T}_{\mathbf{f}}^{-1}$ and inserting Equation (2.9) into Equation (2.19),

$$\tilde{\mathcal{F}}_{\mathbf{x},\mathbf{L}}(\omega) = \alpha \Phi_{\mathbf{x},\mathbf{L}} \mathbf{D}(\omega) \Phi_{\mathbf{f},\mathbf{L}}^T \tilde{\mathcal{F}}_{\mathbf{f},\mathbf{L}}(\omega) \quad (2.21)$$

can be derived with

$$\begin{aligned} \Phi_{\mathbf{x},\mathbf{L}} &= \mathbf{T}_{\mathbf{x}} \Phi_{\mathbf{x},\mathbf{G}}, \\ \Phi_{\mathbf{f},\mathbf{L}} &= \mathbf{T}_{\mathbf{f}} \Phi_{\mathbf{f},\mathbf{G}}, \text{ and} \\ \tilde{\mathcal{F}}_{\mathbf{f},\mathbf{G}}(\omega) &= \mathbf{T}_{\mathbf{f}}^{-1} \tilde{\mathcal{F}}_{\mathbf{f},\mathbf{L}}(\omega). \end{aligned} \quad (2.22)$$

Consequently, the local spectral response

$$\tilde{\mathcal{F}}_{\mathbf{x},\mathbf{L}}(\omega) = \mathbf{H}_{\mathbf{x}\mathbf{f},\mathbf{L}}(\omega) \tilde{\mathcal{F}}_{\mathbf{f},\mathbf{L}}(\omega) \quad (2.23)$$

is defined by using the local frequency response function

$$\mathbf{H}_{\mathbf{x}\mathbf{f},\mathbf{L}}(\omega) = \alpha \Phi_{\mathbf{x},\mathbf{L}} \mathbf{D}(\omega) \Phi_{\mathbf{f},\mathbf{L}}^T \quad (2.24)$$

and the locally defined finite Fourier transform of excitation $\tilde{\mathcal{F}}_{\mathbf{f},\mathbf{L}}(\omega)$.

2.2.4 White noise excitation

One example of random excitation is the white noise excitation. Although the assumption of white noise excitation is of theoretical nature and does not represent a realistic excitation, it leads to reasonable results in many applications. For example, white noise is commonly used to represent ambient vibrations.

An approach to describe a white noise excitation as a discrete signal was given in [Bucher 2009]. In this study, the white noise is represented by independent and identically distributed (i.i.d.) random variables with a constant value for the time interval Δt . The random variables have a mean value of $\mathbf{E}(\{\mathbf{f}\}_{i,n}) = 0$ and a certain variance of $\mathbf{V}(\{\mathbf{f}\}_{i,n}) = \sigma^2 \forall n \in \mathbb{Z}$ and $n = 0, \dots, N-1$ with even $N \in \mathbb{Z}$. The variance itself can be related to the intensity of white noise S_0 in terms of spectral density, i.e.

$$\sigma^2 = \frac{S_0}{\Delta t}. \quad (2.25)$$

Based on Equation (2.16), it can be derived that the mean values of real and imaginary part of the Fourier transform vanish.

$$\mathbf{E}\left(\left\{\tilde{\mathcal{F}}_{\mathbf{f}}\right\}_k\right) = \Delta t \sum_{n=0}^{N-1} \mathbf{E}(\{\mathbf{f}\}_n) \left(\cos\left(-\frac{2\pi}{N}kn\right) + \iota \sin\left(-\frac{2\pi}{N}kn\right) \right) = 0 \quad (2.26)$$

The discrete circular frequency steps $k \in \mathbb{Z}$ with $k = 0, \dots, \frac{N}{2}$ are equidistantly spaced by $\Delta\omega = \frac{2\pi}{T}$. The variance of the real part of the Fourier transform related to white noise random excitation is expressed by

$$\begin{aligned} & \mathbf{V}\left(\operatorname{Re}\left(\left\{\tilde{\mathcal{F}}_{\mathbf{f}}\right\}_k\right)\right) \\ &= \Delta t^2 \sum_{n_1=0}^{N-1} \sum_{n_2=0}^{N-1} \sqrt{\mathbf{V}(\{\mathbf{f}\}_{n_1}) \circ \mathbf{V}(\{\mathbf{f}\}_{n_2})} \cos\left(-\frac{2\pi}{N}kn_1\right) \cos\left(-\frac{2\pi}{N}kn_2\right) \\ &= \Delta t^2 \sum_{n=0}^{N-1} \mathbf{V}(\{\mathbf{f}\}_n) \cos^2\left(-\frac{2\pi}{N}kn\right), \end{aligned} \quad (2.27)$$

which can be simplified to

$$\mathbf{V}\left(\operatorname{Re}\left(\left\{\tilde{\mathcal{F}}_{\mathbf{f}}\right\}_k\right)\right) = \begin{cases} N\Delta t^2\sigma^2 & : k = 0, \frac{N}{2} \\ \frac{1}{2}N\Delta t^2\sigma^2 & : k = 1, \dots, \frac{N}{2} - 1 \end{cases}. \quad (2.28)$$

Analogously, the variance of the imaginary part of the Fourier transform can be derived.

$$\mathbf{V}\left(\operatorname{Im}\left(\left\{\tilde{\mathcal{F}}_{\mathbf{f}}\right\}_k\right)\right) = \begin{cases} 0 & : k = 0, \frac{N}{2} \\ \frac{1}{2}N\Delta t^2\sigma^2 & : k = 1, \dots, \frac{N}{2} - 1 \end{cases} \quad (2.29)$$

The covariance between the real and imaginary part of the Fourier transform, related to a certain frequency step k , can be analytically derived

$$\mathbf{C}\left(\operatorname{Re}\left(\left\{\tilde{\mathcal{F}}_{\mathbf{f}}\right\}_k\right), \operatorname{Im}\left(\left\{\tilde{\mathcal{F}}_{\mathbf{f}}\right\}_k\right)\right) = \frac{\Delta t^2}{2} \sum_{n=0}^{N-1} \mathbf{E}\left(\{\mathbf{f}\}_n \{\mathbf{f}\}_n^T\right) \sin\left(-\frac{4\pi}{N}kn\right) = \mathbf{0}. \quad (2.30)$$

This is governed by the property $\sum_{n=0}^{N-1} \sin\left(-\frac{4\pi}{N}kn\right) = 0 \forall k, n \in \mathbb{Z}$. $\mathbf{0}$ indicates a matrix with Frobenius norm zero. Due to the assumed independent random process, the covariances between the real parts of a specific circular frequency step k with respect to space are zero. Equivalently, this is also valid for the imaginary parts.

2.2.5 Multiple impulse excitation

A more realistic random excitation is the multiple impulse excitation with respect to time and space, which can also be designed as a wide sense stationary process. According to [Natke 1992], a typical single impulse function $p^{(i)}(t)$, where the impulse with an impulse duration $T^{(i)}$ and a maximal amplitude of $p_0^{(i)}$ starts at time $t_0^{(i)}$, can be represented by

$$p^{(i)}(t) = \begin{cases} p_0^{(i)} \sin^2\left(\frac{\pi}{T^{(i)}}(t - t_0^{(i)})\right) & : t_0^{(i)} \leq t \leq t_0^{(i)} + T^{(i)} \\ 0 & : \text{elsewhere} \end{cases}. \quad (2.31)$$

Using the shift property of the Fourier transform and the formulation in [Natke 1992], its Fourier transform is given by

$$\mathcal{F}_p^{(i)}(\omega) = -\frac{p_0^{(i)}}{\omega} \left(\frac{1}{1 - \left(\frac{\omega T^{(i)}}{2\pi}\right)^2} \right) \sin \frac{\omega T^{(i)}}{2} \exp\left(-i\omega \left(\frac{T^{(i)}}{2} - t_0^{(i)}\right)\right). \quad (2.32)$$

Then, a multiple impulse can be formulated as superposition of single impulse functions $p^{(i)}(t)$ in time and frequency domain

$$p(t) = \sum_i p^{(i)}(t) \quad (2.33)$$

and

$$\mathcal{F}_p(\omega) = \sum_i \mathcal{F}_p^{(i)}(\omega), \quad (2.34)$$

respectively.

If the durations of the impulses $T^{(i)}$, the maximal amplitudes $p_0^{(i)}$, and the times of impulse occurrences $t_0^{(i)}$ are defined as random variables, a random multiple impulse process can be obtained. A closed form of Equation (2.34), based on random variables, is not available. Nevertheless, if the properties of the impulses are known, a simulation can be conducted to extract the first two statistical moments of Equation (2.34). Alternatively, several measurements of multiple impulse time histories and subsequent evaluation with the Fourier transform can help to derive the required second order statistics of the excitation Fourier transform. Both approaches will typically result in non-smooth discrete curves of the statistical moments depending on the frequencies. Simulations show that the mean value of the Fourier transform of a multiple impulse excitation converges to zero.

To identify the variances at each frequency of interest, surrogate models are used to smooth the variances. The discrete non-smooth approximations of the variances obtained from simulations or measurements will serve as training data.

One possibility to approximate the variances is offered by a surrogate model that is created by the product of a Gaussian function and a potential function based on parameters b_1 , b_2 , b_3 , b_4 , and b_5

$$\begin{aligned} \mathbf{V}(\operatorname{Re}(\mathcal{F}_p(\omega))) &= \mathbf{V}(\operatorname{Im}(\mathcal{F}_p(\omega))) \\ &= b_1 \omega^{b_5} \exp(b_2 \omega + b_3 \omega^2) + b_4. \end{aligned} \quad (2.35)$$

The free parameters b_i can be determined, for instance, by curve fitting using a gradient-based optimization strategy. Similar to white noise excitation, the covariances between real and imaginary part for a certain frequency step k vanish in case of a multiple impulse excitation. This has been proved by simulations.

Another possibility to approximate the variances is given by a surrogate model using a moving least squares approach. [Lancaster et al. 1986] defined a local moving least squares approximation by

$$\tilde{y}(\omega, \omega_j) = \sum_{i=1}^{n_b} h_i(\omega_j) a_i(\omega), \quad (2.36)$$

whereas n_b is the predefined number of basis functions h_i with corresponding coefficients a_i . The pairs ω_j and $y(\omega_j)$ are the n_s support points, which are used to determine the coefficients a_i with the weighted least squares postulate

$$M(\omega) = \sum_{j=1}^{n_s} w(\omega - \omega_j) (\tilde{y}(\omega, \omega_j) - y(\omega_j))^2 \rightarrow \min. \quad (2.37)$$

Assuming symmetry, the weighting $w(\omega - \omega_j) = w(\|\omega - \omega_j\|^{L_2})$ is defined by

$$w(\|\omega - \omega_j\|^{L_2}) = \begin{cases} \exp\left(-\left(\frac{\|\omega - \omega_j\|^{L_2}}{R(-\log 0.001)^{-\frac{1}{2}}}\right)^2\right) & : \|\omega - \omega_j\|^{L_2} \leq R \\ 0 & : \|\omega - \omega_j\|^{L_2} > R \end{cases} \quad (2.38)$$

with an influence radius R . More theoretical aspects about this approach and extensions were given in [Lancaster et al. 1986] and [Most et al. 2005]. In the present application, y corresponds to the variances of real and imaginary part of the Fourier transform and \tilde{y} to the respective approximations.

In general, the moving least squares approach is more flexible and can fit simulated or measured data more accurately. However, the analytical function can be used, if insufficient information is available about the multiple impulses. Both surrogate models will be tested by means of an example. This example relies on a simulation conducted with 100,000 multiple impulse time histories represented by the sum of single impulse time histories according to Equation (2.33). The single impulse time histories are generated

Table 2.1: Statistical properties of random input parameters used for simulation, whereas $p_0^{(i)} = p_0^{(i_s)} p_0^{(i_m)}$ and $t_0^{(i)} = \sum_{j=0}^i \Delta t_0^{(j)}$.

variable	type of distribution	mean value	variance
duration $T^{(i)}$	lognormal	0.003s	$9 \cdot 10^{-8} \text{s}^2$
sign of amplitude $p_0^{(i_s)}$	binary*	0	1
modulus of amplitude $p_0^{(i_m)}$	normal	100N	400N^2
time between impulses $\Delta t_0^{(j)}$	lognormal	1.5s	2.25s^2

* values are -1 or 1

by Monte Carlo samples with the statistical properties given in Table 2.1. For each time history, the simulation time is 10s with a discrete time step $\Delta t = \frac{1}{4096} \text{s}$. Figure 2.1 shows the comparison between mean values and variances determined by a statistical assessment of 100,000 time histories and the approximated function obtained by curve fitting according to Equations (2.35) and (2.36). The discrete values of the simulation are used as support points for the surrogate models. Using moving least squares with an exponential weighting and influence radius of 100, the variances can be approximated sufficiently well. The proposed analytical function with parameters $b_1 = 0.082982$, $b_2 = -10^{-13}$, $b_3 = -3.3145 \cdot 10^{-7}$, $b_4 = 5 \cdot 10^{-7}$, and $b_5 = 0.01$, obtained with a gradient-based optimization algorithm, is only suitable to approximate the variances related to lower

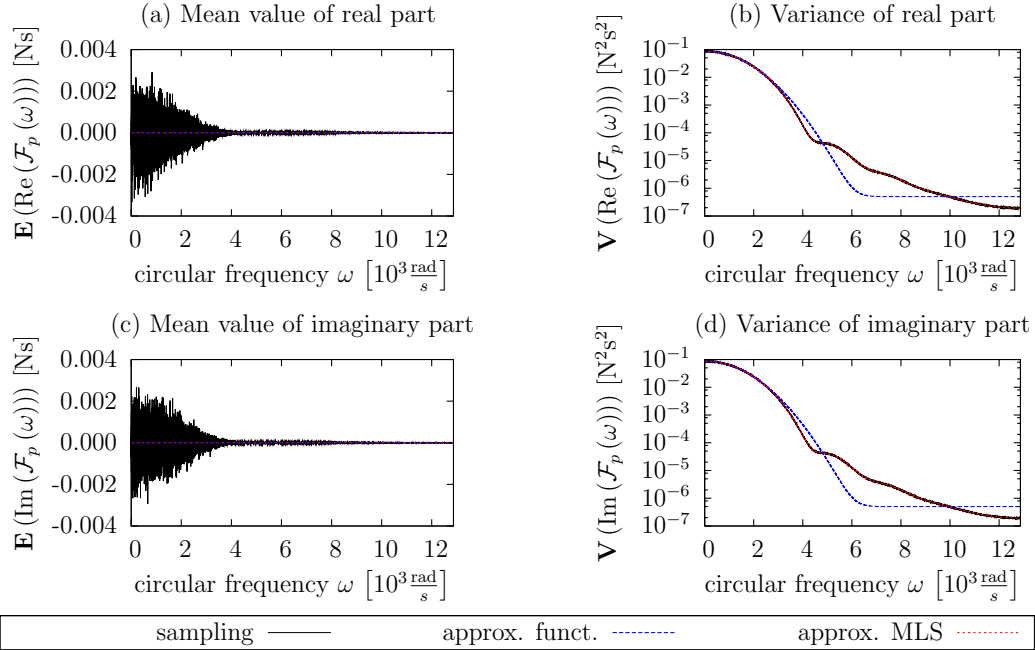


Figure 2.1: Statistical properties of the Fourier transform of a random multiple impulse excitation time history.

frequencies. The approximations of the mean values are set to a constant value of zero. In the later application of searching the best reference sensor positions, the lower frequencies are usually of interest. Therefore, both proposed surrogate models are suitable, whereas the moving least squares approach should be preferred due to higher accuracy and simple application. The analytical function can serve as alternative approximation beyond the moving least squares approach.

The presented approach shows that the statistical parameters of the Fourier transforms can be determined with low numerical effort, if the characteristics of the single impulse are approximately known.

2.3 Determination of optimal reference sensor positions

The described approach in Section 2.2 can be used to evaluate the spectral response at every degree of freedom of the structure depending on the frequency characteristics of the excitation signals, as long as wide sense stationarity is guaranteed.

To assess a set of predefined positions with respect to their suitability as reference sensor positions, the expected values related to the amplitudes of power spectral densities evaluated at the circular eigenfrequencies of the structural system are important. Knowing the statistical properties of the excitation, the expected spectral amplitudes can be easily extracted using Equation (2.12). All n circular eigenfrequencies of interest are assembled in a vector $\boldsymbol{\omega} \in \mathbb{C}^n$. The i th element of vector $\boldsymbol{\omega}$ is denoted by $(\boldsymbol{\omega})_i$. For proportional viscous damping, the circular eigenfrequencies are real numbers. The spectral amplitudes, corresponding to all preselected degrees of freedom m for a set of n modes to be investigated, are arranged column-wise in a matrix

$$\boldsymbol{\Upsilon} = \sum_{i=1}^n \mathbf{1}_i \otimes \sqrt{\mathbf{E} \left(\tilde{\mathbf{S}}_{\mathbf{x}}((\boldsymbol{\omega})_i) \right)} \quad (2.39)$$

with $\boldsymbol{\Upsilon} \in \mathbb{R}^{m \times n}$. Matrix $\mathbf{1}_i = \begin{bmatrix} \mathbf{0}^{1 \times (i-1)} & 1 & \mathbf{0}^{1 \times (n-i)} \end{bmatrix}$ represents a matrix, whereas all entries are zero except for the i th position, which is one. Therefore, $\mathbf{E} \left(\tilde{\mathbf{S}}_{\mathbf{x}}((\boldsymbol{\omega})_i) \right)$ is the expected value of the diagonal of the power spectral density matrix at circular eigenfrequency $(\boldsymbol{\omega})_i$ according to Equation (2.12). To obtain a suitable objective function, the values $\boldsymbol{\Upsilon}$ are normalized by the maximal value of $\boldsymbol{\Upsilon}$.

$$\bar{\boldsymbol{\Upsilon}} = \frac{1}{\max_{j,i} (\boldsymbol{\Upsilon})_{j,i}} \boldsymbol{\Upsilon} \quad (2.40)$$

Once the matrix of normalized spectral amplitudes $\bar{\boldsymbol{\Upsilon}}$ is arranged, the best location j to represent the i th mode is given at the position of the largest value of $\{\bar{\boldsymbol{\Upsilon}}\}_i$. Hence,

the objective function

$$J(j) = 1 - (\bar{\mathbf{Y}})_{j,i} \quad J(j) \rightarrow \min \quad (2.41)$$

has to be minimized.

If n modes should be covered by one reference sensor, the problem can be solved by minimizing

$$J(j) = 1 - (\boldsymbol{\alpha})_j \quad J(j) \rightarrow \min \quad \text{with} \quad (\boldsymbol{\alpha})_j = \min_i (\bar{\mathbf{Y}})_{j,i}. \quad (2.42)$$

Assuming that m measurement positions are possible, the maximal number of evaluations for Equation (2.42) is m .

To find the best set of l sensors to cover n modes of interest is a more general task. The total number of different combinations of sensor positions without repetition will be $\binom{m}{l}$. These combinations are arranged in a binary combinadic matrix $\mathbf{C} \in \mathbb{Z}^{\binom{m}{l} \times m}$ (e.g., [Worden et al. 2001]), also denoted by sensor distribution matrix, consisting of all l -combinations of the set $\{1, 2, \dots, m\}$, whereas zero and one in a certain row j and column k indicate the belonging of sensor position k to the l -combination set j . Then, the problem can be formulated as

$$J(j) = 1 - (\mathbf{A})_j \quad J(j) \rightarrow \min; \quad j = 1, 2, \dots, \binom{m}{l} \quad (2.43)$$

assuming $(\mathbf{A})_j$ is defined as

$$(\mathbf{A})_j = \min_i (\mathbf{B})_{j,i} \quad \mathbf{A} \in \mathbb{R}^{\binom{m}{l}} \quad (2.44)$$

with

$$(\mathbf{B})_{j,i} = \max_k (\mathbf{F}_k)_{j,i} \quad \mathbf{B} \in \mathbb{R}^{\binom{m}{l} \times n}, \quad (2.45)$$

whereas $i = 1, 2, \dots, n$ and $k = 1, 2, \dots, m$ and moreover

$$\mathbf{F}_k = (\mathbf{C} \mathbf{G}_k^T) \otimes (\mathbf{G}_k \bar{\mathbf{Y}}) \quad \mathbf{F}_k \in \mathbb{R}^{\binom{m}{l} \times n} \quad \forall k = 1, 2, \dots, m. \quad (2.46)$$

The one row matrix \mathbf{G}_k is defined by $\mathbf{G}_k = \begin{bmatrix} \mathbf{0}^{1 \times k-1} & 1 & \mathbf{0}^{1 \times m-k} \end{bmatrix}$. Consequently, matrix \mathbf{F}_k represents the normalized spectral amplitude at position k of all sets j and all modes i . The matrix \mathbf{B} contains the maximal normalized spectral amplitudes of each set j for all modes n . The vector \mathbf{A} determines the normalized spectral amplitude of the mode that is least represented in set j . If a certain j has been identified by applying Equation (2.43), the sensor positions are represented by the j th row of the binary combinadic matrix \mathbf{C} .

It is assumed that all combinations of reference sensor sets can be evaluated and assessed by the proposed criterion to find the best set. However, the computational effort increases fast with an increasing number of reference sensors. Although, the operations are mainly based on comparisons, the computational effort is not neglectable. Hence, the algorithm has to be implemented as efficiently as possible. Furthermore, the algorithm is

suitable for sequential parallel computing that will additionally reduce the computation time. Other strategies to reduce the computational expense are discussed in the Section 2.5.

As minimum and maximum functions are applied, it is likely that many possible sensor configurations are equally assessed. Consequently, a secondary criterion needs to be added to the objective. Such a criterion is, for instance, the norm of normalized spectral amplitudes derived for a certain set of positions. A larger norm indicates a higher redundancy. The Euclidean norm based on the matrices \mathbf{F}_k is appropriate

$$(\mathbf{N})_{j,i} = \sqrt{\frac{1}{l} \sum_{k=1}^m (\mathbf{F}_k)_{j,i}^2}. \quad (2.47)$$

Hence, a modified weighted objective function

$$J(j) = w_1 (1 - (\mathbf{A})_j) + w_2 \left(1 - \min_i (\mathbf{N})_{j,i}\right) \quad J(j) \rightarrow \min, \quad (2.48)$$

can be derived. The values of scaling factors w_1 and w_2 can be specified depending on the application. The weighting factor w_1 forces that the least represented mode is covered with a normalized spectral amplitude of $(\mathbf{A})_j$ at least at one position. The normalized spectral amplitudes of other positions are not recognized. Therefore, the best signal to noise ratio can be obtained with a high value of w_1 with respect to w_2 . In contrast, the weighting factor w_2 is related to the norm of normalized spectral amplitudes of all sensor positions in a certain configuration for the least represented mode. Therefore, w_2 accentuates the redundancy of a certain sensor setup configuration. As the norm itself does not guarantee that all modes of interest are covered appropriately, w_1 should be larger than w_2 . A recommended combination of weighting factors, derived from experience, is $w_1 = 0.9$ and $w_2 = 0.1$. Due to the scaling of the normalized spectral amplitudes according to Equation (2.40), both objectives, $(1 - (\mathbf{A})_j)$ and $(1 - \min_i (\mathbf{N})_{j,i})$, range between 0 and 1. Of course, if the number of reference sensors is one, it follows $\mathbf{B} = \mathbf{N}$.

For a sufficiently large finite number of sensors and $w_1 + w_2 = 1$, the minimal expected objective value

$$\tilde{J} = 1 - \min_i \left(\max_k (\tilde{\mathbf{Y}})_{i,k} \right) \quad (2.49)$$

is determined by the minimal maximum values of the normalized spectral amplitudes corresponding to each mode of interest. However, this optimal objective value is based on the assumption that the determining mode i has l equal maximal values and that all modes are covered better than mode i for the corresponding sensor position set. Even if this approximation of the minimal expected objective value is unlikely to be achieved, it can serve as a criterion for the assessment whether the application of more reference sensors has the potential to improve the objective significantly.

2.4 Possible simplifications for ambient excitation

In case of ambient excitation, the computational effort to calculate spectral response amplitudes increases with increasing degrees of freedom of the structure. Under certain conditions, the spectral response amplitudes can be approximated by the eigenvectors of the system.

If the ambient excitation can be represented by white noise, the mean value of the finite Fourier transform is zero and the variances of real and imaginary part are identical for all circular frequencies:

$$\mathbf{V} \left(\operatorname{Re} \left(\tilde{\mathcal{F}}_{\mathbf{f}}(\omega) \right) \right) = \mathbf{V} \left(\operatorname{Im} \left(\tilde{\mathcal{F}}_{\mathbf{f}}(\omega) \right) \right) = \mathbf{V}_{\mathbf{f}}. \quad (2.50)$$

Furthermore, the mode shape matrices of response and excitation are identical with the eigenvector matrix, if the response positions are not restricted:

$$\Phi_{\mathbf{x}} = \Phi_{\mathbf{f}} = \Phi. \quad (2.51)$$

Therefore, the frequency response function

$$\mathbf{H}_{\mathbf{x}\mathbf{f}}((\omega)_i) = \alpha \Phi_{\mathbf{x}} \mathbf{D}((\omega)_i) \Phi_{\mathbf{f}}^{\mathbf{T}} \quad (2.52)$$

is given for a circular eigenfrequency $(\omega)_i$, if proportional viscous damping is assumed.

Consequently, Equation (2.12) can be simplified

$$\mathbf{E} \left(\tilde{\mathbf{S}}_{\mathbf{x}}((\omega)_i) \right) = \frac{2}{T} (\mathbf{H}_{\mathbf{x}\mathbf{f}}((\omega)_i) \circ \mathbf{H}_{\mathbf{x}\mathbf{f}}((\omega)_i)^*) \mathbf{V}_{\mathbf{f}}. \quad (2.53)$$

For n modes and k degrees of freedom, the row sum of the squared frequency response matrix yields

$$\begin{aligned} \sum_{k=1}^m (\mathbf{H}_{\mathbf{x}\mathbf{f}}((\omega)_i))_{j,k} (\mathbf{H}_{\mathbf{x}\mathbf{f}}((\omega)_i))_{j,k}^* \approx \\ \sum_{k=1}^m \sum_{l=1}^n (\Phi)_{j,l} (\Phi)_{j,l} \alpha \alpha^* (\mathbf{D}((\omega)_i))_{l,l} (\mathbf{D}((\omega)_i))_{l,l}^* (\Phi)_{k,l} (\Phi)_{k,l} \end{aligned} \quad (2.54)$$

assuming $(\mathbf{D}((\omega)_i))_{l_1,l_1} (\mathbf{D}((\omega)_i))_{l_2,l_2} \approx 0 \quad \forall l_1 \neq l_2$. If a constant value $(\mathbf{V}_{\mathbf{f}})_k = V_0 \quad \forall k = 1, \dots, m$ can be expected, Equation (2.53) derives

$$\begin{aligned} \mathbf{E} \left(\tilde{\mathbf{S}}_{\mathbf{x}}((\omega)_i) \right) \approx \\ \frac{2V_0}{T} \sum_{l=1}^n \left(\left(\alpha \alpha^* (\mathbf{D}((\omega)_i))_{l,l} (\mathbf{D}((\omega)_i))_{l,l}^* \{ \Phi \}_l^{\mathbf{T}} \{ \Phi \}_l \right) \left(\{ \Phi \}_l \circ \{ \Phi \}_l \right) \right). \end{aligned} \quad (2.55)$$

Introducing a factor

$$(\gamma((\omega)_i))^2 = \alpha \alpha^* (\mathbf{D}((\omega)_i))_{i,i} (\mathbf{D}((\omega)_i))_{i,i}^* \{ \Phi \}_i^{\mathbf{T}} \{ \Phi \}_i \quad (2.56)$$

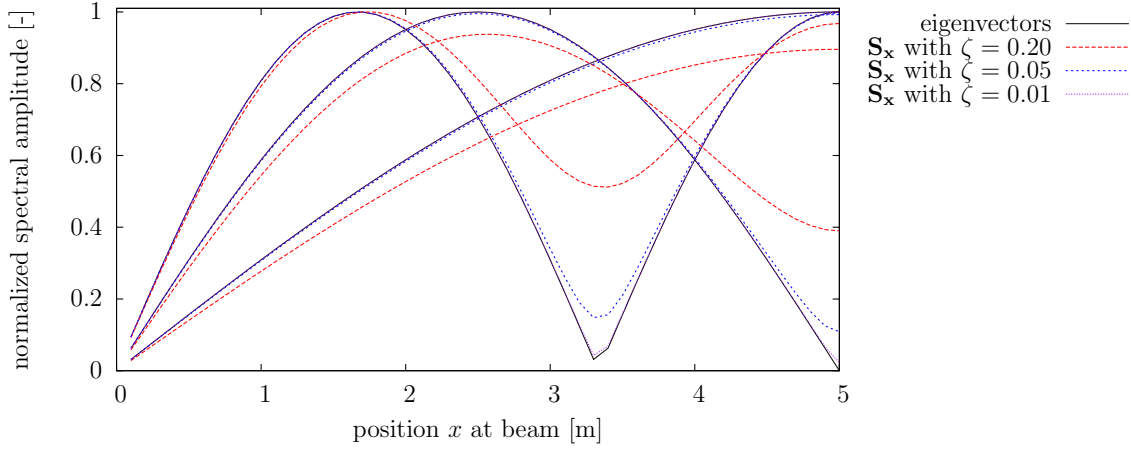


Figure 2.2: Comparison of predicted spectral amplitudes using eigenvectors and power spectral amplitudes. The spectral response based on the first three bending modes of a simply supported beam are shown separately. The modal damping varies by 1%, 5%, and 20%.

and applying Equation (2.10), Equation (2.55) can be reformulated

$$\mathbf{E} \left(\tilde{\mathbf{S}}_{\mathbf{x}}((\omega)_i) \right) \approx \frac{2V_0}{T} (\gamma((\omega)_i))^2 \sum_{l=1}^n \left(\left(\frac{4(\zeta)_l^2 (\omega)_i^4}{((\lambda)_l - (\omega)_i)^2 + 4(\zeta)_l^2 (\lambda)_l (\omega)_i^2} \frac{\{\Phi\}_l^T \{\Phi\}_l}{\{\Phi\}_i^T \{\Phi\}_i} \right) \left(\{\Phi\}_l \circ \{\Phi\}_l \right) \right) \quad (2.57)$$

with $(\zeta)_l \neq 0 \forall l = 1, 2, \dots, n$. If the modal damping ratios $(\zeta)_l$ are small, but not zero, and the circular eigenfrequencies $(\omega)_l$ are well separated, the expected value of the power spectral density can be approximated by

$$\mathbf{E} \left(\tilde{\mathbf{S}}_{\mathbf{x}}((\omega)_i) \right) \approx \frac{2V_0}{T} (\gamma((\omega)_i))^2 \{\Phi\}_i \circ \{\Phi\}_i. \quad (2.58)$$

On the premise that the factors $(\gamma((\omega)_i))^2 = \gamma_0^2$ are constant for all modes i , the spectral response amplitude matrix according to Equation (2.39) can be reduced to

$$\mathbf{\Upsilon} = \gamma_0 \hat{\Phi} \quad \text{with} \quad (\hat{\Phi})_{i,j} = \|(\Phi)_{i,j}\|^{L^2}. \quad (2.59)$$

As the normalized matrix $\tilde{\mathbf{\Upsilon}}$ according to Equation (2.40) is the basis of the algorithm, $\mathbf{\Upsilon} = \hat{\Phi}$ can be applied directly.

One example, which fulfils all requirements, is a simply supported beam with a sufficient stiffness to mass ratio, where only the bending modes in one direction are considered and accelerations are supposed to be measured. The excitation is assumed to be a perfect white noise. Furthermore, the modal damping ratios are small and constant for all modes i . For an equidistantly discretized, homogeneous beam, the norms of the eigenvectors $\{\Phi\}_i^T \{\Phi\}_i$ are constant for all modes i . Due to measured accelerations, the value α is

equal to $-(\omega)_i^2$. The variances of the Fourier transform of the white noise excitation are constant as well. All these requirements lead to a constant value γ_0^2 for all modes i . Therefore, the simplification to use directly the mass normalized eigenvectors as basis for the determination of optimal reference sensor positions is appropriate.

To visualize the effect of insufficient small modal damping ratios, the simply supported beam described in Section 2.6 is investigated with different modal damping values that are constant for the first three modes. Figure 2.2 shows a comparison of the normalized spectral amplitudes based on Equation (2.39) with the approximation of normalized spectral amplitudes using the mass normalized eigenvectors according to Equation (2.59). The discrepancies between the correct curves and the approximation with eigenvectors decrease with decreasing modal damping ratios. In this case, a modal damping ratio below 5% may be acceptable.

However, other examples can be found where the simplification is reasonable. In general, the simplification needs to be approved for each structure. If Equation (2.58) is approximately fulfilled together with their specific conditions, the simplification can be applied.

In the context of optimal experimental design of one-setup configurations, Bayard [Bayard et al. 1988] also states that the sensors can be placed optimally by using only mode shape information, if lightly damped systems are considered. This demonstrates that the simplification is widely used also for other applications. Nevertheless, the conditions for the simplification have to be fulfilled.

2.5 Search strategy

In Section 2.3, it was assumed that all possible sets of sensor positions can be evaluated to extract the best set. As already discussed, the drawback of this search strategy is the computational expense. Many authors (e.g., [Liu et al. 2008], [Papadimitriou 2004], [Papadimitriou 2005], [Stabb et al. 1995]) solved similar problems using optimization methods. They tried to find the optimal set of sensor positions with respect to model updating or structural health monitoring, that includes not only the identification of frequencies, but also the separation of mode shapes. Hence, it is obvious that at least as many sensors are needed as modes should be identified. For the intended application in this chapter, the identification of mode shapes is not of primary interest and the number of reference sensors is typically smaller than the number of modes of interest.

Even if the objective functions are different, the optimization search strategy has to deal with the same demands. [Liu et al. 2008] proposed to use the ordering of the identification number of the degrees of freedom as design variables, which is an appropriate strategy for simple structures with one measurement direction. Of course, as the numbering of degrees of freedom or the node numbering itself is not necessarily coherent with the

geometrical information of the nodes, many isolated local minima can be present. Many researchers (e.g., [Liu et al. 2008], [Stabb et al. 1995]) applied genetic algorithms or evolutionary algorithms as optimization method with a high number of generations and a large population size to deal with resulting weak convergence rates. Therefore, the approaches are not applicable for complex structures with different measurement directions and a high number of possible combinations of sensor positions.

For a satisfying convergence of the optimization algorithms, the objective function needs to be as smooth as possible with a minimal number of local minima. In contrast to available approaches in literature, the innovative contribution of this chapter is the definition of design variables based on geometrical information of possible sensor positions instead of using directly degree of freedom numbers or any other numbering. Consequently, the design variables are parameters of the sensor positions representing the spatial location. For example, the longitudinal distance to a reference point (e.g., one support) can be an appropriate design parameter, in case of a beam structure for one measurement direction. If different measurement directions are necessary or in case of more complicated structures, the set of possible sensor positions has to be divided into subsets with simple geometries and one measurement direction. For example, if vertical and lateral modes of a beam are of interest, the two measurement directions need to be separated into two subsets.

In the next step, several smaller optimization problems will be created. The optimization problem itself depends mainly on the number of design variables, which should represent the location of possible sensor positions. If the possible reference sensor positions need to be divided into t subsets, whereas a near-optimal set of l reference sensors is required, a number of $\binom{t+l-1}{l}$ optimization subproblems have to be solved. The minimum of all suboptima $J(j_s)$ is the final global optimum

$$J(j) = \min_s J(j_s) \quad \forall s = 1, 2, \dots, \binom{t+l-1}{l}. \quad (2.60)$$

An advantage of this approach is that the suboptimization problems are well defined and the respective objective functions are relatively smooth. Hence, a fast convergence can be expected. This approach reduces the total computational effort and increases the probability to determine the global optimum of the problem. An example with a benchmark comparing several search strategies is presented in Section 2.7.

To summarize the proposed algorithm, a workflow is presented in Figure 2.3. Therein, three phases are distinguished: (1) Preparation of numerical model and excitation, (2) Determination of normalized spectral response amplitudes, and (3) Optimization. The three phases have to be applied in succession.

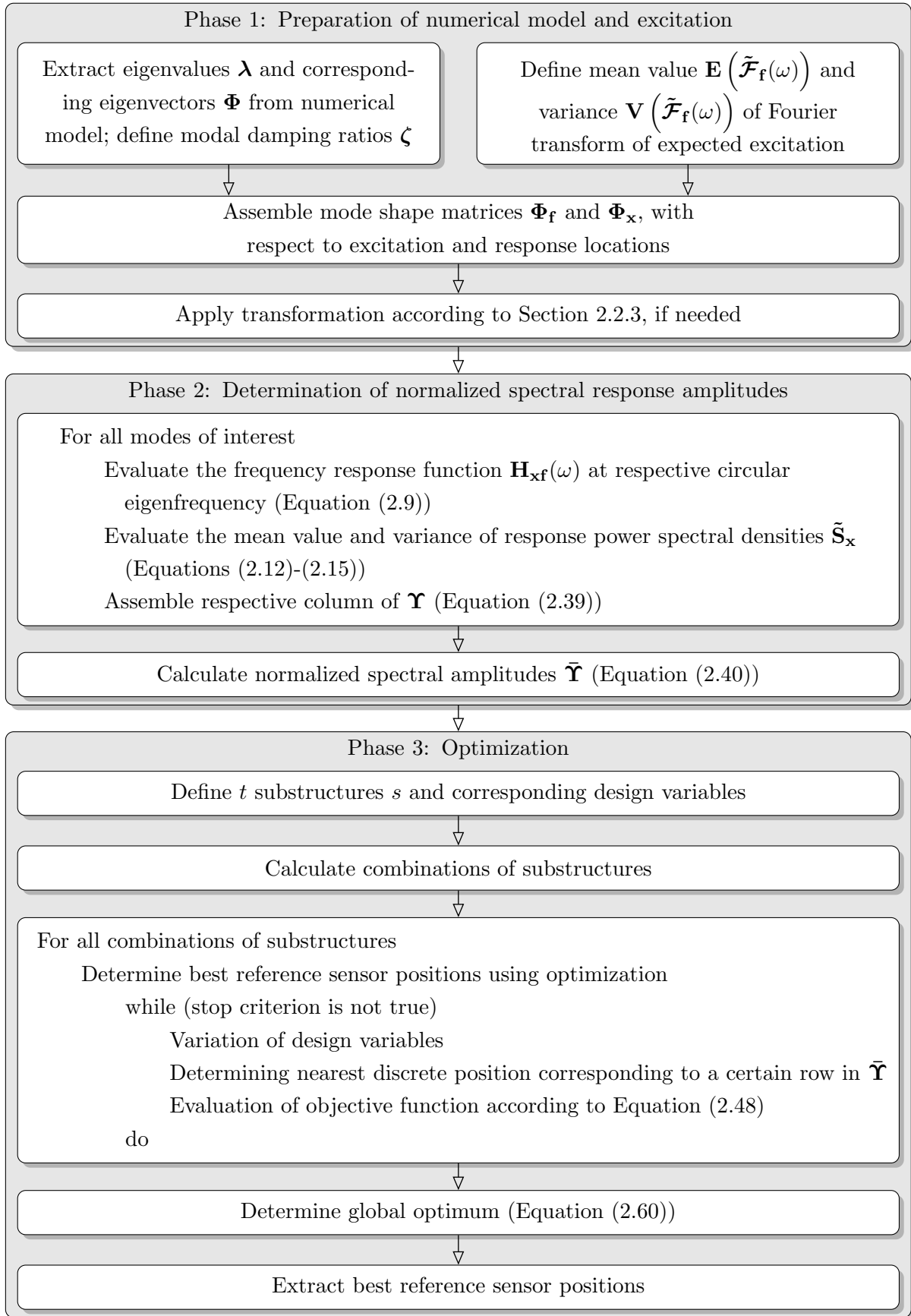


Figure 2.3: Workflow for optimal reference sensor placement.

2.6 Benchmark study: Simply supported beam

2.6.1 System description

The described approach of Section 2.3 will be investigated within a benchmark study of a simply supported beam. The beam is 10m long and has a rectangular cross-section as described in Figure 2.4. It is supposed to be made of concrete. Hence, the Young's modulus is assumed to be $3 \cdot 10^{10} \frac{\text{N}}{\text{m}^2}$, the Poisson ratio is given as 0.2, and the mass density is set to $2500 \frac{\text{kg}}{\text{m}^3}$. The beam is modeled using finite elements. The 1000 twelve degree of freedom beam elements are equidistantly distributed along the structure. All modal damping ratios are set to 3%. Then, the complex frequency response function can be calculated by Equation (2.9) for each natural frequency of the system assuming measured accelerations.

Only the first n vertical bending modes are of interest, whereas each mode is equally important. The 500 possible sensor positions are distributed at the left half of the beam between $x = 0.01\text{m}$ and $x = 5.00\text{m}$. Possible positions of the reference sensors are identical to the positions of the finite element nodes. In the following, the best reference sensor positions for an ambient excitation and a random multiple impulse excitation will be determined while the number of reference sensors and the number of modes of interest will be varied. As only vertical bending modes are of interest, the reference sensors are assumed to measure always in vertical direction.

2.6.2 Ambient excitation

The ambient excitation, which is applied for all frequencies to each translational degree of freedom in vertical and longitudinal direction, is realized by applying white noise with a zero mean and a constant variance of the real and imaginary part of the Fourier spectrum, according to the investigations in Subsection 2.2.4. The rotational degrees of freedom are assumed to be not excited. The normalized spectral amplitudes are calculated by using Equations (2.39) and (2.40). The columns of the matrix of normalized spectral amplitudes represent the modes of interest. Figure 2.5 shows the normalized spectral amplitudes up to the 8th vertical mode of the system. It can be observed that the shape of the spectral

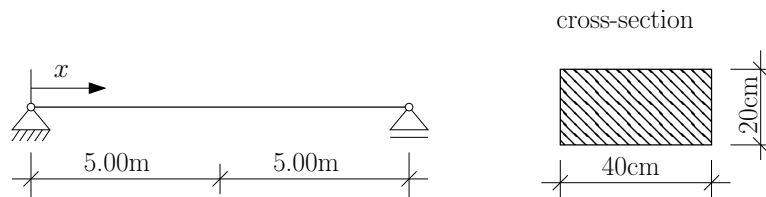


Figure 2.4: Simply supported beam with rectangular cross-section.

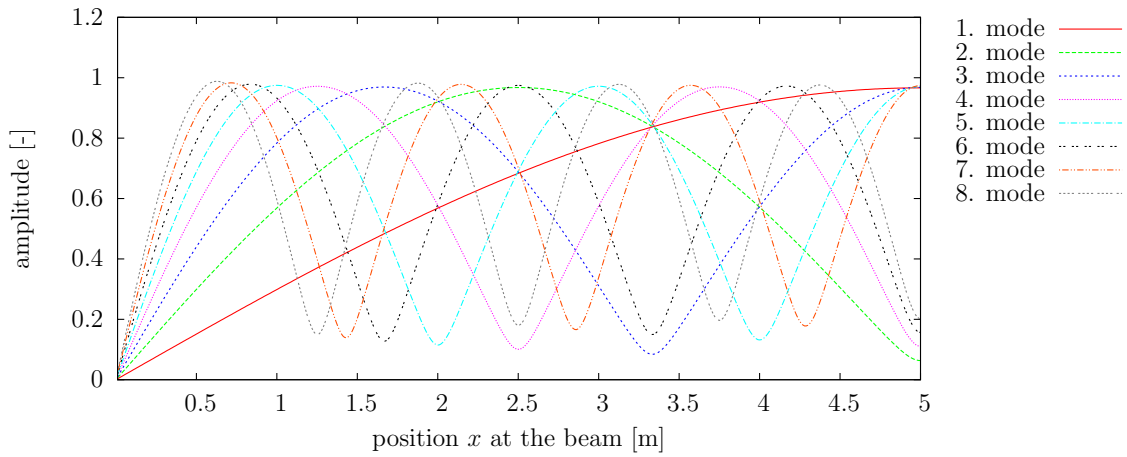


Figure 2.5: Normalized spectral amplitudes of the simply supported beam in case of ambient excitation. (only left half span is considered due to symmetry)

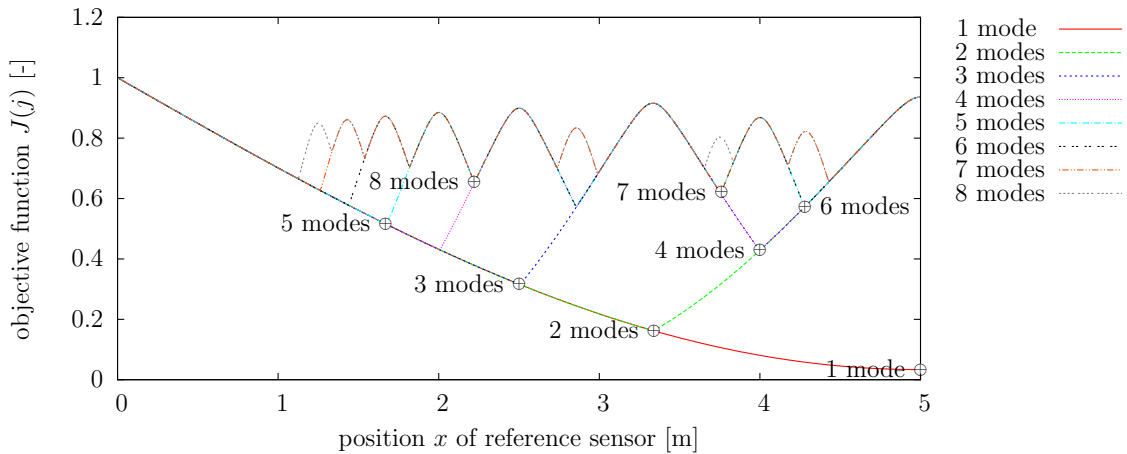


Figure 2.6: Objective functions assuming one reference sensor detecting a certain number of vertical modes of a simply supported beam. \oplus indicates the optimal position with respect to the number of modes of interest.

amplitudes is similar to the mode shapes with respect to the observed degrees of freedom. Section 2.4 discussed this phenomenon in detail.

Based on the normalized spectral amplitudes, the objective function according to Equation (2.48) can be evaluated for all combinations of reference sensor positions. The optimal reference sensor positions are found at the minimum of the objective function. Of course, the best configuration depends on the number of reference sensors, the number of modes of interest, and the weightings w_1 and w_2 . The dependency on the number of modes of interest in case of one reference sensor is visualized in Figure 2.6. In total, 500 positions are available in the present study. Obviously, if only the first vertical mode

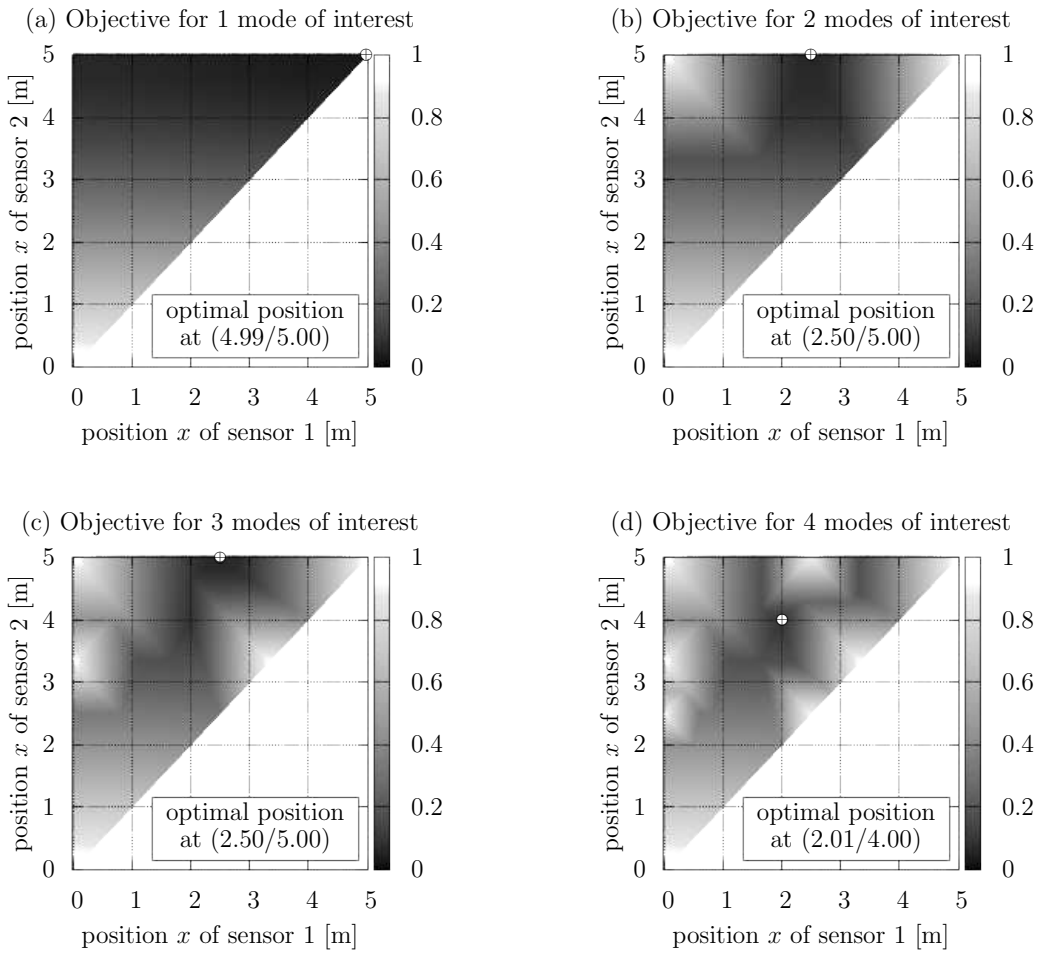


Figure 2.7: Objective function using two reference sensors to detect a certain number of vertical modes of a simply supported beam assuming ambient excitation. \oplus indicates the optimal position.

is of interest, the best reference position will be in the midspan of the simply supported beam at position 5m. The first three vertical modes are best represented using a reference sensor at position 2.5m. This is the crossing point of the normalized spectral amplitudes of modes one and three and the maximal normalized spectral amplitude of mode two. Derived from practical applications, [Wenzel et al. 2005, p. 33] recommended a position of 40% of the maximal span width to capture the modal information of the first few modes. Actually, the proposed approach shows that this position represents an optimal position, if the first four vertical modes need to be investigated. Furthermore, it is a suboptimal position in case the first three vertical modes are of interest.

With an increasing number of modes to be investigated, the minimal achievable objective function values increase. Depending on the normalized spectral noise level, it is possible that the spectral amplitudes of a certain mode are below the noise level. Conse-

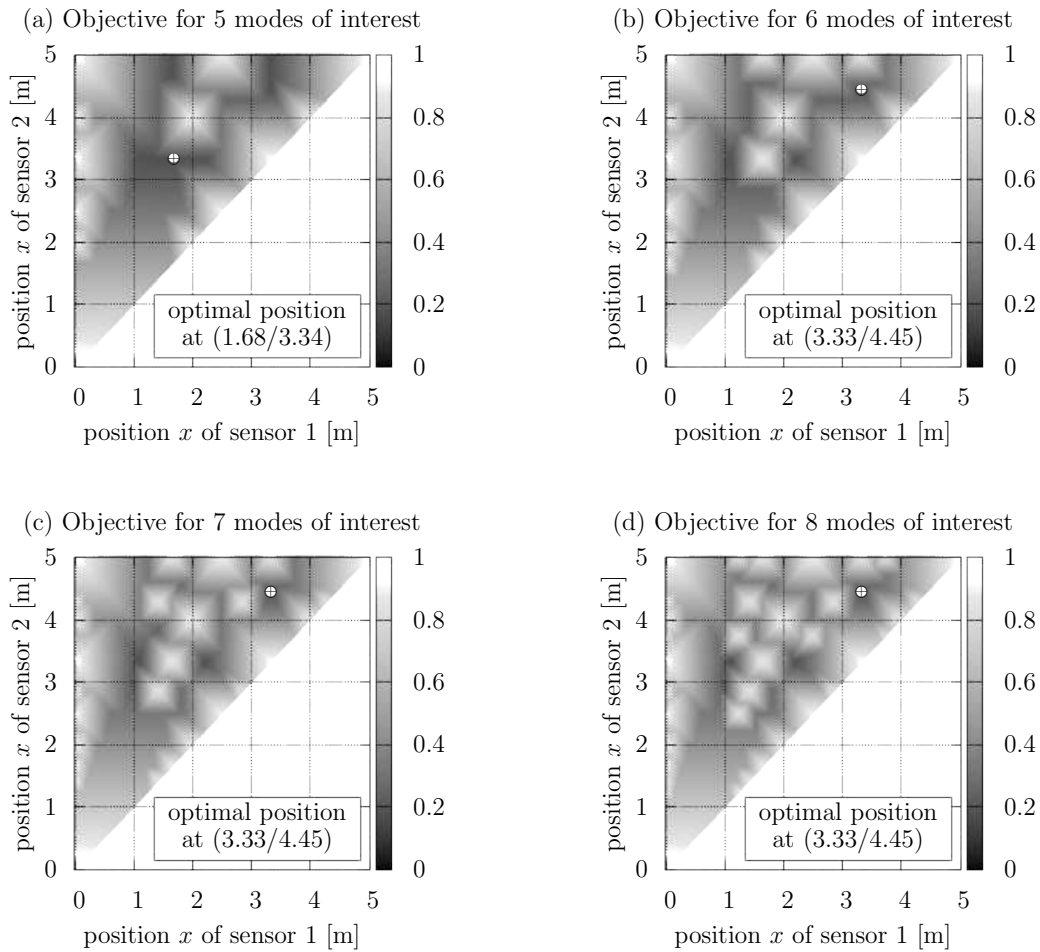


Figure 2.8: Objective function using two reference sensors to detect a certain number of vertical modes of a simply supported beam assuming ambient excitation. \oplus indicates the optimal position.

quently, additional reference sensors have to be used to capture a large number of modes. As a next step, the number of available reference sensors is extended to two. That is related to 124,750 possible combinations of reference sensor sets. The objective functions are evaluated for an increasing number of modes of interest up to eight modes. The weighting factors are chosen to be $w_1 = 0.9$ and $w_2 = 0.1$. Figures 2.7 and 2.8 show the results. As expected, the best positions to detect up to three modes are at the maximum points of the respective normalized spectral amplitudes according to Figure 2.5. For six, seven, or eight modes to be detected, the optimal positions do not change significantly, which cannot be generalized for an increasing number of modes. When using two reference sensors instead of one reference sensor, while eight modes are of interest, the minimal objective value can be significantly reduced from 0.65 to 0.19.

To investigate a further improvement of the objective function and thus, an improve-

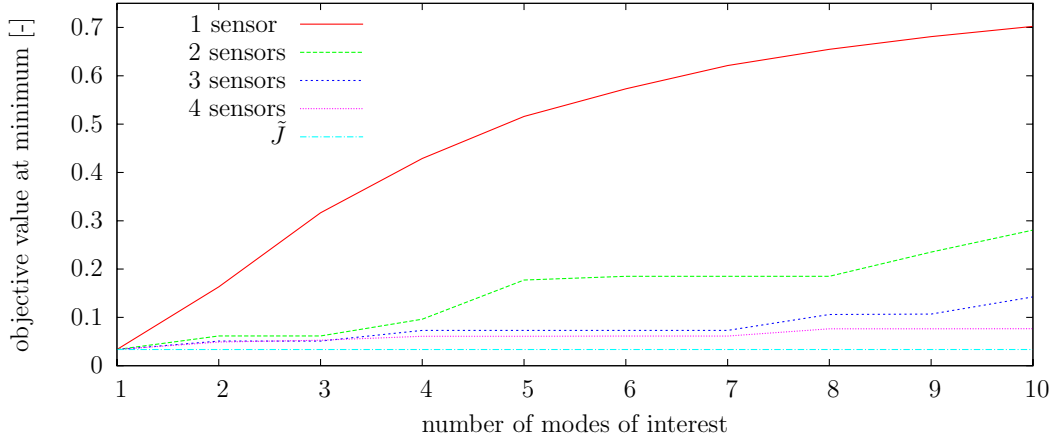


Figure 2.9: Objective function value at the optimum for different numbers of available reference sensors and modes to be detected assuming white noise excitation.

Table 2.2: Objective function value and respective optimal positions assuming ambient excitation. The positions are related to the distance of the sensor to the left support.

# of modes	1 sensor		2 sensors		3 sensors		4 sensors (PSO)					
	objective value	position [m]	objective value	positions [m]	objective value	positions [m]	objective value	positions [m]				
1	0.033516	5.00	0.033516	4.99 5.00	0.033517	4.98 4.99 5.00	0.065894	4.97 4.98 4.99 5.00				
2	0.163304	3.34	0.061603	2.50 5.00	0.051084	2.51 2.52 5.00	0.048941	2.57 2.98 3.00 5.00				
3	0.316581	2.50	0.061603	2.50 5.00	0.051084	2.51 2.52 5.00	0.052859	1.88 2.43 3.43 5.00				
4	0.428804	4.00	0.096235	2.01 4.00	0.073138	1.25 2.58 4.94	0.061034	1.28 2.43 3.72 5.00				
5	0.515869	1.67	0.177338	1.68 3.34	0.073138	1.25 2.58 4.94	0.061034	1.28 2.43 3.72 5.00				
6	0.573101	4.28	0.185096	3.33 4.45	0.073200	1.25 2.57 5.00	0.061320	1.23 2.50 3.70 5.00				
7	0.621318	3.76	0.185096	3.33 4.45	0.073200	1.25 2.57 5.00	0.061320	1.23 2.50 3.70 5.00				
8	0.654878	2.22	0.185096	3.33 4.45	0.105985	1.02 2.00 4.41	0.076504	0.64 1.17 2.57 4.94				
9	0.681027	2.99	0.235301	1.01 3.01	0.106869	2.99 4.00 4.85	0.076504	0.64 1.17 2.57 4.94				
10	0.702232	2.74	0.280632	1.82 4.55	0.142414	0.91 1.83 4.36	0.076639	0.64 1.17 2.44 4.94				

ment of the signal to noise ratio, a variation is performed with respect to the number of reference sensors and the number of modes of interest. The results are visualized in Figure 2.9. It can be observed that with increasing numbers of reference sensors, the optimal objective function value decreases. However, for a certain number of sensors, the objective function improvement may be not significant enough to justify the application of more reference sensors. Moreover, the numerical effort increases with a higher number of available reference sensors. For example, 20,708,500 evaluations of the objective function are needed for three reference sensors and 2,573,031,125 evaluations of the objective function are possible for four reference sensors. To determine the best set of four reference sensor positions, an evaluation of all combinations is not efficient. Hence, an optimization procedure using a particle swarm optimization (PSO) (e.g., [Kennedy et al. 1995]) with passive congregation ([He et al. 2004]) and fly-back mechanism according to [Li et al. 2007b] is applied. The design variables, which are related to the discrete nodal information of the structure, are the distances from the left support. The objective function is

identical to the one used in the sequential evaluations for up to three reference sensors. In addition, the limit defined in Equation (2.49) is drawn in Figure 2.9. For this special benchmark example with white noise excitation, the limit is almost independent from the number of modes of interest. This could be not observed for a random multiple impulse excitation as described in Section 2.6.3.

Table 2.2 summarizes all optimal objective function values with their corresponding sets of sensor positions regarding the number of modes to be investigated and the available number of reference sensors. As already observed for the determination of the best sensor positions, in case of one and two reference sensor positions, the number of local optima increases with increasing number of sensors and modes of interest. Hence, it is difficult to find the best set of positions, if it is not possible to evaluate all combinations. However, the local minima have objective values similar to the global optimum. Therefore, it may be sufficient for applications to use a local optimum as reference sensor position.

2.6.3 Multiple impulse excitation

In many applications, the low spectral amplitudes usually obtained from ambient excitations are not sufficient. Higher spectral amplitudes of a random excitation can be achieved, for example, by generating an artificial noise signal with shakers mounted on the structure. Practical problems may arise due to additional masses on the structure, the interaction with the structure, or the additional effort to install and to operate the shakers. The application of random multiple impulses is an easy and efficient alternative, if a representative total excitation time and sufficient excitation energy can be guaranteed.

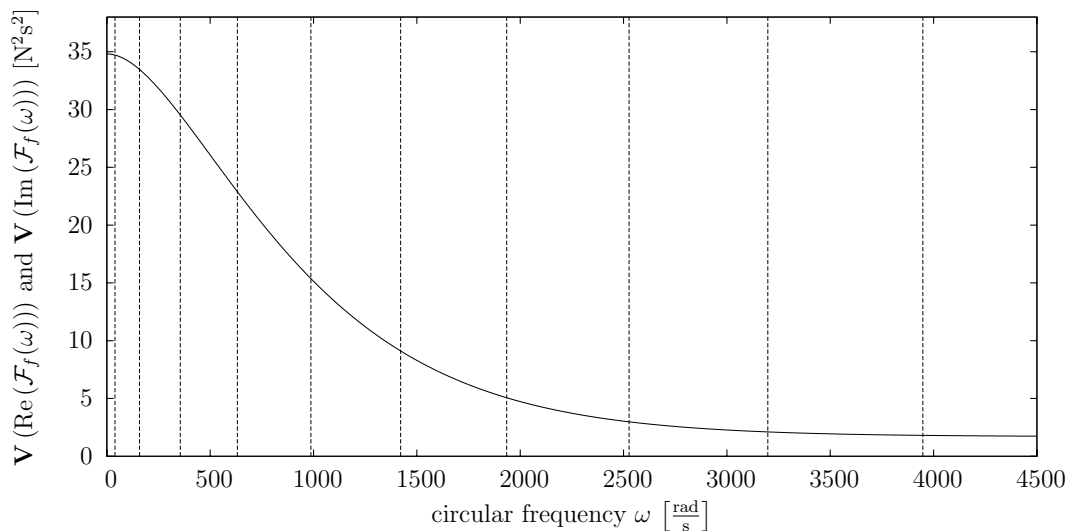


Figure 2.10: Variance of the real and imaginary part of the Fourier spectrum of random multiple impulse excitation. Vertical lines indicate the position of circular eigenfrequencies corresponding to vertical bending modes of the simply supported beam.

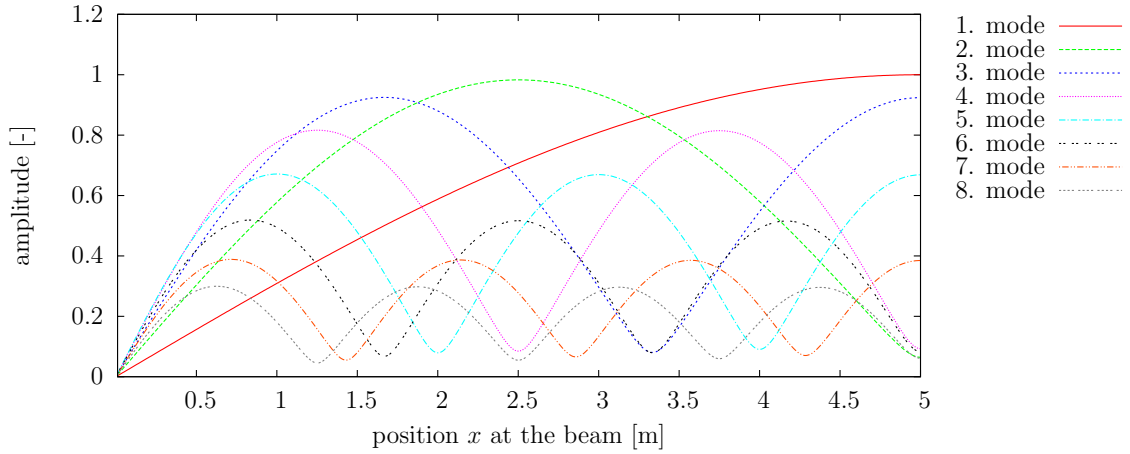


Figure 2.11: Normalized spectral amplitudes expecting random multiple impulse excitation on a simply supported beam.

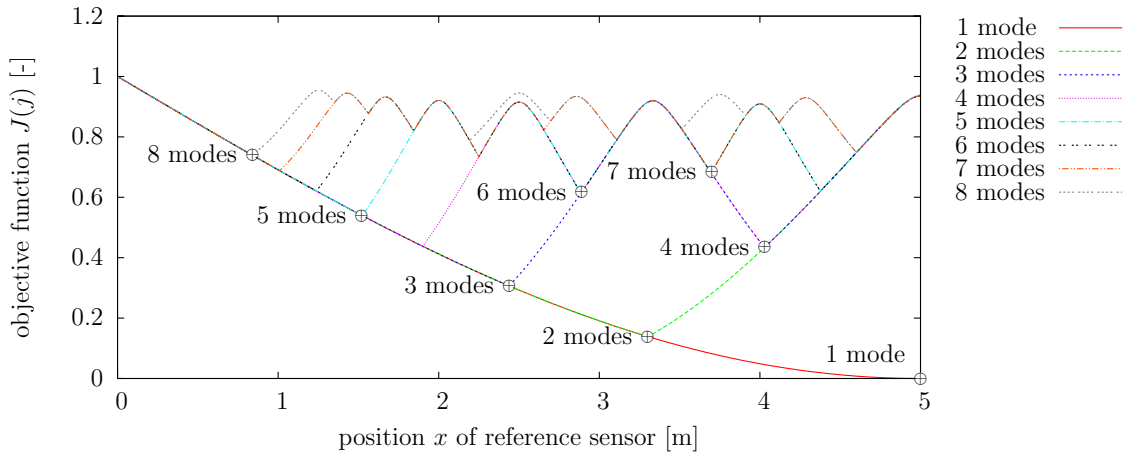


Figure 2.12: Objective functions assuming one reference sensor detecting a certain number of vertical modes of a simply supported beam assuming random multiple impulse excitation. \oplus indicates the optimal position with respect to the number of modes of interest.

The single impulses do not need to be measured in terms of intensity or spatial distribution, as long as the statistical characteristics are available. In the presented benchmark study, the impulses are only applied at the right half of the beam between $x = 5.05\text{m}$ and $x = 9.99\text{m}$. Furthermore, only vertical degrees of freedom in positive and negative direction can be excited. A random number represents the excitation of each degree of freedom with respect to a certain time instant. The distribution of the random numbers are identical for all degrees of freedom and all instants of time. These random numbers are independent concerning time and space. The expected value of the Fourier spectrum is zero and the variance of imaginary and real part can be represented similar to Equation

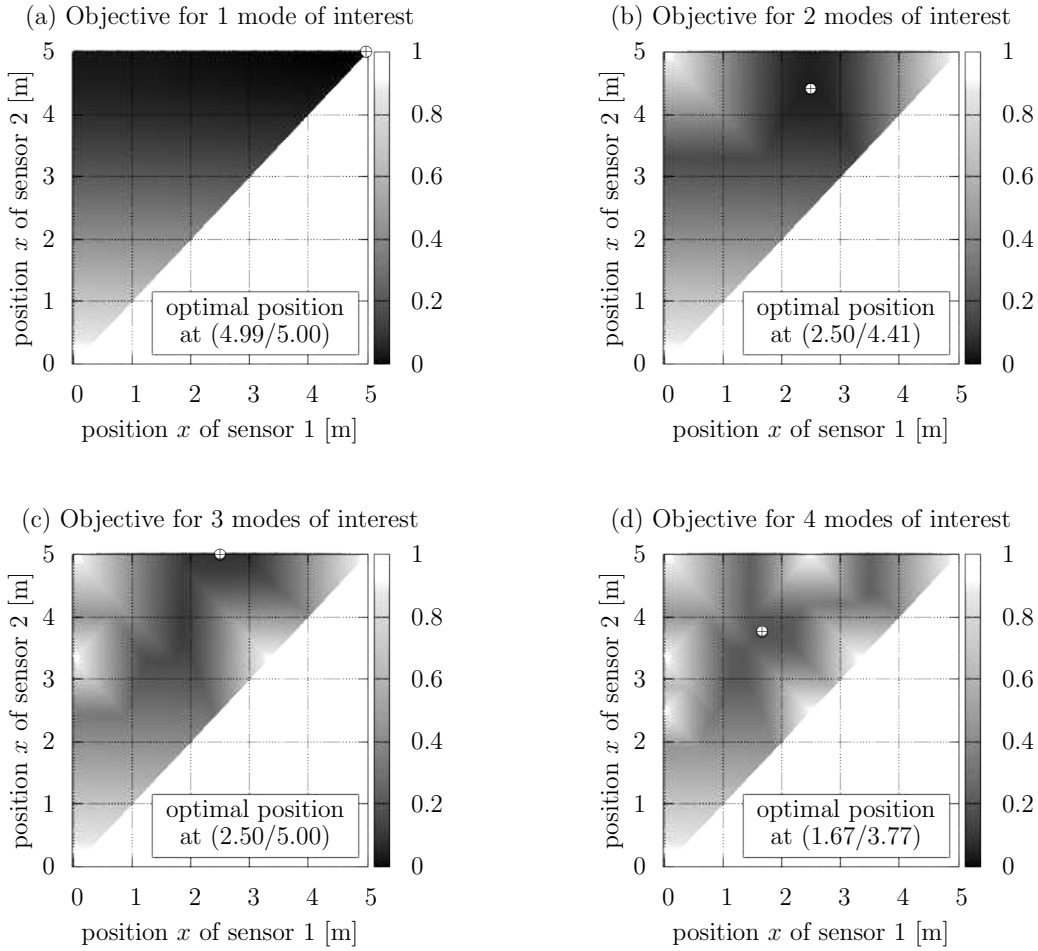


Figure 2.13: Objective function using two reference sensors to detect a certain number of vertical modes of a simply supported beam assuming random multiple impulse excitation. \oplus indicates the optimal position.

(2.35) by

$$\begin{aligned} \mathbf{V}(\operatorname{Re}(\mathcal{F}_f(\omega))) &= \mathbf{V}(\operatorname{Im}(\mathcal{F}_f(\omega))) \\ &= 0.18(\omega + 500) \exp(-0.002(\omega + 500)) + 1.7 \quad \forall \omega > 0. \end{aligned} \quad (2.61)$$

This function is shown in Figure 2.10. The vertical lines in Figure 2.10 are related to the circular eigenfrequencies of the first ten vertical bending modes of the beam. As typical for an impulse excitation, the excitation energy decreases with higher frequencies.

Once the statistical properties are known, the normalized spectral amplitudes can be calculated according to Equation (2.40). They are visualized in Figure 2.11. The effect of decreasing excitation energy with increased circular eigenfrequency is clearly visible. Based on the normalized spectral amplitudes, the best reference sensor position can be determined using Equation (2.48) with weightings $w_1 = 0.9$ and $w_2 = 0.1$.

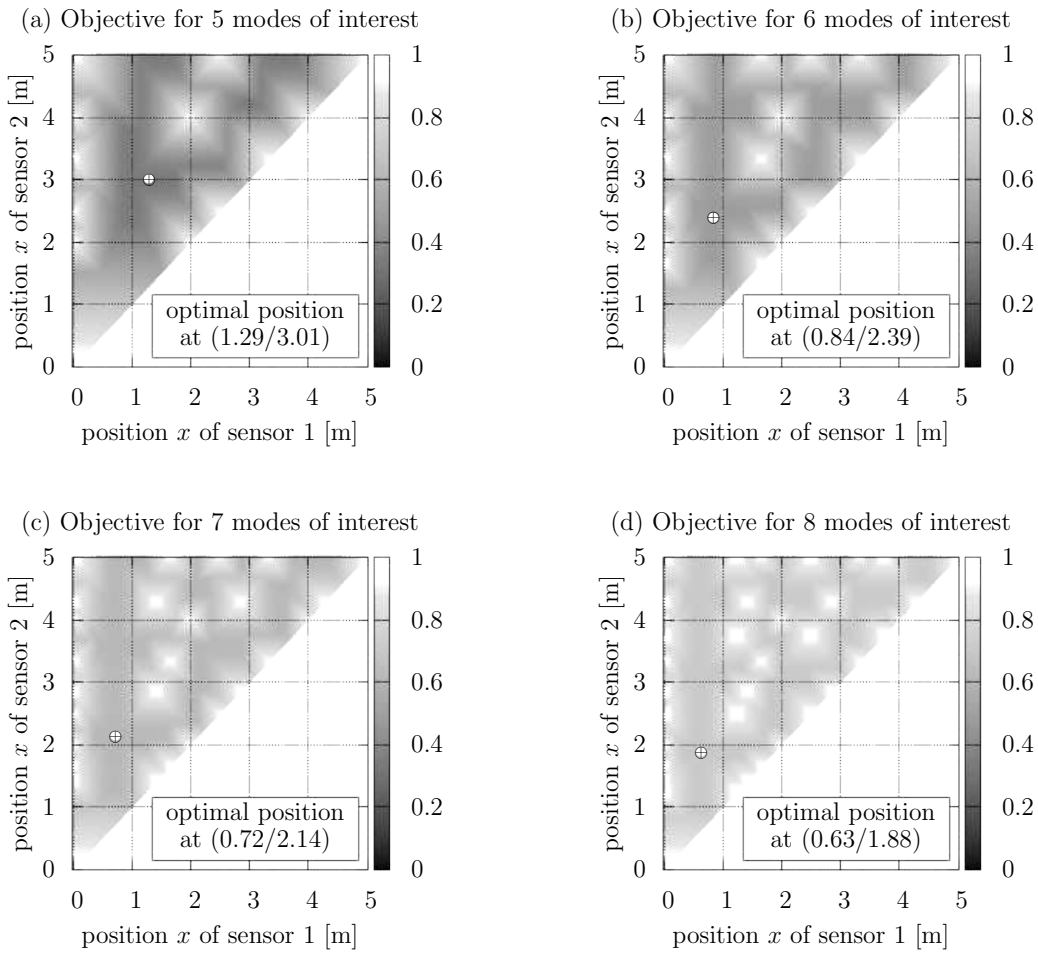


Figure 2.14: Objective function using two reference sensors to detect a certain number of vertical modes of a simply supported beam assuming random multiple impulse excitation. \oplus indicates the optimal position.

In a first investigation, only one reference sensor is assumed to be available. The results are given in Figure 2.12. The determined best reference positions are similar to the positions obtained for white noise excitation, presented in Figure 2.6. The only exceptions occur with six and eight modes of interest. It is obvious that the best positions are in the vicinity of crossing normalized spectral amplitudes of the determining modes. For example, if eight modes are of interest, the best position is at the crossing of the normalized spectral amplitude of the first and eighth mode.

The best positions of two reference sensors in combination with random multiple impulse excitation are presented in Figures 2.13 and 2.14. If less than six modes are of interest, the obtained positions are comparable to those of white noise excitation. In cases of six, seven, or eight modes to be detected, the determined positions deviate clearly from the positions obtained for white noise excitation. The objective function shapes

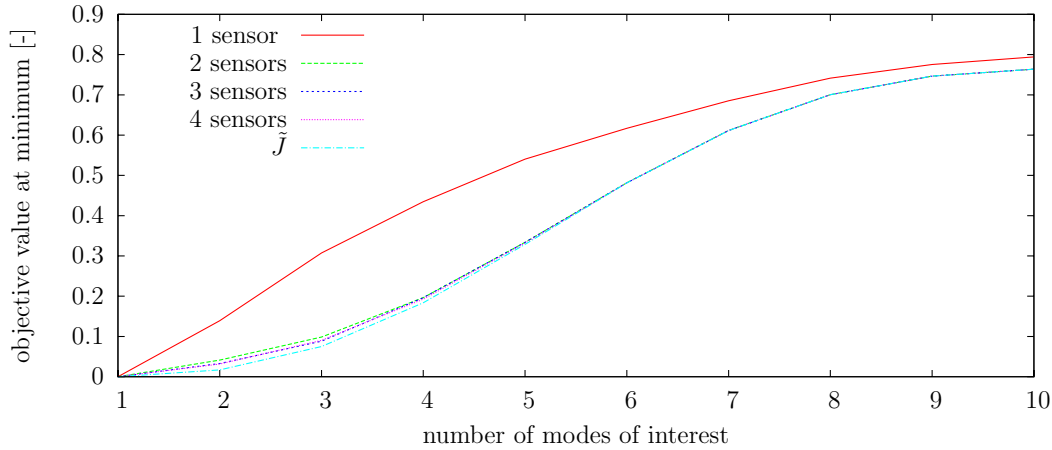


Figure 2.15: Objective function value at optimum for different numbers of available reference sensors and modes to be detected assuming random multiple impulse excitation.

Table 2.3: Objective value and respective optimal positions assuming random multiple impulse excitation.

# of modes	1 sensor		2 sensors		3 sensors		4 sensors (PSO)			
	objective value	position [m]	objective value	positions [m]	objective value	positions [m]	objective value	positions [m]		
1	0.000000	5.00	0.000000	4.99 5.00	0.000001	4.98 4.99 5.00	0.000002	4.97 4.98 4.99 5.00		
2	0.139250	3.30	0.041362	2.50 4.41	0.032870	2.50 2.73 4.42	0.031571	2.51 3.04 3.05 4.42		
3	0.307436	2.44	0.098687	2.50 5.00	0.088374	2.29 2.45 5.00	0.090217	1.67 2.17 3.31 5.00		
4	0.434647	4.03	0.196376	1.67 3.77	0.196325	1.25 2.14 3.94	0.192396	1.66 1.67 3.75 4.10		
5	0.540408	1.52	0.333965	1.29 3.01	0.333622	1.01 3.24 4.65	0.331338	1.01 1.24 3.12 4.77		
6	0.616970	2.89	0.481886	0.84 2.39	0.481510	0.84 0.90 4.11	0.481313	0.83 0.84 2.50 4.17		
7	0.685214	3.70	0.611533	0.72 2.14	0.611502	0.71 0.72 2.14	0.611520	0.71 0.72 0.73 3.57		
8	0.741497	0.84	0.700511	0.63 1.88	0.700482	0.62 0.63 1.88	0.700471	0.62 0.63 0.64 1.88		
9	0.775433	0.73	0.746643	0.56 1.67	0.746616	0.55 0.56 1.67	0.746606	0.55 0.56 0.57 1.66		
10	0.794130	0.66	0.763842	0.50 1.50	0.763814	0.50 0.51 1.50	0.763802	0.49 0.50 0.51 1.50		

themselves are similar, but with a lower objective value. This lower objective value results from the high differences of excitation energy between lower and higher frequencies. As the optimal reference sensor positions are at locations of maximal normalized spectral amplitudes of the respective last mode of interest, the best position is only determined by this mode. For instance, in case of eight modes of interest, the optimal positions are at locations of the maximal normalized spectral amplitudes of the eighth mode. This differs from the white noise excitation, where the best positions are at crossing points of the normalized spectral amplitudes.

The investigation can be continued by increasing the number of available reference sensors. Figure 2.15 shows this effect for different numbers of modes of interest. It is noticeable that the objective value at the minimum cannot be significantly improved for increasing numbers of available reference sensors. This is typical for impulse excitations as the objective is mainly determined by the mode with the highest frequency. The limit according to Equation (2.49), presented graphically in Figure 2.15, shows that more than

two sensors are not feasible for the current benchmark study.

A summary of all results with best objective values and respective positions for several combinations of sensor numbers and number of modes of interest is given in Table 2.3.

2.7 Case study: Test specimen

2.7.1 System description

While the benchmark study of a simply supported beam, presented in Section 2.6, explained and validated the proposed algorithm, the case study in this section considers a test specimen with a more complex geometry. For this example, the optimal reference sensor positions cannot be determined exclusively by experience. The test specimen, made of welded steel plates and a standard C-section, has dimensions of about 75cm by 50cm by 70cm and weighs approximately 160kg. Its first eleven calculated global mode shapes are presented in Figure 2.16. In the tests, the specimen is supported by a rubber rope to ensure free-free conditions. Figure 2.17 shows the test configuration.

The presented case study investigates two issues. Firstly, the accuracy of theoretically derived spectral response amplitudes are validated by a specific test configuration. And secondly, the best reference sensor configuration is determined by the proposed strategy. As the measurement direction and the excitation direction are always perpendicular to the surfaces, a transformation needs to be applied. This transformation is described in Section 2.2.3.

2.7.2 Description of finite element model

An initial finite element model is created using the software Ansys Workbench [ANSYS, Inc. 2009]. The model is only based on pretest knowledge. The geometry and the material are modeled as accurate as possible based on drawings and additional geometry measurements. As the test specimen is assumed to be decoupled from the supporting structure, the finite element model does not contain supports. The welds are connected by the bonded contact formulation with standard penalty formulation provided in [ANSYS, Inc. 2009]. It is assumed that the welded parts are in direct contact with each other. This is modeled again by the same bonded contact formulation. The final model has 132,792 nodes and 38,295 volume and contact elements. It is assumed that welds and structural steel have identical material properties, namely a Young's modulus of 2.12MPa, a Poisson's ratio of 0.3, and a density of $7850 \frac{\text{kg}}{\text{m}^3}$.

The finite element model is shown in Figure 2.18 and the first eleven non-local, non-rigid body mode shapes obtained from the numerical model are presented in Figure 2.16. In addition, six rigid body modes at frequencies close to 0Hz and eight local modes at

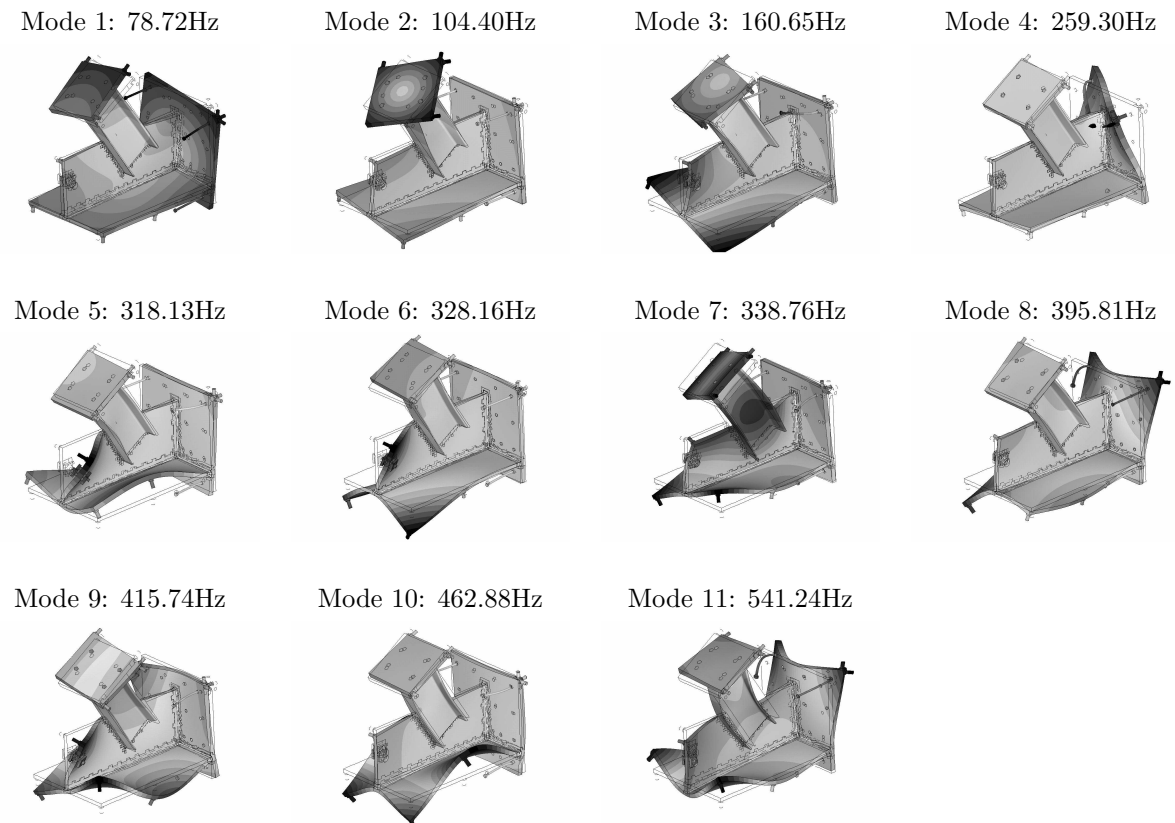


Figure 2.16: First 11 non-local, non-rigid body modes obtained by numerical modal analysis.



Figure 2.17: Left: Test specimen with free-free support conditions. Right: Accelerometers PCB338B35 mounted with magnets at lower flange.

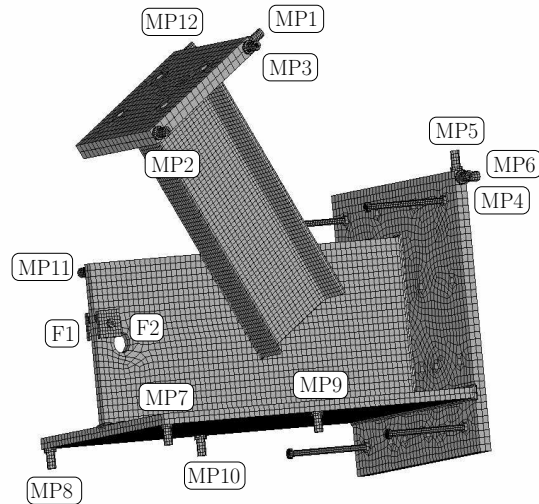


Figure 2.18: Finite element model. The measurement points and excitation points are indicated with MP and F, respectively.

natural frequencies between 195.19Hz and 198.16Hz are observed. The local modes are mainly associated with bending modes of the four support plate screws mounted as safety support for the rope.

2.7.3 Validation of spectral response amplitudes

To validate the theory described in Section 2.2, a multiple impulse test has been performed, whereas random excitation is applied at two specific positions. This test is conducted as a one-setup configuration and does not primarily aim at identifying the best reference sensor positions. The investigation shows a comparison between experimentally obtained and theoretically derived power spectral densities.

The data acquisition system consists of an NI DAQ6062E card connected to an NI SCXI1000DC with four modules NI SCXI1531. The data acquisition software LabVIEW [National Instruments 2009] is applied on a standard notebook. The hammer impacts are introduced by a standard rubber mallet at the two predefined positions. Two force sensors PCB200B05 are utilized to measure the force over time. Twelve accelerometers PCB338B35 measure the response at twelve predefined positions denoted by MP1 to MP12.

The locations of force sensors and accelerometers are described in Figure 2.18. The measurement duration of a single test is 180 seconds. This test has been repeated 107 times. Figures 2.19-2.23 show representative time histories of force and acceleration with corresponding averaged power spectral densities for a single test. It can be observed that the most energy of the impulses is concentrated within a frequency range up to

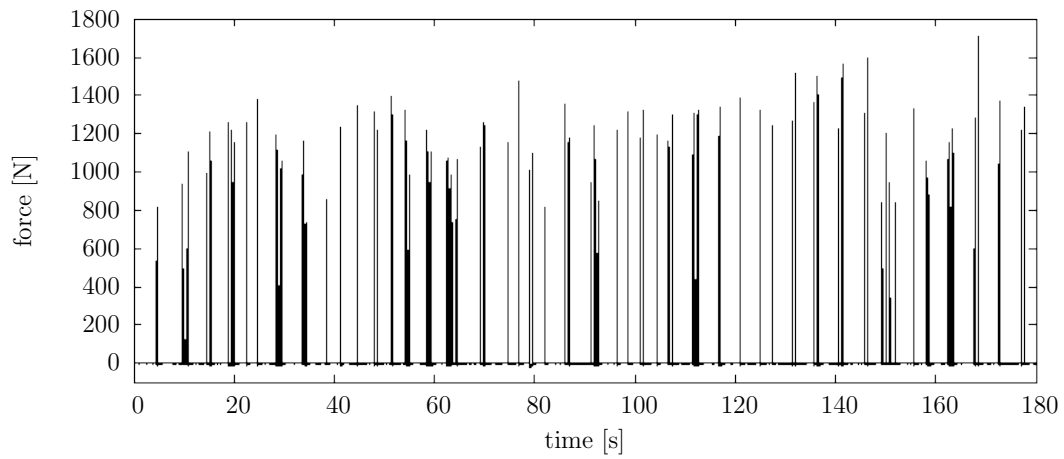


Figure 2.19: Example of a time history of the force signal at position F1.

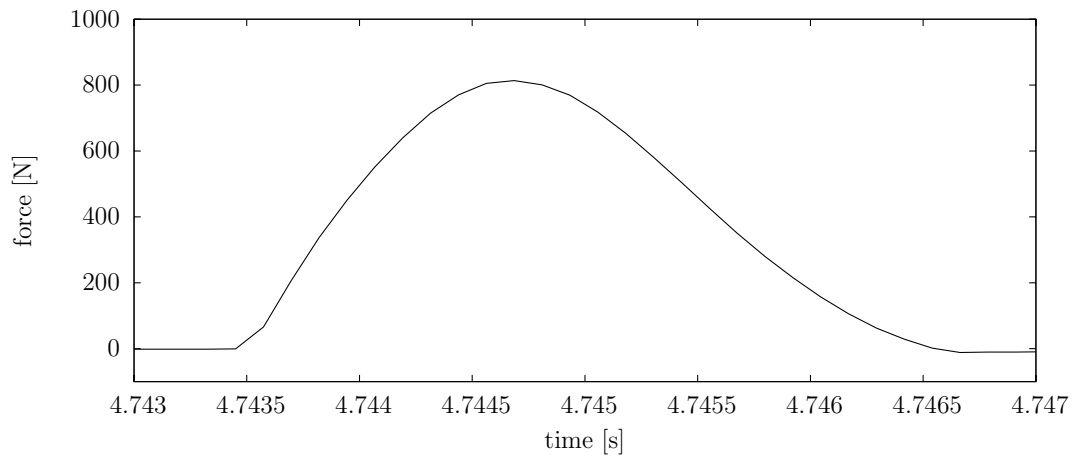


Figure 2.20: First impulse of the force time history given in Figure 2.19.

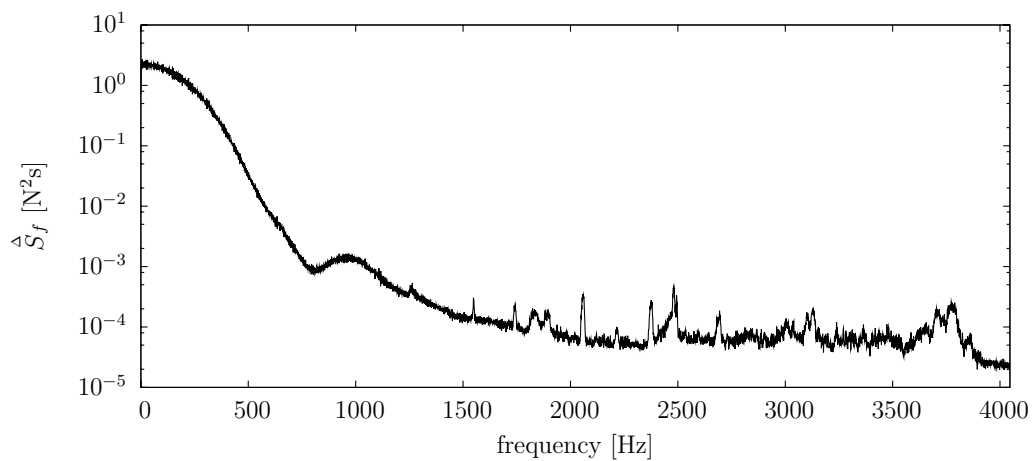


Figure 2.21: Example of an averaged power spectral density of the force signal at position F1 using 180 statistically independent blocks of a 180s time history.

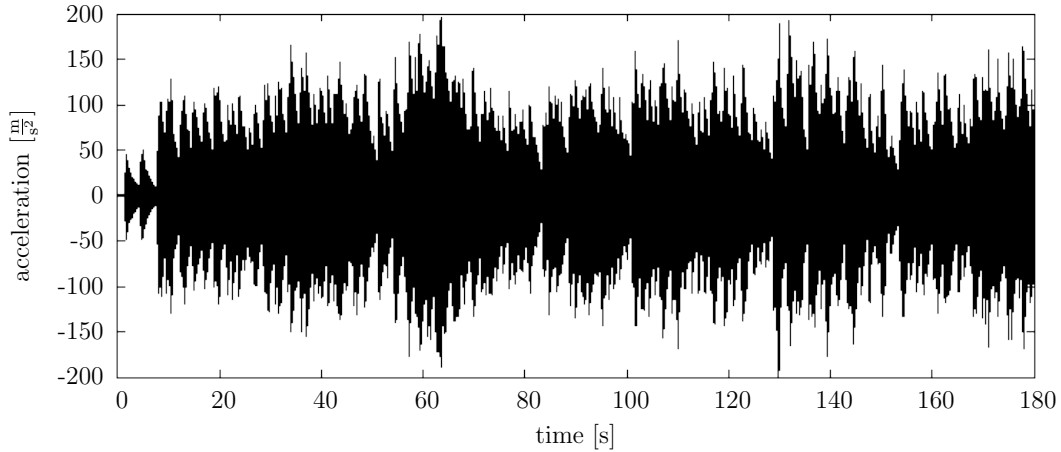


Figure 2.22: Example of a time history of the response signal at position MP12.

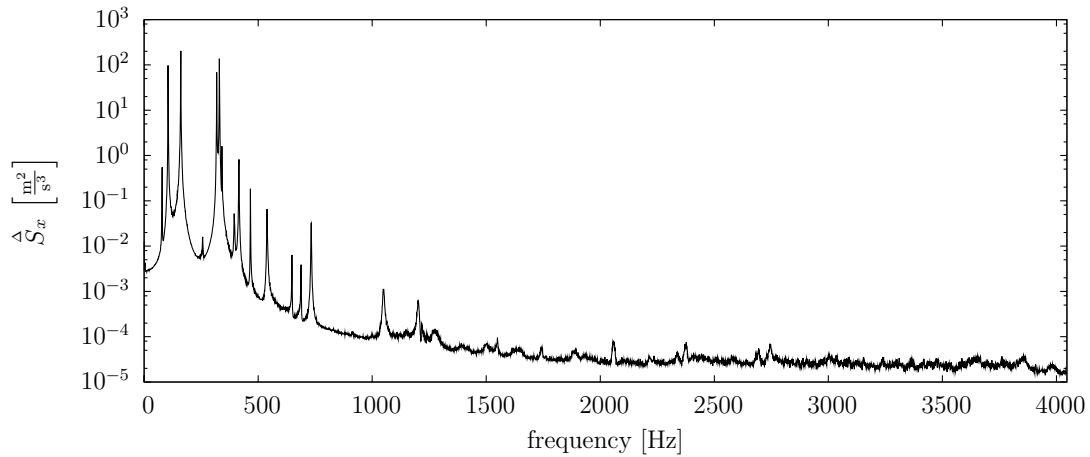


Figure 2.23: Example of an averaged power spectral density of the response signal at position MP12 using 180 statistically independent blocks of a 180s time history.

600Hz. Therefore, the following assessment is limited to frequencies not greater than 600Hz. For subsequent analyses, the first 18s of each 180s test are removed to assure stationarity in the remaining signals. The remaining time histories are cut into six 27s blocks without overlapping. An advanced model updating of the described finite element model is not the intention of this investigation. To validate the confidence of the model with the experiments, each 27s block is evaluated by the covariance-based stochastic subspace identification algorithm [Peeters et al. 1999]. Based on these results, erroneous measurements and outliers are identified and removed manually from the total set. Finally, 507 blocks of 27s are included in the statistics. The sample mean and sample standard deviation of the obtained modal parameters are presented in Table 2.4. The sample mean value and sample standard deviation of the magnitudes of the complex modal assurance criterion [Allemang et al. 1982] between experimentally obtained and numerically derived modal displacements using the twelve measurement points are given as well.

Table 2.4: Comparison of numerically derived and experimentally obtained modal properties. The statistics rely on 507 stochastic subspace identification (SSI) evaluations of data sets with time duration of 27s. The modal assurance criterion is calculated between the mode shapes obtained from the SSI algorithm and numerical mode shapes.

mode	experimental		numerical	
	frequency	damping	frequency	MAC
	mean(stdv) [Hz]	mean(stdv) [%]	[Hz]	mean(stdv) [-]
1	78.737 (0.0270)	0.1773 (0.0627)	78.721	0.9994 (0.0000)
2	105.13 (0.0176)	0.0640 (0.0184)	104.40	0.9996 (0.0000)
3	160.69 (0.0181)	0.0324 (0.0103)	160.65	0.9982 (0.0000)
4	256.62 (0.2228)	0.5637 (0.0747)	259.30	0.9980 (0.0002)
5	318.18 (0.1199)	0.0447 (0.0082)	318.13	0.9890 (0.0008)
6	330.26 (0.0373)	0.0479 (0.0083)	328.16	0.9786 (0.0018)
7	340.91 (0.0266)	0.0554 (0.0065)	338.76	0.9634 (0.0031)
8	394.95 (0.2036)	0.3757 (0.0186)	395.81	0.9955 (0.0004)
9	415.58 (0.0637)	0.1271 (0.0133)	415.74	0.9980 (0.0001)
10	466.19 (0.0296)	0.0352 (0.0068)	462.88	0.9983 (0.0001)
11	538.91 (0.0647)	0.2231 (0.0261)	541.24	0.9936 (0.0004)

The fast Fourier transformation is applied to each of the 507 27s blocks without any further data processing except an offset removal. The complex Fourier spectra are evaluated separately for each block. Thereafter, the statistical properties, sample mean and sample standard deviation, of the Fourier transforms are calculated. The mean values of the power spectral densities are calculated according to Equation (2.12). They are visualized for each measurement point in Figures 2.25 and 2.26 indicated with the black lines.

The data processing of the force time histories is exactly the same as for the response time histories up to the evaluation of the sample mean and sample standard deviation of their Fourier transforms. The power spectral densities are not needed for further calculations. Figure 2.24 shows that the mean values are close to zero. A moving least squares algorithm [Lancaster et al. 1986] with exponential weighting and an influence radius $R = 600$ is applied to smooth the curve of sample variances. It is assumed that the real and imaginary parts are equal and that the mean values are zero. The sample variances and mean values of the imaginary and real parts are given in Figure 2.24 exemplarily for the first excitation point.

Applying Equations (2.13), (2.14), (2.15), and (2.12), the mean value of the response power spectral density can be calculated analytically, based on the smoothed variances and a zero mean of the excitation Fourier spectra. The first 32 rigid body, global, and local

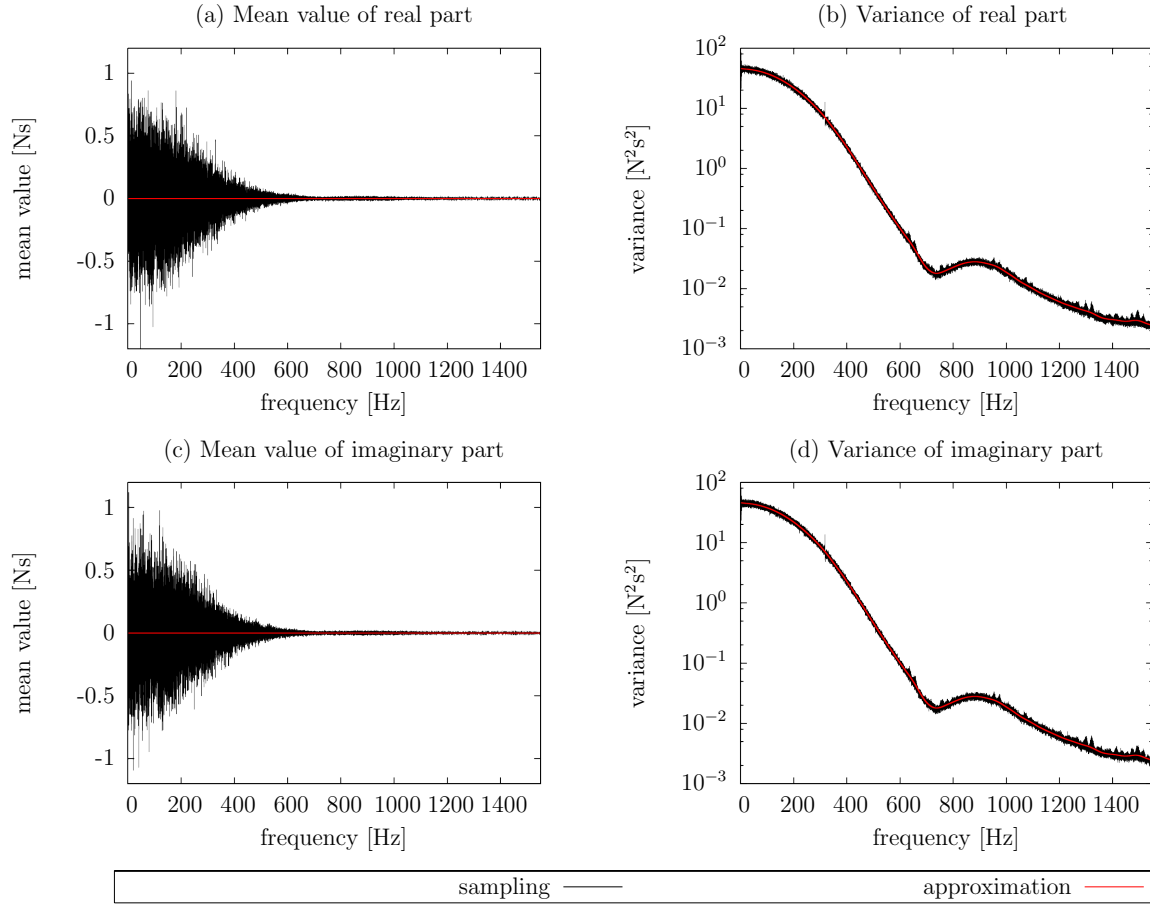


Figure 2.24: Sample mean values and sample variances of the Fourier transform of the force signal at position 1 with respect to the multiple impulse excitation. The smoothed curves for the variances are based on a moving least squares algorithm. The sample means are approximated by a constant value zero.

modes, which are required to assemble the frequency response function, are extracted from the numerical model described in Section 2.7.2. Assuming proportional viscous damping, the modal damping ratios of the first eleven global modes are set to the mean values of the modal damping ratios derived from the stochastic subspace identification evaluations, which are presented in Table 2.4. The modal damping ratios of the local modes between 170Hz and 200Hz are set to 0.15%. All other modal damping ratios are set to 0.1%. The results for each measurement point are given in Figures 2.25 and 2.26, indicated with the red lines.

To investigate the influence of model assumptions (e.g., proportional viscous damping, support conditions) and deviations of the numerical model, two alternative approaches are chosen to describe the frequency response function in Equations (2.13), (2.14), and (2.15). The first alternative approach uses the modal data (frequencies, damping ratios, modal displacements) of the first eleven global modes obtained from the stochastic subspace

identification to assemble the frequency response function. The results are indicated by the blue lines in Figures 2.25 and 2.26. The second alternative approach relies on the experimental frequency response function obtained from averaging all 507 experimental input and output relations. This is visualized as green line in Figures 2.25 and 2.26. Both alternative approaches use the same statistical values of the force Fourier transforms like in the structural model based approach.

In general, all power spectral densities of the alternative approaches agree well in comparison to the pure experimentally obtained power spectral densities. The experimental power spectral densities, corresponding to the black line, are less smooth compared to those obtained by the approaches indicated by the red and blue line. This can be explained by the statistical scatter. In addition, measurement noise influences the smoothness of the curves. If the noise can be approximated by a normally distributed zero mean independent variable with respect to amplitude and frequency, the variance of the noise is included as an additional summand in the mean value of the experimental power spectral density. Test measurements without external excitation showed that the mean value of the power spectral density of measurement noise is approximately $10^{-6} \frac{\text{m}^2}{\text{s}^4}$ for all acceleration signals in the frequency range between 50Hz and 600Hz.

The approach, indicated by the green color in Figures 2.25 and 2.26, uses directly the spectral input output relation by establishing the experimental frequency response function. Therefore, no structural model assumptions are included. The green and the black lines are very similar to each other. The amplitudes and positions of the natural frequencies agree perfectly. Discrepancies are obvious in the lower amplitudes. This can be partially explained by nonlinear effects and measurement noise that are disregarded. Due to averaging effects, the calculated frequency response function is less sensitive to noise than the experimentally obtained power spectral densities, which include the variance of the noise as a summand.

An additional assumption is made by using the modal parameters from the stochastic subspace identification, as performed in the approach indicated by the blue line. There, proportional viscous damping is presumed, which is reflected in the calculation of the frequency response function. However, the amplitudes and positions of the natural frequencies agree almost perfectly with the experimental power spectral amplitudes. Larger discrepancies are observed for lower amplitudes. As only the eleven global modes are included, the amplitudes near the boundaries of the covered frequency range have higher deviations. This can be explained by the missing interaction effects with modes outside the considered frequency range. A very clear example for this phenomenon is the measurement point MP3 around the frequency of 500Hz. Furthermore, the local modes between 160Hz and 250Hz cannot be recognized.

The approach, corresponding to the red line in Figures 2.25 and 2.26, uses the modal damping ratios from the measurement. The natural frequencies and mode shapes are

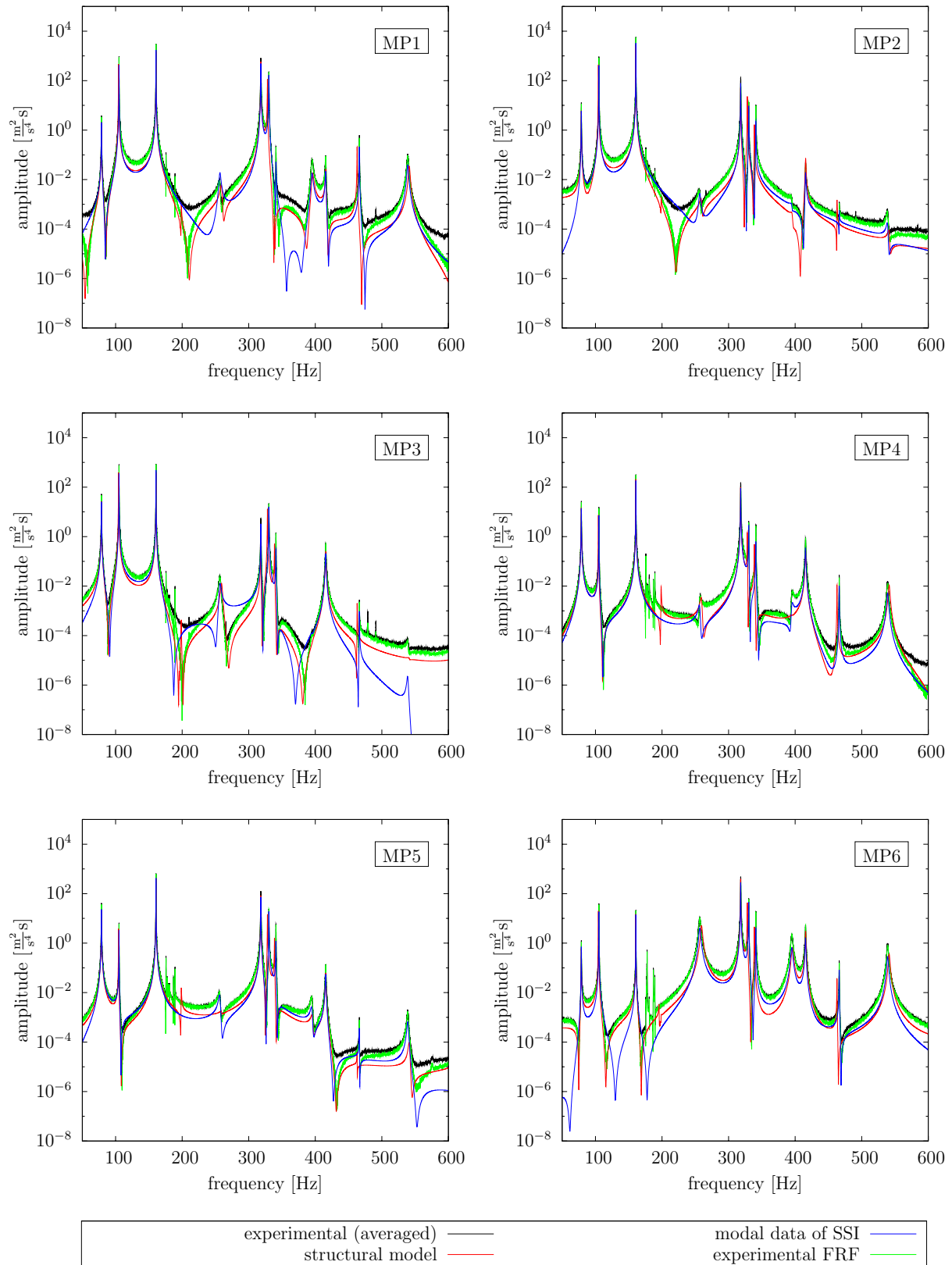


Figure 2.25: Comparison of mean values of auto power spectral amplitudes of the responses at MP1 to MP6 using different approaches.

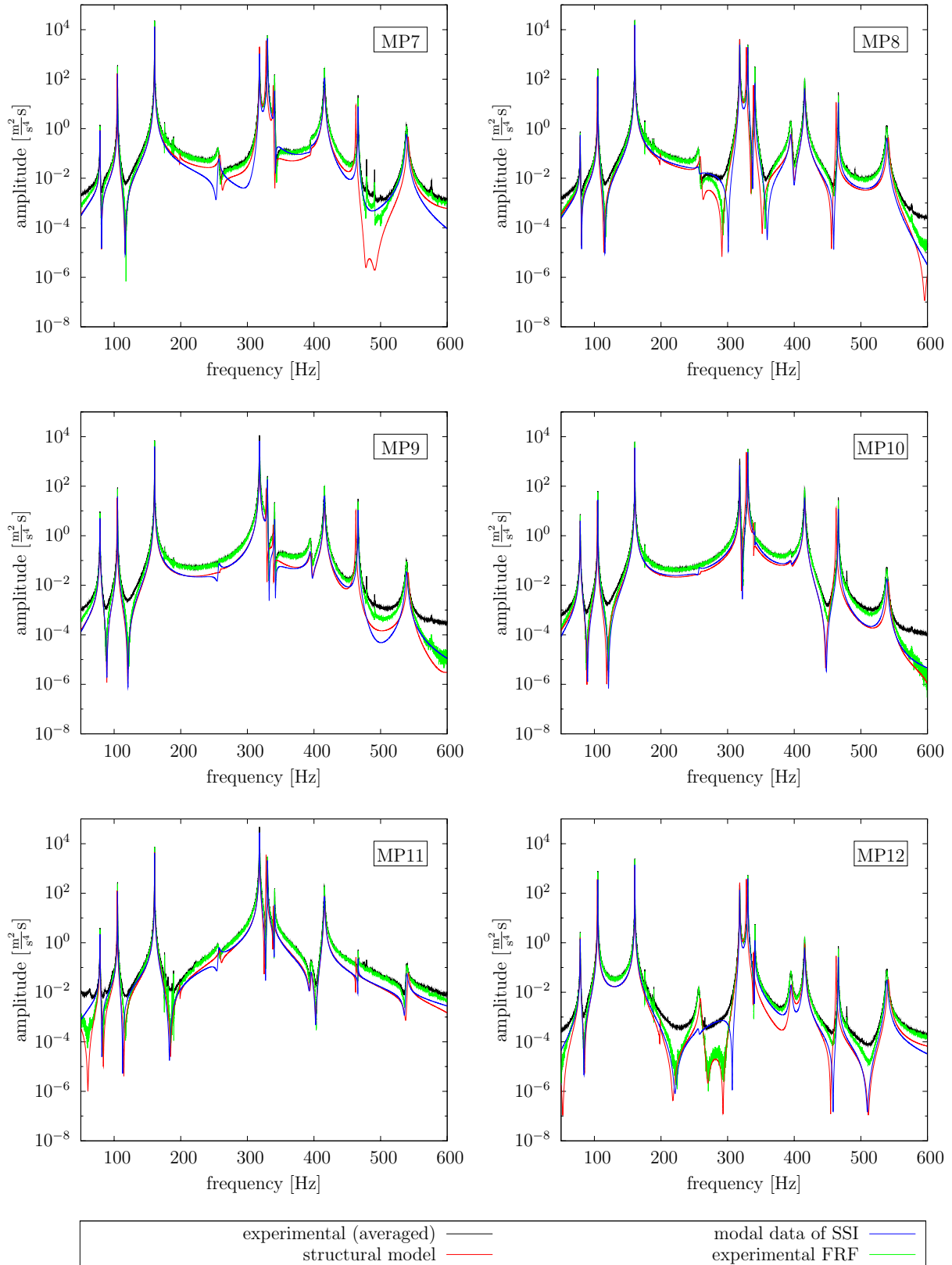


Figure 2.26: Comparison of mean values of auto power spectral amplitudes of the responses at MP7 to MP12 using different approaches.

extracted from the numerical structural model. Therefore, additional model uncertainties are introduced, which lead to higher deviations in the spectral amplitudes and positions of the natural frequencies. Nevertheless, the deviations are small especially in the range of the natural frequencies. As this approach assumes a proportional viscous damping model, the results are very similar to those obtained from the stochastic subspace identification approach, indicated by the blue color.

The different approaches show how different assumptions and simplifications of the model can lead to deviations. However, it can be shown that the proposed method to estimate the power spectral densities, based on a numerical model, is appropriate to predict power spectral densities obtained by a vibration test. These estimated power spectral amplitudes constitute the basis to validate possible sensor positions.

2.7.4 Determination of optimal reference sensor positions

2.7.4.1 One reference sensor using measured positions

Now, the twelve previously defined measurement points are investigated concerning their suitability for a reference sensor position in a roving sensor setup configuration with one reference sensor, where the first eleven global modes need to be covered. For each possible sensor position, Equation (2.48) will be evaluated based on the power spectral densities of both, the experimental data and the approach, which relies on the numerical structural model marked by the red color in Figures 2.25 and 2.26.

As the experimental power spectral amplitudes are not smooth, the peak values at the position of the natural frequencies of the experimental power spectral densities are obtained from a moving least squares (MLS) smoothed curve around the natural frequencies. The spectral amplitudes corresponding to the numerical model approach are calculated directly at the position of the natural frequencies.

Figure 2.27 shows the objective function value according to Equation (2.48). Even though significant deviations are observed at positions MP1 and MP6, the results, based on experiments and numerical structural model, are very similar. Assuming a required signal to noise ratio of 100, defined by the ratio of power spectral densities, possible reference sensor positions are at MP6, MP7, MP8, and MP11, which are revealed by both approaches. Furthermore, both approaches indicate MP7 as best position.

The investigation shows impressively that the predicted best reference position is equal to the experimentally obtained position. This validates the methodology proposed in Section 2.3. However, these perfect results rely on an almost perfect numerical model and the experimentally obtained modal damping ratios. For more imprecise models and less accurate predicted modal damping ratios, the prediction may be less reliable. The influence of those uncertainties needs to be investigated more detailed, which is out of the scope of these investigations.

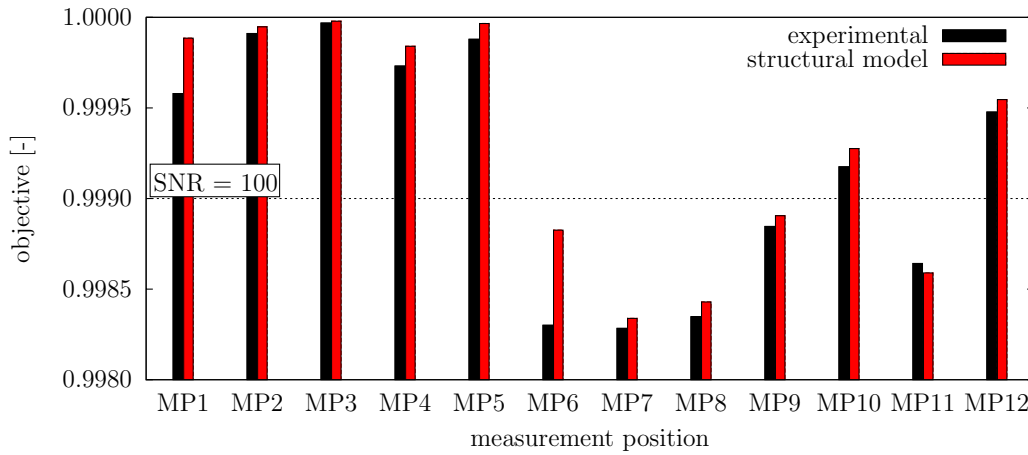


Figure 2.27: Objective function value of each measurement position according to Equation (2.48). black: calculation based on measured data; red: prediction based on structural model; The dotted line is related to a signal to noise ratio of 100 derived from the spectral density of measurement noise.

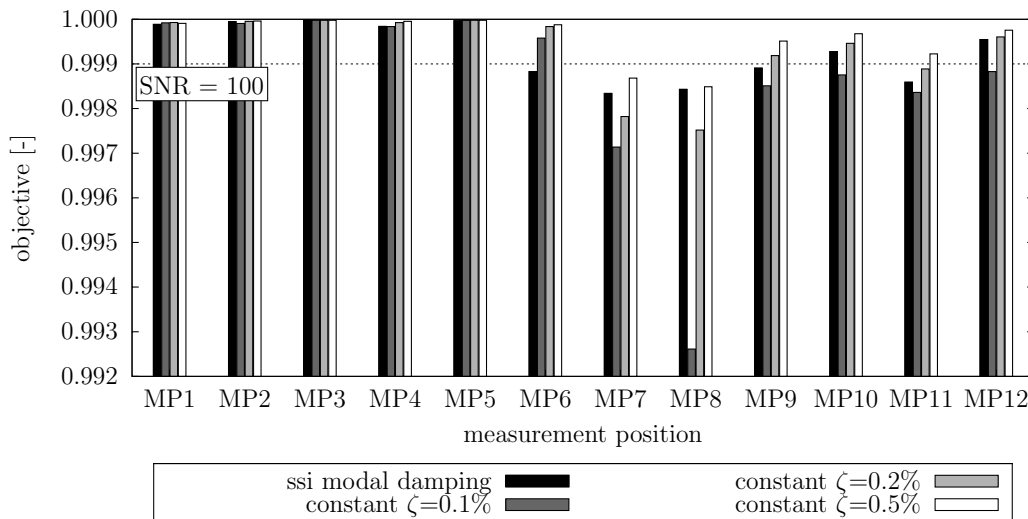


Figure 2.28: Objective function value of each measurement position according to Equation (2.48) depending on the distribution and size of modal damping ratios.

Nevertheless, a small investigation of the variation of modal damping ratios has been performed. This study uses the previously described approach related to the structural model indicated by the red color. The modal damping ratios are modified and set to a certain constant value for all 32 considered modes to calculate the frequency response function. Figure 2.28 shows the result using the original modal damping values obtained from the stochastic subspace identification method and assuming constant modal damping ratios with values of 0.1%, 0.3%, and 0.5% for all included modes. All spectral amplitudes are scaled with the maximal value $\max_{j,i}(\Upsilon)_{j,i}$ according to the reference approach using

modal damping ratios extracted from the stochastic subspace identification.

It can be observed that the objective function is sensitive to the size of modal damping and the distribution over the modes. However, for all constant damping ratios of 0.1%, 0.2%, and 0.5%, the measurement point MP8 is indicated as best reference sensor position, which is one of the four best positions identified by the approach related to the experimental data.

The objective values in Figures 2.27 and 2.28 are all close to one. Nevertheless, the differences are significant, when they are related to the minimal expected objective value according to Equation (2.49). The results derived with the structural model approach, presented in Figure 2.27, need to be related to the best objective value of 0.9952443. To obtain this value a large number of reference sensors and additional other assumptions and simplifications are required, as discussed in Section 2.3.

2.7.4.2 One reference sensor

On the basis of the previously validated model, the optimal sensor position for one reference sensor to represent the first eleven global modes will be investigated. 22,706 degrees of freedom are selected as possible sensor positions. The measurement directions are always perpendicular to the respective surfaces. From each plate, only one side is chosen to represent the behavior in orthogonal direction. As the direction cannot be defined within one global coordinate system, the transformation described in Subsection 2.2.3 is applied. The positions of the selected degrees of freedom are illustrated in Figure 2.29. With the weighting factors $w_1 = 0.9$ and $w_2 = 0.1$, Equation (2.48) is applied as objective function to assess the suitability of each preselected degree of freedom. Due to the small number

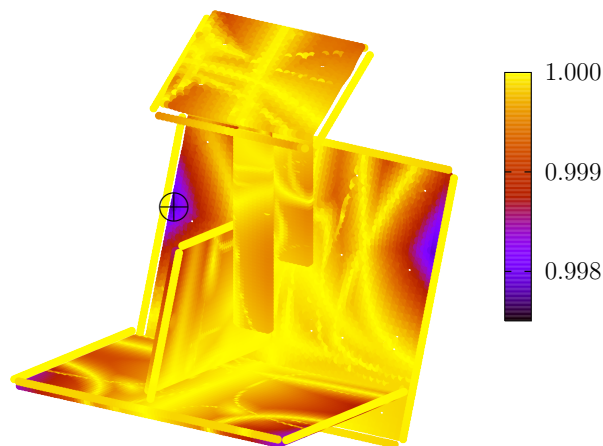


Figure 2.29: Objective function for the placement of one reference sensor for the detection of the first 11 global modes of the structure. The symbol \oplus indicates the optimal position with an objective value of 0.99781.

of possible reference sensor positions, all possibilities can be evaluated. The objective function values associated with the degrees of freedom are visualized in Figure 2.29. As the structure is almost symmetric, two possible suitable positions can be identified. The best position with an objective value of 0.99781 is marked with the symbol \oplus .

2.7.4.3 Two reference sensors

For the previously described test specimen, the optimal sensor positions of two reference sensors will be studied in this subsection. This investigation intends to find the optimal positions regarding the first eleven global modes of the finite element model. The total number of combinations for the preselected 22,706 measurement positions is 257,769,865. Even though the time to evaluate one combination is approximately 0.3ms at a single cpu with a Six-Core AMD Opteron(tm) Processor 8439 SE, a calculation of all combinations would need about 1 day, which is computationally too expensive for a practical application. Therefore, an optimization strategy is needed to find the best combination of reference sensor positions.

Following search strategies will be compared with each other:

- (i) optimization with a genetic algorithm using design variables that are related to the geometry of the structure,
- (ii) optimization with a particle swarm optimization using design variables that are related to the geometry of the structure,
- (iii) optimization with a genetic algorithm using design variables that are related to the degrees of freedom of the model,
- (iv) optimization with a particle swarm optimization using design variables that are related to the degrees of freedom numbering of the model,
- (v) optimization with a genetic algorithm using design variables that are related to a randomly reordered degree of freedom numbering of the model,
- (vi) optimization with a particle swarm optimization using design variables that are related to a randomly reordered degree of freedom numbering of the model, and
- (vii) evaluation of samples of combinations generated by the plain Monte Carlo method.

Strategies (i) and (ii) are related to the proposed innovative concept described in Subsection 2.5. In contrast to other strategies, the design variables are the coordinates of a local coordinate system of defined subdomains. The 22,706 possible positions are sorted into 20 subdomains. The subdomains, indicated in Figure 2.30, are related to the corresponding planes of the positions. Therefore, an optimization run needs to be

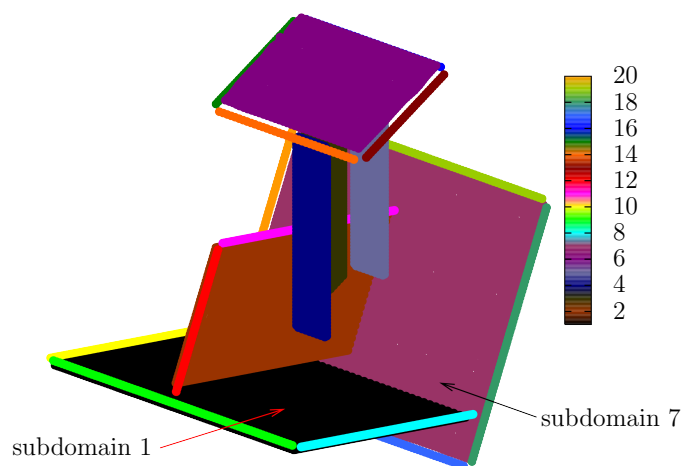


Figure 2.30: Subdomains of preselected degrees of freedom.

Table 2.5: Most important configuration parameters of the genetic algorithm (GA) depending on a total number of design evaluations b .

parameters	value
number of parents	$\sqrt{\frac{b}{5}}$
number of individuals	$2\sqrt{\frac{b}{5}}$
number of generations	$5\sqrt{\frac{b}{5}}$
crossover probability	0.5
mutation rate	0.5
mutation standard deviation	0.01

Table 2.6: Most important configuration parameters of the particle swarm optimization (PSO) depending on a total number of design evaluations b .

parameters	value
number of iterations	$2\sqrt{\frac{b}{2}}$
number of particles	$\sqrt{\frac{b}{2}}$
c_1	0.5
c_2	0.5
c_3	0.5
ω at first iteration	0.9
ω at last iteration	0.6

conducted for a total of 210 combinations of subdomains assuming that both reference sensor positions can be mounted in one subdomain. For the optimization, the total geometrical dimensions of the subdomains are normalized in each direction. Hence, the design variables are constrained between 0 and 1. Each reference sensor position within a certain subdomain has two design variables to describe the position in plain. As the design variables are defined as continuous variables and the spectral information is only available at the nodes of the finite element structure, the nearest available finite element node has to be detected. To determine two reference sensor positions, four design variables have to be defined. The most important configuration parameters of the optimization approaches, genetic algorithm and particle swarm optimization, are presented in Tables 2.5 and 2.6. A general description of the algorithms are given in Appendix B.

Strategies (iii) and (iv) are related to the common strategies found in literature, where only the ordering of possible positions according to the degree of freedom numbering of the finite element model is used to define a certain sensor position. In this investigation, the preselected 22,706 possible sensor positions are sorted according to their subdomains depicted in Figure 2.30 and then numbered from 1 to 22,706. This configuration is referred to as the original degree of freedom numbering. For the most important subdomains one and seven, the ordering is given in Figure 2.31. It can be observed that a certain relation to the geometry is present. The configuration of the applied optimization approaches is identical to the configuration used in strategies (i) and (ii). But in contrast to strategy (i) and (ii), only two discrete design variables are required to define the reference sensor positions.

Strategies (v) and (vi) are similar to strategies (iii) and (iv). The only difference is the numbering of possible sensor positions, which is randomly reordered to reduce the dependency of the numbering on the geometry. The random numbering of subdomains one and seven is given in Figure 2.31. To increase convergence and computational efficiency of the optimization algorithms in strategies (i) to (vi), permutations with repetition instead of combinations without repetition are generated as design sample sets.

The simplest strategy is a search with a plain Monte Carlo sampling, which is proposed for strategy (vii). The combinations without repetition are defined by using the design variable definition of strategies (iii) and (iv). This unguided search algorithm is very easy to apply.

The seven investigated strategies will be compared regarding their efficiency in terms of generated number of design samples and with respect to the ability to detect the optimum in terms of location and objective function value. The objective function is evaluated according to Equation (2.48) using the weighting factors 0.9 and 0.1 for w_1 and w_2 , respectively. Due to the symmetry properties of the test specimen, many suboptimal sensor position sets with almost equal objectives are possible. Therefore, the best four suboptima are considered in the assessment. The four suboptimal sensor positions are

visualized in Figure 2.32, whereas the global optimum is represented by the first suboptimum. The minimal distance d_p between the location vector $\boldsymbol{\theta}_j \in \mathbb{R}^4$ of the currently detected optimum and the location vector $\boldsymbol{\theta}_p \in \mathbb{R}^4$ of the suboptimum p is defined as

$$d_p = \|\boldsymbol{\theta}_p - \boldsymbol{\theta}_j\| \quad \text{with} \quad p = 1, 2, 3, 4. \quad (2.62)$$

The criterion to assign a certain position to the most likely suboptimum \bar{p} is

$$\bar{p} = \underset{p}{\operatorname{argmin}} d_p. \quad (2.63)$$

The optimization is declared as failed, when the optimum cannot be found on the subdomains one and seven, or when the detected positions are not within a range of 10cm of the position of the corresponding suboptimum. To investigate the efficiency of the search strategies, the number of maximal allowed design sample sets is restricted and reduced in seven steps. The seven steps are performed with 2,150,895, 1,127,892, 616,370, 360,634, 232,767, 168,840, and 84,396 design sample sets. As the genetic algorithm and the particle swarm optimization are stochastic optimization strategies, they do not deliver repeatable results. The natural randomness of the search strategies is considered by generating 20 runs for each search. The mean values of the distance and the objective function value of the detected optimum are calculated separately for each suboptimum. The results are presented in Figures 2.33 - 2.39.

The implemented genetic algorithm performs better in case of optimal positions on the boundary. This can be explained by the constraint handling. If a new design point is not within the defined boundaries, it will be set to the respective violated boundary value.

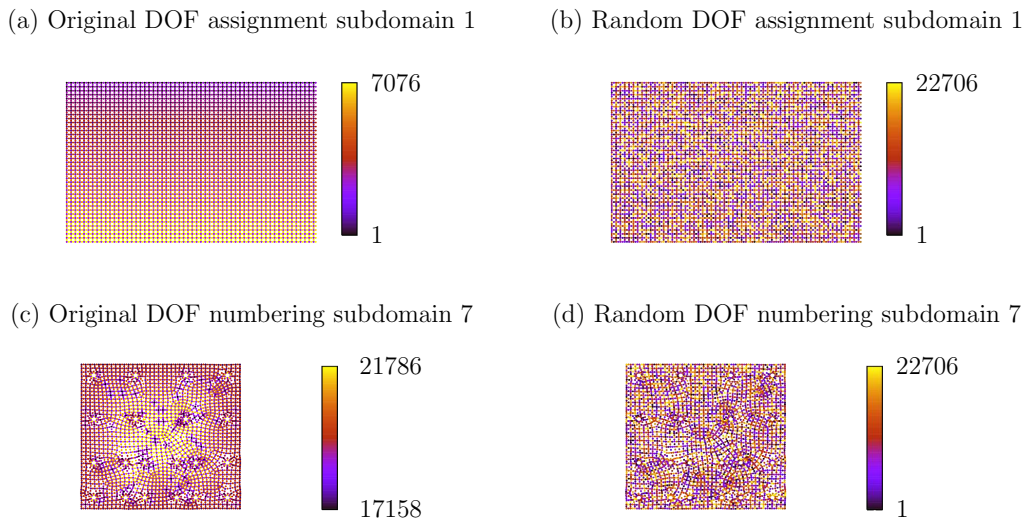


Figure 2.31: Original and random degree of freedom (DOF) numbering for subdomains 1 and 7.

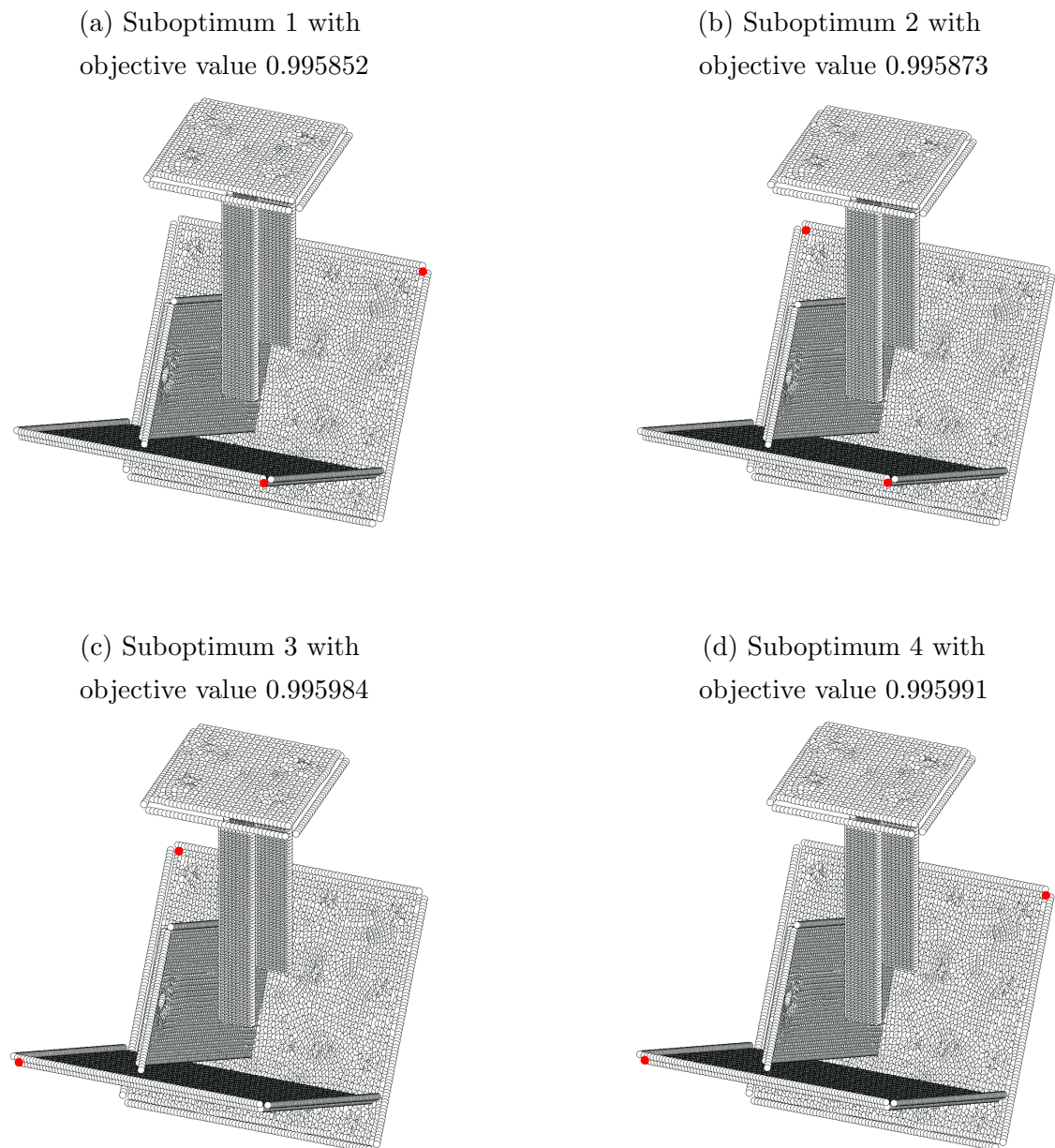


Figure 2.32: Position of best four suboptima. The first suboptimum is the global optimum. The red dots mark the reference sensor positions.

Table 2.7: Averaged calculation time to evaluate one design sample set.

strategy	(i)	(ii)	(iii)	(iv)	(v)	(vi)	(vii)
time per design [ms]	1.87	1.93	0.30	0.34	0.30	0.34	0.38

Therefore, more designs are generated at the boundaries, which improves the detection of optimal positions at the boundaries.

If the boundary condition is not fulfilled when using the particle swarm optimization algorithm, the unsuitable design sample set is replaced by a randomly chosen design from a collection of best design sample sets. Thus, the implemented particle swarm optimization is more suitable for optima in the center of a design domain. This effect can be recognized for the search strategies (i) and (ii), where the boundaries are very important for the search. Only for the lower number of design sample sets, the genetic algorithm is not able to detect one of the four suboptima. In contrast, the particle swarm optimization frequently identifies suboptimal positions near the center of the design spaces, which are not assignable to one of the considered suboptima. However, this effect is not observed in case of search strategies (iii) to (vi), in which the boundaries are represented by the available number of sensor positions.

Furthermore, it can be concluded that the innovative proposal to use geometry-based design variables, as applied in strategies (i) and (ii), is more suitable to detect the optimum correctly. The optimum can be identified, even if the number of available design sample sets is very low compared to the total number of available combinations. With a decreasing geometry association of the design variables, the accuracy of the obtained optimum decreases as well. This is proven by comparing the results from strategies (iii) and (iv) with the results from strategies (v) and (vi). For search strategies (v) and (vi), the design variables are totally disconnected from the geometry. Thus, it is obvious that the accuracy of obtained results is similar to the search strategy (vii), in which a Monte Carlo sampling is performed.

The time to evaluate a single design is not identical for all strategies. A benchmark with respect to the average time to evaluate a single design is conducted on a single cpu of a Six-Core AMD Opteron(tm) Processor 8439 SE. The results are presented in Table 2.7. The average time includes also the calculation of the search directions, necessary sampling of designs, and the observation of constraints. The implemented genetic algorithm is always faster than the particle swarm optimization. Strategies (i) and (ii) are slower than the others, because the search for the nearest discrete possible finite element node is required. The Monte Carlo based search strategy is surprisingly slow in comparison to strategies (iii) to (vi). The explanation therefor is the increased computational effort to gain combinations without repetition. All other strategies are based on permutations with repetition, which can be generated more efficiently.

Summarizing, the best search strategy is strategy (i) with a genetic algorithm and the

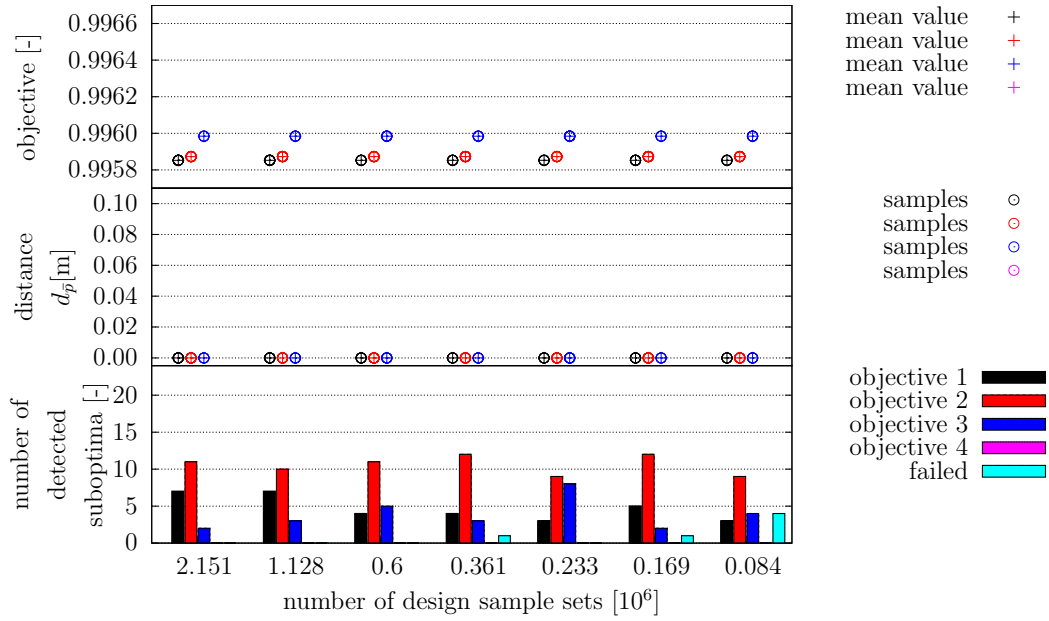


Figure 2.33: Results of search strategy (i) with geometry-based design variables and genetic algorithm.

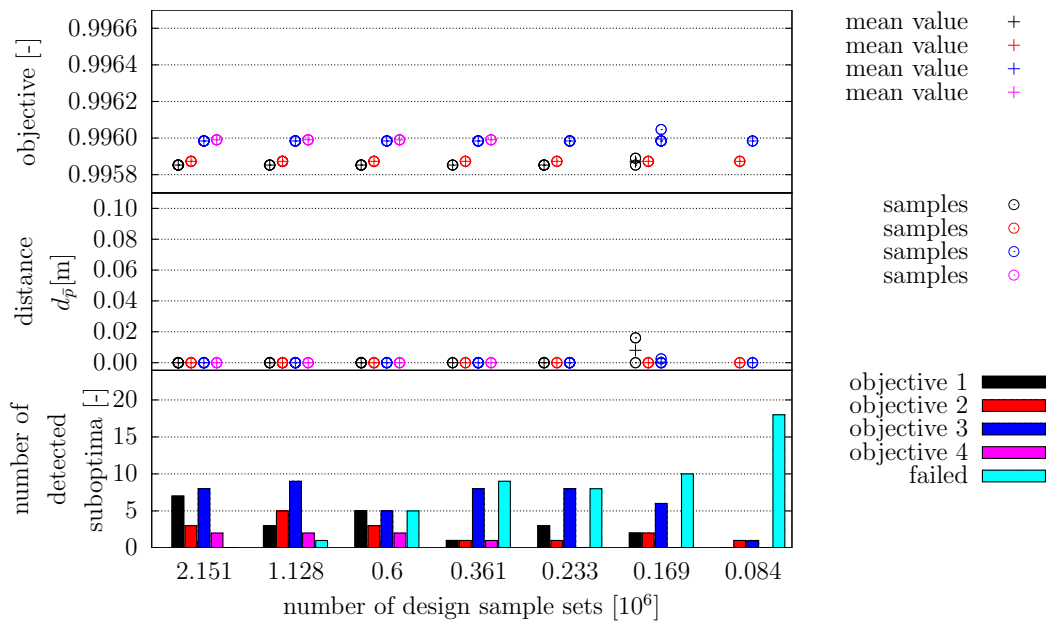


Figure 2.34: Results of search strategy (ii) with geometry-based design variables and particle swarm optimization.

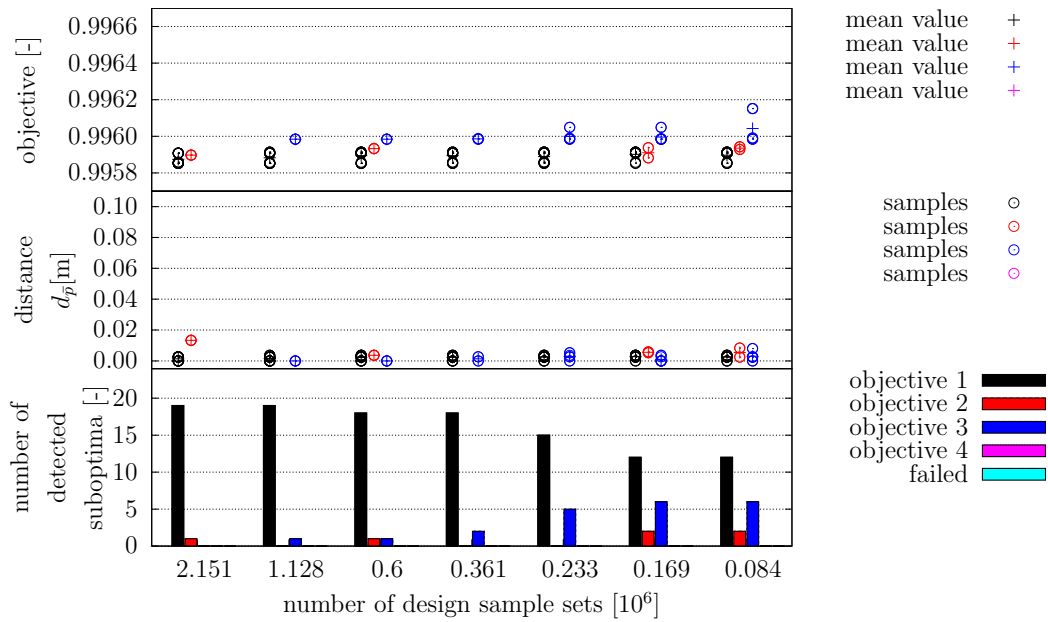


Figure 2.35: Results of search strategy (iii) with design variables based on a modified degree of freedom numbering and genetic algorithm.

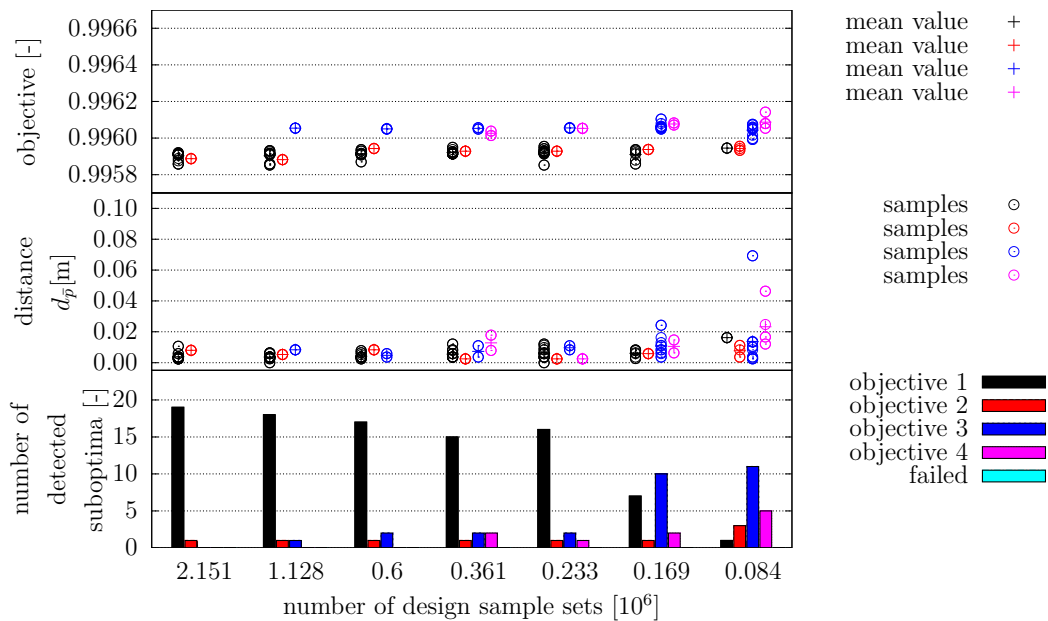


Figure 2.36: Results of search strategy (iv) with design variables based on a modified degree of freedom numbering and particle swarm optimization.

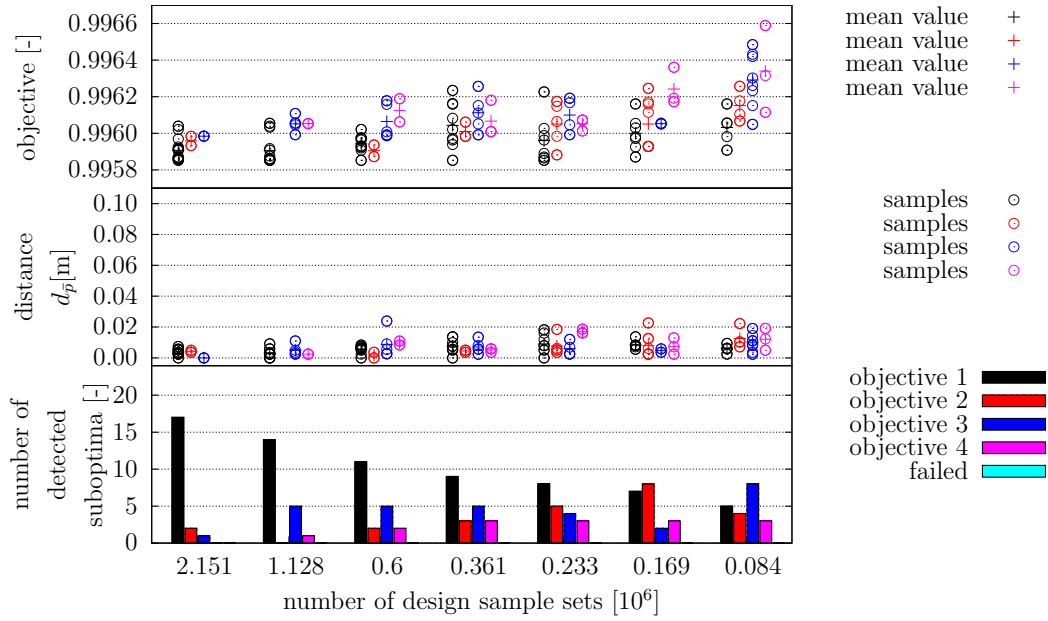


Figure 2.37: Results of search strategy (v) with design variables based on a randomly reordered degree of freedom numbering and genetic algorithm.

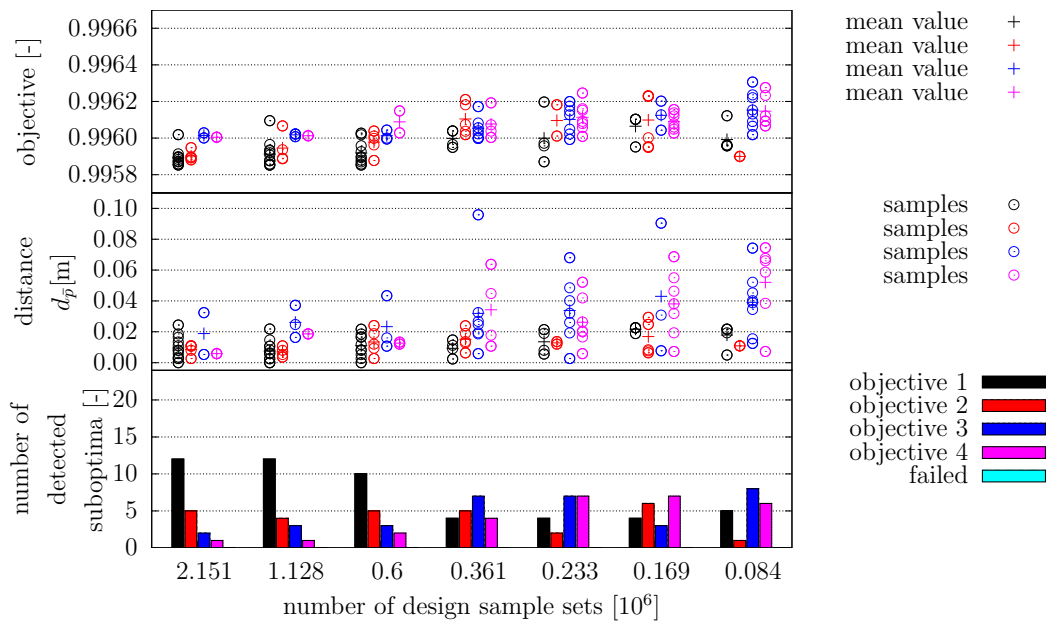


Figure 2.38: Results of search strategy (vi) with design variables based on a randomly reordered degree of freedom numbering and particle swarm optimization.

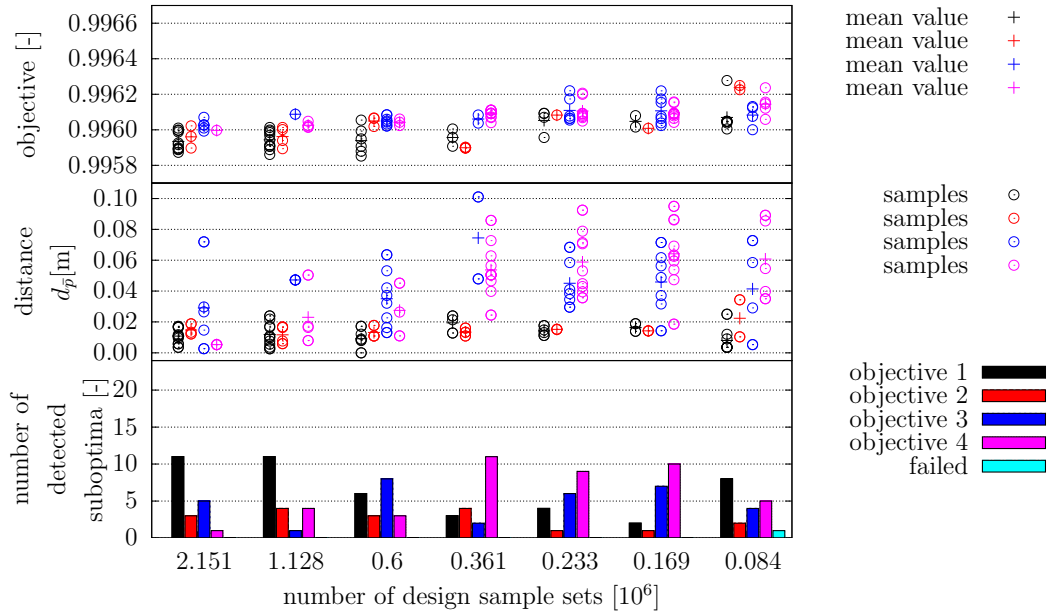


Figure 2.39: Results of search strategy (vii) based on Monte Carlo sampling.

geometry-based design variables. Like every other investigated strategy, even the best strategy will not be able to find one of the suboptima with a certain accuracy, if the number of available design sample sets is too small. However, very satisfying results can be obtained with only 168,840 assessed design sample sets. These are approximately 0.066 per cent of the total number of combinations. Nevertheless, the other search strategies can also provide suitable results with an increased but acceptable number of design sample sets.

By applying two reference sensors, the objective function can be reduced from 0.99781 to 0.99585. Following the limits of the applied objective function, it is not worthy to consider a higher number of reference sensors. According to Equation (2.49), the limit is given by 0.9952443.

2.8 Discussion

The presented chapter proposed an innovative strategy to determine optimal reference sensor positions for a roving sensor setup configuration. In contrast to alternative methods, this approach can be applied to all structures where vibration quantities like displacements, velocities, or accelerations, need to be measured. Moreover, the predicted spectral response can be related to a certain measurement noise level. The strategy relies on a prediction of expected power spectral amplitudes of the responses assuming a random weak stationary excitation. Such excitations are, for example, ambient vibrations or multiple impulse excitations. Based on the predicted power spectral amplitudes, an objective function could be mathematically formulated to detect the best positions for a set of ref-

erence sensors at a structure. To solve the optimization problem, a search strategy using nature inspired optimization algorithms, namely genetic algorithm and particle swarm optimization algorithm, were proposed. The inventive design variable description, which defined the sensor positions based on the geometry of the structure, improved the convergence and accuracy of the proposed standard optimization algorithms. Unfortunately, this advantage was partly neutralized by the increased computational effort.

The proposed approach was demonstrated by means of a numerical benchmark study on a simply supported beam. The derived results met experience-based expectations. Especially the derived position for one reference sensor, in case of ambient excitation to investigate the first four bending modes, met experience-based expectations. Furthermore, the approach has been applied on a real test specimen. As the computational effort was not neglectable for this case study, intensive investigations were performed with respect to computational effort and accuracy of various search strategies. Finally, a genetic algorithm with a geometry-based design variable description performed best. Only 0.066 percent of all possible combinations needed to be evaluated to obtain one of the best four suboptima. In addition, the predicted analytically derived and experimentally obtained power spectral densities of the responses were compared. The results showed an almost perfect agreement at the investigated measurement points for a random multi impulse excitation. Repeated identical tests assured statistical confidence.

Of course, the obtained results relied on an accurate finite element model and experimentally derived modal damping ratios. As the definition of reference sensor positions is a task in the pretest phase, such information is typically very uncertain. Hence, model uncertainties need to be considered. The resulting task of determining a robust optimal reference sensor configuration should be the topic of subsequent studies. Nevertheless, the proposed approach to determine optimal reference sensor positions contributes to a reduction of uncertainties with respect to extracted features from vibration measurements.

The energy-based modal assurance criterion

3.1 Problem overview

According to the framework for model updating described in Section 1.2, vibration-based model updating and prior sensitivity analysis need to compare and assign modal parameters obtained from experiments and numerical analyses. Regardless of which methods are applied for model updating or sensitivity analysis, the reliability of the obtained results is strongly related to a correct pairing of numerically derived and experimentally obtained mode shapes. This can be a challenge not only because of changes in the order of mode shapes due to a change of model input parameters, but also due to the fact that only a limited number of degrees of freedom are included in experimentally obtained mode shapes.

Most mode assignment strategies are based on criteria that were developed to investigate the correlation between an experimentally identified modal vector and the respective mode shape of a numerical model. These indicators were analyzed by several authors and were described in standard text books on experimental modal analysis such as [Ewins 2000a], [Maia and Silva 1997], and [Heylen et al. 1999].

One of these measures for the correlation of two mode shapes is the modal scale factor (MSF), originally developed in [Allemang et al. 1982]. This measure is a non-normalized indicator that depends on the scaling of two vectors. Accordingly, the magnitude of the MSF is strongly related to the applied normalization that is used in the analysis. This normalization can cause problems in context with a correct assignment of respective modes. The most widely used approach to check the correlation between experimental and numerical modal vectors is the modal assurance criterion (MAC). It was introduced in [Allemang et al. 1982] and has been discussed in several references (e.g., [Allemang 2003], [Ewins 2000b]) as well as in the aforementioned text books. The main advantages of the MAC are its independence of the scaling of mode shapes and its straightforward implementation, as it does not require coordinate-complete experimental eigenvectors or

system matrices [Morales 2005]. The possible range of the MAC is from zero to one. An application of the MAC in the context of topology optimization using reduced nodal information is given in [Kim et al. 2000]. Another criterion that is related to both, the MAC and the MSF, was suggested in [Waters 1995] and [Maia and Silva 1997]. It is based on normalized modal differences (NMD) and indicates maximal correlation by zero. The NMD indicator is not bounded and yields infinity in case of perfect orthogonal mode shapes. This can be a drawback in practice.

Several other correlation measures were derived from the MAC. For example, the linear modal assurance criterion (LMAC) proposed by [Morales 2005], linearizes the nonlinear behavior of the MAC. This results in a higher sensitivity in case of almost identical modal vectors. The coordinate modal assurance criterion (COMAC) [Lieven et al. 1988] and the enhanced coordinate modal assurance criterion (ECOMAC) [Hunt 1992] highlight the discrepancy of particular degrees of freedom and require a preliminary mode pairing. An overview and further discussion is given in [Allemang 2003] and [Morales 2005]. The weighted modal assurance criterion, also known as normalized cross orthogonality (NCO) (e.g., [Lieven et al. 1994], [Ewins 2000a], [Morales 2005]), includes additional physical information of the structure by using reduced or expanded mass or stiffness matrices of a finite element model. [Morales 2005] discussed this measure and indicated advantages compared to the MAC. However, one disadvantage is the introduction of additional errors and inaccuracies due to the necessary reduction or expansion procedure.

Unfortunately, the previously described criteria tend to fail under certain, but typical, conditions. There are cases in which a defined sensor setup can only capture the global dynamic behavior but not local modes, such as vibrations of certain structural elements or substructures. If one considers, for example, a space frame structure with sensors placed at structural nodes, the global bending and torsional modes of the system can be identified very well, but not the mode shapes of the truss rods. Due to small modal displacements of local modes at the measured global positions of the structure, artificial modes could be detected that can impair a correct mode assignment. Another example is an arch bridge, where only the bridge deck may be accessible for vibration measurements but not the arch. Here, it can become very difficult to distinguish the modes of the arch and the modes of the deck. This can be explained to a certain extent by the existence of vibration modes of the arch and bending and torsional modes of the bridge deck that have similar vibration shapes at the bridge deck [Ribeiro et al. 2009].

These problems mainly arise, if the spatial information in the experimentally identified mode shapes is incomplete. In an interactive analysis, the recognition of correct mode assignment can be managed by engineering judgment. However, automated processes, such as optimization or sensitivity analysis in the context with finite element model updating, require a different approach.

This chapter emphasizes on situations where the mentioned mode correlation criteria

may fail in the correct assignment of numerical to experimental modes due to incomplete spatial information in the experimental data. A novel mode assignment strategy is presented that enhances the purely mathematical modal assurance criterion (MAC) by physical information about stiffness distributions. In case of using mass-normalized eigenvectors, a relation with modal strain energies of numerically obtained mode shapes is achieved. Therefore, the new criterion is denoted by the energy-based modal assurance criterion (EMAC). Typical applications are systems where only unidirectional measurements are possible. The proposed method can also be applied to systems with several weakly coupled substructures, for which sufficient modal information is not available for all substructures. The developed method is suitable to be applied to an automatic mode assignment, for example, within an optimization procedure.

Even though modal strain energies have been applied to manifold problems, their use in combination with mode assignment is novel, as presented in this chapter. For example, various approaches that use modal strain energies to detect and locate structural damage were described in literature (e.g., [Shi et al. 1998], [Shi et al. 2000], [Li et al. 2006], [Cornwell et al. 1999]). In [Doebeling et al. 1997], it was suggested using modal strain energies to select the most relevant modes with respect to certain structural damage. Those modes were taken into account in model updating to detect and localize damage. Also in context with damage detection, [Reynders et al. 2007] suggested an approach that used measured modal strains to derive modal curvatures, which were applied as a damage indicator. Some of these approaches require a numerical model of the considered structure that has to describe the respective structural behavior with sufficient accuracy. This is usually obtained by updating the parameters of an initial model. If the available experimental modes are spatially incomplete, especially for systems with several substructures, the correct assignment of the respective modes is of great importance to the updating process.

For an enhanced understanding, the theory of the most relevant mode pairing criteria is briefly described in the following section, before the suggested criterion is defined. A numerical benchmark study and an experimental case study are presented. For these studies, the suggested approach leads to satisfying results with limited additional numerical effort while the application of the modal assurance criterion (MAC) fails to find the correct mode shapes.

3.2 Most important existing mode pairing criteria

3.2.1 Modal assurance criterion (MAC)

According to [Allemang et al. 1982], the modal assurance criterion (MAC) is defined as

$$(\mathbf{MAC})_{i,j} = \frac{\left(\{\hat{\Phi}\}_i^T \{\hat{\Phi}\}_j\right)^2}{\left(\{\hat{\Phi}\}_i^T \{\hat{\Phi}\}_i\right) \left(\{\hat{\Phi}\}_j^T \{\hat{\Phi}\}_j\right)}, \quad (3.1)$$

where $\{\hat{\Phi}\}_j$ is the reduced numerical eigenvector of mode j containing only the measured degrees of freedom. $\{\hat{\Phi}\}_i$ is the corresponding experimental eigenvector of the experimental derived mode i . The modal assurance criterion is a purely mathematical criterion for checking the consistency between two eigenvectors. The relation

$$(\bar{\mathbf{j}})_i = \underset{j}{\operatorname{argmax}}((\mathbf{MAC})_{i,j}) \quad (3.2)$$

assigns the numerical mode $(\bar{\mathbf{j}})_i$ to the experimental mode i . For perfectly correlated mode shapes that are in an appropriate order, the numbers i and $(\bar{\mathbf{j}})_i$ should agree with each other. As long as the modes are evidently separated based on the available sparse spatial information and the measurement noise is negligible, the modes can be assigned with high reliability. Some applications can be found in [Ribeiro et al. 2009], [Zabel et al. 2008b], [Cantieni et al. 2008b], [Keye 2003], [Kim et al. 2000], and [Doebbling et al. 1997].

According to [Morales 2005], the linearized version of the MAC, the linear modal assurance criterion (LMAC) is formulated by

$$(\mathbf{LMAC})_{i,j} = 1 - \frac{2}{\pi} \arccos \sqrt{(\mathbf{MAC})_{i,j}} \quad \text{with} \quad \arccos \sqrt{(\mathbf{MAC})_{i,j}} = \left[0, \frac{\pi}{2}\right]. \quad (3.3)$$

The possible values of the MAC and the LMAC range between zero and one, where one indicates a perfect fit. [Morales 2005] showed that the LMAC becomes more sensitive if two modes are almost identical. Advantages of the MAC and the LMAC are a convenient implementation and their independence of system matrices. The MAC and the LMAC do not consider system properties like an inhomogeneous mass or stiffness distribution [Allemang 2003]. Therefore, the application in those cases is not recommended.

3.2.2 Normalized cross orthogonality (NCO)

An extension of the MAC is the weighted modal assurance criterion (WMAC) [Allemang 2003], also denoted by modified MAC (ModMAC) [Penny et al. 1994] or normalized cross orthogonality (NCO) check, proposed by [Lieven et al. 1994] and [Ewins 2000b]. This normalized cross orthogonality is expressed by

$$(\mathbf{NCO})_{i,j} = \frac{\left(\{\hat{\Phi}\}_i^T \mathbf{W} \{\hat{\Phi}\}_j\right)^2}{\left(\{\hat{\Phi}\}_i^T \mathbf{W} \{\hat{\Phi}\}_i\right) \left(\{\hat{\Phi}\}_j^T \mathbf{W} \{\hat{\Phi}\}_j\right)}, \quad (3.4)$$

where \mathbf{W} is a weighting matrix. Usually, either the mass or the stiffness matrix of the numerical model are used as weighting matrix (e.g., [Lieven et al. 1994], [Penny et al. 1994], [Morales 2005], [Ewins 2000b]). If the mass matrix is applied, those modal components that are related to high kinetic energy contributions are accentuated while the application of the stiffness matrix highlights the high strain energy contributions [Penny et al. 1994]. Since usually only limited information about the total degrees of freedom is available from tests, reduced system matrices have to be used. It has to be recognized that a reduction of the system matrices introduces additional errors into the system. A frequently applied method to generate reduced system matrices is the Guyan reduction, also called static condensation [Guyan 1965]. The numerical effort increases with a smaller ratio between known and unknown degrees of freedom (DOFs). This increased numerical effort can be critical for some applications. A numerically more efficient method, the system equivalent reduction and expansion process (SEREP), has been proposed by [Avitabile et al. 1988] and [O'Callahan et al. 1989] and was briefly explained in [Ewins 2000a]. The condensed mass matrix \mathbf{M}_a^S and the condensed stiffness matrix \mathbf{K}_a^S are calculated by

$$\mathbf{M}_a^S = \mathbf{T}^T \mathbf{M} \mathbf{T} \quad \text{and} \quad \mathbf{K}_a^S = \mathbf{T}^T \mathbf{K} \mathbf{T}. \quad (3.5)$$

The full size mass and stiffness matrices are denoted by \mathbf{M} and \mathbf{K} , respectively.

The transformation matrix $\mathbf{T} = \mathbf{\Phi} \hat{\mathbf{\Phi}}^+$ is given by the numerical eigenvector matrix $\mathbf{\Phi}$ with dimension of the numerical model and the generalized inverse of the reduced eigenvector matrix $\hat{\mathbf{\Phi}}$. If $\hat{\mathbf{\Phi}}$ consists of a independent rows (measured DOFs) and m independent columns (number of considered modes), the generalized inverse $\hat{\mathbf{\Phi}}^+$ can be calculated using the singular value decomposition $\hat{\mathbf{\Phi}} = \mathbf{L} \mathbf{S} \mathbf{R}^T$ [Ewins 2000b] as $\hat{\mathbf{\Phi}}^+ = \mathbf{R} \mathbf{S}^+ \mathbf{L}^T$. Assuming the weighting matrix of Equation (3.4) is given by a SEREP-condensation, the normalized cross orthogonality is also referred to as SEREP cross orthogonality (SCO) [Ewins 2000b].

Similar to the linearized modal assurance criterion, an extension of the NCO has been proposed by [Morales 2005].

$$(\mathbf{LNCO})_{i,j} = 1 - \frac{2}{\pi} \arccos \sqrt{(\mathbf{NCO})_{i,j}} \quad \text{with} \quad \arccos \sqrt{(\mathbf{NCO})_{i,j}} = \left[0, \frac{\pi}{2} \right] \quad (3.6)$$

The values of NCO and LNCO range between zero and one. One indicates a perfect fit.

3.3 Mode assignment using the energy-based modal assurance criterion

In case of a mass normalized eigenvector matrix $\mathbf{\Phi}$, where the j th column corresponds to the eigenvector of the j th eigenvalue $(\omega)_j^2$, one has

$$\mathbf{\Phi}^T \mathbf{M} \mathbf{\Phi} = \mathbf{I} \quad (3.7)$$

and

$$\Phi^T \mathbf{K} \Phi = \mathbf{I}(\omega \circ \omega) \quad (3.8)$$

with the positive definite mass matrix \mathbf{M} , the positive definite stiffness matrix \mathbf{K} , and an identity matrix \mathbf{I} . According to Equation (3.8), the total modal strain energy for each mode j is $\frac{1}{2}(\omega)_j^2$. By separating the available degrees of freedom into n independent clusters, the eigenvector of mode j can be rewritten as

$$\{\Phi\}_j^T = \left[\{\Phi\}_j^{(1)T} \quad \{\Phi\}_j^{(2)T} \quad \dots \quad \{\Phi\}_j^{(n)T} \right]^T. \quad (3.9)$$

Then, the corresponding clustered stiffness matrices $\mathbf{K}^{(k,l)} \forall k, l = 1, 2, \dots, n$ are given by

$$\mathbf{K} = \begin{bmatrix} \mathbf{K}^{(1,1)} & \mathbf{K}^{(1,2)} & \dots & \mathbf{K}^{(1,n)} \\ \mathbf{K}^{(2,1)} & \mathbf{K}^{(2,2)} & \dots & \mathbf{K}^{(2,n)} \\ \vdots & \vdots & \ddots & \vdots \\ \mathbf{K}^{(n,1)} & \mathbf{K}^{(n,2)} & \dots & \mathbf{K}^{(n,n)} \end{bmatrix}. \quad (3.10)$$

Hence, the modal strain energy for mode j with respect to cluster k is obtained.

$$(\text{MSE})_j^{(k)} = \frac{1}{2} \sum_{l=1}^n \{\Phi\}_j^{(k)T} \mathbf{K}^{(k,l)} \{\Phi\}_j^{(l)} \quad (3.11)$$

Accordingly, the total strain energy of mode j is represented by

$$\sum_{k=1}^n (\text{MSE})_j^{(k)} = \frac{1}{2} \sum_{k=1}^n \sum_{l=1}^n \{\Phi\}_j^{(k)T} \mathbf{K}^{(k,l)} \{\Phi\}_j^{(l)} = \frac{1}{2} \{\Phi\}_j^T \mathbf{K} \{\Phi\}_j = \frac{1}{2}(\omega)_j^2. \quad (3.12)$$

Equations (3.11) and (3.12) yield the relative modal strain energy of mode j with respect to cluster k

$$(\Pi)_j^{(k)} = \frac{(\text{MSE})_j^{(k)}}{\sum_{k=1}^n (\text{MSE})_j^{(k)}} = \frac{\sum_{l=1}^n \{\Phi\}_j^{(k)T} \mathbf{K}^{(k,l)} \{\Phi\}_j^{(l)}}{\{\Phi\}_j^T \mathbf{K} \{\Phi\}_j} \quad \text{with} \quad \sum_{k=1}^n (\text{MSE})_j^{(k)} \neq 0. \quad (3.13)$$

Therefore, multiplying Equation (3.1) by Equation (3.13), results in an energy-based modal assurance criterion for each cluster k

$$(\text{EMAC})_{i,j}^{(k)} = (\Pi)_j^{(k)} (\text{MAC})_{i,j}. \quad (3.14)$$

Based on the linearized modal assurance criterion (LMAC), an equivalent energy-based linear modal assurance criterion can be defined.

$$(\text{ELMAC})_{i,j}^{(k)} = (\Pi)_j^{(k)} (\text{LMAC})_{i,j} \quad (3.15)$$

The assignment of modes is given similarly to the modal assurance criterion, where the numerical mode with the largest value is assigned to the respective experimental mode. Analogously to Equation (3.2) the assignment can be formulated with

$$(\bar{\mathbf{j}})_i^{(k)} = \operatorname{argmax}_j \left((\mathbf{EMAC})_{i,j}^{(k)} \right). \quad (3.16)$$

The chosen numerically derived mode $(\bar{\mathbf{j}})_i^{(k)}$ depends on the experimentally obtained mode i and the corresponding cluster k . The relative modal strain energy $(\mathbf{\Pi})_j^{(k)}$, which ranges between zero and one, and the modal assurance criterion $(\mathbf{MAC})_{i,j}$ are connected by multiplication. Therefore, the range of the energy-based modal assurance criterion $(\mathbf{EMAC})_{i,j}^{(k)}$ is bounded between zero and one. The relative modal strain energy of the observed cluster reflects the amount of energy, which can be covered by the measurements. By this interpretation, the EMAC involves the possibility that a numerical mode can be represented by both, the measurements and the purely mathematical correlation between scaled measured and scaled numerical modes. The workflow, visualized in Figure 3.1, summarizes the procedure of pairing modes by the proposed energy-based modal assurance criterion.

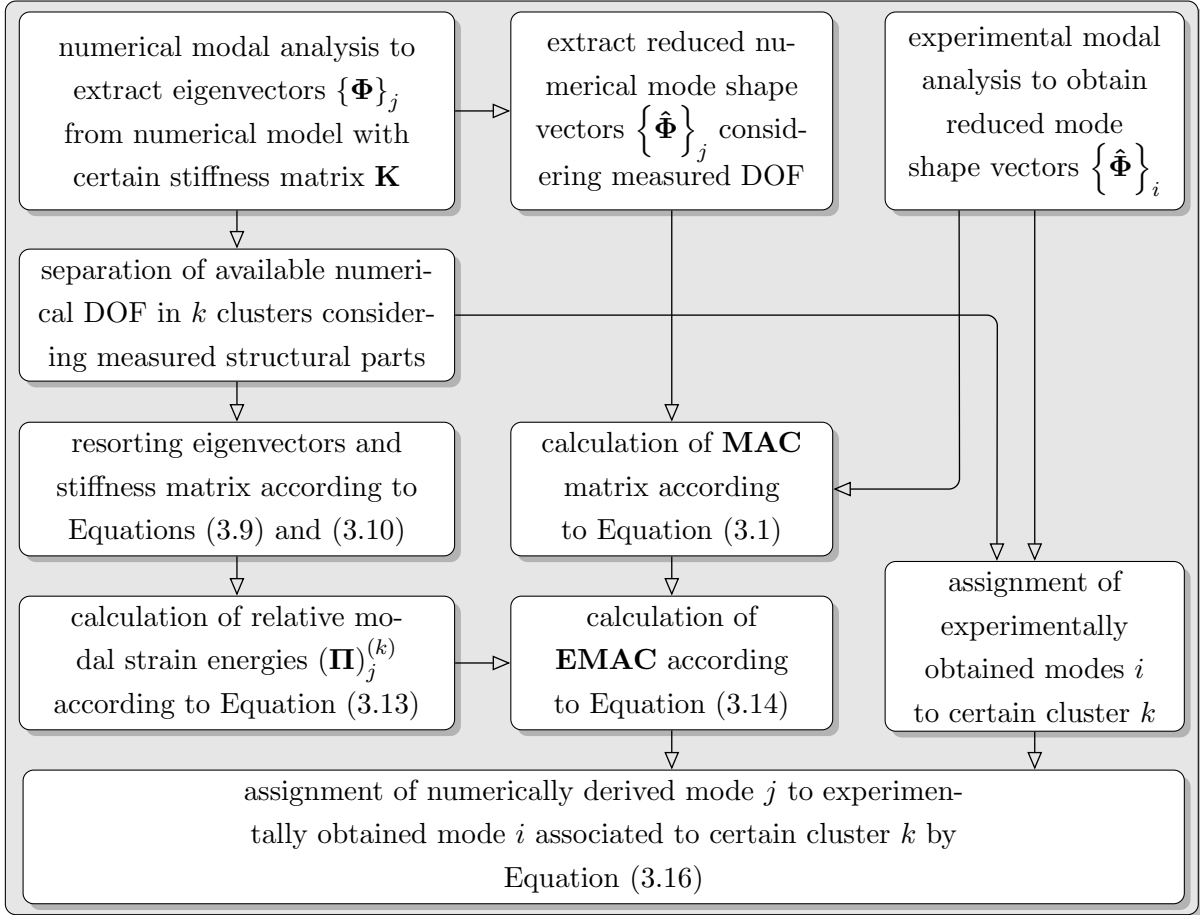


Figure 3.1: Workflow for mode pairing using the energy-based modal assurance criterion.

The success of the proposed method depends on the selected numerical degrees of freedom, which will be clustered. Since this selection strongly hinges on the specific structure to be investigated and the applied experimental setup, it is difficult to present a general guideline. However, the clusters should be chosen in a way that the measured degrees of freedom can be separated from those degrees of freedom that were not considered in the tests. In case of a structure that consists of several substructures, the selection of clusters should be also related to the substructures. For example, if an arch bridge is only instrumented at the main slab and not at the arch itself, it is more likely that a certain experimentally obtained mode is associated with a mode that activates high energies in the main slab. Therefore, the EMAC should be related to the cluster that contains all degrees of freedom of the main slab. Another example is the test specimen described in Section 2.7. The twelve chosen measurement points can cover all global modes of the structure, but not the local modes of the screws. Therefore, the degrees of freedom of the main structure and the degrees of freedom of the screws should be separated in two clusters. Then, the mode assignment for the global modes can be related to the cluster associated with the main structure. For a better understanding how to choose appropriate clusters, further examples of typical cases are presented in the following section.

3.4 Benchmark study: Cantilever truss

3.4.1 Description of the system

The numerical example is based on a 20 degree of freedom cantilever truss consisting of 12 nodes and 21 truss members. It has been suggested in [Khodaparast et al. 2008b] for a numerical model updating benchmark. The geometry is presented in Figure 3.2. The cross-sectional area and the mass density of all truss members are defined to 0.03m^2 and $2700\frac{\text{kg}}{\text{m}^3}$, respectively. The material is linearly elastic with a Young's modulus of $7 \cdot 10^{10}\frac{\text{N}}{\text{m}^2}$.

For the numerical test example, it is assumed that the vertical modal displacements at the four measurement points (MP), indicated in Figure 3.2, are available for identifying

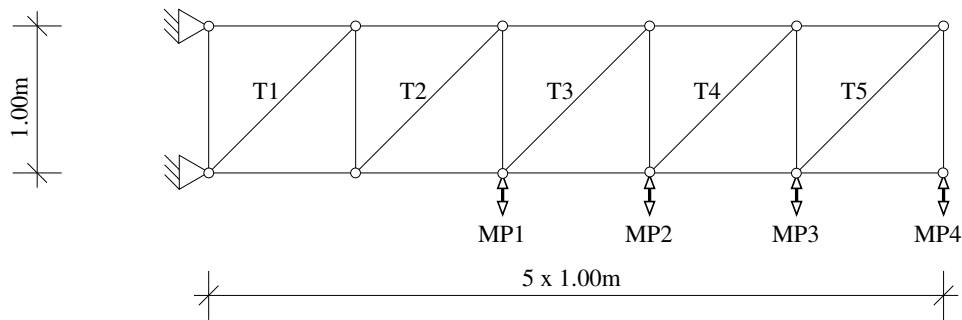


Figure 3.2: Geometrical description of the cantilever truss system.

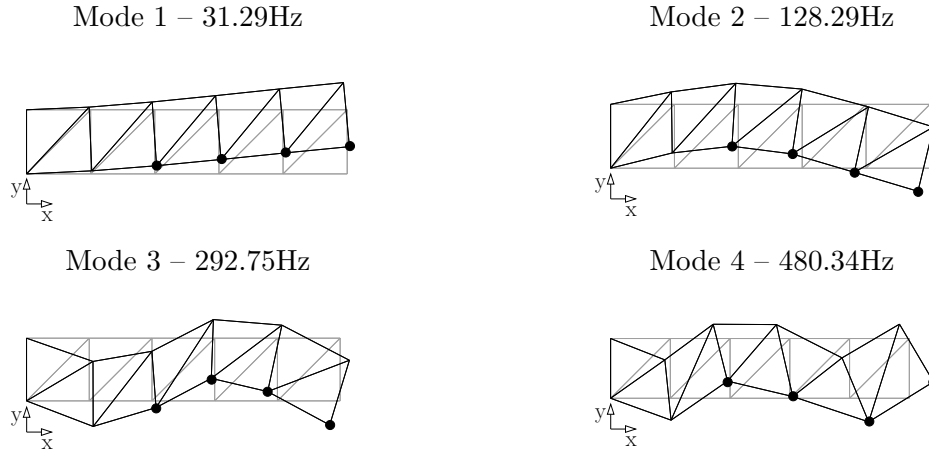


Figure 3.3: First four experimental mode shapes of the system obtained by simulation. Only the vertical modal displacements of the marked positions (●) are assumed to be available from tests.

Table 3.1: Original modal displacements.

	Mode 1	Mode 2	Mode 3	Mode 4
MP1	-0.0127	0.0344	0.0107	0.0287
MP2	-0.0225	0.0224	-0.0360	0.0029
MP3	-0.0327	-0.0064	-0.0149	-0.0395
MP4	-0.0425	-0.0362	0.0384	0.0275

Table 3.2: Perturbations of modal displacements.

	Mode 1	Mode 2	Mode 3	Mode 4
MP1	0.0010	0.0007	-0.0001	-0.0015
MP2	-0.0002	0.0043	-0.0001	-0.0002
MP3	-0.0004	-0.0003	-0.0002	0.0016
MP4	-0.0012	0.0041	0.0016	-0.0014

the first four vertical modes. The corresponding mode shapes are shown in Figure 3.3. Furthermore, it is assumed that the mode shapes, supposed to be identified from tests, are affected by some inaccuracies. These inaccuracies are simulated by adding independent normally distributed perturbations with a mean value of 0 and a coefficient of variation of 0.05 to the calculated modal displacements. These noise disturbed mode shapes are referred to as experimental mode shapes in the following. The original modal displacements and one set of random perturbations of noisy modal displacements are given in Table 3.1 and 3.2, respectively.

3.4.2 Application of mode assignment

It is assumed that one design of an optimization run or one sample of a sensitivity analysis leads to a change of the Young's moduli of the diagonal elements T2 and T4 to $2.2 \cdot 10^{11} \frac{\text{N}}{\text{m}^2}$. The first nine modes of the changed system are presented in Figure 3.4. For reliable results in the subsequent analyses, it is essential that the experimentally obtained modes are assigned to the most likely numerical modes based only on the vertical modal displacements of the four measurement points. The MAC values between numerical and noise disturbed experimental modes are presented in Figure 3.5. It can be observed that the MAC values between the second experimental mode and the second and third numerical mode are close to one. This indicates an almost perfect agreement in both cases. If the original MAC is used to select the mode, the wrong third numerical mode, which is mainly a longitudinal mode, will be assigned to the second experimental mode, because the MAC value is slightly higher. The results are illustrated in Figures 3.6 and 3.7. This wrong mode assignment can cause significant problems for some investigations, such as sensitivity analysis or model updating.

The proposed alternative approach uses the energy-based modal assurance criterion to pair correct modes. Therefore, the total degrees of freedom are separated into two clusters. Cluster 1 contains the vertical degrees of freedom and cluster 2 contains the horizontal degrees of freedom. The relative modal strain energies $(\mathbf{\Pi})_j^{(k)}$ according to Equation (3.13) are visualized in Figure 3.8. By this criterion, the modes can be distinguished into primary horizontal and primary vertical modes. The EMAC according to Equation (3.14)

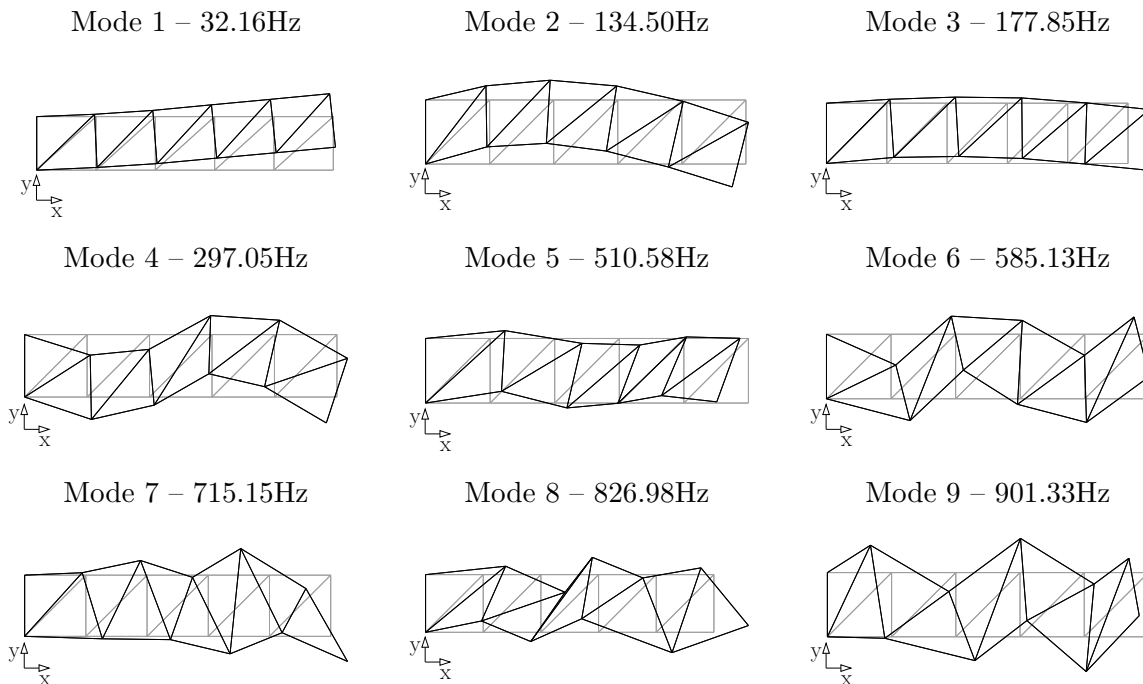


Figure 3.4: First nine mode shapes of the modified numerical model.

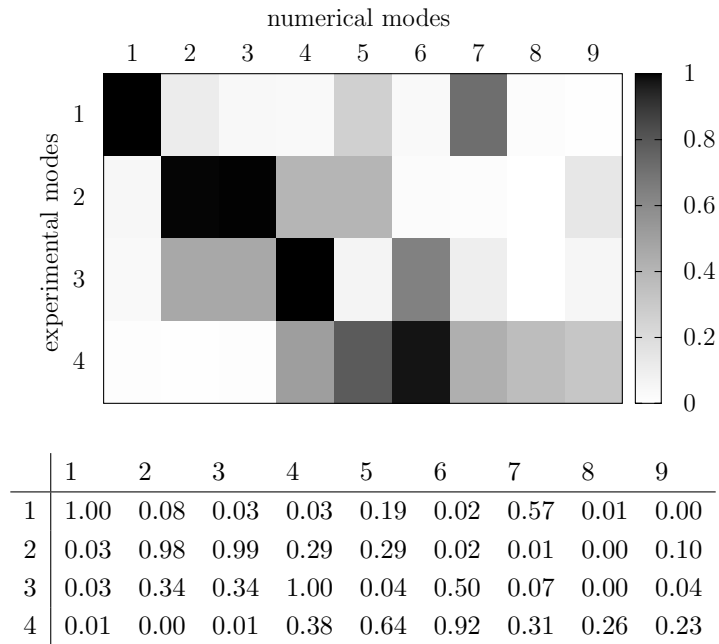


Figure 3.5: Modal assurance criterion (MAC) – numerical vs. experimental modes.

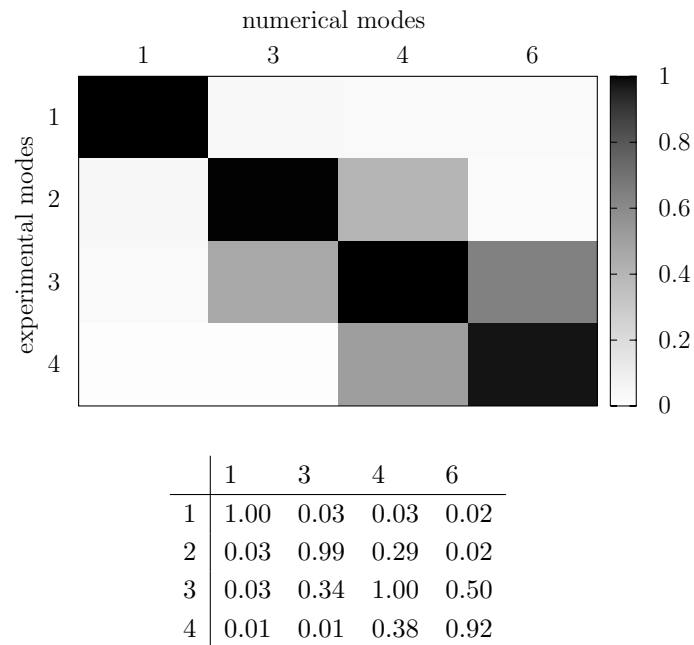


Figure 3.6: Modal assurance criterion (MAC) – identified numerical vs. experimental modes.

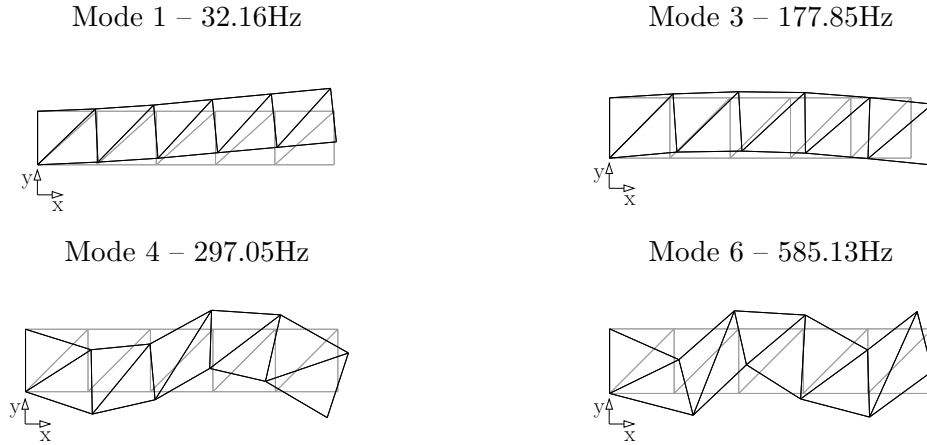


Figure 3.7: Identified mode shapes from numerical modal analysis using MAC.

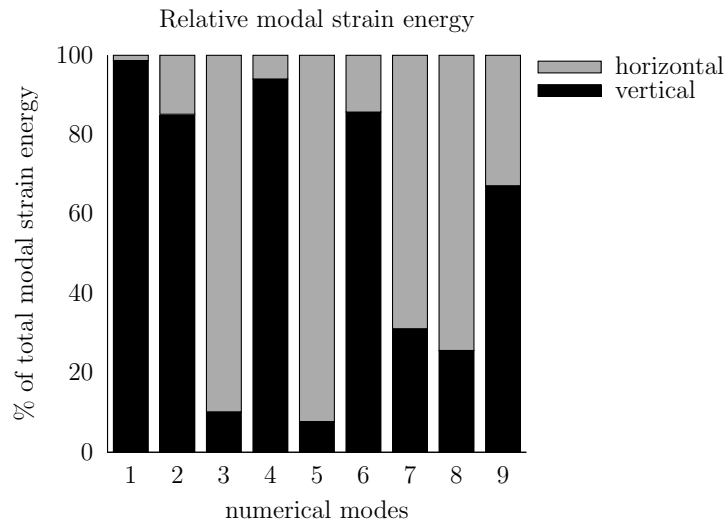


Figure 3.8: Relative modal strain energies for vertical and horizontal degrees of freedom.

is presented in Figure 3.9. The largest value in each row indicates to which numerical mode the respective experimental mode has to be assigned. The EMAC and the original MAC of the identified modes are shown in Figures 3.10 and 3.11, respectively. Figure 3.12 presents the selected numerical mode shapes. It can be observed that the correct second numerical mode can be assigned to the second experimental mode.

This numerical benchmark study shows that the MAC is able to pair the correct modes as long as the modes can be reliably separated based on the sparse spatial information. If the modes cannot be separated by the available information, the physical information of the modes, namely the modal strain energy, can be used to distinguish between modes with similar MAC values.

Obviously, the size of perturbation is essential for the success of the investigated mode assignment criteria. Therefore, the coefficient of variation that determines the size of

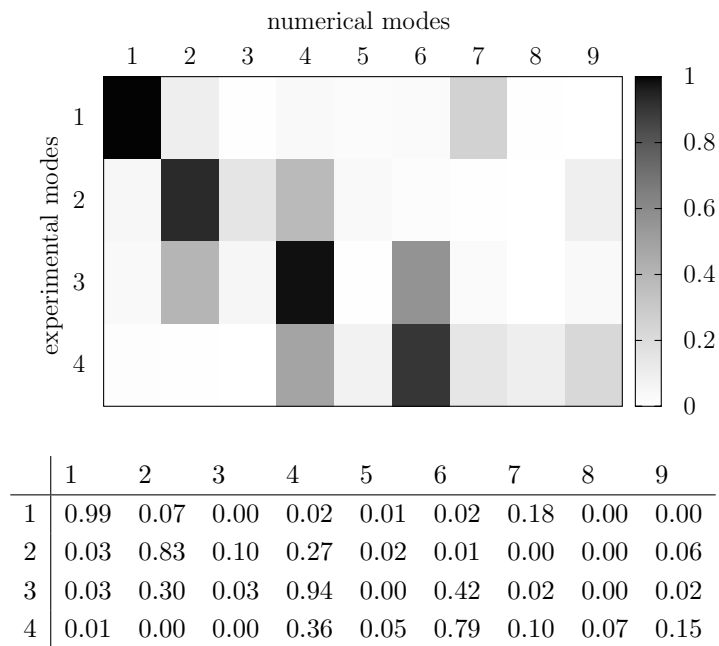


Figure 3.9: Energy-based modal assurance criterion (EMAC) for vertical degrees of freedom – numerical vs. experimental modes.

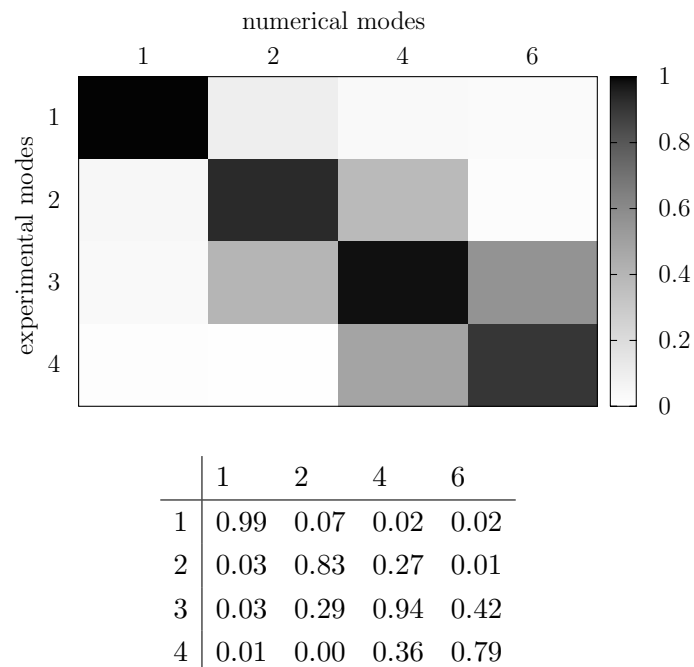


Figure 3.10: Energy-based modal assurance criterion (EMAC) for vertical degrees of freedom – identified numerical vs. experimental modes.

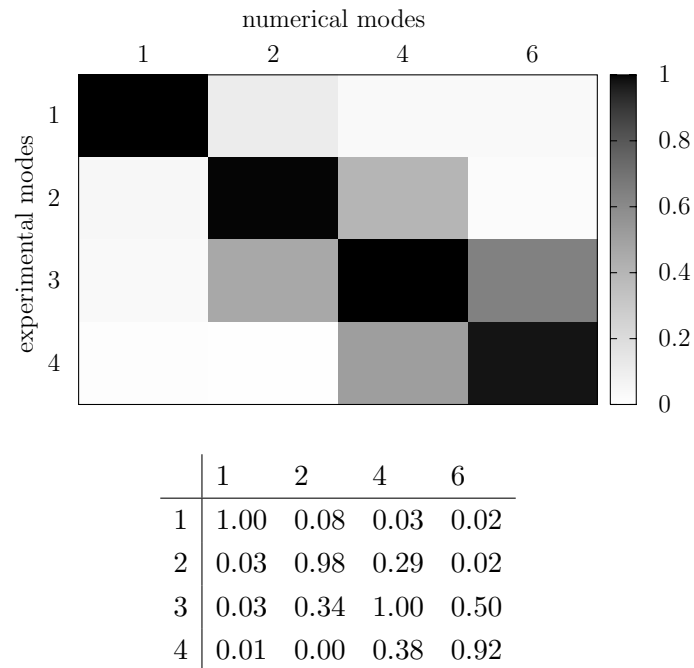


Figure 3.11: Modal assurance criterion (MAC) – identified numerical vs. experimental modes. Numerical modes are previously selected by the energy-based modal assurance criterion (EMAC).

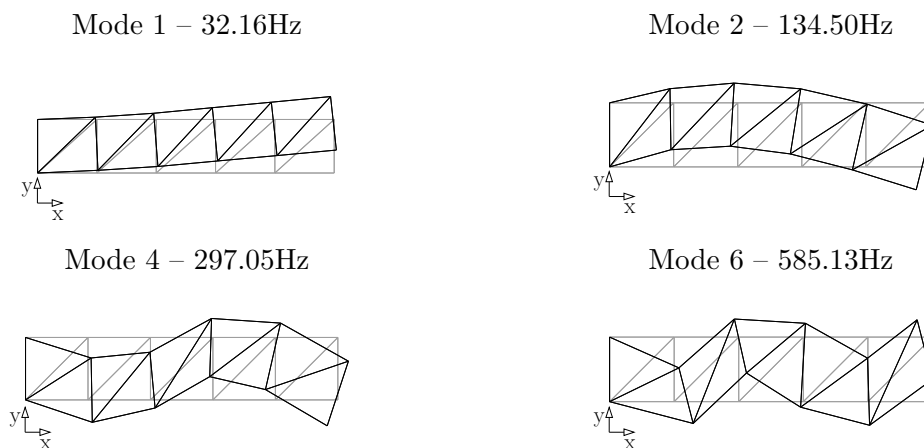


Figure 3.12: Identified mode shapes from numerical modal analysis using the energy-based modal assurance criterion (EMAC).

Table 3.3: Dependency of successful mode assignment on the degree of noise.

degree of noise (coefficient of variation)	mode assignment criterion	assignment	
		successful	failed
0.02	MAC	1000	0
	EMAC	1000	0
0.05	MAC	920	80
	EMAC	1000	0
0.10	MAC	787	213
	EMAC	1000	0

perturbation is varied by 2%, 5%, and 10%. For each value, 1000 samples are generated based on a normal distribution using the Monte Carlo method. Table 3.3 shows the success of both mode assignment criteria, MAC and EMAC. It can be concluded that the EMAC is very robust and is always able to assign the right modes. The MAC criterion shows good results for the lowest level of perturbations. However, with increasing size of perturbations, the possibility of getting a failed mode assignment increases by using the MAC criterion. For a coefficient of variation of 10%, more than 20% of the mode assignments failed.

Hence, the success of using the MAC as mode pairing criterion in the presented benchmark study depends strongly on the size and distribution of the perturbations itself, while the success of the proposed EMAC is less sensitive to a usually acceptable size of perturbations.

3.4.3 Optimization

Assuming that only the Young's moduli of the diagonal element T2 and T4 are unknown, an optimization problem can be established. The Young's moduli are defined by $E(T2) = 7k_2 \cdot 10^{10} \frac{N}{m^2}$ and $E(T4) = 7k_4 \cdot 10^{10} \frac{N}{m^2}$, respectively. Based on the values $k_2 = 1$ and $k_4 = 1$, the artificial experimentally derived modal parameters are defined and presented in Figure 3.3. The subsequently applied measured noise disturbed modal displacements are obtained by adding the perturbations given in Table 3.2 to the original values of Table 3.1. Hence, the measured feature vector

$$\mathbf{z}_m = \left[(\mathbf{f}_m)_1 \quad (\mathbf{f}_m)_2 \quad (\mathbf{f}_m)_3 \quad (\mathbf{f}_m)_4 \quad 1 \quad 1 \quad 1 \quad 1 \right]^T \quad (3.17)$$

is assembled by the first four measured known natural frequencies $(\mathbf{f}_m)_i$ and the four values of 1 assuming the best value for the MAC of the first four paired modes. The updated feature vector is given by

$$\mathbf{z}_p = \left[(\mathbf{f}_p)_1 \quad (\mathbf{f}_p)_2 \quad (\mathbf{f}_p)_3 \quad (\mathbf{f}_p)_4 \quad (\mathbf{MAC}_p)_{1,1} \quad (\mathbf{MAC}_p)_{2,2} \quad (\mathbf{MAC}_p)_{3,3} \quad (\mathbf{MAC}_p)_{4,4} \right]^T \quad (3.18)$$

where $(\mathbf{f}_p)_i$ are the four updated numerical natural frequencies at optimization step p obtained by the mode pairing strategy. The MAC values are related to the four measured modes and the corresponding identified numerical modes. The objective function

$$J = \sqrt{(\mathbf{z}_m - \mathbf{z}_p)^T \mathbf{W} (\mathbf{z}_m - \mathbf{z}_p)} \quad \text{with} \quad J(\mathbf{z}_p(\boldsymbol{\theta}_p)) \rightarrow \min \quad (3.19)$$

is a weighted Euclidean distance between the measured feature vector \mathbf{z}_m and the updated feature vector \mathbf{z}_p , whereas \mathbf{z}_p depends on the unknown parameters $\boldsymbol{\theta}_p = \begin{bmatrix} k_2 & k_4 \end{bmatrix}^T$. The weighting matrix \mathbf{W} is a diagonal matrix defined by

$$\mathbf{W} = \text{diag} \left((\mathbf{f}_m)_1^{-2}, (\mathbf{f}_m)_2^{-2}, (\mathbf{f}_m)_3^{-2}, (\mathbf{f}_m)_4^{-2}, 1, 1, 1, 1 \right). \quad (3.20)$$

The initial estimates for the optimization are $\boldsymbol{\theta}_0 = \begin{bmatrix} 1.05 & 0.90 \end{bmatrix}^T$.

Using the adaptive response surface approach (e.g., [Etman et al. 1996], [Kurtaran et al. 2002]) of the software optiSLang [Dynardo GmbH 2009], optimal values can be obtained for $\boldsymbol{\theta}_p$. The optimization at the approximated surfaces is based on a combination of the gradient-based method SQP (sequential quadratic programming) and genetic algorithm (GA) (e.g., [Holland 1992], [Goldberg 1989]). Details about the optimization method are described in Appendix B.3. The results are independent from the starting values $\boldsymbol{\theta}_0$ within the given range.

The application of the MAC-based mode pairing strategy results in optimal values $\boldsymbol{\theta}_p = \begin{bmatrix} 0.70182 & 0.70768 \end{bmatrix}^T$, which do not reflect the nominal values $\begin{bmatrix} 1.00000 & 1.00000 \end{bmatrix}^T$. This effect is explained by an inappropriate mode assignment.

The correct values $\boldsymbol{\theta}_p = \begin{bmatrix} 1.00010 & 0.99994 \end{bmatrix}^T$ were found by using the EMAC-based mode pairing strategy. As the optimization itself is performed on the response surface, 250 objective function evaluations were required in total to define the supporting points for the response surface approximations. On a computer with an Intel Xeon 5130 (2.00GHz) processor, the total computation time for the model updating is 10 minutes. The high number of objective function evaluations and the total computational time is mainly caused by the desired accuracy of the parameters. Analogously to the previous study, the relative modal strain energies are related to all vertical degrees of freedom of the numerical model. The shapes of the objective functions are given in Figures 3.13 and 3.14. The respective minima are marked by white dots, which coincides with the identified values. Accordingly, one can deduce that inaccurately identified values are not caused by the choice of an inappropriate optimization strategy. The objective function related to a MAC-based mode assignment is incorrectly established. Note that the sharp edges in Figures 3.13 and 3.14 indicate discontinuities in the objective functions due to mode switches. Furthermore, the optimum using the MAC-based approach is coincident with the discontinuity of the objective function, where the gradients in the vicinity of the optimum are small along the edge, which is visualized in Figure 3.13b. This causes an additional challenge for an optimization strategy.

These observations verify that the application of an inappropriate mode assignment strategy in a model updating algorithm can lead to wrong results for the optimization.

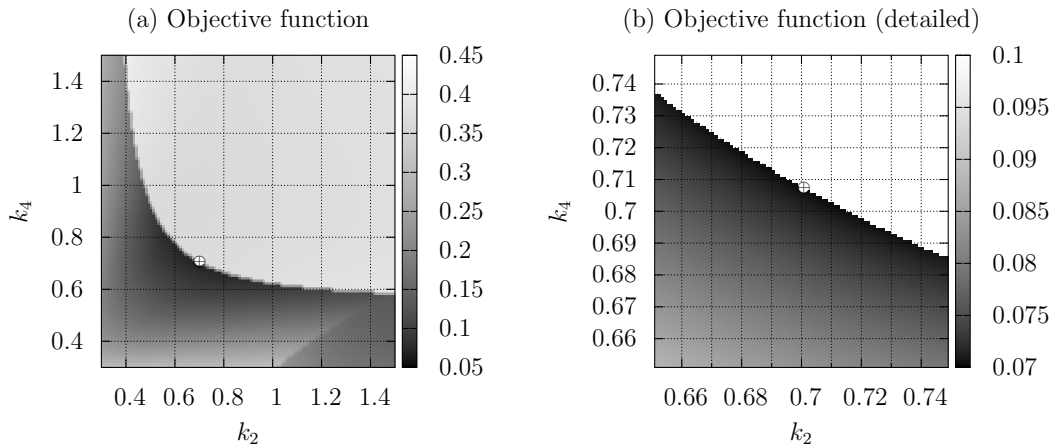


Figure 3.13: Objective function using MAC-based mode pairing strategy. The minimum is obtained at $(k_2, k_4) = (0.70182, 0.70768)$ and marked by the white dot. Diagram (b) shows a detail of diagram (a).

Objective function using EMAC-based mode pairing strategy

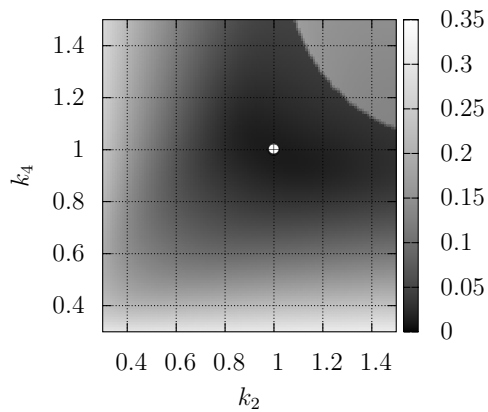


Figure 3.14: Objective function using EMAC-based mode pairing strategy. The minimum is obtained at $(k_2, k_4) = (1.00010, 0.99994)$ and is marked by the white dot.

3.5 Case study: High-speed railway bridge EÜ Erfttalstraße

3.5.1 Description of the system

The numerical model describes a high-speed railway bridge on the line between Cologne and Brussels, which was discussed in several references, like [Brehm et al. 2009a], [Cantieni et al. 2008a], and [Cantieni et al. 2008b]. This filler beam bridge consists of two main superstructures, each carrying one rail line. The rail is installed on ballast, which is continuously distributed over both superstructures and the transition zones between the bridge and the embankment. Figures 3.15, 3.16, and 3.17 show the simplified bridge model and the resulting finite element model. A set of seven experimental mode shapes and corresponding natural frequencies are available from an experimental campaign, which was described in [Cantieni et al. 2008a] and [Cantieni et al. 2008b]. The mode shapes and the natural frequencies obtained from the experimental campaign are listed in Table 3.4. Due to limitations in the experimental setup, the modal displacements are only available in vertical direction at 44 points at the bottom side of the composite slabs.

As the model is supposed to be used for model updating, a correct mode assignment is essential. A total number of 35 uncertain material parameters was initially defined. These parameters are listed in Table 3.5.

3.5.2 Application of mode assignment

One particular set of 35 unknown model parameters was generated by a stochastic sampling scheme. For this set, a numerical modal analysis has been performed to extract the first 200 mode shapes and natural frequencies, which represent a frequency range between 0Hz and 50Hz. Many modes are primary modes of the rail system containing a small modal deflection amplitude of the bridge deck. Due to noise influences, these modes are unlikely to be detected with the measured data acquired at the bottom side of the slabs.

First, the original modal assurance criterion (MAC) is used to assign the experimental to the corresponding numerical mode shapes. The **MAC** matrix for all 200 numerical and seven experimental modes is depicted in Figure 3.18a. The largest value in each row indicates the numerical mode that has to be assigned to the respective experimental mode. Based on this assignment, the **MAC** matrix, illustrated in Figure 3.18a, can be reduced. The reduced **MAC** matrix is presented in Figure 3.18b. Since some MAC values between a certain measured mode and the numerical modes are almost identical, the selection is sensitive to noise and small changes of the input parameter values.

Alternatively, the energy-based modal assurance criterion (EMAC) is applied for mode

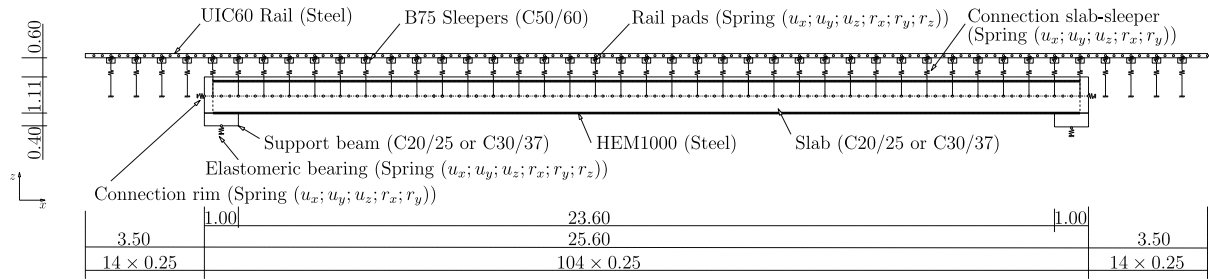


Figure 3.15: Longitudinal section of the simplified bridge model.

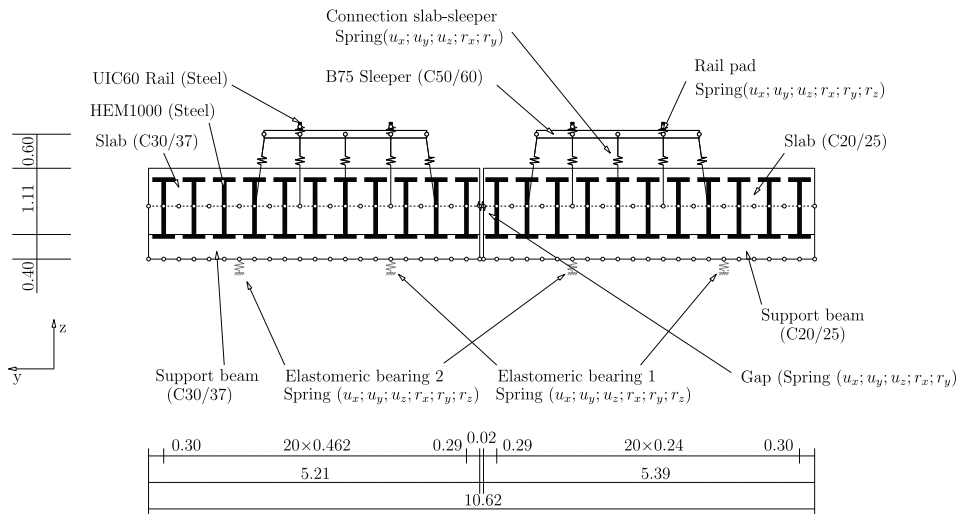


Figure 3.16: Cross section of the simplified bridge model.

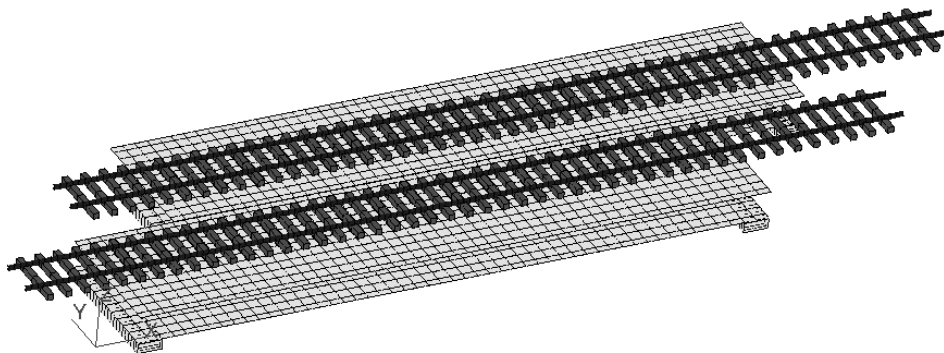


Figure 3.17: Finite element model of the bridge.

assignment. As the sensors are homogeneously distributed at the bottom side of the main slabs in a vertical direction, the relative modal strain energies $(\mathbf{\Pi})_j^{(k)}$, and therefore the corresponding EMAC values, are based on a cluster with all vertical degrees of freedom of the composite slabs with respect to the numerical model. The resulting **EMAC** matrix is visualized in Figure 3.19a. Figure 3.19b shows the EMAC values for the identified numerical modes. The MAC values of the selected numerical modes are illustrated in Figure 3.20. It has been assumed that the main modal strain energy is present in the vertical components of the two main composite slabs. Since only one large EMAC value is present in each row, the selection is insensitive with respect to noise and small input parameter value changes.

The compared mode selection methods, based on MAC and EMAC, assign some different numerical modes. The obtained modes are compared in Table 3.4. It should be

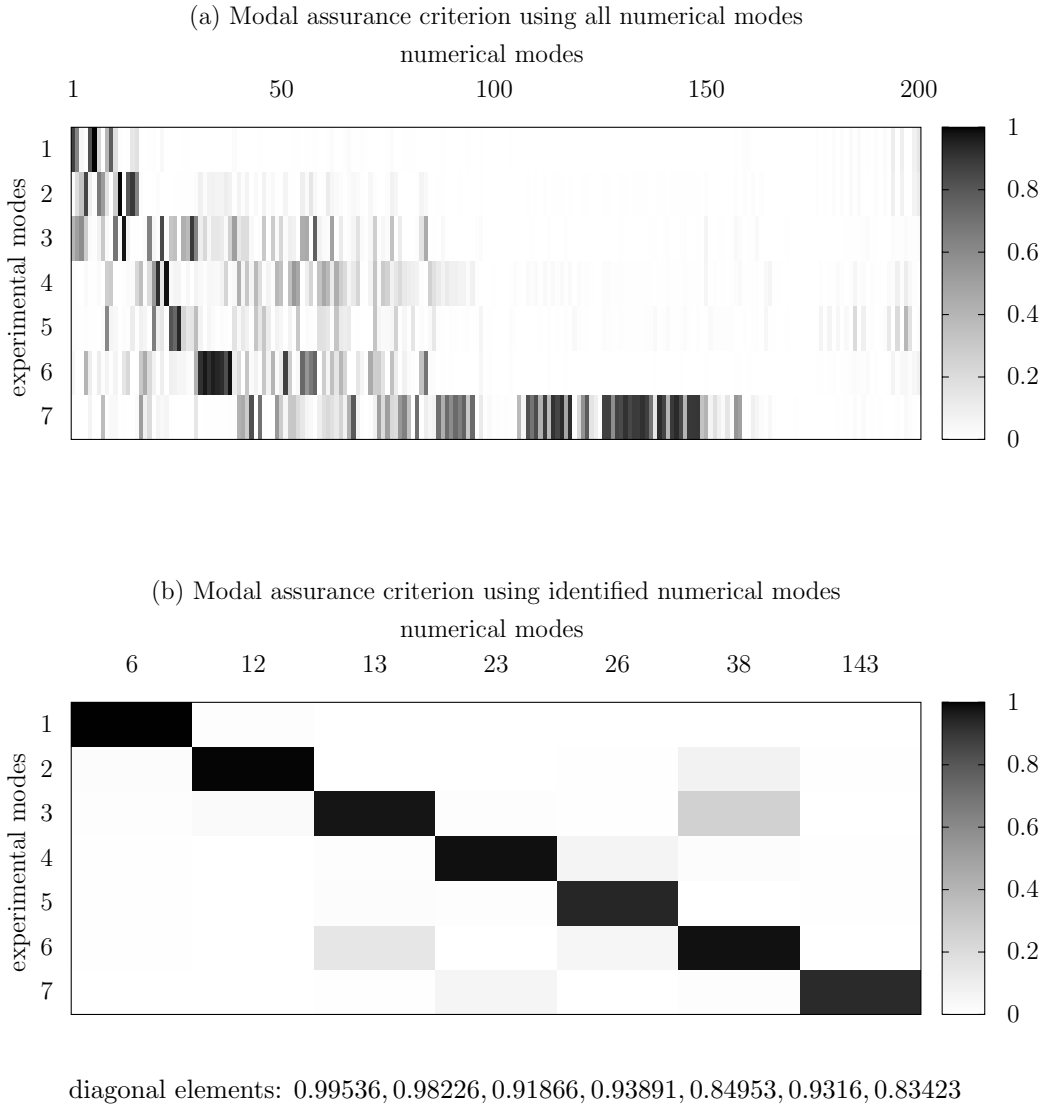


Figure 3.18: Modal assurance criterion (MAC) – (a) all numerical vs. experimental modes of the Erfttal bridge; (b) identified numerical vs. experimental modes of the Erfttal bridge.

noted that these numerical modes do not correspond to a model that was obtained by an optimization, but with a parameter set that could be generated within one optimization step or during a sensitivity analysis. In the cases of measured modes 3, 5, 6, and 7, it can be observed that the assignments fail using the original MAC, whereas the EMAC values constitute a more reliable result. This is mainly caused by the scaling of the MAC. The MAC does not recognize the size of modal displacement compared to the largest modal displacement of a respective numerical mode of the complete system. Some of the modes, primarily related to the rails, have small modal deflections of the bridge decks, which are of similar shape as some of the global modes. Due to the lack of scaling of the reduced mo-

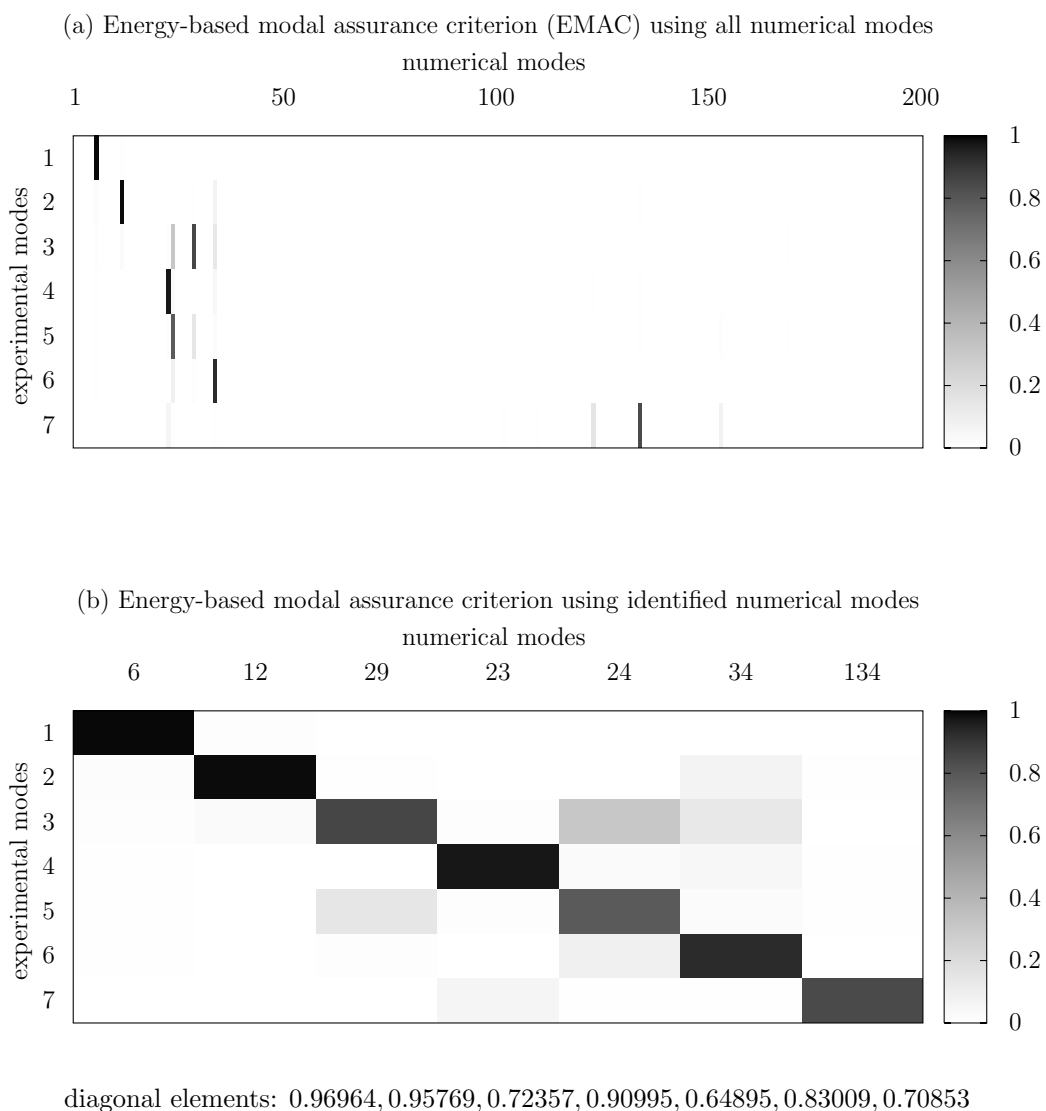
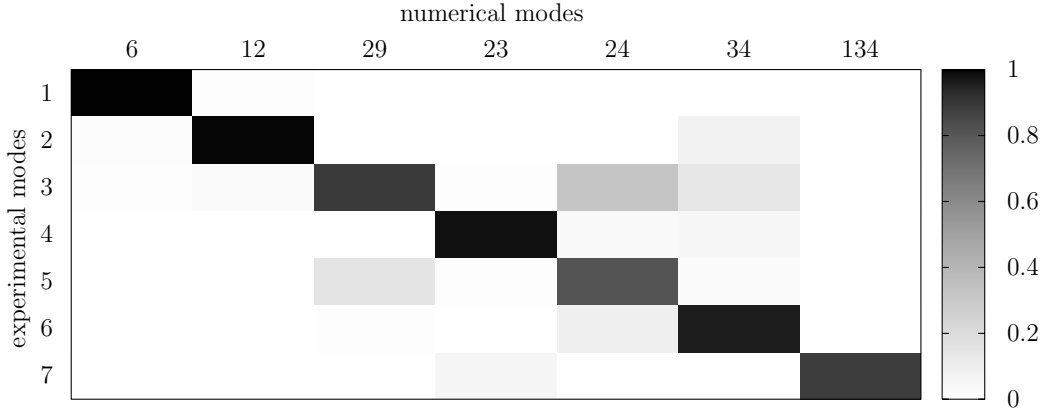


Figure 3.19: Energy-based modal assurance criterion (EMAC) for vertical degrees of freedom of the slab – (a) all numerical vs. experimental modes of the Erfttal bridge; (b) identified numerical vs. experimental modes of the Erfttal bridge.



diagonal elements: 0.99536, 0.98226, 0.77112, 0.93891, 0.67214, 0.88729, 0.76423

Figure 3.20: Modal assurance criterion – identified numerical vs. experimental modes of the Erfttal bridge. The numerical modes are selected previously by the energy-based modal assurance criterion.

dal vectors, the MAC indicates an almost perfect fit. For some parameter configurations and a certain level of noise, the MAC indicates a higher correlation between a global measured mode and a rail mode, which is an unlikely pairing. The proposed EMAC scales the MAC by the relative modal strain energy with respect to the vertical degrees of freedom of the bridge deck. Therefore, the rail modes with low relative modal strain energy will generate a small EMAC value. Finally, the EMAC is able to separate the modes and to assign the most likely global numerical modes to the respective experimentally obtained modes.

3.5.3 Global sensitivity analysis

The following investigation demonstrates the influence of an inappropriate mode selection algorithm on a global sensitivity analysis. The 35 selected, uncertain independent input parameters of the model are varied by a stochastic sampling scheme, the Latin hypercube sampling. For each parameter, a uniform distribution is assumed. The boundaries are listed in Table 3.5, in which the numbering corresponds to the numbering of the vertical axis in Figure 3.21. The parameter's boundaries are related to physically reasonable ranges. The Latin hypercube sampling uses 750 classes, whereas one representative of each class, the mean value, will be selected. Thus, the number of cubes is 750^{35} . The modal parameters are calculated for all 750 generated sample sets. All moduli of the linear Spearman correlation coefficient [Spearman 1904] between each input and output parameter pair are assembled into a matrix. The matrix is used to assess the sensitivity of each parameter with respect to a certain calculated modal parameter. Applications of the Spearman correlation in the context of model updating can be found in [Mares

Table 3.4: Comparison of identified numerical mode shapes with the mode shapes obtained from measurements.

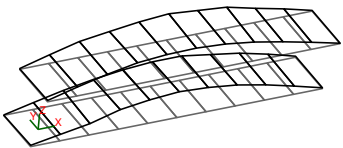
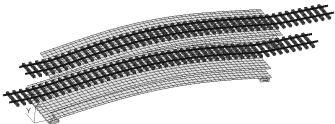
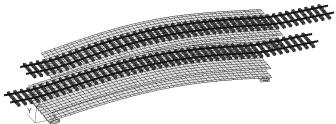
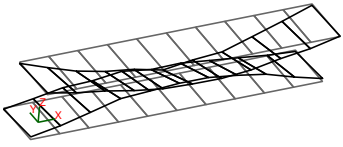
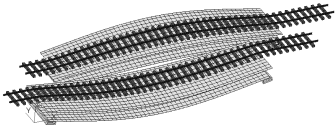
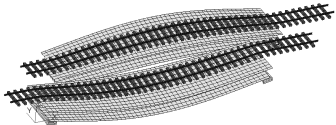
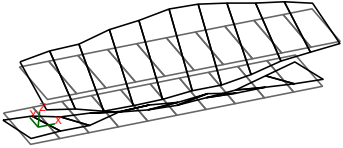
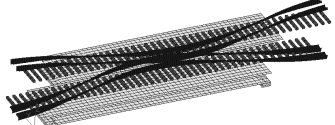
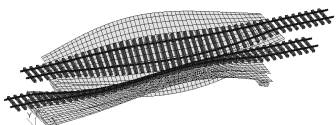
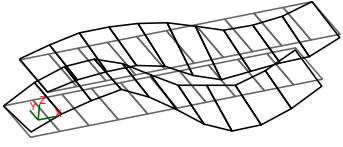
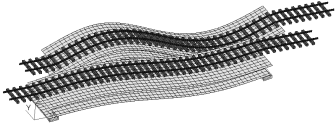
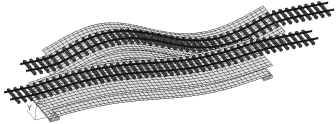
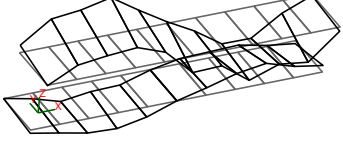
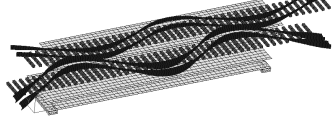
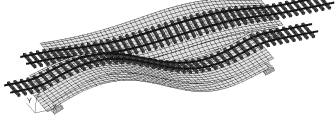
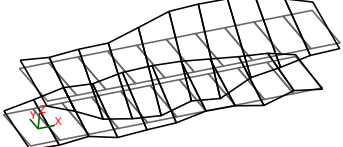
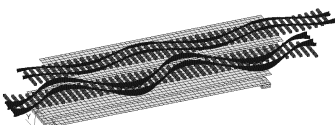
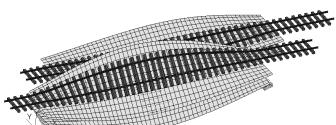
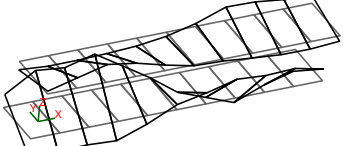
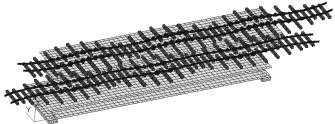
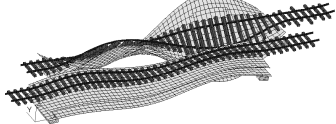
	measured mode shape	numerical mode shape identified by	
		MAC	EMAC
1	3.67Hz 	3.67Hz 	3.67Hz 
2	5.24Hz 	5.82Hz 	5.82Hz 
3	9.36Hz 	7.28Hz 	15.14Hz 
4	13.17Hz 	12.69Hz 	12.69Hz 
5	13.71Hz 	14.38Hz 	13.89Hz 
6	15.09Hz 	18.86Hz 	18.38Hz 
7	20.98Hz 	31.41Hz 	30.75Hz 

Table 3.5: Notation, lower bounds, and upper bounds for all input variables.

#	parameter	unity	lower bound	upper bound
1	Young's modulus of concrete B25 including ballast	$\frac{\text{N}}{\text{m}^2}$	$2.70 \cdot 10^{10}$	$4.50 \cdot 10^{10}$
2	Poisson ratio of concrete B25 including ballast	-	$1.80 \cdot 10^{-1}$	$2.20 \cdot 10^{-1}$
3	density of concrete B25 including ballast	$\frac{\text{kg}}{\text{m}^3}$	$3.00 \cdot 10^3$	$4.00 \cdot 10^3$
4	Young's modulus of concrete B25 including ballast	$\frac{\text{N}}{\text{m}^2}$	$2.90 \cdot 10^{10}$	$4.50 \cdot 10^{10}$
5	Poisson ratio of concrete B25 including ballast	-	$1.80 \cdot 10^{-1}$	$2.20 \cdot 10^{-1}$
6	density of concrete B25 including ballast	$\frac{\text{kg}}{\text{m}^3}$	$3.00 \cdot 10^3$	$4.00 \cdot 10^3$
7	Young's modulus of HEM1000	$\frac{\text{N}}{\text{m}^2}$	$2.00 \cdot 10^{11}$	$2.30 \cdot 10^{11}$
8	Poisson ratio of HEM1000	-	$2.50 \cdot 10^{-1}$	$3.50 \cdot 10^{-1}$
9	density of HEM1000	$\frac{\text{kg}}{\text{m}^3}$	$7.70 \cdot 10^3$	$8.00 \cdot 10^3$
10	Young's modulus of sleeper	$\frac{\text{N}}{\text{m}^2}$	$3.00 \cdot 10^{10}$	$5.00 \cdot 10^{10}$
11	Poisson ratio of sleeper	-	$2.00 \cdot 10^{-1}$	$3.00 \cdot 10^{-1}$
12	density of sleeper	$\frac{\text{kg}}{\text{m}^3}$	$2.10 \cdot 10^3$	$3.00 \cdot 10^3$
13	shear modulus of elastomer 1	$\frac{\text{N}}{\text{m}^2}$	$9.40 \cdot 10^6$	$4.50 \cdot 10^6$
14	shear modulus of elastomer 2	$\frac{\text{N}}{\text{m}^2}$	$9.40 \cdot 10^6$	$4.50 \cdot 10^6$
15	stiffness of ballast gap u_x	$\frac{\text{N}}{\text{m}}$	$3.00 \cdot 10^5$	$3.00 \cdot 10^{11}$
16	stiffness of ballast gap u_y	$\frac{\text{N}}{\text{m}}$	$5.00 \cdot 10^5$	$5.00 \cdot 10^{11}$
17	stiffness of ballast gap u_z	$\frac{\text{N}}{\text{m}}$	$3.00 \cdot 10^5$	$9.49 \cdot 10^7$
18	stiffness of ballast gap r_x	$\frac{\text{Nm}}{\text{rad}}$	$1.00 \cdot 10^1$	$1.00 \cdot 10^5$
19	stiffness of ballast gap r_y	$\frac{\text{Nm}}{\text{rad}}$	$1.00 \cdot 10^1$	$1.00 \cdot 10^8$
20	stiffness of ballast rim-soil u_x	$\frac{\text{N}}{\text{m}}$	$3.00 \cdot 10^4$	$3.00 \cdot 10^{11}$
21	stiffness of ballast rim-soil u_y	$\frac{\text{N}}{\text{m}}$	$5.00 \cdot 10^4$	$5.00 \cdot 10^{11}$
22	stiffness of ballast rim-soil u_z	$\frac{\text{N}}{\text{m}}$	$3.00 \cdot 10^5$	$3.00 \cdot 10^8$
23	stiffness of ballast rim-soil r_x	$\frac{\text{Nm}}{\text{rad}}$	$1.00 \cdot 10^1$	$1.00 \cdot 10^6$
24	stiffness of ballast rim-soil r_y	$\frac{\text{Nm}}{\text{rad}}$	$1.00 \cdot 10^1$	$1.00 \cdot 10^{10}$
25	stiffness of slab-sleeper connection u_x	$\frac{\text{N}}{\text{m}}$	$5.00 \cdot 10^4$	$5.00 \cdot 10^{11}$
26	stiffness of slab-sleeper connection u_y	$\frac{\text{N}}{\text{m}}$	$1.58 \cdot 10^5$	$5.00 \cdot 10^{11}$
27	stiffness of slab-sleeper connection u_z	$\frac{\text{N}}{\text{m}}$	$5.00 \cdot 10^5$	$5.00 \cdot 10^{11}$
28	stiffness of slab-sleeper connection r_x	$\frac{\text{Nm}}{\text{rad}}$	$1.00 \cdot 10^1$	$1.00 \cdot 10^5$
29	stiffness of slab-sleeper connection r_y	$\frac{\text{Nm}}{\text{rad}}$	$1.00 \cdot 10^1$	$1.00 \cdot 10^5$
30	stiffness of rail pad u_x	$\frac{\text{N}}{\text{m}}$	$1.00 \cdot 10^5$	$1.00 \cdot 10^{10}$
31	stiffness of rail pad u_y	$\frac{\text{N}}{\text{m}}$	$1.00 \cdot 10^5$	$1.00 \cdot 10^{10}$
32	stiffness of rail pad u_z	$\frac{\text{N}}{\text{m}}$	$5.01 \cdot 10^6$	$1.58 \cdot 10^9$
33	stiffness of rail pad r_x	$\frac{\text{Nm}}{\text{rad}}$	$1.00 \cdot 10^1$	$1.00 \cdot 10^5$
34	stiffness of rail pad r_y	$\frac{\text{Nm}}{\text{rad}}$	$1.00 \cdot 10^1$	$1.00 \cdot 10^5$
35	stiffness of rail pad r_z	$\frac{\text{Nm}}{\text{rad}}$	$1.00 \cdot 10^1$	$1.00 \cdot 10^5$

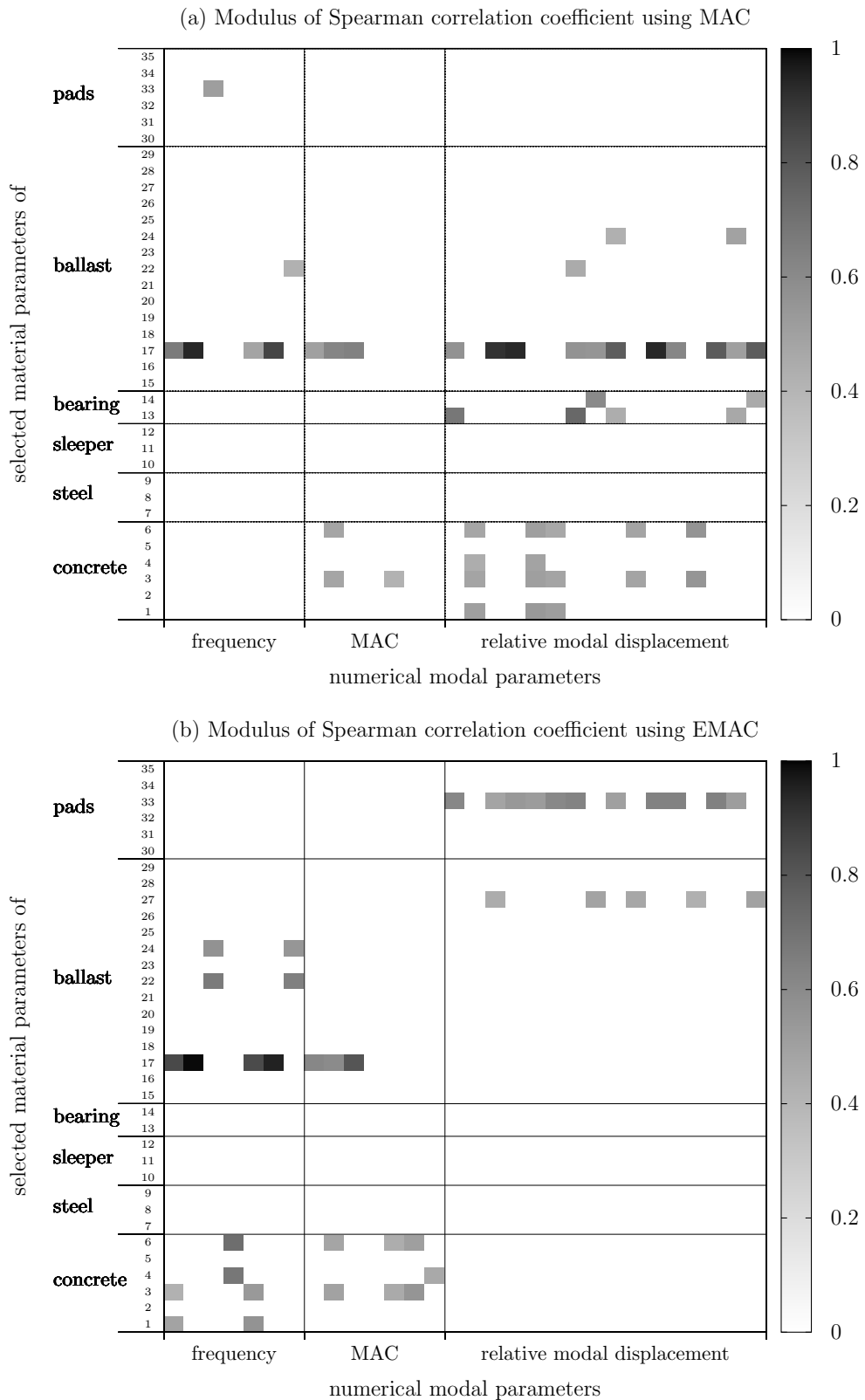


Figure 3.21: Modulus of the linear Spearman correlation coefficient based on 750 sample sets. Coefficients smaller than 0.3 are set to 0. (a) using the modal assurance criterion (MAC) for mode assignment (b) using the energy-based modal assurance criterion (EMAC) for mode assignment.

et al. 2006] and [Mottershead et al. 2006]. A compact theoretical description is given in Appendix A.1.

The assignment of numerical modes to experimental modes is important. Figure 3.21a shows the result of the global sensitivity analysis in case the traditional modal assurance criterion (MAC) is applied for mode assignments. By using the same design space, but applying the energy-based modal assurance criterion (EMAC) for mode assignments, different results are obtained, as presented in Figure 3.21b. For example, the MAC approach indicates a significant sensitivity of the bearings, which disappears, when the energy-based criterion is applied. Therefore, in the case of using the MAC, the sensitivity of the bearings are overvalued. As the most sensitive parameters should be used in a subsequent finite element model updating, a disadvantageous parameter set would be selected. This would lead to an inaccurate identification of the bearing parameters and an unfavorable convergence rate within the optimization. By using the EMAC as mode pairing criterion, the bearing parameters would not be selected for finite element model updating.

3.6 Discussion

This chapter emphasized the problem of wrong mode selection by using the traditional modal assurance criterion (MAC) in certain cases. An innovative criterion combined the common mathematical modal assurance criterion with additional physical information, the modal strain energies of the numerical eigenvectors. This energy-based modal assurance criterion was denoted by EMAC. It has been shown that additional information leads to a more reliable mode assignment.

The problem has been explained extensively by means of a numerical example with artificially generated and noise disturbed measured data. It was shown that an optimization can lead to a wrong identification of parameters when using an inappropriate mode pairing algorithm. However, by applying the proposed EMAC, the most likely numerically derived modes could be assigned correctly to the respective experimentally determined mode. This is an important issue in the context with automated model updating, which is focused on the correct identification of uncertain model input parameters. The proposed EMAC-based mode assignment has been tested on a high-speed railway bridge, for which experimentally identified modal data were available. On the example of an finite element model of a bridge with a single arbitrarily chosen model input parameter set, it was demonstrated that the most likely mode pairing was found by using the EMAC. In this case, the application of the MAC as mode pairing criterion failed. Furthermore, the effect of a wrong mode assignment within a global sensitivity analysis became obvious.

An important step in the application of the energy-based modal assurance criterion (EMAC) is the selection of appropriate clusters, which is needed to define the relative modal strain energies. A general and detailed guideline for the selection of clusters could

not be given, because the selection always depends on the specifics of each individual structure. The clusters always have to be defined in accordance with the kind of the underlying structure and the measurement setup used in the tests. In this context, it is important

- (i) that the degrees of freedom that are instrumented with sensors in the tests can represent the considered mode shapes sufficiently well and
- (ii) that the selected clusters of the stiffness matrix have to be strongly related to those components of the numerical model that are known from the tests.

Finally, the proposed methodology cannot replace a careful preparation of modal tests. However, it can significantly reduce uncertainties associated with mode assignments in situations when only limited spatial information is available due to unavoidable reasons.

Objective functions for stochastic model updating

4.1 Problem overview

4.1.1 Motivation

Model updating is a procedure to improve the correlation between a mathematical or numerical model and a realistic structure using extracted features from measured data (e.g., [Steenackers et al. 2006]). In the context of vibration measurements, typical features are modal parameters, like natural frequencies, modal damping ratios, or modal displacements. The purpose of model updating is the generation of a model that cannot only represent the involved features or measurements. Depending on the intended use, the updated model should also be able, for example, to predict other loading scenarios under different conditions or to estimate the residual life time of the realistic structure. Typically, uncertain input parameters of the model will be modified to increase the agreement between numerically derived and experimentally obtained features. The measure of agreement is termed cost function or objective function. A general framework for model updating and its relation to model verification and model validation is described in Section 1.2.

Of course, several sources of uncertainties are present in the model updating process. Uncertainties may be associated with the measurements, the postprocessing and extraction of features, the simplification of the realistic structure, and the calculation of numerically derived features. Another possibility is the variability of test structures or test conditions. Examples are the experimental investigation of several nominally identical structures or the repeated measurement of a disassembled and reassembled structure. A comprehensive overview about uncertainties in model updating using dynamic test data was given in [Friswell et al. 1995], [Natke 1998], and [Mottershead et al. 2010]. The results of experimental evaluations of uncertainties were documented in [Adhikari et al. 2009]

and [Govers et al. 2010b]. An additional example of the variability of modal parameters from experimental modal analysis was presented in Chapter 2.

Different approaches are available to treat uncertainties in the process of model updating. The standard deterministic model updating does not consider uncertainties directly. The features, as well as, the adjusted model parameters are often assumed to be deterministic. However, if the uncertainty of experimentally obtained features can be estimated and the source of uncertainty is not modeled explicitly, the uncertainty of identified model parameters can be minimized or quantified even in deterministic approaches. The application of an estimator is evidently required. An overview about several estimators, such as maximum likelihood estimators, minimum variance estimators (e.g., [Collins et al. 1974], [Friswell 1989]), or Bayesian estimators (e.g., [Bucher 2009], [Lombaert et al. 2010a], [Lombaert et al. 2010b]) was given in [Teughels 2003]. An appropriate weighting of residuals, for instance, by applying the inverse of the covariance matrix, may reduce the influence of uncertainties [Doebeling et al. 2000]. [Mares et al. 2002] tried to reduce the uncertainties by a robust estimation technique. In stochastic model updating methods, the source of uncertainty can be integrated within the updating as model parameter. The variability of test structures or test conditions are applications for such methods. The results are distributions of the unknown model parameters that correspond to the distributions of experimentally obtained features. Hence, the identified statistical properties of model parameters are no indicators of confidence.

In this chapter, an approach is presented, which is affiliated to stochastic model updating methods. In contrast to existing sensitivity-based methods, optimization strategies are applied to determine the optimum. The resulting group of methods is denoted by optimization-based stochastic model updating. A special emphasis is put on the investigation of information theory based measures with respect to their suitability as objective functions.

4.1.2 Literature review

Sensitivity-based stochastic model updating procedures were developed by [Mares et al. 2006] and [Mottershead et al. 2006], as well as, by [Khodaparast et al. 2008b]. Besides some numerical benchmark studies, also realistic case studies with measured data were specified. [Brehm et al. 2009a] improved the perturbation approach of [Khodaparast et al. 2008b] regarding decreasing computational expenses using a Latin hypercube sampling strategy combined with neural network approximations of the output parameters. For the presented benchmark study, the evaluations within the stochastic structural analysis could be reduced by 99.7% in comparison to the original approach. [Govers et al. 2009] and [Govers et al. 2010a] introduced a sensitivity-based stochastic model updating procedure, in which the mean values and variances can be updated separately. That was demon-

strated by numerical examples. However, this method is only asymptotically correct, if the distribution of numerical model responses is a linear function of the distribution of model parameters. An application on an aircraft-like structure with experimentally obtained data was presented in [Govers et al. 2010b]. An alternative to probabilistic approaches is the interval model updating given in [Khodaparast et al. 2010]. In this approach, kriging has been applied to approximate model responses.

For a successful application of sensitivity methods, the initial input parameters need to be close to the optimal solution. This can be difficult in some applications. Hence, [Khodaparast et al. 2008a] and [Zabel et al. 2009a] applied successfully classical optimization methods (i.e., genetic algorithm, adaptive response surface methods). [Khodaparast et al. 2008a] chose a combination of squared weighted Euclidean norm and Frobenius norm of the mean value vector and covariance matrix as objective function. In contrast, [Zabel et al. 2009a] used information theory measures, like Kullback-Leibler divergence and Bhattacharyya distance. A subsequent optimization of mean values using the Mahalanobis distance and the covariances using the Kullback-Leibler divergence was proposed by [Doebeling et al. 2000]. The optimization method was based on a quasi Newton approach on response surfaces. An alternative objective function, the constitutive relation error estimator, was suggested by [Ladevèze et al. 2006].

The distribution of numerically derived model responses and experimentally obtained features need to be compared by using an objective function. The distributions can be uniquely defined by their cumulative distribution functions, probability density functions, their statistical moments, or other parameters. For example, a multivariate normal distribution is defined by its mean value vector and the covariance matrix. Therefore, an Euclidean norm combined with a Frobenius norm, as applied by [Khodaparast et al. 2008a] and investigated in detail by [Zabel et al. 2009a], may be appropriate. However, the type of distribution is not recognized. In a general case, the objective function should be able to consider different distribution types. Dissimilarity measures, commonly applied and developed in information theory, are measures that can compare distributions by their probability density functions. Such dissimilarity measures are also termed divergence measures.

Comprehensive lists of dissimilarity measures were given in [Baseville 1989], [Bock and Diday 2000], [Pekalska et al. 2005], and [Escolano et al. 2009]. A large parametric class of f -divergences was introduced by [Csiszár 1967a], [Csiszár 1967b], and [Ali et al. 1966]. These divergences were investigated in detail by [Vajda 1972], [Vajda 2009], and [Jain et al. 2007]. The most common dissimilarity measures are the Kullback-Leibler (e.g., [Kullback et al. 1951], [Kullback 1997], [Prasanth et al. 2003]), Bhattacharyya (e.g., [Bhattacharyya 1943], [Thacker et al. 1997]), Chernoff ([Chernoff 1952]), Patrick-Fisher ([Patrick et al. 1969]), and Hellinger ([Hellinger 1909]) dissimilarities. Alternative measures were proposed by [Kannappan 1974], [Burbea et al. 1982], [Rao et al. 1985],

[Chung et al. 1989], [Ullah 1996], [Kumar et al. 2005b], and [Kumar et al. 2005a]. Typically, information theory based dissimilarity measures rely on integrals of functions depending on probability distributions functions. Explicite formulas are available for some measures comparing multivariate normal distributions. Examples were presented in [Kailath 1967], [Shen 1998], [Kullback 1997], and [Bock and Diday 2000]. Properties and inequalities of various dissimilarity measures were investigated in [Kobayashi et al. 1967], [Kobayashi 1970], [Taneja 1989], [Topsøe 2000], [Dragomir et al. 2000], and [Sahoo 1999]. Typical applications are face recognition [Singh et al. 2002], speech recognition [Jeon et al. 2004][Lee 1991], and pattern recognition (e.g., [Rauber et al. 2008a], [Rauber et al. 2008b], [De Maesschalck et al. 2000], [Ramakrishnan et al. 2006]) in disciplines like chemistry ([Mekenyan et al. 2004]), biology ([Stoll et al. 2006]), and finance ([Brigo et al. 2001],[Brigo et al. 2005]). Applications closer related to structural engineering disciplines are fault detection of engines ([Basir et al. 2007]) and sensors ([Wang et al. 2003]), discrimination analysis of ground vibrations ([Kakizawa et al. 1998]), and model selection problems ([Shibata 1997]).

The previously presented non-exhaustive list of various dissimilarity measures leads to the problem of selecting the best suitable measure for a specific application. This task is recognized by some authors, but it is not well analyzed in literature. The problem of selecting the best measure for hypothesis testing or assignment of pattern to the most suitable class was investigated by [Nayak et al. 2009] and [Abrahams 1982]. They concluded that the suitability of measures depends strongly on the kind of problem and that there is no preferred dissimilarity measure at all. [Nayak et al. 2009] stated that topological rather than non-topological f -divergences should be considered. [Ullah 1996] observed that the Kullback-Leibler divergence measure is the most frequently applied measure to compare probability density functions even though there is no real reason to promote the Kullback-Leibler divergence measure against others. In contrast, [Kulhavý 1996] stated that the Kullback-Leibler dissimilarity measure is a natural way to be consistent with probability theory. Similarities of the Kullback-Leibler distance estimator with the maximum likelihood estimators and Bayesian estimators are obvious (e.g., [Kulhavý 1996], [Ullah 1996]).

Some dissimilarity measures, like α -divergences and β -divergences, need to be configured with a parameter. Hence, the problem to find the best parameter for a specific application arises. [Minka 2005] systematically investigated this problem for a specific type of α -divergence. Extreme values of the parameter α try to cover the mass or all modes of a distribution P with respect to a distribution Q . For α values between zero and one, the mass and the modes of the distributions are almost equally considered in the divergence. In these cases, the α -divergence is close to the Kullback-Leibler or reversed Kullback-Leibler divergence. The Rényi α -divergence was investigated by [Hero et al. 2001]. The best results were obtained for an image indexing problem with α -values of

1 and $\frac{1}{2}$, corresponding to the Kullback-Leibler divergence and the Bhattacharyya distance, respectively. However, if the discrimination between the distributions was small, the Bhattacharyya distance performed better. [Zabel et al. 2009a] compared the suitability of Kullback-Leibler divergence and Bhattacharyya distance as objective functions for model updating using different optimization methods. The Kullback-Leibler distance in combination with an adaptive response surface method was the most suitable approach for the investigated benchmark study.

4.1.3 Proposed methodology

The available sensitivity-based stochastic model updating methods are suitable for a large class of problems. In general, a fast convergence can be achieved within few iterations. Certainly, the numerical derivation to calculate the sensitivities needs various objective function evaluations. The computational effort to calculate the first order sensitivity matrix is increasing quadratically with the number of features included in the target distribution and the number of uncertain model parameters. Nevertheless, some of the sensitivity-based stochastic model updating methods are asymptotically not correct, if the connection between the model parameters and the model responses is nonlinear. Furthermore, they are based on residuals of mean values and covariance matrices, which limits the application with respect to the feasible distribution type of the features. Moreover, an initial distribution close to the optimal distribution needs to be chosen to assure the success of the methods.

A promising alternative is the application of standard optimization methods, such as adaptive response surface method, genetic algorithm, or particle swarm optimization. Of course, the success of these methods depends strongly on the definition of the objective function. Some initial investigations from [Zabel et al. 2009a] showed that dissimilarity measures are suitable for the application in optimization-based stochastic model updating. These measures are based on the comparison of probability density functions. Therefore, the type of distribution is less important. Most optimization methods require the definition of input parameter bounds. Hence, unrealistic values of adjusted model parameters can be avoided. Initial distributions are only needed for some optimization methods. Usually, a random set of parameters is chosen from the design space to define the initial distributions. Although, a near-optimal initial parameter set is beneficial for optimization methods, it is not essentially required for the success of the method.

The novel contribution of the presented approach is the investigation of information theory based dissimilarity measures in combination with conventional optimization methods in the field of optimization-based stochastic model updating using vibration test data. The aim is to assess various dissimilarity measures, with respect to their application as objective functions. The dissimilarity measures depend on several input pa-

rameters, which describe the distribution of uncertain model parameters. An analytical investigation of the objective function properties is not possible. Thus, some parts of the multi-dimensional objective function will be mapped onto several one-dimensional functions. Such one-dimensional functions can be assessed easily regarding monotonicity, convexity, and first derivatives. Based on the properties of the one-dimensional functions, a monotonicity, convexity, and gradient indicator of the objective function are defined. The objective functions are tested with several optimization strategies to proof their suitability for stochastic model updating. The capability of the methodology will be tested in two representative numerical benchmark studies, a three degree of freedom mass-spring system and a 20 degree of freedom cantilever truss.

4.2 Optimization-based stochastic model updating

Like every optimization problem, also the stochastic model updating intends to find a set of input parameters that is most suitable to represent a certain set of target output parameters. Therefore, the optimization problem in context of optimization-based stochastic model updating can be defined by six important quantities:

- the input parameters \mathbf{x} , sometimes denoted by design variables, defining the distribution of an unknown model parameter vector $\boldsymbol{\theta}$,
- the output parameters \mathbf{y} , defining the numerically derived distribution of a model response vector \mathbf{z} ,
- the function or relation to calculate the model responses depending on the model parameters,
- the target output parameters \mathbf{y}_m , defining the distribution of an experimentally obtained feature vector \mathbf{z}_m ,
- the objective function $J(\mathbf{x})$ that should be typically minimized, and
- the optimization method.

In case of stochastic model updating, the input parameters $\mathbf{x} \in \mathbb{R}^{m_x}$ are statistical parameters describing the probability distribution of the random vector associated with the uncertain model parameters $\boldsymbol{\theta}$. For example, mean values $\mathbf{E}_{\boldsymbol{\theta}}$, variances $\mathbf{V}_{\boldsymbol{\theta}}$, and correlation coefficients $\mathbf{r}_{\boldsymbol{\theta}}$ of material properties, geometry data, modeling parameters, or loads are possible input parameters. The distribution type of the model parameter vector can be added as discrete input parameter or is assumed to be known. Obviously, all input parameters need to be restricted by lower bounds \mathbf{x}_l and upper bounds \mathbf{x}_u to avoid unreasonable identification results or to avoid numerical problems. Typical restrictions

are the requirement of a positive standard deviation and a correlation coefficient between -1 and 1. Additional equality or inequality constraints, $h_e(\mathbf{x}) = 0$ or $h_i(\mathbf{x}) > 0$, can limit the valid input parameter space. For example, the covariance matrix of the multivariate model parameter vector $\boldsymbol{\theta}$ needs to be positive definite, which can be written as $|\mathbf{C}_\theta| > 0$.

The output parameters $\mathbf{y} \in \mathbb{R}^{m_y}$ are the statistical parameters describing the probability distribution of the random vector associated with the model responses \mathbf{z} . Typical output parameters are mean values \mathbf{E}_z and covariances \mathbf{C}_z of the modal parameters (natural frequencies, modal damping ratios, modal displacements) or features extracted from response time histories of displacements, velocities, accelerations, strains, or stresses.

Of course, to obtain the output parameters \mathbf{y} , a function or relation between the model parameter vector $\boldsymbol{\theta}$ and the model response vector \mathbf{z} is required. This can be an analytical function or another mathematical description of the relation, for instance, a solution obtained from a finite element model. An analytical derivation of the relation between input parameters \mathbf{x} and output parameters \mathbf{y} is advantageous. If this is not possible, a sample-based stochastic structural analysis, as described in [Bucher 2009], can be applied. This analysis relies on systematic sampling schemes (e.g., D-optimal design, Koshal design, full factorial design [Myers et al. 2009]) or stochastic sampling schemes (e.g., plain Monte Carlo sampling, Latin hypercube sampling [Verma et al. 2010][Bucher 2009]) to generate a certain number of samples from the multivariate distributions of model parameters $\boldsymbol{\theta}$ defined by a certain set of input parameters \mathbf{x} . For each model input parameter sample, a sample of model responses \mathbf{z} can be determined by using the known relation between model parameters and model responses. Performing a statistical analysis on the obtained model response sets, the output parameters \mathbf{y} can be derived.

The target output parameters \mathbf{y}_m are the statistical properties specifying the probability distribution of the random vector based on the experimentally obtained features \mathbf{z}_m . The vector \mathbf{y}_m can be determined by a statistical analysis of the respective extracted features obtained from several measurements. Obviously, the target output parameters \mathbf{y}_m and the output parameters \mathbf{y} need to describe the same kind and number of features.

To evaluate the suitability of the input parameter vector \mathbf{x}_j corresponding to a certain iteration step j , the random vector of experimentally obtained features \mathbf{z}_m and model response random vector \mathbf{z}_j have to be compared, for example, by means of a function depending on the target output parameters \mathbf{y}_m and output parameters \mathbf{y}_j . Such a function is termed objective function. If the optimization problem is formulated as a positively defined minimization problem, the objective function

$$J(\mathbf{x}) \rightarrow \min \quad \text{with} \quad J: \mathbb{R}^{m_x} \rightarrow \mathbb{R} \quad (4.1)$$

should at least satisfy the properties

$$J(\mathbf{y}_m || \mathbf{y}_j(\mathbf{x}_j)) \geq 0 \quad \text{and} \quad J(\mathbf{y}_m || \mathbf{y}_j(\mathbf{x}_j)) = 0, \quad \text{if and only if } \mathbf{y}_m = \mathbf{y}_j(\mathbf{x}_j). \quad (4.2)$$

A very common example of an objective function is the weighted Euclidean distance. In the presented contribution, dissimilarity measures originally developed for information theory problems are used as objective functions. These dissimilarity measures are described in Section 4.3. To reduce computational expenses, explicit formulas assuming multivariate normal distributions are applied in this study.

By using the previous description of input parameters, output parameters, and objective function, any standard optimization method (e.g., gradient-based methods, response surface methods, or nature inspired methods) can be applied. If the relation between the input parameters \mathbf{x}_j and the output parameters \mathbf{y}_j cannot be derived analytically and a sample-based stochastic analysis needs to be applied, the topology of the objective function can be very rough. Therefore, gradient-based methods are not recommended, as demonstrated in [Zabel et al. 2009a].

If a sample-based stochastic structural analysis is integrated in stochastic model updating, the most computational effort is required for the evaluation of the samples generated according to the distribution of model parameters. The accuracy of the obtained output parameter vector \mathbf{y} depends on the number of evaluated samples. Hence, the convergence of the optimization depends on both, the configuration of the optimization method (e.g., number of iterations) and the number of samples used to determine the output parameters \mathbf{y} . The challenge is to minimize the total number of sample evaluations by optimizing the configuration parameters of the optimization method. However, this is not the major emphasis of this contribution. The main aim is to investigate the general suitability of various objective functions and optimization methods by means of benchmark studies as described in Sections 4.5 and 4.6.

4.3 Dissimilarity measures

4.3.1 Definitions

A typical task in several scientific and engineering disciplines is the comparison of two t -variate distributions P and Q described by their probability density functions $p(\mathbf{u})$ and $q(\mathbf{u})$. Those probability density functions need to satisfy the conditions

$$\begin{aligned} \int_{\mathbb{R}^t} p(\mathbf{u}) d\mathbf{u} = 1 \quad \text{and} \quad p(\mathbf{u}) \geq 0 \quad \forall \mathbf{u} \in \mathbb{R}^t \quad \text{resp.} \\ \int_{\mathbb{R}^t} q(\mathbf{u}) d\mathbf{u} = 1 \quad \text{and} \quad q(\mathbf{u}) \geq 0 \quad \forall \mathbf{u} \in \mathbb{R}^t. \end{aligned} \quad (4.3)$$

Most of the dissimilarity measures between two distributions P and Q can be represented by a general function

$$D(P||Q) = g \left(\int f(p(\mathbf{u}), q(\mathbf{u}), \mathbf{r}) d\mathbf{u}, \mathbf{s} \right) \quad (4.4)$$

depending on a set of parameters \mathbf{r} and \mathbf{s} . $g(\cdot)$ and $f(\cdot)$ are functions to be specified. Dissimilarity measures are usually no metrics in the classical sense, because they do not necessarily satisfy the symmetry and triangular condition, but they meet the positive definiteness condition

$$D(P\|Q) \geq 0 \quad \text{and} \quad D(P\|Q) = 0 \quad \text{if and only if} \quad p(\mathbf{u}) = q(\mathbf{u}), \quad (4.5)$$

which is essential for the application onto model updating problems. Many dissimilarity measures can be derived from similarity measures $S(P\|Q)$. They satisfy the condition

$$S(P\|P) \geq S(P\|Q) \quad \text{and} \quad S(P\|P) \geq S(Q\|P), \quad (4.6)$$

but not necessarily the symmetry and triangular condition. Therefore, the maximal value for the similarity measure will be obtained if and only if $p(\mathbf{u}) = q(\mathbf{u})$. The most important similarity measures are listed in Subsection 4.3.2.

The dissimilarity measure integrals according to Equation (4.4) can only be solved analytically for few distribution types. For example, explicit formulas are available for various dissimilarity measures comparing normal distributions. If a closed form is not existing, the integral needs to be solved numerically, for instance, by rectangle rule, Monte Carlo method, or Metropolis Hastings algorithm [Evans et al. 2005]. Probability density estimates need to be applied, if the probability density functions cannot be expressed as analytical function. [Scott 1992] proposed various methods, like histograms, averaged shifted histograms, and kernel density estimates. The accuracy of the estimation strongly depends on the number of available sample sets.

In the presented thesis, the dissimilarity measures are only applied with their explicit formula assuming a multivariate normal distribution. Symmetric and unsymmetric dissimilarity measures are indicated by $D(P, Q)$ and $D(P\|Q)$, respectively. In case the distributions P and Q are t -variate normal distributions, they can be described by the mean value vectors \mathbf{E}_p and \mathbf{E}_q and the positive definite covariance matrices \mathbf{C}_p and \mathbf{C}_q . The unity matrix of size t is indicated by \mathbf{I}_t with entries

$$(\mathbf{I}_t)_{i,j} = \begin{cases} 1 & : i = j \\ 0 & : i \neq j \end{cases}. \quad (4.7)$$

The congruent transformation of a vector \mathbf{A} and matrix \mathbf{B} is abbreviated by

$$\|\mathbf{A}\|_{\mathbf{B}}^2 = \mathbf{A}^T \mathbf{B} \mathbf{A}. \quad (4.8)$$

If the vector \mathbf{A} is a difference between two vectors, $\|\mathbf{A}\|_{\mathbf{B}}^2$ is denoted by the squared weighted Euclidean distance. The term $\|\mathbf{E}_p - \mathbf{E}_q\|_{\mathbf{C}_p^{-1}}^2$ represents the squared Mahalanobis distance. In the following, $|\cdot|$ indicates the determinant of a matrix.

4.3.2 Similarity measures based on probability density functions

4.3.2.1 Hellinger coefficient

The Hellinger coefficient $S_{HC}(P||Q, s)$ of order s with $0 < s < 1$ is a similarity measure bounded within $[0, 1]$ (e.g., [Bock and Diday 2000], [Pekalska et al. 2005]). It is defined by

$$S_{HC}(P||Q, s) = \int_{\mathbb{R}^t} p(\mathbf{u})^{1-s} q(\mathbf{u})^s d\mathbf{u}. \quad (4.9)$$

For two t -variate normal distributions P and Q the explicit equation

$$\begin{aligned} S_{HC}^{\mathcal{N}}(P||Q, s) &= |s\mathbf{I}_t + (1-s)\mathbf{C}_p^{-1}\mathbf{C}_q|^{-\frac{s}{2}} |(1-s)\mathbf{I}_t + s\mathbf{C}_q^{-1}\mathbf{C}_p|^{-\frac{1-s}{2}} \\ &\exp\left(\frac{1}{2} \left\| s\mathbf{C}_q^{-1}\mathbf{E}_q + (1-s)\mathbf{C}_p^{-1}\mathbf{E}_p \right\|_{(s\mathbf{C}_q^{-1} + (1-s)\mathbf{C}_p^{-1})}^2 \right. \\ &\quad \left. - \frac{s}{2} \|\mathbf{E}_q\|_{\mathbf{C}_q^{-1}}^2 - \frac{1-s}{2} \|\mathbf{E}_p\|_{\mathbf{C}_p^{-1}}^2 \right) \end{aligned} \quad (4.10)$$

can be derived according to [Bock and Diday 2000]. It is required that the matrix $(s\mathbf{C}_q^{-1} + (1-s)\mathbf{C}_p^{-1})$ is positive definite.

Based on this similarity measure, several dissimilarity measures, like the Chernoff distance, can be derived. For the calculation of α -divergence and β -divergence, the restrictions of $0 < s < 1$ can be extended to $s > 0$.

4.3.2.2 Hellinger integral

The Hellinger integral was originally introduced by [Hellinger 1909] and referenced, for example, by [Escolano et al. 2009] and [Hazewinkel 2002]. With $s = \frac{1}{2}$, the Hellinger integral is a special case of the Hellinger coefficient. Therefore, its general form is given by

$$S_{HI}(P, Q) = S_{HC}\left(P||Q, \frac{1}{2}\right) = \int_{\mathbb{R}^t} \sqrt{p(\mathbf{u})q(\mathbf{u})} d\mathbf{u} \quad (4.11)$$

and the explicit formula for two t -variate normal distributions

$$\begin{aligned} S_{HI}^{\mathcal{N}}(P, Q, s) &= 2^{\frac{t}{2}} |2\mathbf{I}_t + \mathbf{C}_p^{-1}\mathbf{C}_q + \mathbf{C}_q^{-1}\mathbf{C}_p|^{-\frac{1}{4}} \\ &\exp\left(\frac{1}{4} \left\| \mathbf{C}_q^{-1}\mathbf{E}_q + \mathbf{C}_p^{-1}\mathbf{E}_p \right\|_{(\mathbf{C}_q^{-1} + \mathbf{C}_p^{-1})}^2 \right. \\ &\quad \left. - \frac{1}{4} \|\mathbf{E}_q\|_{\mathbf{C}_q^{-1}}^2 - \frac{1}{4} \|\mathbf{E}_p\|_{\mathbf{C}_p^{-1}}^2 \right) \end{aligned} \quad (4.12)$$

can be derived from Equation (4.10). The Hellinger integral is the basis of the dissimilarity measures Bhattacharyya distance and Hellinger distance. [Escolano et al. 2009] denoted the Hellinger integral by Bhattacharyya coefficient.

4.3.3 Dissimilarity measures based on probability density functions

4.3.3.1 Patrick-Fisher distance

The Patrick-Fisher distance

$$D_{PF}(P, Q) = \sqrt{\int_{\mathbb{R}^t} (p(\mathbf{u}) - q(\mathbf{u}))^2 d\mathbf{u}}, \quad (4.13)$$

was introduced by [Patrick et al. 1969] and is identical to the Minkowski L_2 distance (e.g., [Walter-Williams et al. 2010]). In [Shen 1998] and [Zhou et al. 2006], an explicit equation for two t -variate normal distributions was presented.

$$D_{PF}^{\mathcal{N}}(P, Q) = \left(\frac{1}{\sqrt{(2\pi)^t |\mathbf{C}_p|}} + \frac{1}{\sqrt{(2\pi)^t |\mathbf{C}_q|}} - \frac{2}{\sqrt{(2\pi)^t |\mathbf{C}_p + \mathbf{C}_q|}} \exp\left(-\frac{1}{2} \|\mathbf{E}_p - \mathbf{E}_q\|_{(\mathbf{C}_p + \mathbf{C}_q)^{-1}}^2\right) \right)^{\frac{1}{2}} \quad (4.14)$$

The matrix $(\mathbf{C}_p + \mathbf{C}_q)$ needs to be positive definite. [Baseville 1989] also listed the Patrick-Fisher distance. According to [Rauber et al. 2008a], an analytical solution for the Patrick-Fisher distance is not existing for two Dirichlet distributions.

4.3.3.2 Squared Patrick-Fisher distance

The squared Patrick-Fisher distance or squared Minkowski distance of order two is defined as (e.g., [Bock and Diday 2000], [Pekalska et al. 2005])

$$D_{SPF}(P, Q) = \int_{\mathbb{R}^t} (p(\mathbf{u}) - q(\mathbf{u}))^2 d\mathbf{u}. \quad (4.15)$$

The explicit formula for two t -variate normal distributions can be derived directly from Equation (4.14).

$$D_{SPF}^{\mathcal{N}}(P, Q) = (D_{PF}^{\mathcal{N}}(P, Q))^2 \quad (4.16)$$

[Bock and Diday 2000] presented an alternative for the comparison of two t -variate normal distributions

$$D_{SPF}^{\mathcal{N}}(P, Q) = \frac{1}{2^t \pi^{\frac{t}{2}}} \left(\frac{1}{|\mathbf{C}_p|^{\frac{1}{2}}} + \frac{1}{|\mathbf{C}_q|^{\frac{1}{2}}} \right) - \frac{2}{(2\pi)^{\frac{t}{2}} |\mathbf{C}_p + \mathbf{C}_q|^{\frac{1}{2}}} \exp\left(\frac{1}{2} \|\mathbf{C}_p^{-1} \mathbf{E}_p + \mathbf{C}_q^{-1} \mathbf{E}_q\|_{(\mathbf{C}_p^{-1} + \mathbf{C}_q^{-1})^{-1}}^2 - \|\mathbf{E}_p\|_{\mathbf{C}_p^{-1}}^2 - \|\mathbf{E}_q\|_{\mathbf{C}_q^{-1}}^2\right). \quad (4.17)$$

This version is computationally more expensive and numerically unstable for ill-conditioned matrices \mathbf{C}_p and \mathbf{C}_q . Besides $(\mathbf{C}_p + \mathbf{C}_q)$, also $(\mathbf{C}_p^{-1} + \mathbf{C}_q^{-1})$ need to be positive definite. Hence, Equation (4.16) is preferred in the subsequent benchmark studies.

4.3.3.3 Chernoff distance

Chernoff's distance of order s , introduced in [Chernoff 1952], can be derived from the Hellinger coefficient $S_{HC}(P||Q, s)$ according to Equation (4.9) by

$$D_{CH}(P||Q, s) = -\ln S_{HC}(P||Q, s) \quad (4.18)$$

with $0 < s < 1$. Applying Equation (4.10), the formula for two t -variate normal distributions can be directly expressed. A numerically more stable explicit formula

$$D_{CH}^{\mathcal{N}}(P||Q, s) = \frac{1}{2} \ln \frac{|s\mathbf{C}_p + (1-s)\mathbf{C}_q|}{|\mathbf{C}_p|^s |\mathbf{C}_q|^{1-s}} + \frac{1}{2} s(1-s) \|\mathbf{E}_p - \mathbf{E}_q\|_{(s\mathbf{C}_p + (1-s)\mathbf{C}_q)^{-1}}^2 \quad (4.19)$$

was presented in [Zhou et al. 2006] and [Shen 1998].

[Rauber et al. 2008a] showed an explicit form of the Chernoff distance for two Dirichlet distributions, as well as, for two Beta distributions.

4.3.3.4 Bhattacharyya distance

A symmetric version of the Chernoff distance is obtained for order $s = \frac{1}{2}$, which is referred to as Bhattacharyya distance [Bhattacharyya 1943]

$$D_{BH}(P, Q) = D_{CH}\left(P||Q, \frac{1}{2}\right) = -\ln S_{HI}(P, Q). \quad (4.20)$$

Presuming two t -variate normal distributions, [Kailath 1967] and [Zhou et al. 2006] provided an analytical solution

$$D_{BH}^{\mathcal{N}}(P, Q) = \frac{1}{2} \ln \frac{|\frac{1}{2}(\mathbf{C}_p + \mathbf{C}_q)|}{\sqrt{|\mathbf{C}_p||\mathbf{C}_q|}} + \frac{1}{8} \|\mathbf{E}_p - \mathbf{E}_q\|_{\left(\frac{\mathbf{C}_p + \mathbf{C}_q}{2}\right)^{-1}}^2. \quad (4.21)$$

An explicit formula of the Bhattacharyya distance for other exponential densities was given in [Kailath 1967]. For the cases of two Dirichlet distributions and two Beta distributions, explicit formulas were derived in [Rauber et al. 2008b] and [Rauber et al. 2008a]. The properties of the Bhattacharyya distance were extensively discussed in [Thacker et al. 1997].

4.3.3.5 Hellinger distance

The Hellinger distance $D_{HD}(P, Q)$ can be directly derived from the Hellinger integral. A common representation (e.g., [Hazewinkel 2002], [Nguyen et al. 2005]) is

$$\begin{aligned} D_{HD}(P, Q) &= \sqrt{2 - 2S_{HI}(P, Q)} \\ &= \sqrt{\int_{\mathbb{R}^t} (\sqrt{p(\mathbf{u})} - \sqrt{q(\mathbf{u})})^2 d\mathbf{u}}. \end{aligned} \quad (4.22)$$

With this definition, the symmetric Hellinger distance is bounded within $[0, \sqrt{2}]$. The closed equation for two t -variate normal distributions can be obtained by applying Equation (4.12). The derivation from the Chernoff distance, according to Equation (4.19), is numerically more stable.

$$D_{HD}^{\mathcal{N}}(P, Q) = \sqrt{2 - 2 \exp\left(-D_{CH}^{\mathcal{N}}\left(P\|Q, \frac{1}{2}\right)\right)} \quad (4.23)$$

Another representation of the Hellinger distance was defined in [Escolano et al. 2009], which only differs in the prefactor $\frac{1}{2}$. [Rauber et al. 2008a] termed the Hellinger distance, as described in Equation (4.22), Jeffreys-Matusita distance, because the Hellinger distance is a special case of the generalized Matusita distance ([Toussaint 1974]).

4.3.3.6 Squared Hellinger distance

The squared variant of the Hellinger distance is

$$D_{SHD}(P, Q) = 2 - 2S_{HI}(P, Q) = \int_{\mathbb{R}^t} (\sqrt{p(\mathbf{u})} - \sqrt{q(\mathbf{u})})^2 d\mathbf{u}. \quad (4.24)$$

It is bounded within $[0, 2]$ and is a true metric (e.g., [Hero et al. 2001], [Brigo et al. 2005], [Vajda 2009]), as it fulfills the positive definiteness, symmetry, and triangular condition. An analytical calculation for two t -variate normal distributions can be performed with Equation (4.12) or (4.23). In general, the latter version is numerically more stable.

Other terms for the squared Hellinger distance are Matusita distance ([Nayak et al. 2009]) and Jeffreys distance ([Sahoo 1999][Chung et al. 1989]).

4.3.3.7 χ^2 -divergence

In the general case of two continuous probability distribution functions, the directed χ^2 -divergence is a weighted form of the squared Patrick-Fisher distance and can be calculated by

$$D_{\chi^2}(P\|Q) = \int_{\mathbb{R}^t} \frac{(p(\mathbf{u}) - q(\mathbf{u}))^2}{p(\mathbf{u})} d\mathbf{u}. \quad (4.25)$$

According to [Bock and Diday 2000], an explicite formula

$$D_{\chi^2}^{\mathcal{N}}(P\|Q) = \frac{|\mathbf{C}_{\mathbf{p}}\mathbf{C}_{\mathbf{q}}^{-1}|}{|2\mathbf{C}_{\mathbf{p}}\mathbf{C}_{\mathbf{q}}^{-1} - \mathbf{I}_t|^{\frac{1}{2}}} \exp\left(\frac{1}{2}\|2\mathbf{C}_{\mathbf{q}}^{-1}\mathbf{E}_{\mathbf{q}} - \mathbf{C}_{\mathbf{p}}^{-1}\mathbf{E}_{\mathbf{p}}\|_{(2\mathbf{C}_{\mathbf{q}}^{-1} - \mathbf{C}_{\mathbf{p}}^{-1})}^2 - \|\mathbf{E}_{\mathbf{q}}\|_{\mathbf{C}_{\mathbf{q}}^{-1}}^2 + \frac{1}{2}\|\mathbf{E}_{\mathbf{p}}\|_{\mathbf{C}_{\mathbf{p}}^{-1}}^2\right) - 1 \quad (4.26)$$

is available for two t -variate normal distributions, assuming the matrix $(2\mathbf{C}_{\mathbf{q}}^{-1} - \mathbf{C}_{\mathbf{p}}^{-1})$ is positive definite. In [Sahoo 1999], the χ^2 -divergence was referred to as Kagan affinity measure.

4.3.3.8 Symmetrized χ^2 -divergence

The symmetrized χ^2 -divergence (e.g., [Jain et al. 2007], [Kumar et al. 2005a])

$$\begin{aligned} D_{\chi^2 S}(P, Q) &= D_{\chi^2}(P\|Q) + D_{\chi^2}(Q\|P) \\ &= \int_{\mathbb{R}^t} \frac{(p(\mathbf{u}) - q(\mathbf{u}))^2 (p(\mathbf{u}) + q(\mathbf{u}))}{p(\mathbf{u})q(\mathbf{u})} d\mathbf{u} \end{aligned} \quad (4.27)$$

can be directly obtained from the directed χ^2 -divergence. Positive definite matrices $(2\mathbf{C}_{\mathbf{q}}^{-1} - \mathbf{C}_{\mathbf{p}}^{-1})$ and $(2\mathbf{C}_{\mathbf{p}}^{-1} - \mathbf{C}_{\mathbf{q}}^{-1})$ are required for the explicite formula derived from Equation (4.26) expecting two t -variate normal distributions.

4.3.3.9 Kullback-Leibler divergence

The Kullback-Leibler divergence [Kullback 1997, p. 189] is defined by

$$D_{KL}(P\|Q) = \int_{\mathbb{R}^t} q(\mathbf{u}) \ln \frac{q(\mathbf{u})}{p(\mathbf{u})} d\mathbf{u}. \quad (4.28)$$

[Kakizawa et al. 1998] showed that Equation (4.28) simplifies to

$$\begin{aligned} D_{KL}^{\mathcal{N}}(P\|Q) &= \frac{1}{2} \ln \frac{|\mathbf{C}_{\mathbf{p}}|}{|\mathbf{C}_{\mathbf{q}}|} + \frac{1}{2} \text{tr}(\mathbf{C}_{\mathbf{q}}(\mathbf{C}_{\mathbf{p}}^{-1} - \mathbf{C}_{\mathbf{q}}^{-1})) + \\ &\quad \frac{1}{2} (\mathbf{E}_{\mathbf{p}} - \mathbf{E}_{\mathbf{q}})^{\text{T}} \mathbf{C}_{\mathbf{p}}^{-1} (\mathbf{E}_{\mathbf{p}} - \mathbf{E}_{\mathbf{q}}), \end{aligned} \quad (4.29)$$

for t -variate normal distributions P and Q , whereas $\text{tr}(\cdot)$ is the trace of a matrix.

[Rauber et al. 2008a] derived that the explicite formula for the Kullback-Leibler divergence between two Dirichlet distributions is not defined.

4.3.3.10 Symmetrized Kullback-Leibler divergence

The symmetrized Kullback-Leibler divergence is also known as J -divergence [Bock and Diday 2000] in honor of Jeffrey, who first used this divergence. According to [Kullback 1997, p. 190], it is defined by

$$D_{KLS}(P, Q) = D_{KL}(P\|Q) + D_{KL}(Q\|P) = \int_{\mathbb{R}^t} (p(\mathbf{u}) - q(\mathbf{u})) \ln \frac{p(\mathbf{u})}{q(\mathbf{u})} d\mathbf{u}. \quad (4.30)$$

For two t -variate normal distributions, an explicite formula can be deduced [Kullback 1997, p. 190]

$$D_{KLS}^{\mathcal{N}}(P, Q) = \frac{1}{2} \text{tr} \left((\mathbf{C}_p - \mathbf{C}_q) (\mathbf{C}_q^{-1} - \mathbf{C}_p^{-1}) \right) + \frac{1}{2} (\mathbf{E}_p - \mathbf{E}_q)^T (\mathbf{C}_p^{-1} + \mathbf{C}_q^{-1}) (\mathbf{E}_p - \mathbf{E}_q). \quad (4.31)$$

Alternatively, Equation (4.29) can be applied to define an explicite formula.

The L -divergence and K -divergence, established by [Burbea et al. 1982], are identical to the symmetrized Kullback-Leibler divergence for special parameters. An explicite formula of the symmetrized Kullback-Leibler divergence for exponential densities was provided by [Kailath 1967].

4.3.3.11 Rényi α -divergence

Rényi's α -divergence (e.g., [Rényi 1961], [Escolano et al. 2009]) of order s , also well known as information gain (e.g., [Sibson 1969], [Bock and Diday 2000]), is defined by

$$D_{\alpha}(P\|Q, s) = \frac{1}{s-1} \ln \int_{\mathbb{R}^t} p(\mathbf{u})^{1-s} q(\mathbf{u})^s d\mathbf{u}. \quad (4.32)$$

The integral is identical to the Hellinger coefficient, but the parameter $s \in \mathbb{R}$ with $s > 0$ has no upper bound. In the limit $s \rightarrow 1$, the information gain

$$\lim_{s \rightarrow 1} D_{\alpha}(P\|Q, s) = D_{KL}(P\|Q) \quad (4.33)$$

is equal to the Kullback-Leibler divergence according to Equation (4.28). For $s = 2$, one half of the χ^2 -distance defined in Equation (4.25) is obtained. Within a range of $0 < s < 1$, the Rényi α -divergence is up to a factor $\frac{1}{1-s}$ identical to the Chernoff distance.

Using the Hellinger coefficient according to Equation (4.10), an explicite equation for two t -variate normal distributions can be derived for $s > 0$.

$$D_{\alpha}^{\mathcal{N}}(P\|Q, s) = \frac{1}{s-1} \ln (S_{HC}^{\mathcal{N}}(P\|Q, s)) \quad (4.34)$$

An explicite formula based on Equation (4.19) is numerically more stable, but is restricted to $0 < s < 1$.

$$D_{\alpha}^{\mathcal{N}}(P\|Q, s) = \frac{1}{1-s} (D_{CH}^{\mathcal{N}}(P\|Q, s)) \quad (4.35)$$

4.3.3.12 β -divergence

Another generalized directed measure is the β -divergence, for example, proposed and investigated by [Ullah 1996]. Based on the Hellinger coefficient, according to Equation (4.9), it is defined by

$$D_{\beta}(P\|Q, s) = \frac{1}{s-1} \left(\int_{\mathbb{R}^t} p(\mathbf{u})^{1-s} q(\mathbf{u})^s d\mathbf{u} - 1 \right). \quad (4.36)$$

The parameter s needs to be restricted to $s \in \mathbb{R}$ with $s > 0$ to obtain a reasonable distance with $D_\beta(P\|Q, s) \geq 0$. For $s \rightarrow 1$, the β -divergence is identical to the Kullback-Leibler divergence according to Equation (4.28).

$$\lim_{s \rightarrow 1} D_\beta(P\|Q, s) = D_{KL}(P\|Q) \quad (4.37)$$

The squared Hellinger distance (4.24) and the χ^2 -distance (4.25) can be obtained with values $s = \frac{1}{2}$ and $s = 2$, respectively.

An explicit equation for two t -variate normal distributions can be derived from the Hellinger coefficient according to Equation (4.10), whereas the parameter s is only restricted by $s > 0$.

$$D_\beta^{\mathcal{N}}(P\|Q, s) = \frac{1}{s-1} (S_{HC}^{\mathcal{N}}(P\|Q, s) - 1) \quad (4.38)$$

For $0 < s < 1$, the numerically more stable formula based on the Chernoff distance according to Equation (4.19) is recommended.

$$D_\beta^{\mathcal{N}}(P\|Q, s) = \frac{1}{s-1} (\exp(-D_{CH}^{\mathcal{N}}(P\|Q, s)) - 1) \quad (4.39)$$

In [Sahoo 1999] and [Chung et al. 1989], an α -divergence was given, which is identical to the β -divergence, where the factor $\frac{1}{s-1}$ is replaced by $\frac{1}{2^{s-1}-1}$. An alternative factor $\frac{1}{s(s-1)}$ was utilized in [Minka 2005] with an unbounded $s \in \mathbb{R}$.

4.3.3.13 Symmetrized β -divergence

The symmetrized form of the β -divergence is expressed by

$$\begin{aligned} D_{\beta S}(P, Q, s) &= D_\beta(P\|Q, s) + D_\beta(Q\|P, s) \\ &= \frac{1}{s-1} \left(\int_{\mathbb{R}^t} p(\mathbf{u})^{1-s} q(\mathbf{u})^s + p(\mathbf{u})^s q(\mathbf{u})^{1-s} d\mathbf{u} - 2 \right) \end{aligned} \quad (4.40)$$

with $s \in \mathbb{R}$ and $s > 0$. The limit $s \rightarrow 1$ results in the symmetrized Kullback-Leibler distance and for $s = 2$ the symmetrized χ^2 -distance is obtained.

A closed solution for t -variate normal distributions can be derived from the Hellinger coefficient according to Equation (4.10) using $s > 0$.

$$D_{\beta S}^{\mathcal{N}}(P\|Q, s) = \frac{1}{s-1} (S_{HC}^{\mathcal{N}}(P\|Q, s) + S_{HC}^{\mathcal{N}}(Q\|P, s) - 2) \quad (4.41)$$

The numerically more stable version based on the Chernoff distance, but restricted to $0 < s < 1$, is

$$D_{\beta S}^{\mathcal{N}}(P\|Q, s) = \frac{1}{s-1} (\exp(-D_{CH}^{\mathcal{N}}(P\|Q, s)) + \exp(-D_{CH}^{\mathcal{N}}(Q\|P, s)) - 2). \quad (4.42)$$

[Burbea et al. 1982] denoted the symmetrized β -divergence as L -divergence. The factor $\frac{1}{s-1}$ was replaced by $\frac{1}{2^{s-1}-1}$ in [Chung et al. 1989].

4.3.4 Dissimilarity measures based on statistical moments

4.3.4.1 Euclidean Frobenius norm

To compare the first two statistical moments of two distributions P and Q , a combined Euclidean Frobenius norm can be defined by

$$D_{EF}^S(P||Q, w_1, w_2) = w_1 \|\mathbf{E}_p - \mathbf{E}_q\|_{\mathbf{I}_t}^2 + w_2 \|\mathbf{C}_p - \mathbf{C}_q\|^F. \quad (4.43)$$

The scalars $w_1, w_2 \in \mathbb{R}$ with $w_1, w_2 > 0$ are weighting parameters. A similar measure was proposed by [Khodaparast et al. 2008a] in the context of stochastic model updating.

4.3.4.2 Weighted Euclidean Frobenius norm

To avoid a non-uniform weighting of the mean value differences, the Euclidean distance can be weighted by a matrix \mathbf{W}_1 with entries

$$(\mathbf{W}_1)_{i,j} = \begin{cases} ((\mathbf{E}_p)_i + \delta((\mathbf{E}_p)_i, 0))^{-2} & : i = j \\ 0 & : i \neq j \end{cases} \quad \forall i = 1, \dots, t. \quad (4.44)$$

$\delta(a, b)$ is the Kronecker delta, which is specified by

$$\delta(a, b) = \begin{cases} 1 & : a = b \\ 0 & : a \neq b \end{cases}. \quad (4.45)$$

The resulting weighted Euclidean Frobenius norm is expressed as

$$D_{WEF}^S(P||Q, w_1, w_2) = w_1 \|\mathbf{E}_p - \mathbf{E}_q\|_{\mathbf{W}_1}^2 + w_2 \|\mathbf{C}_p - \mathbf{C}_q\|^F \quad (4.46)$$

with $w_1, w_2 \in \mathbb{R}$ and $w_1, w_2 > 0$.

4.3.4.3 Mahalanobis Frobenius norm

A dimensionless quantity can be obtained by applying the Mahalanobis distance and the Frobenius norm of the scaled difference between the covariance matrices. Hence, a combined Mahalanobis distance and Frobenius norm

$$D_{MF}^S(P||Q, w_1, w_2) = w_1 \|\mathbf{E}_p - \mathbf{E}_q\|_{\mathbf{C}_p^{-1}}^2 + w_2 \|(\mathbf{C}_p - \mathbf{C}_q) \mathbf{C}_p^{-1}\|^F \quad (4.47)$$

is deduced for $w_1, w_2 \in \mathbb{R}$ and $w_1, w_2 > 0$.

4.3.4.4 Weighted Euclidean norm of statistical moments

The first four statistical moments, mean value \mathbf{E} , variance \mathbf{V} , skewness \mathbf{S} , and kurtosis \mathbf{K} of the marginal distributions of the t -variate distributions P and Q , are assembled in vectors

$$\mathbf{m}_{4Sp} = \left(\mathbf{E}_p^T \quad \mathbf{V}_p^T \quad \mathbf{S}_p^T \quad \mathbf{K}_p^T \right)^T \quad \text{and} \quad \mathbf{m}_{4Sq} = \left(\mathbf{E}_q^T \quad \mathbf{V}_q^T \quad \mathbf{S}_q^T \quad \mathbf{K}_q^T \right)^T, \quad (4.48)$$

respectively. The definition of the statistical moments is given in Appendix A. Thereafter, a dissimilarity measure can be established by a squared weighted Euclidean norm

$$D_{E4S}^S(P\|Q) = \|\mathbf{m}_{4S\mathbf{p}} - \mathbf{m}_{4S\mathbf{q}}\|_{\mathbf{W}_{4S}}^2 \quad (4.49)$$

with

$$(\mathbf{W}_{4S})_{i,j} = \begin{cases} ((\mathbf{m}_{4S\mathbf{p}})_i + \delta((\mathbf{m}_{4S\mathbf{p}})_i, 0))^{-2} & : i = j \\ 0 & : i \neq j \end{cases} \quad \forall i = 1, \dots, 4t \quad (4.50)$$

using the Kronecker delta $\delta(a, b)$ defined in Equation (4.45).

As a sufficient accuracy of higher statistical moments requires a large number of samples, it can be reasonable to exclude the skewness and the kurtosis from the measure. This measure is expressed as $D_{E2S}^S(P\|Q)$.

4.3.4.5 Weighted Euclidean norm of statistical moments with correlation coefficients

By implementing the correlation coefficients, another measure

$$D_{E4SC}^S(P\|Q) = \|\mathbf{m}_{4SC\mathbf{p}} - \mathbf{m}_{4SC\mathbf{q}}\|_{\mathbf{W}_{4SC}}^2 \quad (4.51)$$

with

$$\begin{aligned} \mathbf{m}_{4SC\mathbf{p}} &= \left(\mathbf{E}_{\mathbf{p}}^T \quad \mathbf{V}_{\mathbf{p}}^T \quad \mathbf{S}_{\mathbf{p}}^T \quad \mathbf{K}_{\mathbf{p}}^T \quad (\mathbf{r}_{\mathbf{p}})_{1,2} \quad \dots \quad (\mathbf{r}_{\mathbf{p}})_{t-1,t} \right)^T, \\ \mathbf{m}_{4SC\mathbf{q}} &= \left(\mathbf{E}_{\mathbf{q}}^T \quad \mathbf{V}_{\mathbf{q}}^T \quad \mathbf{S}_{\mathbf{q}}^T \quad \mathbf{K}_{\mathbf{q}}^T \quad (\mathbf{r}_{\mathbf{q}})_{1,2} \quad \dots \quad (\mathbf{r}_{\mathbf{q}})_{t-1,t} \right)^T, \end{aligned} \quad (4.52)$$

and

$$(\mathbf{W}_{4SC})_{i,j} = \begin{cases} ((\mathbf{m}_{4SC\mathbf{p}})_i + \delta((\mathbf{m}_{4SC\mathbf{p}})_i, 0))^{-2} & : i = j \\ 0 & : i \neq j \end{cases} \quad \forall i = 1, \dots, 4t + \frac{1}{2}(t^2 - t) \quad (4.53)$$

can be derived from Equation (4.49).

If the skewness and the kurtosis are of minor importance or cannot be calculated with sufficient accuracy, they can be excluded from the measure in Equation (4.51). The resulting measure is indicated by $D_{E2SC}^S(P\|Q)$.

4.3.4.6 Weighted Euclidean norm of L moments

The accuracy of statistical moments depends on the sample size. Especially for the higher statistical moments, large sample sizes are needed to achieve a sufficient accuracy. With the same sample size, L moments [Hosking 1990] and their sample estimates [Wang 1996] can be calculated with higher accuracy than the traditional statistical moments. The calculation is described in Appendix A.

By replacing the traditional statistical moments \mathbf{E} , \mathbf{V} , \mathbf{S} , and \mathbf{K} by \mathbf{L}_1 , \mathbf{L}_2 , \mathbf{L}_3 , and \mathbf{L}_4 in Equation (4.49), respectively, the dissimilarity measures based on L moments $D_{E4L}^S(P\|Q)$ and $D_{E2L}^S(P\|Q)$ can be derived.

4.3.5 Numerical and computational aspects

In the subsequent benchmark studies, the dissimilarity measures are utilized as objective functions. Due to similar dependencies of the output parameters with respect to the input parameters, covariance matrices of the outputs are typically not well conditioned. In addition, the accuracy of the sample covariance matrix depends on the number of samples used for the estimation. Therefore, it is not guaranteed that the covariance matrices and their linear combinations are always positive definite or well conditioned.

Several techniques are available to improve the condition of a matrix. Suitable regularization techniques are the Tikhonov regularization and approaches based on singular value decomposition [Friswell 2001]. The quality of improvement depends strongly on the chosen regularization parameters, which can be determined by L-curves or minimizing cross validation functions [Friswell 2001]. In the current work, the sensitivity of dissimilarity measures with respect to ill-conditioned covariance matrices is one subject of interest. Therefore, no regularization techniques are applied.

However, to avoid failed designs within the optimization process, all objective function values need to be numerically representable. Furthermore, the optimization algorithm performs additional calculations using the objective function values. This additionally limits the range of allowed numerical values for the objective function. The numerical calculation of the listed dissimilarity measures is conducted with the software package `Slang` [Dynardo GmbH and Bauhaus University Weimar 2010], which is based on C, C++, and FORTRAN routines. The used datatype is an 8 Byte double, which implies that the minimal positive and maximal representable numerical values are $2.2250738585072014 \cdot 10^{-308}$ and $1.7976931348623157 \cdot 10^{308}$, respectively. The accuracy can be described by $\epsilon \approx 2.2204460492503131 \cdot 10^{-16}$. If the result of an operation is higher than the maximal representable numerical value, INF (infinity) is obtained. The result of an invalid operation is declared as NAN (not a number). Examples are the division by zero and the square root of a negative number. Hence, adjustments during the evaluation of dissimilarity measures are required to avoid failed designs. In addition, the maximal value of the dissimilarity measure needs to be reduced, because the optimization methods

Table 4.1: Adjustments applied during the calculation of the dissimilarity measures to avoid unrepresentable numerical values.

adjusted values	original values and conditions
$ \mathbf{A} = 2.2250738585072014 \cdot 10^{-308}$	$ \mathbf{A} \leq 0$
$a = 10^{292}$	$a > 10^{292}$
$\exp(a) = 10^{292}$	$a > 6.72354847154261392461 \cdot 10^2$
$\ln a = -1 \cdot 10^{292}$	$a = 0$
$a^{-b} = 10^{292}$	$a = 0$ and $b > 1$

usually perform additional mathematical operations by using objective function values. Typical examples of adjustments to avoid unrepresentable values are given in Table 4.1 represented by the matrix \mathbf{A} and two real scalar values a and b .

To increase the readability of the diagrams shown in the benchmark studies, abbreviations are introduced to indicate the respective formula applied in the calculations. An overview on introduced abbreviations is presented in Table 4.2.

Table 4.2: Abbreviations and respective formula applied in the diagrams of the benchmark studies in Sections 4.5 and 4.6.

abbreviation	exact formula symbol	formula
PF	$D_{PF}^N(P, Q)$	according to Equation (4.14)
SPF	$D_{SPF}^N(P, Q)$	according to Equation (4.16)
HD	$D_{HD}^N(P, Q)$	based on Equation (4.12)
HD^\dagger	$D_{HD}^N(P, Q)$	according to Equation (4.23)
SHD	$D_{SHD}^N(P, Q)$	based on Equation (4.12)
SHD^\dagger	$D_{SHD}^N(P, Q)$	based on Equation (4.23)
BH	$D_{BH}^N(P, Q)$	according to Equation (4.21)
$CH(\cdot)$	$D_{CH}^N(P\ Q, \cdot)$	according to Equation (4.19)
χ^2	$D_{\chi^2}^N(P\ Q)$	according to Equation (4.26)
$r\chi^2$	$D_{\chi^2}^N(Q\ P)$	according to Equation (4.26)
χ^2S	$D_{\chi^2S}^N(P, Q)$	based on Equation (4.26)
$\alpha(\cdot)$	$D_{\alpha}^N(P\ Q, \cdot)$	according to Equation (4.34)
KL	$D_{KL}^N(P\ Q)$	according to Equation (4.29)
rKL	$D_{KL}^N(Q\ P)$	according to Equation (4.29)
KLS	$D_{KLS}^N(P, Q)$	according to Equation (4.31)
$\beta(\cdot)$	$D_{\beta}^N(P\ Q, \cdot)$	according to Equation (4.38)
$\beta^\dagger(\cdot)$	$D_{\beta}^N(P\ Q, \cdot)$	according to Equation (4.39)
$\beta S(\cdot)$	$D_{\beta S}^N(P, Q, \cdot)$	according to Equation (4.41)
$\beta S^\dagger(\cdot)$	$D_{\beta S}^N(P, Q, \cdot)$	according to Equation (4.42)
$WEF(\cdot, \cdot)$	$D_{WEF}^S(P\ Q, \cdot, \cdot)$	according to Equation (4.46)
$MF(\cdot, \cdot)$	$D_{MF}^S(P\ Q, \cdot, \cdot)$	according to Equation (4.47)
$EF(\cdot, \cdot)$	$D_{EF}^S(P\ Q, \cdot, \cdot)$	according to Equation (4.43)
$E2S$	$D_{E2S}^S(P\ Q)$	based on Equation (4.49)
$E2L$	$D_{E2L}^S(P\ Q)$	based on Equation (4.49)
$E4S$	$D_{E4S}^S(P\ Q)$	according to Equation (4.49)
$E4L$	$D_{E4L}^S(P\ Q)$	based on Equation (4.49)
$E2SC$	$D_{E2SC}^S(P\ Q)$	based on Equation (4.51)
$E4SC$	$D_{E4SC}^S(P\ Q)$	according to Equation (4.51)

4.4 Numerical evaluation of objective function properties

Independent from the optimization algorithm, the objective function $J(\mathbf{x})$ should satisfy certain properties. If the optimization problem is a positive defined minimization problem according to Equation (4.1), the properties

- (i) positive definiteness according to Equation (4.2),
- (ii) strict monotonicity with respect to the optimum,
- (iii) strict convexity with respect to the optimum,
- (iv) existence and suitable size of the gradient, and
- (v) positive definiteness of the Hessian matrix

are convenient for the objective function.

If the objective function is strictly monotone decreasing (ii) with respect to the optimum, suboptima will not exist. The convexity (iii) is a stronger property, as it implies the monotonicity. In general, the topology of strictly convex functions is very suitable for objective functions. Especially objective functions in combination with response surface methods and gradient-based methods will benefit from this property. However, even convex functions can have rapid gradient changes that are inappropriate for objective functions. Also small gradients can be disadvantageous as inaccuracies for the numerical calculations and numerical noise can strongly influence the objective. Hence, a suitable size of the gradient (iv) is required. The size itself depends on the optimization problem and the accuracy to determine the objective function. Property (v) is stronger than property (iv). A positive definite Hessian matrix is essential for gradient-based optimization methods, in which it is required for the line search. The entries of the Hessian matrix are the second partial derivatives, which are indicators for the change of gradients. The existence and the positive definiteness of the Hessian will further ensure a well-shaped smooth function.

If an analytical objective function is given, the properties can be analyzed analytically. However, the analytical objective function depending on the input parameters is not always available. Therefore, the properties have to be determined numerically with acceptable computational effort.

Since analytical objective functions are not available for the following benchmark studies, a numerical investigation of the properties needs to be conducted. To reduce the computational expenses, the properties of the objective function will be investigated at discrete design space points $(\mathbf{X})_{k,l} \in \mathbb{R}^{m_x}$ with $k = 1, \dots, m$ and $l = 1, \dots, n$ assembled

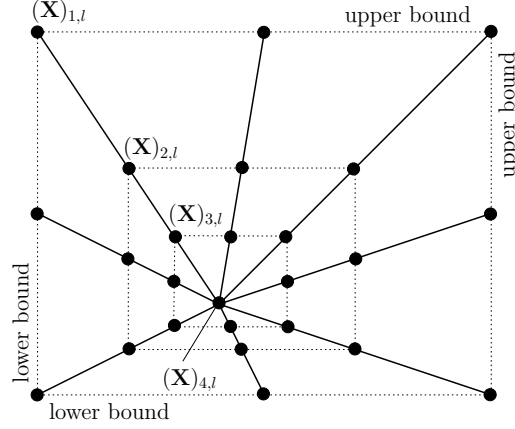


Figure 4.1: Definition of discrete points based on a full factorial design for a two-dimensional parameter space.

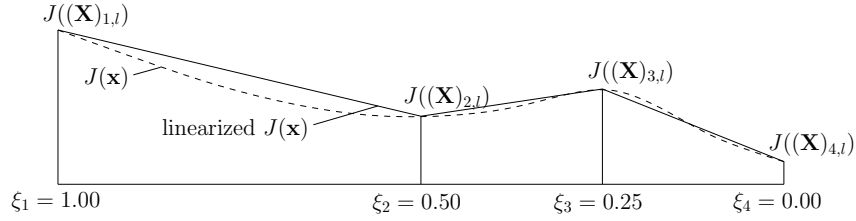


Figure 4.2: Example of a slice l of the objective function using four points per slice.

in a tensor $[\mathbf{X}] \in \mathbb{R}^{m \times n \times m_x}$. Based on a design-of-experiment (DOE) sampling scheme at the boundaries of the design space, the points $(\mathbf{X})_{1,l}$ of a slice l can be defined. Suitable DOE schemes are, for example, full factorial design, central composite design, or Koshal design. The central points are neglected for the present application. The total number of slices n depends on the DOE scheme and the number of design variables m_x . For example, a configuration based on a full factorial design will provide $n = 3^{m_x} - 1$ slices, whereas configurations based on a central composite design will have $n = 2^{m_x} + 2m_x - 1$ slices. Each slice l consists of $m > 1$ points $(\mathbf{X})_{k,l}$, which are assembled at a line between $(\mathbf{X})_{1,l}$ and $(\mathbf{X})_{m,l}$. All points $(\mathbf{X})_{m,l}$ are identical to the optimum. Defining normalized coordinates $\boldsymbol{\xi} \in \mathbb{R}^m$ by

$$(\boldsymbol{\xi})_k = 2^{1-k} \quad \forall k = 1, \dots, m-1 \quad \text{and} \quad (\boldsymbol{\xi})_m = 0, \quad (4.54)$$

the points of the design space are specified as

$$(\mathbf{X})_{k,l} = (\mathbf{X})_{m,l} + (\boldsymbol{\xi})_k ((\mathbf{X})_{1,l} - (\mathbf{X})_{m,l}) \quad \forall k = 1, \dots, m. \quad (4.55)$$

Figure 4.1 shows a configuration for two design variables based on a full factorial design. The number of points m for each slice l is four. Presuming two design variables, the full factorial and face centered central composite sampling scheme are identical. An example of slice l with the corresponding objective function values are given in Figure 4.2.

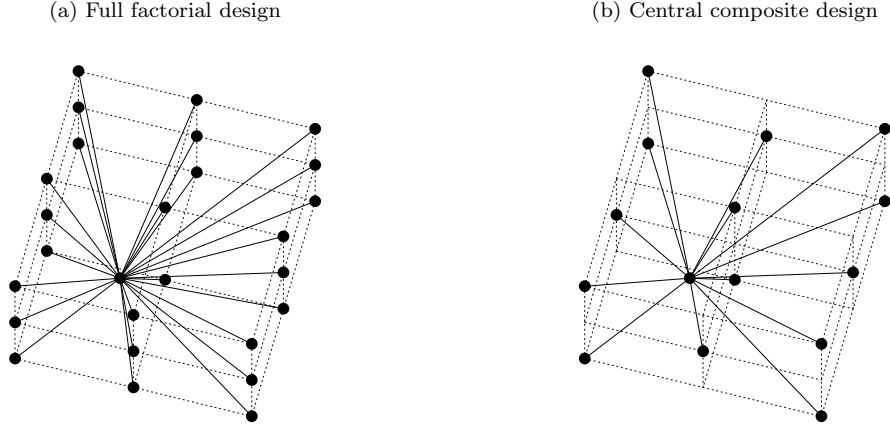


Figure 4.3: Definition of discrete points $(\mathbf{X})_{k,l}$ for a three-dimensional parameter space with two points per slice.

Figure 4.3 visualizes the configuration for three design variables based on full factorial and central composite design using two points per slice.

To proof the required properties of an objective function, three indicators will be defined based on the properties of the slices using the discrete points $(\mathbf{X})_{k,l}$. The convexity in the interval $](\xi)_k, (\xi)_m[\forall k = 1, \dots, m-2$ and $m > 2$ of the discrete objective function slice l is indicated by

$$(\mathbf{o}_c)_{k,l} = \begin{cases} 0 : J((\mathbf{X})_{j,l}) < \frac{(\xi)_j - (\xi)_m}{(\xi)_k - (\xi)_m} J((\mathbf{X})_{k,l}) + \frac{(\xi)_k - (\xi)_j}{(\xi)_k - (\xi)_m} J((\mathbf{X})_{m,l}) & \forall k < j < m \\ 1 : \text{else} \end{cases} \quad (4.56)$$

The convexity indicator $(\mathbf{O}_c)_k$ is obtained by averaging all $(\mathbf{o}_c)_{k,l}$ over all slices l . Hence, it is defined by

$$(\mathbf{O}_c)_k = \frac{1}{n} \sum_{l=1}^n (\mathbf{o}_c)_{k,l} \quad \forall k = 1, \dots, m-2. \quad (4.57)$$

Obviously, the indicator $(\mathbf{O}_c)_k$ is bounded by 0 and 1, whereas $(\mathbf{O}_c)_k = 0$ indicates a strict convexity of the objective function in the interval $](\xi)_k, (\xi)_m[$.

The monotonicity within the interval $](\xi)_k, (\xi)_{k+1}[\forall k = 1, \dots, m-1$ and $m > 1$ are tested by

$$(\mathbf{o}_m)_{k,l} = \begin{cases} 0 : J((\mathbf{X})_{k,l}) > J((\mathbf{X})_{k+1,l}) \\ 1 : J((\mathbf{X})_{k,l}) \leq J((\mathbf{X})_{k+1,l}) \end{cases} \quad (4.58)$$

and the corresponding monotonicity indicator yields

$$(\mathbf{O}_m)_k = \frac{1}{n} \sum_{l=1}^n (\mathbf{o}_m)_{k,l} \quad \forall k = 1, \dots, m-1. \quad (4.59)$$

This indicator ranges between 0 and 1. $(\mathbf{O}_m)_k = 0$ refers to a monotone decreasing function in all slices with respect to the interval $](\xi)_k, (\xi)_{k+1}[$.

By using the single sided finite differences approach, the first derivatives of each slice l at a position $k = 1, \dots, m - 1$ are calculated.

$$(\mathbf{o}_{\mathbf{g}})_{k,l} = \frac{1}{\|(\mathbf{X})_{1,l} - (\mathbf{X})_{m,l}\|^{L_2}} \frac{J((\mathbf{X})_{k+1,l}) - J((\mathbf{X})_{k,l})}{(\boldsymbol{\xi})_{k+1} - (\boldsymbol{\xi})_k} \quad (4.60)$$

A gradient indicator

$$(\mathbf{O}_{\mathbf{g}})_k = \frac{\sum_{l=1}^n (\mathbf{o}_{\mathbf{g}})_{k,l}}{\max_k \sum_{l=1}^n (\mathbf{o}_{\mathbf{g}})_{k,l}} \quad (4.61)$$

is derived. Applying this definition, a positive value of $(\mathbf{o}_{\mathbf{g}})_{k,l}$ is related to a decrease of the objective function with respect to the optimum. In general, it is possible that some of the values $(\mathbf{o}_{\mathbf{g}})_{k,l}$ are negative even though the gradient indicator $(\mathbf{O}_{\mathbf{g}})_k$ is positive. Therefore, the gradient indicator needs to be related to the monotonicity indicator. A monotone decrease of the gradient indicators is convenient for an objective function. However, the gradient indicators should be not too small to avoid high influences from inaccurately calculated objective function values or numerical noise.

The three presented indicators are applied within the benchmark studies in Sections 4.5 and 4.6. Of course, the numerically derived properties rely on the discrete slices of the objective function. They can only indicate and not determine the properties of the objective function. The quality of the indicators can be improved by increasing the number of slices and points. Unfortunately, this is related to an additional computational effort.

4.5 Benchmark study: Three degree of freedom mass-spring system

4.5.1 Description

A three degree of freedom system [Khodaparast et al. 2008b] is considered with known deterministic masses $m_1 = m_2 = m_3 = 1.0 \text{ kg}$ and stiffnesses $k_3 = k_4 = 1.0 \frac{\text{N}}{\text{m}}$, $k_6 = 3.0 \frac{\text{N}}{\text{m}}$. It is depicted in Figure 4.4. The stiffnesses k_1 , k_2 , and k_5 are the unknown model input parameters, which are assembled in a random vector $\boldsymbol{\theta} = \begin{bmatrix} k_1 & k_2 & k_5 \end{bmatrix}^T$. It is assumed that the random vector entries are independently lognormal distributed. The multivariate distribution is described by the mean value vector $\mathbf{E}_{\boldsymbol{\theta}}$ and the standard deviation vector $\boldsymbol{\sigma}_{\boldsymbol{\theta}}$. Thus, the input parameters $\mathbf{x} = [(\mathbf{E}_{\boldsymbol{\theta}})_1 \quad (\mathbf{E}_{\boldsymbol{\theta}})_2 \quad (\mathbf{E}_{\boldsymbol{\theta}})_3 \quad (\boldsymbol{\sigma}_{\boldsymbol{\theta}})_1 \quad (\boldsymbol{\sigma}_{\boldsymbol{\theta}})_2 \quad (\boldsymbol{\sigma}_{\boldsymbol{\theta}})_3]^T$ are used in the optimization process. Assuming the system's natural frequencies are the known target features given as a random vector $\mathbf{z}_{\mathbf{m}} = \begin{bmatrix} f_1 & f_2 & f_3 \end{bmatrix}^T$ obtained from several experiments, the inverse problem is established.

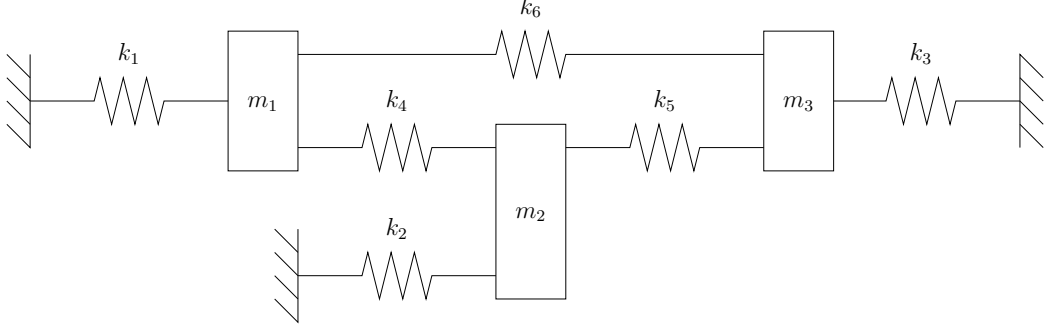


Figure 4.4: Three degree of freedom mass-spring system

Of course, the experimental data needs to be generated artificially for this benchmark study. The properties describing the distribution of the random vector \mathbf{z}_m are obtained from 1,000,000 Latin hypercube samples based on the nominal values of the stiffnesses $\hat{\boldsymbol{\theta}} = \begin{bmatrix} \hat{k}_1 & \hat{k}_2 & \hat{k}_5 \end{bmatrix}^T \in \mathcal{LN}(\mathbf{E}_{\hat{\boldsymbol{\theta}}}, \mathbf{C}_{\hat{\boldsymbol{\theta}}})$ with

$$\mathbf{E}_{\hat{\boldsymbol{\theta}}} = \begin{bmatrix} 1 & 1 & 1 \end{bmatrix}^T \quad \text{and} \quad (\mathbf{C}_{\hat{\boldsymbol{\theta}}})_{i,j} = \begin{cases} 0.04 & : i = j \\ 0.00 & : i \neq j \end{cases}. \quad (4.62)$$

The obtained mean values, covariance matrix, skewness, kurtosis, and L moments of the target output features are respectively:

$$\begin{aligned} \mathbf{E}_{\mathbf{z}_m} &= \begin{bmatrix} 1.5861569206 \cdot 10^{-1} & 3.1785414404 \cdot 10^{-1} & 4.5040703469 \cdot 10^{-1} \end{bmatrix}^T, \\ \mathbf{C}_{\mathbf{z}_m} &= \begin{bmatrix} 5.4013635699 \cdot 10^{-5} & 3.4854959899 \cdot 10^{-5} & 1.4801754616 \cdot 10^{-5} \\ 3.4854959899 \cdot 10^{-5} & 1.6615287298 \cdot 10^{-4} & 3.8101343173 \cdot 10^{-5} \\ 1.4801754616 \cdot 10^{-5} & 3.8101343173 \cdot 10^{-5} & 1.6981213650 \cdot 10^{-5} \end{bmatrix}, \\ \mathbf{S}_{\mathbf{z}_m} &= \begin{bmatrix} 2.2005156916 \cdot 10^{-1} & 2.5019213736 \cdot 10^{-1} & 5.6342856633 \cdot 10^{-1} \end{bmatrix}^T, \\ \mathbf{K}_{\mathbf{z}_m} &= \begin{bmatrix} 5.8981458043 \cdot 10^{-2} & 5.0541817841 \cdot 10^{-2} & 7.0438472870 \cdot 10^{-1} \end{bmatrix}^T, \\ \mathbf{L}_{1\mathbf{z}_m} &= \begin{bmatrix} 1.5861569206 \cdot 10^{-1} & 3.1785414404 \cdot 10^{-1} & 4.5040703469 \cdot 10^{-1} \end{bmatrix}^T, \\ \mathbf{L}_{2\mathbf{z}_m} &= \begin{bmatrix} 4.1412783652 \cdot 10^{-3} & 7.2631368837 \cdot 10^{-3} & 2.2958859280 \cdot 10^{-3} \end{bmatrix}^T, \\ \mathbf{L}_{3\mathbf{z}_m} &= \begin{bmatrix} 1.5007058955 \cdot 10^{-4} & 3.0596503399 \cdot 10^{-4} & 1.9761198197 \cdot 10^{-4} \end{bmatrix}^T, \quad \text{and} \\ \mathbf{L}_{4\mathbf{z}_m} &= \begin{bmatrix} 5.0648855561 \cdot 10^{-4} & 8.8362809194 \cdot 10^{-4} & 3.0285439088 \cdot 10^{-4} \end{bmatrix}^T. \end{aligned}$$

The histograms of the marginal distributions of the random vectors corresponding to nominal model input parameters and target features are shown in Figure 4.5. The distributions of the nominal stiffnesses are known to be lognormal, whereas the best fitting distributions of corresponding frequencies are determined by a χ^2 -test [Montgomery et al.

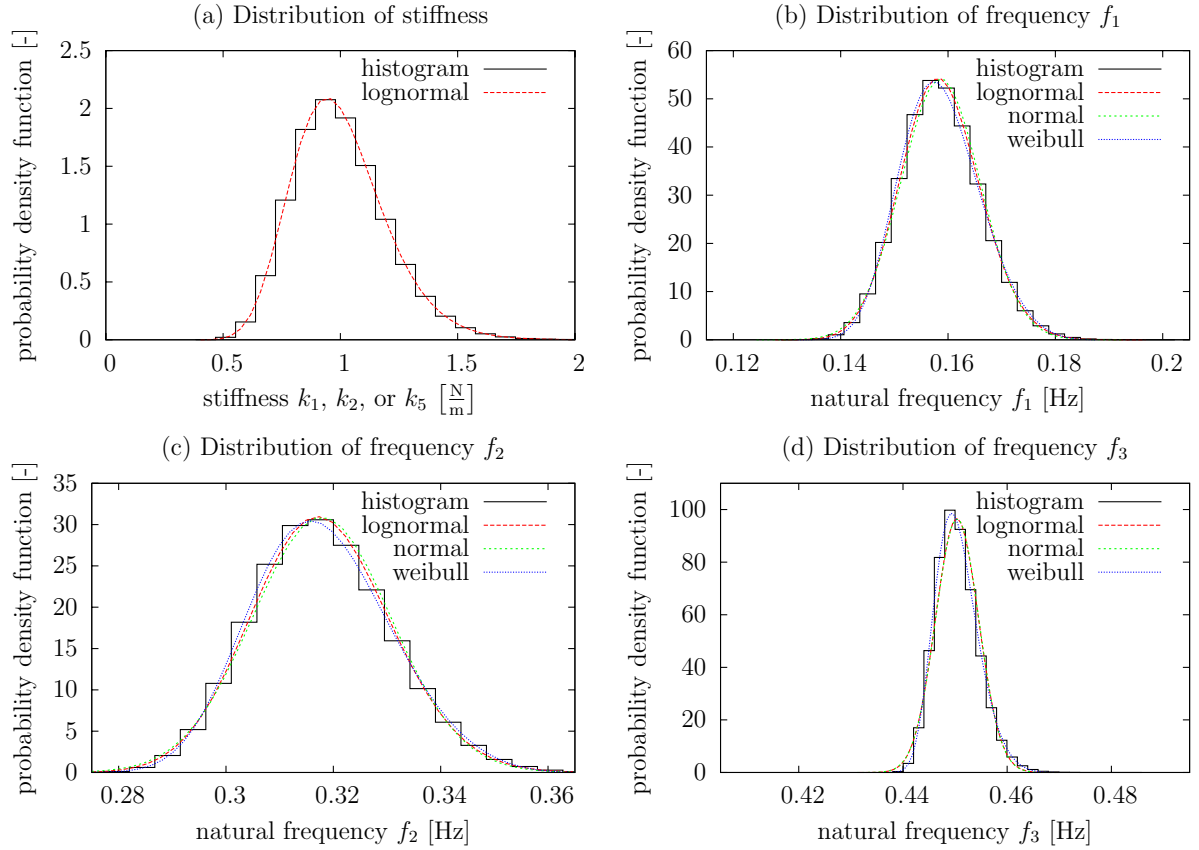


Figure 4.5: Probability density functions of the nominal stiffness and corresponding natural frequencies. The histograms are density estimations based on 1,000,000 Latin hyper-cube samples.

2002]. The Weibull, as well as, the lognormal distribution provide a valid description of the frequencies. However, the Weibull distribution is closer to the histogram, especially for the third natural frequency. The estimated probability density functions are also close to a probability density function of a normal distribution, which justifies the application of the explicit formulas of dissimilarity measures as objective functions.

This benchmark study investigates the suitability of dissimilarity measures, defined in Sections 4.3.3 and 4.3.4, with respect to their applicability as objective functions in the stochastic model updating process. The input parameter space is bounded by $[10^{-3}, 5]$ and $[10^{-3}, 0.5]$ for the mean values \mathbf{E}_{θ_j} and the standard deviations σ_{θ_j} of the unknown stiffnesses, respectively. The model input parameters are assumed to be uncorrelated. The accuracy of estimated statistical properties of the model responses \mathbf{E}_{z_j} and \mathbf{C}_{z_j} derived from a certain distribution of θ_j , depends on the sample size of the sample-based stochastic structural analysis.

In a first step, the properties of each objective function are numerically assessed by means of the convexity, monotonicity, and gradient indicator. Subsequently, the results of two nature inspired optimization methods, genetic algorithm (GA) and particle swarm

optimization (PSO), are compared. As an alternative to nature inspired optimization methods, the adaptive response surface method (ARSM) using a linear regression polynomial with a quadratic D-optimal sampling scheme is investigated.

4.5.2 Numerically derived properties of the objective functions

The gradients of the objective functions, as well as, the convexity and monotonicity properties are investigated by the indicators defined in Equations (4.61), (4.57), and (4.59), respectively. The investigation is based on a full factorial sampling using six points for each of the 728 slices. A detailed description to define the positions of the resulting 3,641 assessment points is given in Section 4.4. As the accuracy of the objective function value depends on the accuracy of the derived output parameters, the number of Latin hypercube sample sets to be used in the stochastic structural analysis is varied by 10, 100, and 1,000. Based on these calculated data, the objective function values

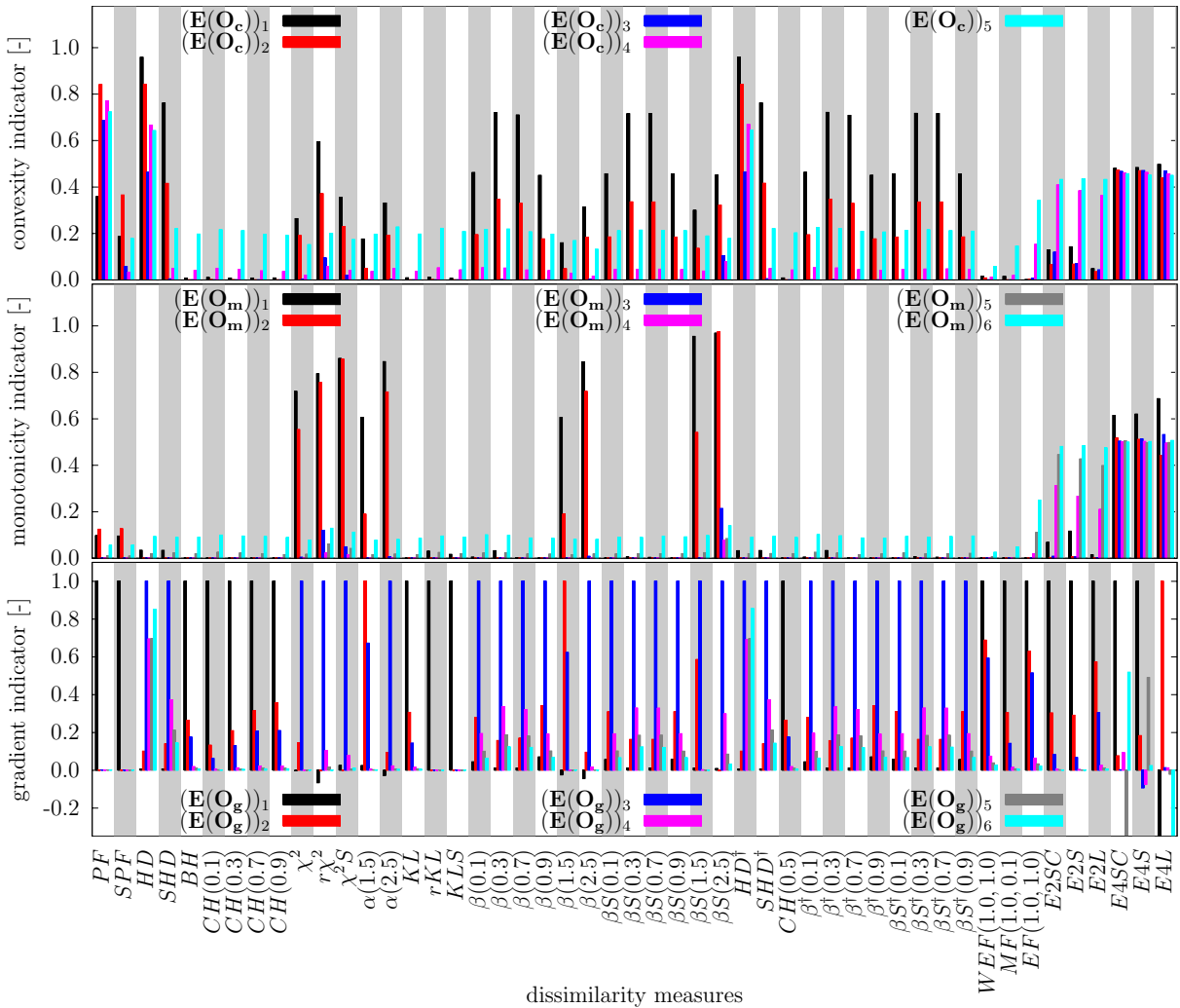


Figure 4.6: Averaged objective function properties of the three degree of freedom benchmark study using 10 Latin hypercube samples. The acronyms are defined in Table 4.2.

are determined. Then, the property indicators are derived relying on these objective function values. To increase the confidence of the obtained indicators, they are averaged over 20 independent evaluations of each objective function. The averaged indicators for all investigated dissimilarity measures are illustrated in Figures 4.6-4.8. The chosen acronyms for the dissimilarity measures are related to specific Equations as listed in Table 4.2. Some examples of objective function slices corresponding to one evaluation of the objective function are visualized in Figures 4.9 and 4.10. Therein, 1,000 Latin hypercube samples are utilized for the stochastic structural analysis.

Comparing Figures 4.6-4.8, the influence of the number of Latin hypercube samples is investigated. As expected, the accuracy of the output parameters is essential in the vicinity of the optimum. Indicators close to the boundaries are less affected. Hence, most fundamental changes are observed for indicators near the optimum. By increasing the samples from 100 to 1,000, only the indicators associated with the Euclidean norm of

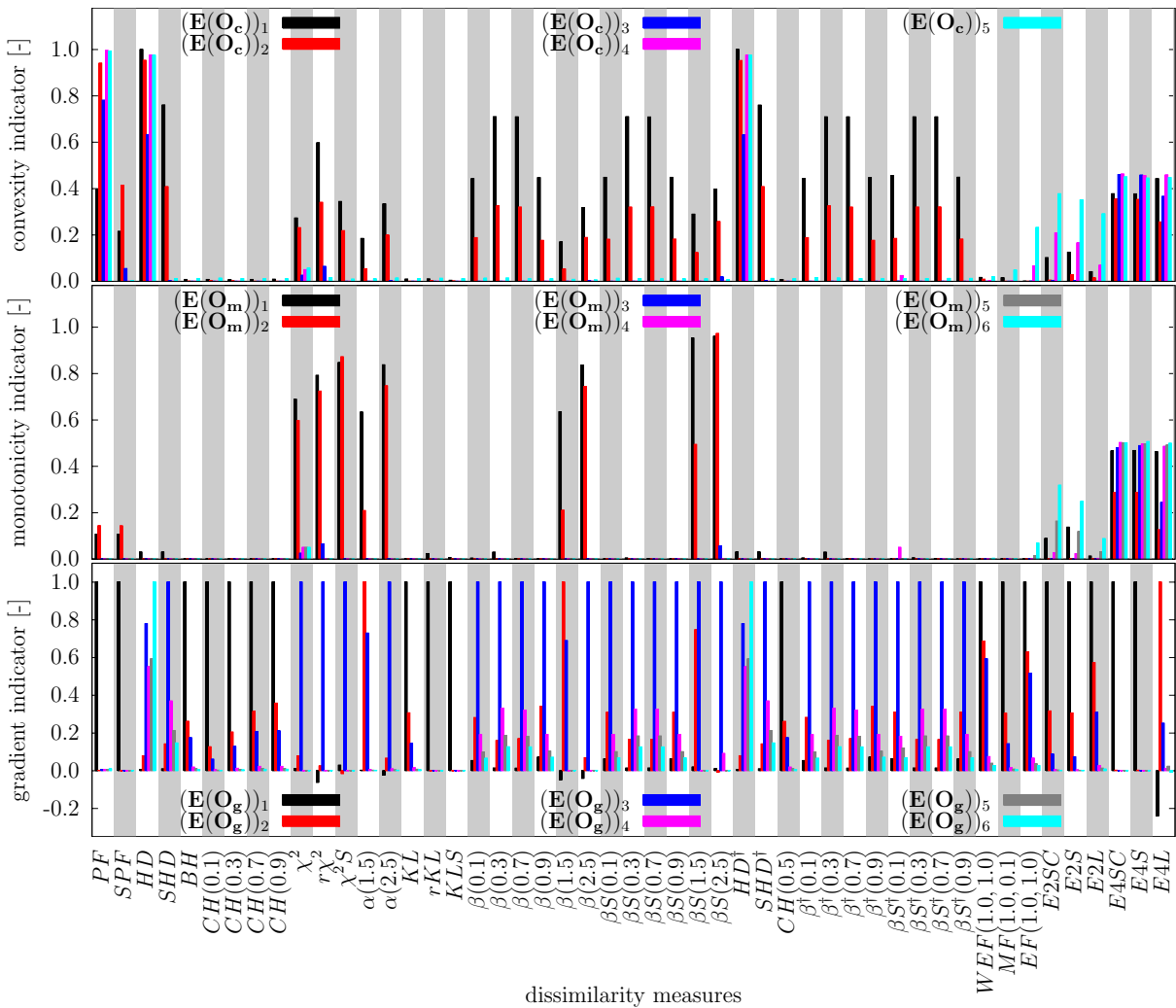


Figure 4.7: Averaged objective function properties of the three degree of freedom benchmark study using 100 Latin hypercube samples. The acronyms are defined in Table 4.2.

statistical moments are significantly influenced. For some measures, two different kinds of formula (e.g., HD vs. HD^\dagger) are used to compute the same dissimilarity measure. The results do not considerably disagree.

The Patrick-Fisher distance (PF) and squared Patrick-Fisher distance (SPF) perform similarly with respect to monotonicity and size of gradients. Both measures show an appreciable monotone behavior near the optimum. The violation of monotonicity at some positions close to the boundaries indicates the existence of local minima. Moreover, the sudden gradient change from $(\mathbf{E}(\mathbf{O}_g))_1$ to $(\mathbf{E}(\mathbf{O}_g))_2$ is not beneficial for the objective function. The squared Patrick-Fisher distance satisfies at least the property of convexity near the optimum.

Both, the Hellinger distance (HD) and the squared Hellinger distance (SHD), are almost monotone functions. The convexity indicator and the gradient indicator demon-

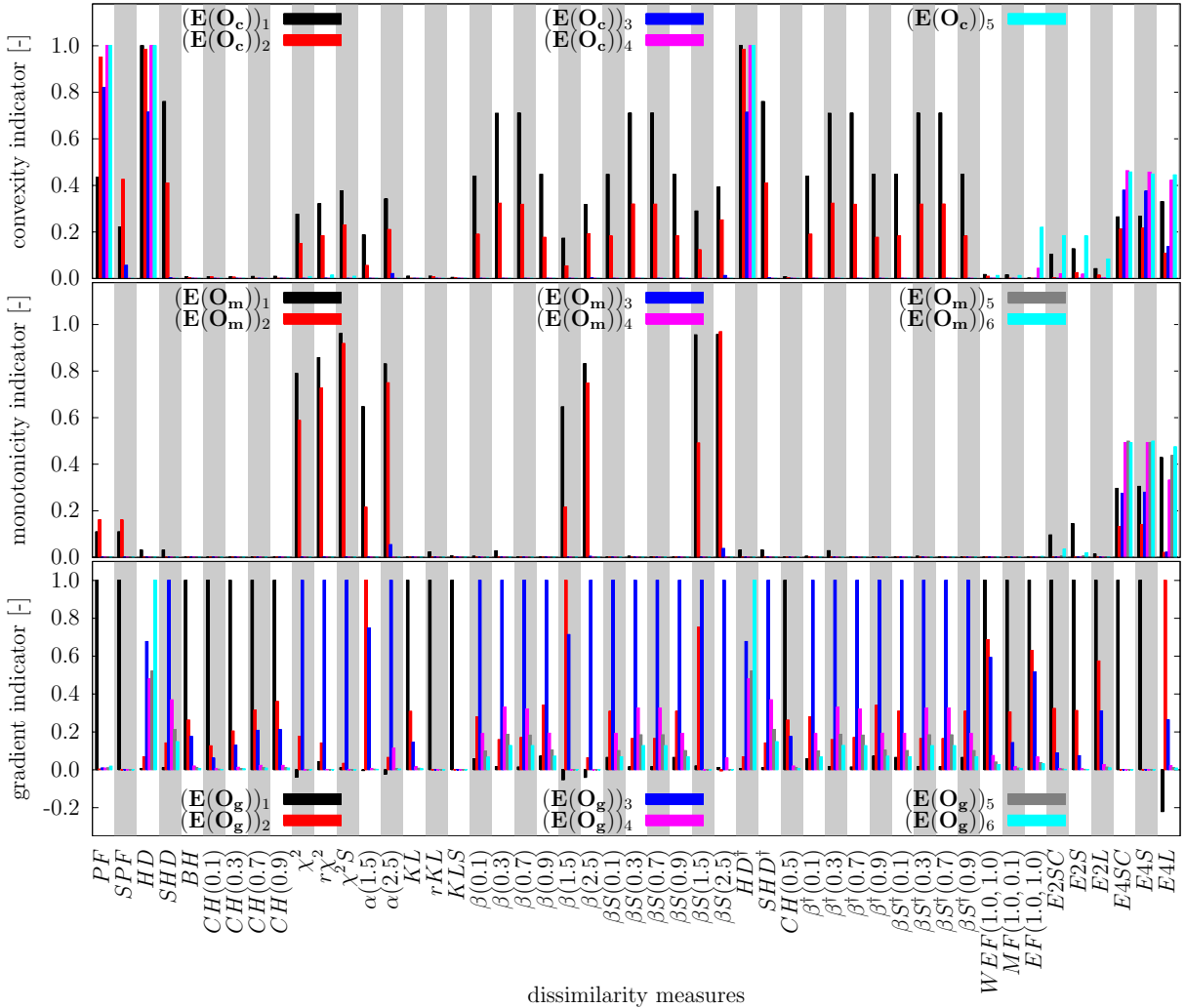


Figure 4.8: Averaged objective function properties of the three degree of freedom benchmark study using 1,000 Latin hypercube samples. The acronyms are defined in Table 4.2.

strate that the Hellinger distance is very irregular. Even if the squared Hellinger distance is convex near the optimum, it is a non-convex function with respect to the whole design space. As the squared Hellinger distance has an upper bound of two, the topology near the boundaries is similar to a plateau with small gradients. Representative slices for one objective function evaluation are depicted in Figures 4.9c and 4.9d.

Independent from its parametric value, the Chernoff distance (CH) has optimal properties to be used as an objective function. The convexity and monotonicity criteria are satisfied at all positions and the gradient changes monotonously using only 100 Latin hypercube samples. For $s = 0.5$, the Chernoff distance is commonly denoted by Bhattacharyya distance (BH). The slices of one representative objective function evaluation are presented in Figure 4.9b.

The χ^2 -divergence, reversed χ^2 -divergence ($r\chi^2$), symmetrized χ^2 -divergence (χ^2S), as well as, the α -divergences, β -divergences, and symmetrized β -divergences (βS) with parameters $s = 1.5$ and $s = 2.5$ are similar in their performance regarding the investigated properties. All of these measures have suitable properties in the vicinity of the optimum. Near the boundaries of the design space, a high degree of non-monotonicity and non-convexity is displayed, which indicates the existence of local minima. Furthermore, the average of all gradients, which coincides with the gradient indicator, is negative in some cases. The unfavorable behavior close to the boundaries is explained by violations of the positive definiteness condition for certain covariance matrix combinations. The positive definiteness condition is an essential requirement for numerical stability, which is defined in Section 4.3.3 for several dissimilarity measures. Examples of representative slices are visualized in Figures 4.9f-4.9h.

If at least 100 Latin hypercube sample sets are utilized in the stochastic structural analysis, the Kullback-Leibler divergence (KL) becomes a well-shaped objective function with respect to convexity and monotonicity. The gradient decreases monotonously with a decreasing distance of the input variables with respect to the optimum. The properties are similar to that of the Chernoff distance. Also the reversed Kullback-Leibler distance (rKL) and the symmetrized Kullback-Leibler distance ($KL S$) show suitable convex and monotone properties. Only the sudden change of the gradient near the boundaries can cause difficulties for certain optimization strategies. Slices of the objective function are presented in Figure 4.9a.

The objective functions based on the β -divergence with parameters $s = 0.1, \dots, 0.9$ are convex in the vicinity of the optimum and concave close to the boundaries of the design space. In general, they are smooth functions. Similar to the squared Hellinger distance, their topology near the boundaries is comparable to a plateau with small gradients. The properties of the symmetrized β -divergences (βS) are not significantly different from those of the β -divergences. Figure 4.9e shows a set of slices of the β -divergence with $s = 0.7$.

The weighted Euclidean Frobenius norm (WEF), Mahalanobis Frobenius norm (MF),

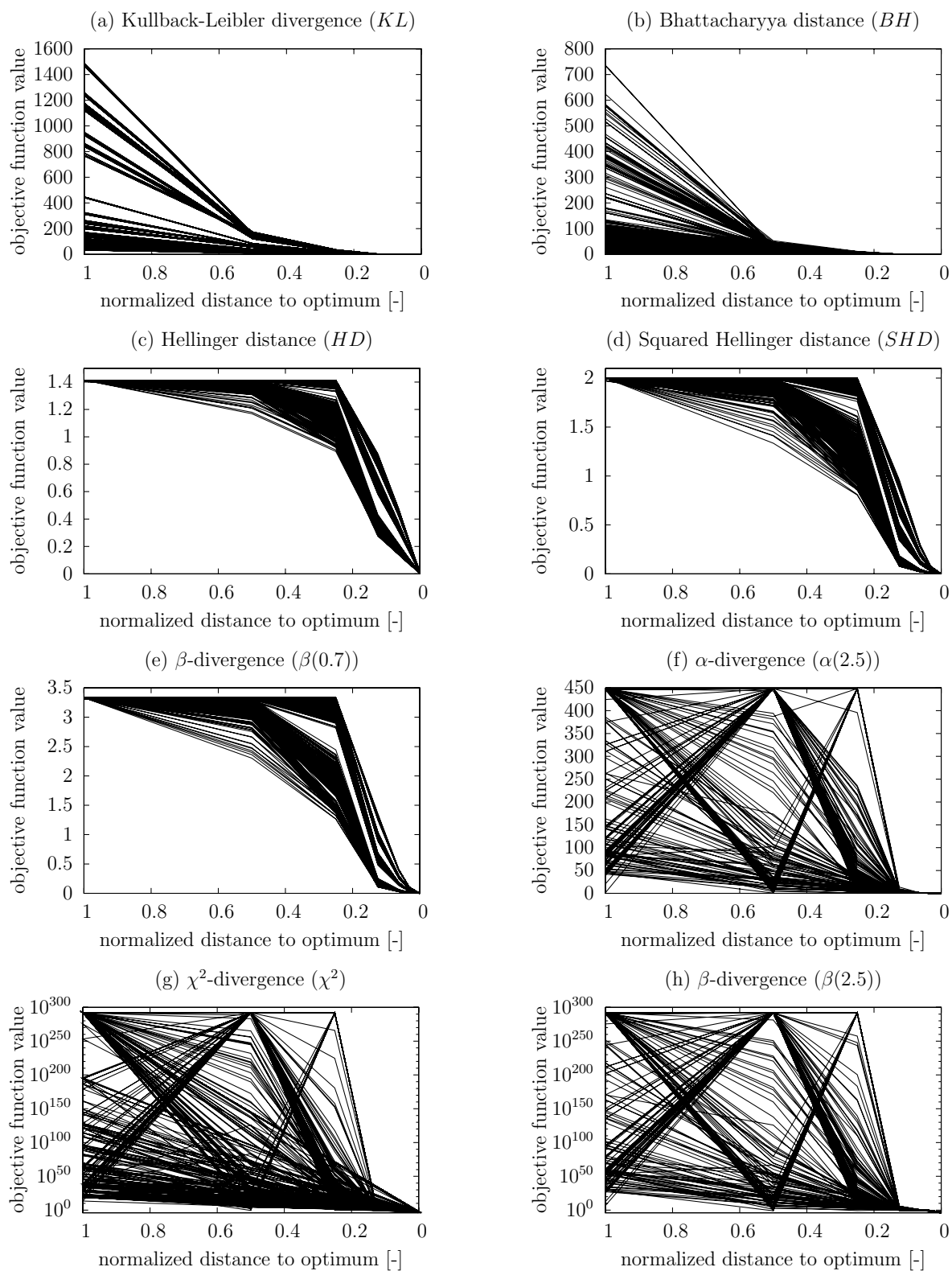


Figure 4.9: Slices of one representative objective function evaluation. The stochastic structural analysis of the three degree of freedom system is based on 1,000 Latin hypercube samples.

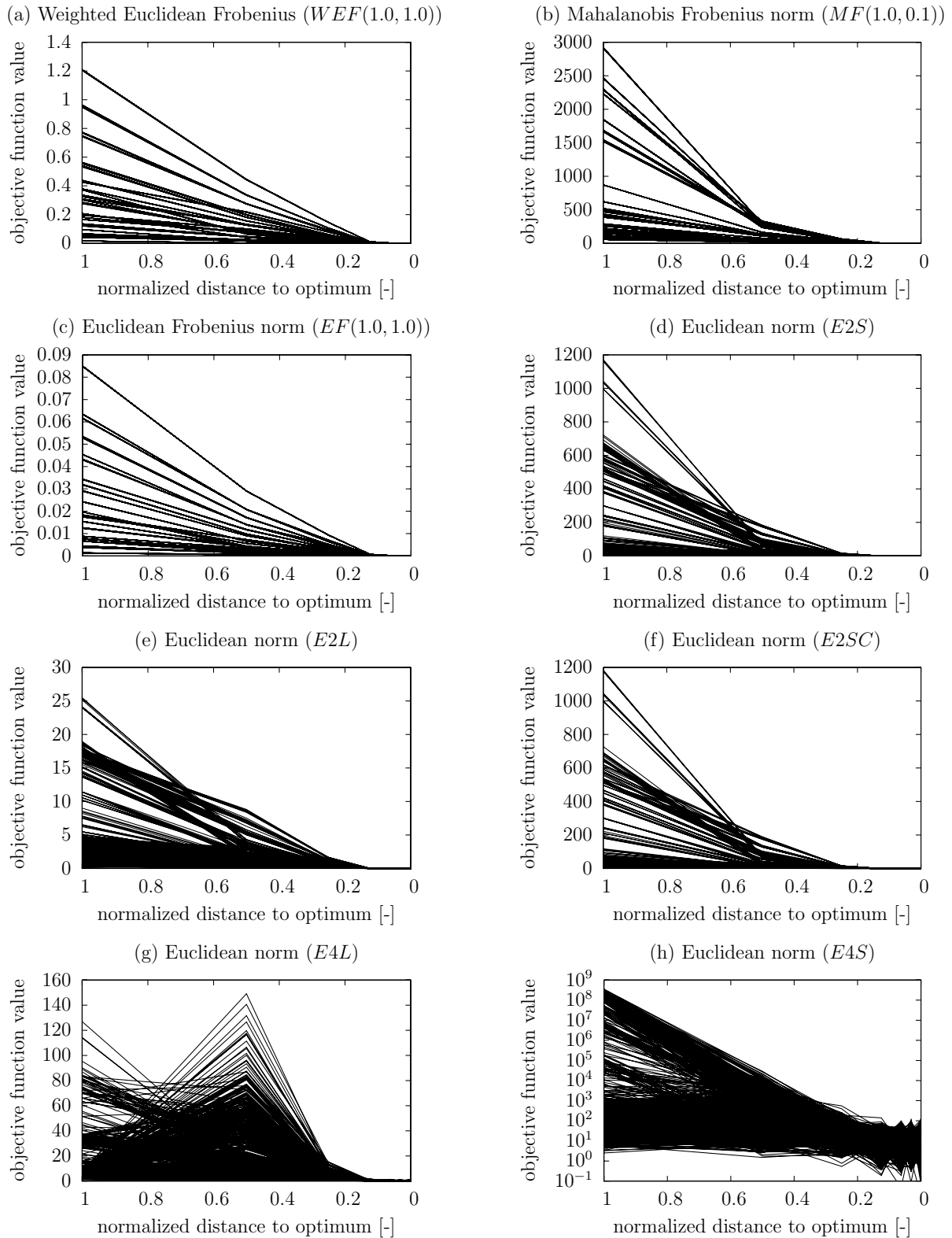


Figure 4.10: Slices of one representative objective function evaluation. The stochastic structural analysis of the three degree of freedom system is based on 1,000 Latin hypercube samples. (continued from Figure 4.9)

and Euclidean Frobenius norm (EF) are monotone at all investigated points. Even if the convexity is not perfectly confirmed close to the optimum, they can serve as an objective function for the considered three degree of freedom system. Also the gradient indicator predicts a smooth and almost convex function. Of course, the suitability of these measures depends on the selection of the weighting parameters w_1 and w_2 . In the present study, the discrepancies related to the mean values and the variances near the optimum are equally weighted. However, as the optimum is typically not known, the suitable choice of weighting factors is always a difficult task.

Another possibility to define a dissimilarity measure is to apply the Euclidean norm of the first two statistical moments (i.e., $E2SC$, $E2S$, $E2L$). These measures are smooth as indicated by the gradients, but they have some drawbacks with respect to convexity and monotonicity nearby the optimum and the boundaries. A significant effect of using the correlation coefficient cannot be observed. Generally, the application of L moments instead of the standard statistical moments is advantageous. In comparison to other investigated measures, the measures based on the first two statistical moments benefit extraordinarily from an increase of Latin hypercube samples used in the stochastic structural analysis.

So far, only the first two statistical moments are applied to the dissimilarity measures, which is not sufficient, if the probability density function is significantly unsymmetric. To consider also unsymmetric probability density functions, measures related to the Euclidean norm of the first four statistical moments represented by the acronyms $E4SC$, $E4S$, and $E4L$ have been introduced. Unfortunately, their properties, especially the non-monotonicity, are not feasible for an objective function. Furthermore, negative gradients are derived. Hence, a high number of local minima can be expected. The undesirable properties are explained by the insufficient accuracy of the third and fourth moments obtained with the investigated number of Latin hypercube samples. Representative objective function slices are given in Figure 4.10g and 4.10h.

In summary, a number of 100 Latin hypercube samples is sufficient to represent the principle behavior of the objective functions at the investigated discrete points. The Bhattacharyya distance, the Kullback-Leibler divergence, the weighted Euclidean Frobenius norm, and the Mahalanobis Frobenius norm are the most suitable dissimilarity measures obtained for this benchmark study. In the following section, all investigated dissimilarity measures will be tested as objective functions for different optimization strategies.

4.5.3 Dissimilarity measures applied as objective functions

The previous section concluded that some dissimilarity measures are qualified to be applied as objective functions. This section aims to demonstrate that optimization methods in combination with the suggested dissimilarity measures can be successfully applied to

Table 4.3: Configuration parameters of the genetic algorithm (GA) applied to the three degree of freedom benchmark study.

parameters	value
number of parents	34
number of individuals	68
number of generations	70

Table 4.4: Configuration parameters of the particle swarm optimization (PSO) applied to the three degree of freedom benchmark study.

parameters	value
number of particles	36
number of iterations	70

Table 4.5: Configuration parameters of the adaptive response surface method (ARSM) applied to the three degree of freedom benchmark study.

parameters	value
maximal iterations or function calls	58
samples for quadratic D-optimal scheme	42

solve stochastic model updating problems. It is not intended to determine the best optimization method with its optimal configuration parameters.

The genetic algorithm and particle swarm optimization method are investigated with a variation of 100 and 10,000 Latin hypercube samples used for the stochastic structural analysis. These investigations are supplemented by the results obtained from an adaptive response surface approach.

For the nature inspired optimization methods, a randomly chosen set is automatically defined as initial input parameter set. In case of the adaptive response surface method, the initial mean values and covariance matrix for the unknown stiffnesses are set to

$$\mathbf{E}_{\theta_0} = \begin{bmatrix} 2 & 2 & 2 \end{bmatrix}^T \quad \text{and} \quad (\mathbf{C}_{\theta_0})_{i,j} = \begin{cases} 0.09 & : i = j \\ 0.00 & : i \neq j \end{cases}, \quad (4.63)$$

which are identical to the values chosen in the investigations by [Khodaparast et al. 2008b]. A short description of the optimization algorithms is given in Appendix B. Tables 4.3 – 4.5 list the corresponding most important configuration parameters, which are related to a similar total number of design point evaluations for each optimization method.

The suitability of each optimization strategy and dissimilarity measure is judged by the error

$$\varepsilon_1 = \sum_{i=1}^{m_x} \left(1 - \frac{(\tilde{\mathbf{x}})_i}{(\hat{\mathbf{x}})_i} \right)^2 \quad (4.64)$$

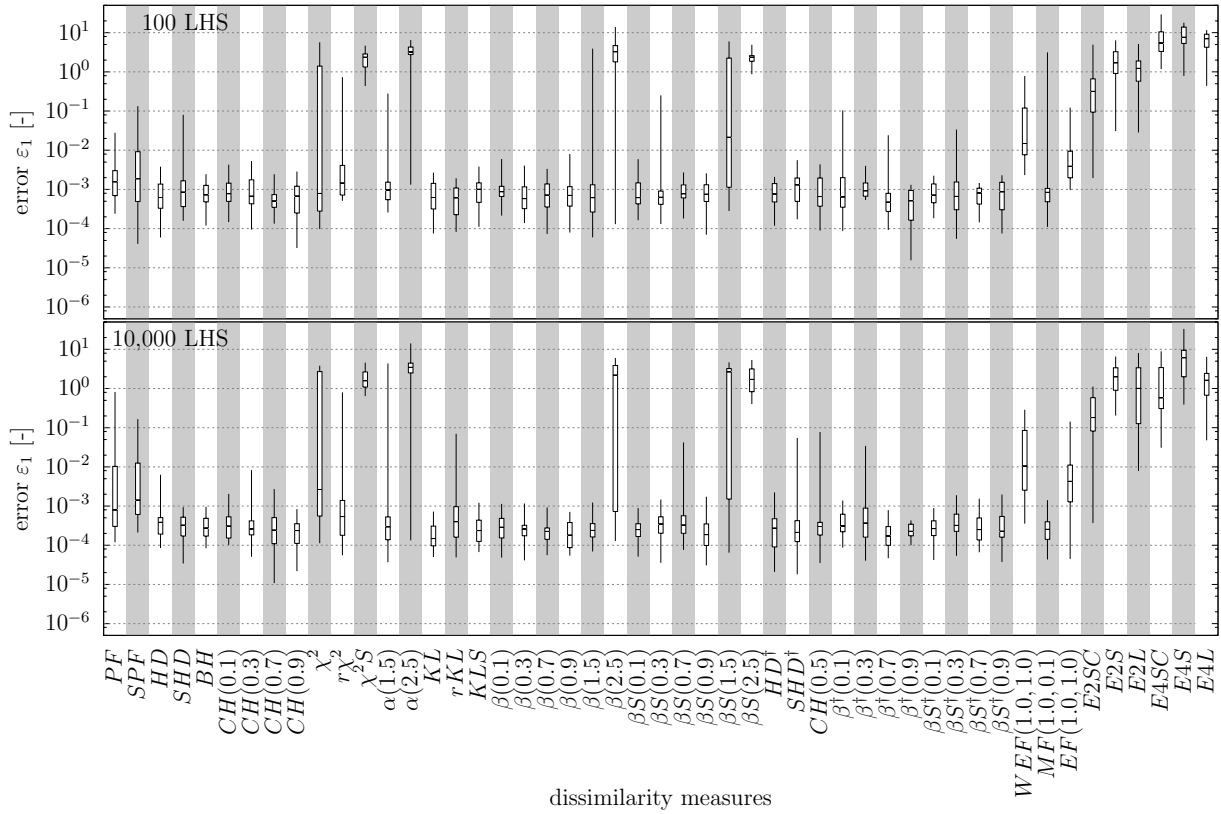


Figure 4.11: Statistics of the error norm ε_1 according to Equation (4.64) using genetic algorithm (GA). The statistics are based on 20 independent optimization runs. To evaluate one objective function value, 100 and 10,000 Latin hypercube samples are applied.

between nominal input parameters $\hat{\mathbf{x}}$ and obtained optimal input parameter values $\tilde{\mathbf{x}}$ with $m_x = 6$. Based on 20 independent optimization runs for each configuration, a statistical assessment is derived and presented in form of a boxplot (e.g., [Falk et al. 2002]). The boxplot indicates minimum, 25-percent quantile, median, 75-quantile, and maximum of the criterion according to Equation (4.64). The results are visualized in Figures 4.11-4.13.

This investigation supports the conclusions drawn from the investigation of objective function properties. The measures χ^2 divergence, reversed χ^2 divergence, symmetrized χ^2 divergence, as well as, all α - and β -divergences with parameters $s = 1.5$ and $s = 2.5$ are not recommended to be used. The only exception is the α -divergence in combination with the adaptive response surface method. With this optimization method and a parameter $s = 1.5$, the best results are obtained with the α -divergence. Furthermore, the dissimilarity measures related to the norms of statistical moments and L moments are not recommended to be applied as objective functions.

By comparing the results of the different optimization methods, some global trends can be observed. The results of the particle swarm optimization method have higher deviations, but are in average more accurate than the results obtained by the genetic algorithm. Applying the adaptive response surface method, a good accuracy with low

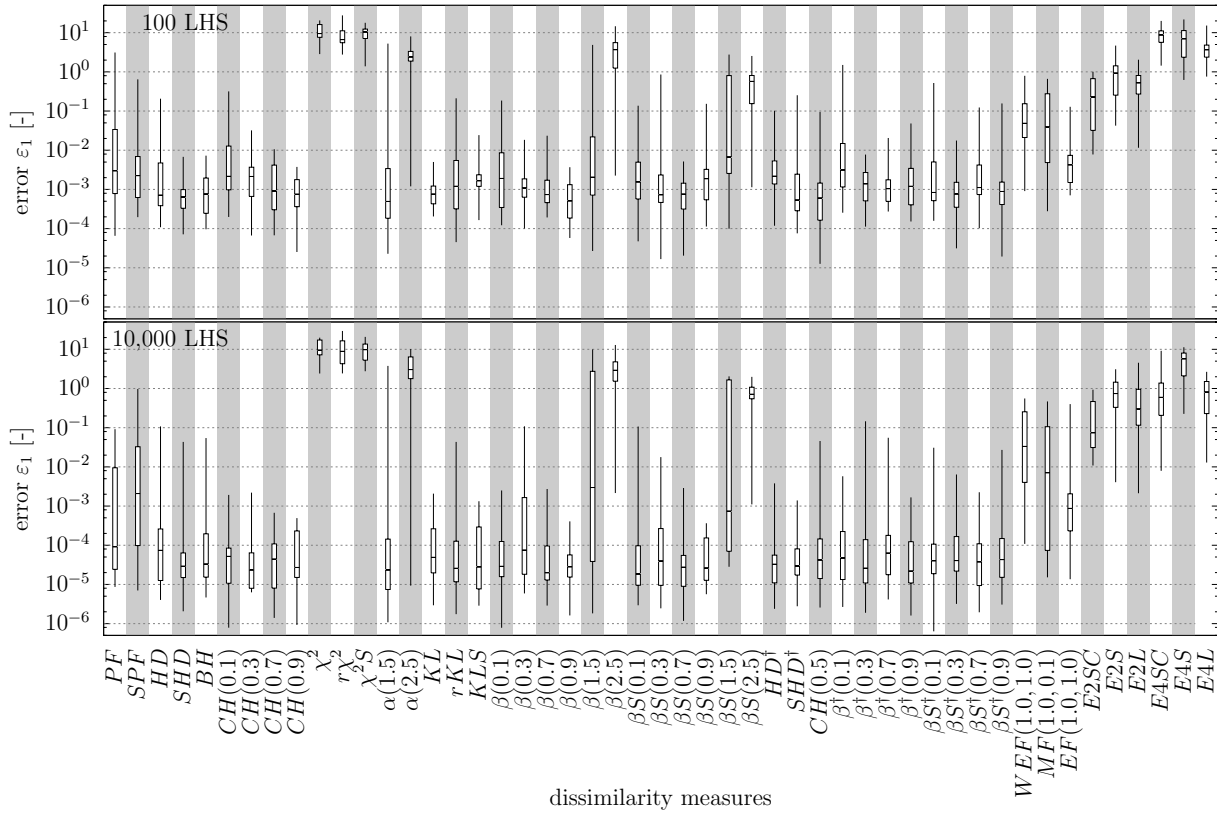


Figure 4.12: Statistics of the error norm ε_1 according to Equation (4.64) using particle swarm optimization (PSO). The statistics are based on 20 independent optimization runs. To evaluate one objective function value, 100 and 10,000 Latin hypercube samples are applied.

deviations can be derived with only 100 Latin hypercube samples.

The improvements resulting from an increased number of Latin hypercube samples are not high enough to justify the increased computational expense. This can be explained to a certain extent by a non-optimal set of configuration parameters applied to the optimization methods.

In summary, the Bhattacharyya distance, the Kullback-Leibler divergence, and the β -divergence with $s = 0.7$ are suitable measures independent from the optimization method. In addition, the α -divergence using $s = 1.5$ in combination with the adaptive response surface method and the Mahalanobis Frobenius norm combined with a genetic algorithm show acceptable results.

Since the Kullback-Leibler divergence is one of the most suitable objective functions, it has been selected for a more detailed investigation. Figure 4.14 shows the convergence of the solution for all optimization algorithms using the Kullback-Leibler distance as objective function. Each line corresponds to a single representative optimization run. The nature inspired optimization methods behave similar. The number of Latin hypercube samples shows no significant influence. As no stagnation is observed, it is advised to

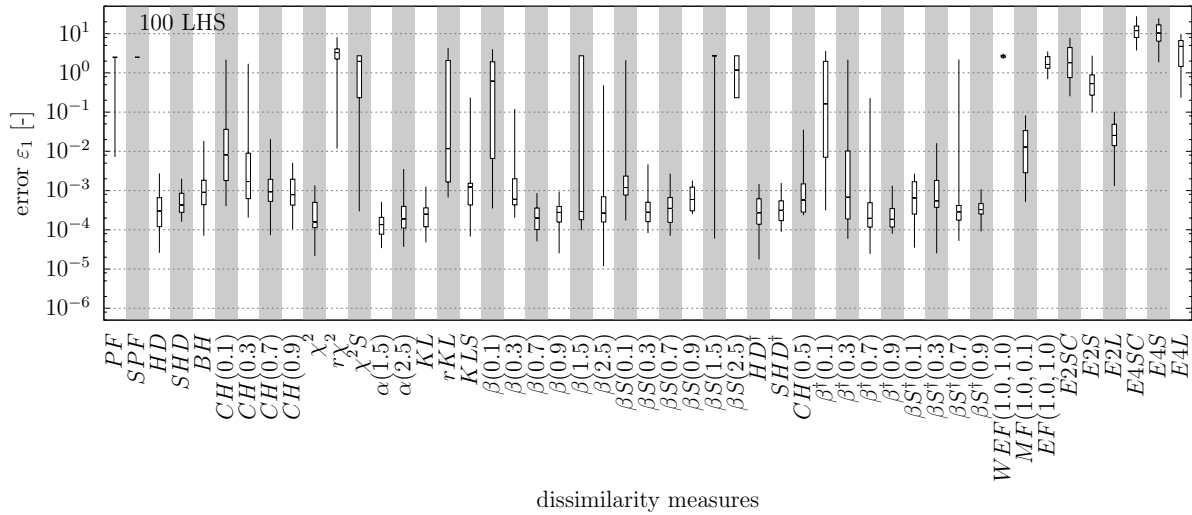


Figure 4.13: Statistics of the error norm ε_1 according to Equation (4.64) using adaptive response surface optimization methods (ARSM). The statistics are based on 20 independent optimization runs. To evaluate one objective function value, 100 Latin hypercube samples are applied.

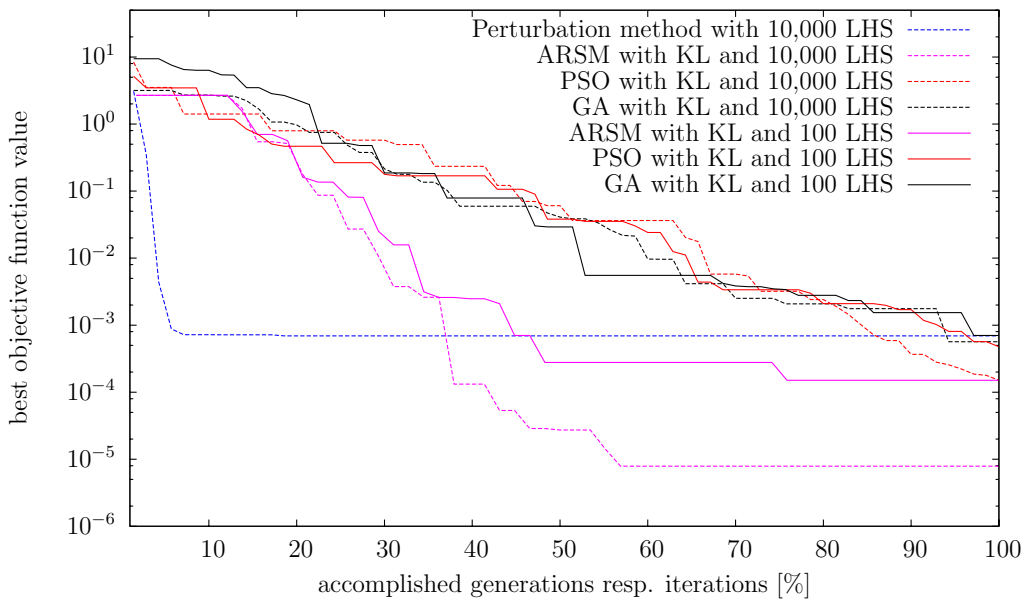


Figure 4.14: Convergence of the solution indicated by the best objective function value depending on the generation or iteration number.

increase the number of generations or iteration steps to improve the quality of the results. The solutions of the adaptive response surface methods converge fast in the first half of the optimization. In the second half, the solutions do not converge significantly, which may be explained by the discrepancy between the true objective function and its approximation. However, the adaptive response surface method performs better than the nature inspired

optimization method investing similar computational effort.

For comparison, the convergence of the sensitivity-based perturbation method proposed by [Khodaparast et al. 2008b] is presented in Figure 4.14. The graph refers to the simplified form of the method, in which the correlation between measured features and model parameters is neglected. The Monte Carlo sampling is replaced by the Latin hypercube sampling as recommended by [Brehm et al. 2009a]. A fast convergence within the first few iteration steps can be observed. Unfortunately, the solution cannot be reduced in the subsequent iteration steps, which indicates a systematic error of the perturbation method.

Table 4.6 presents the statistical information of identified input parameters regarding 20 independent optimization runs for each configuration. The Kullback-Leibler divergence in combination with the genetic algorithm and particle swarm optimization is investigated with respect to 100 and 10,000 Latin hypercube samples. For each input parameter $(\mathbf{x})_i$, the error is defined by

$$\varepsilon_2(i) = 1 - \frac{(\tilde{\mathbf{x}})_i}{(\hat{\mathbf{x}})_i} \quad \forall i = 1, \dots, m_x. \quad (4.65)$$

Based on mean values and standard deviations of the errors $\varepsilon_2(i)$, the two indicators

$$\varepsilon_{3E} = \sqrt{\sum_{i=1}^{m_x} (\mathbf{E}(\varepsilon_2(i)))^2} \quad \text{resp.} \quad \varepsilon_{3\sigma} = \sqrt{\sum_{i=1}^{m_x} (\sigma(\varepsilon_2(i)))^2} \quad (4.66)$$

can be derived with $m_x = 6$. The vectors $\tilde{\mathbf{x}}$ and $\hat{\mathbf{x}}$ are related to the identified and nominal input parameters, respectively. It can be observed that the mean values are identified with a higher accuracy than the standard deviations. Only the accuracy of the standard deviations is significantly improved by increasing the number of samples from 100 to 10,000. With respect to the errors ε_{3E} and $\varepsilon_{3\sigma}$, the genetic algorithm should be preferred. However, the benefit of the genetic algorithm is only marginal.

The results deduced from the adaptive response surface method are shown in Table 4.7. In comparison to the nature inspired optimization algorithms, only the standard deviation error $\varepsilon_{3\sigma}$ is significantly improved. The value of the indicator ε_{3E} is similar to those of the genetic algorithm and particle swarm optimization listed in Table 4.6.

Furthermore, the influence of a variation in the number of parents and generations is investigated for the genetic algorithm. The respective results are presented in Table 4.7. It is observed that the proposed variations do not achieve an improvement of the identified parameters.

To compare the proposed optimization-based stochastic model updating method with the sensitivity-based stochastic model updating method suggested by [Khodaparast et al. 2008b], Table 4.8 collects the results from both approaches. Assuming that the solver runs conducted for the stochastic structural analysis are the most time consuming calculations,

Table 4.6: Comparison between genetic algorithm and particle swarm optimization. The statistical values of identified input parameters are based on 20 independent optimization runs.

method		GA with KL				PSO with KL			
LHS		100		10,000		100		10,000	
total solver runs		$\approx 250,000$		$\approx 25,000,000$		$\approx 250,000$		$\approx 25,000,000$	
		error ε_2 [%]		error ε_2 [%]		error ε_2 [%]		error ε_2 [%]	
i	parameter	$\mathbf{E}(\varepsilon_2(i))$	$\boldsymbol{\sigma}(\varepsilon_2(i))$	$\mathbf{E}(\varepsilon_2(i))$	$\boldsymbol{\sigma}(\varepsilon_2(i))$	$\mathbf{E}(\varepsilon_2(i))$	$\boldsymbol{\sigma}(\varepsilon_2(i))$	$\mathbf{E}(\varepsilon_2(i))$	$\boldsymbol{\sigma}(\varepsilon_2(i))$
1	$\mathbf{E}(\tilde{k}_1)$	0.1069	0.3774	0.0355	0.3053	0.0525	0.2429	0.0203	0.0740
2	$\mathbf{E}(\tilde{k}_2)$	-0.1136	0.2901	0.0207	0.3276	0.0150	0.2270	0.0175	0.0973
3	$\mathbf{E}(\tilde{k}_5)$	0.0882	0.3099	0.0926	0.1988	0.0450	0.1614	-0.0250	0.0807
4	$\boldsymbol{\sigma}(\tilde{k}_1)$	0.6232	2.1620	0.0380	0.8671	0.4170	2.1280	0.1475	1.1131
5	$\boldsymbol{\sigma}(\tilde{k}_2)$	0.1707	1.3498	0.0252	0.8038	0.3432	2.4061	0.2007	1.2347
6	$\boldsymbol{\sigma}(\tilde{k}_5)$	-0.0243	1.2532	0.1250	0.8836	0.5380	1.1078	0.0350	0.7421
ε_{3E} resp. $\varepsilon_{3\sigma}$		0.6710	2.8964	0.1672	1.5553	0.7656	3.4178	0.2542	1.8264

Table 4.7: Results derived from the adaptive response surface method (ARSM) and a variation in configuration parameters of the genetic algorithm (GA). The statistical values of identified input parameters are based on 20 independent optimization runs.

method		ARSM with KL				GA with KL			
LHS		100		10,000		100 ^a		100 ^b	
total solver runs		$\approx 250,000$		$\approx 25,000,000$		$\approx 2,500,000$		$\approx 25,000,000$	
		error ε_2 [%]		error ε_2 [%]		error ε_2 [%]		error ε_2 [%]	
i	parameter	$\mathbf{E}(\varepsilon_2(i))$	$\boldsymbol{\sigma}(\varepsilon_2(i))$	$\mathbf{E}(\varepsilon_2(i))$	$\boldsymbol{\sigma}(\varepsilon_2(i))$	$\mathbf{E}(\varepsilon_2(i))$	$\boldsymbol{\sigma}(\varepsilon_2(i))$	$\mathbf{E}(\varepsilon_2(i))$	$\boldsymbol{\sigma}(\varepsilon_2(i))$
1	$\mathbf{E}(\tilde{k}_1)$	0.0787	0.2611	0.0118	0.0241	0.1147	0.1385	0.0815	0.0813
2	$\mathbf{E}(\tilde{k}_2)$	-0.0044	0.1610	-0.0036	0.0201	-0.0191	0.1287	-0.0237	0.0916
3	$\mathbf{E}(\tilde{k}_5)$	0.2058	0.3016	0.1022	0.1090	-0.0073	0.1361	0.0414	0.1057
4	$\boldsymbol{\sigma}(\tilde{k}_1)$	0.2500	1.1581	0.0520	0.1818	0.7077	0.9870	0.9532	0.9569
5	$\boldsymbol{\sigma}(\tilde{k}_2)$	0.2850	0.8340	-0.0878	0.2136	0.2635	0.8381	-0.0735	0.7759
6	$\boldsymbol{\sigma}(\tilde{k}_5)$	0.4500	0.6849	0.0737	0.1325	0.3057	0.5335	0.1627	0.4029
ε_{3E} resp. $\varepsilon_{3\sigma}$		0.6283	1.6404	0.1626	0.3303	0.8231	1.4197	0.9744	1.3062

^a configuration parameter variation with 70 parents, 350 generations

^b configuration parameter variation with 140 parents, 1750 generations

Table 4.8: Comparison of different updating methods with similar computational expense. The statistical values of identified input parameters are based on 20 independent optimization runs.

method		perturbation method		GA with KL		PSO with KL		ARSM with KL	
LHS		10,000		40		40		40	
total solver runs		$\approx 100,000$		$\approx 100,000$		$\approx 100,000$		$\approx 100,000$	
		error ε_2 [%]		error ε_2 [%]		error ε_2 [%]		error ε_2 [%]	
i	parameter	$\mathbf{E}(\varepsilon_2(i))$	$\boldsymbol{\sigma}(\varepsilon_2(i))$	$\mathbf{E}(\varepsilon_2(i))$	$\boldsymbol{\sigma}(\varepsilon_2(i))$	$\mathbf{E}(\varepsilon_2(i))$	$\boldsymbol{\sigma}(\varepsilon_2(i))$	$\mathbf{E}(\varepsilon_2(i))$	$\boldsymbol{\sigma}(\varepsilon_2(i))$
1	$\mathbf{E}(\tilde{k}_1)$	0.1289	0.0051	0.0143	0.4444	0.0831	0.3534	0.3859	0.4615
2	$\mathbf{E}(\tilde{k}_2)$	-0.0440	0.0048	0.2637	1.0532	-0.0554	0.4008	0.0492	0.3048
3	$\mathbf{E}(\tilde{k}_5)$	-0.0539	0.0024	0.2237	0.4917	0.1462	0.3480	0.2322	0.3289
4	$\boldsymbol{\sigma}(\tilde{k}_1)$	2.2637	0.0185	1.1760	2.2873	0.7407	2.8058	1.9657	1.8117
5	$\boldsymbol{\sigma}(\tilde{k}_2)$	1.3576	0.0350	-0.1340	1.5984	0.4062	2.6342	1.1227	1.1237
6	$\boldsymbol{\sigma}(\tilde{k}_5)$	-0.4315	0.0512	1.0857	1.8946	1.0902	2.5581	1.1472	1.6541
ε_{3E} resp. $\varepsilon_{3\sigma}$		2.6786	0.0652	1.6430	3.5951	1.3906	4.6649	2.5780	2.7740

the computational expenses are comparable for all approaches. Due to the fast converging behavior of the perturbation method, only 10 iteration steps are accomplished. The configuration parameters for the optimization algorithms remain unchanged in comparison to previous calculations.

As the results show, it is not possible to nominate one single method as the best approach for the given limitation of 100,000 solver runs. The optimization methods derive more accurate mean values of the identified input parameters, whereas the input parameters obtained by the perturbation method have lower standard deviations. On average the results found with the particle swarm optimization are the best, but their scatter is the worst in comparison with other methods.

For this benchmark study, it is not possible to determine one preferred optimization method. Of course, the perturbation method converges fast to a solution, but a systematic error is always present. Also, the adaptive response surface method has a fast convergence rate with low computational effort. But due to the approximation, a systematic error cannot be avoided. Furthermore, the success of both approaches depends on the chosen initial input parameter values. In contrast, the nature inspired optimization methods can always find a solution near the optimum. By increasing the computational effort for nature inspired optimization methods, an improvement can be obtained.

It can be constituted that several optimization methods in combination with the proposed dissimilarity measures can be successfully applied for the stochastic model updating problem of this benchmark study. The quality of the derived results obtained by optimization methods and by sensitivity-based methods is almost identical.

4.6 Benchmark study: Truss system

4.6.1 Description

This numerical benchmark study is based on a plain truss cantilever with 20 degrees of freedom consisting of 12 nodes and 21 truss members. The same system has been applied in [Khodaparast et al. 2008b] for a numerical sensitivity-based stochastic model updating benchmark study and in Chapter 3 for the investigation of mode pairing strategies. The geometry is presented in Figure 4.15. The cross-sectional area, the mass density, and the Poisson's ratio of all truss members are set to the known deterministic values of 0.03m^2 , $2700\frac{\text{kg}}{\text{m}^3}$, and 0, respectively. The material is linear elastic. For all non-diagonal truss members, a known Young's modulus of $7 \cdot 10^{10}\frac{\text{N}}{\text{m}^2}$ is chosen and considered as deterministic value.

The Young's moduli of the diagonal elements T1–T5 are unknown and will be represented by $E(T_i) = (\boldsymbol{\theta})_i \cdot 7 \cdot 10^{10}\frac{\text{N}}{\text{m}^2} \forall i = 1, \dots, 5$, whereas $\boldsymbol{\theta}$ is the random vector of model input parameters. The random vector $\boldsymbol{\theta}$ is described by a multivariate

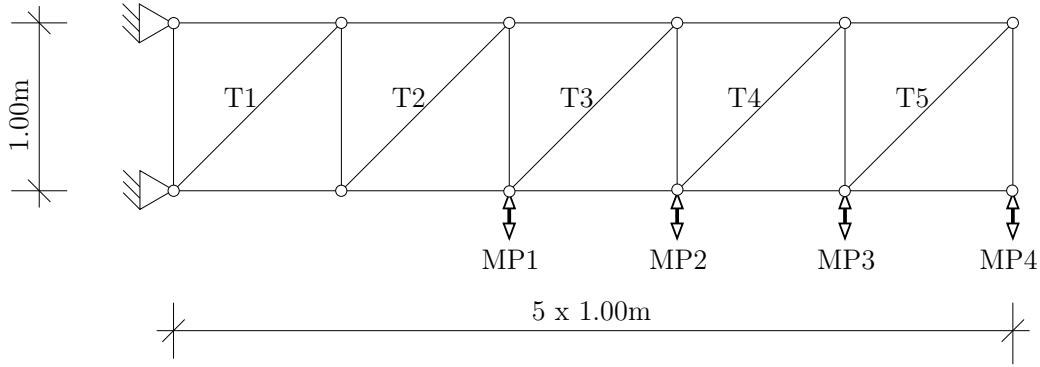


Figure 4.15: Truss system with indicated measurement points (MP) and directions.

lognormal distribution with mean value \mathbf{E}_θ and covariance matrix \mathbf{C}_θ . As the entries of the random vector are assumed to be uncorrelated, it is sufficient to assemble the mean values and standard deviations into the unknown input parameter vector $\mathbf{x} = [(\mathbf{E}_\theta)_1 \dots (\mathbf{E}_\theta)_5 (\sigma_\theta)_1 \dots (\sigma_\theta)_5]^T$. These input parameters are modified during the optimization with the aim to minimize the difference between output parameters \mathbf{y} and target output parameters \mathbf{y}_m .

The statistical properties of the distribution of the random feature vector are obtained by a numerical modal analysis of 1,000,000 Latin hypercube samples generated from the model parameter vector, described by the nominal mean value vector and the nominal covariance matrix

$$\mathbf{E}_{\hat{\theta}} = \begin{bmatrix} 1 & 1 & 1 & 1 & 1 \end{bmatrix} \quad \text{and} \quad (\mathbf{C}_{\hat{\theta}})_{i,j} = \begin{cases} 0.018225 & : i = j \\ 0.000000 & : i \neq j \end{cases}, \quad (4.67)$$

respectively. The target feature vector is representing the natural frequencies of the first four bending modes and the corresponding vertical modal displacements at measurement positions MP1-MP4. Therefore, a total number of 20 features is defined. Figure 4.15 indicates the measurement positions. The first four bending modes related to the nominal mean values of the stiffnesses are illustrated in Figure 4.16. Performing a sample-based stochastic structural analysis, the target output parameters, mean value, covariance matrix, skewness, kurtosis, and the first four L moments, can be extracted. Figure 4.17 shows the estimated and fitted analytical probability density functions of the marginal distributions of some target feature parameters. The target features are typically obtained from experimental data. For this benchmark study, they are generated by performing the previously described artificial experiment.

Mode switches are frequently possible, due to the variation of stiffnesses related to both, the generation of target features and the adjustments during the optimization process. In this benchmark study, the energy-based modal assurance criterion (EMAC) according to Equation (3.14) has been applied to assign numerically derived modes to experimentally obtained modes. The respective cluster includes all vertical degrees of

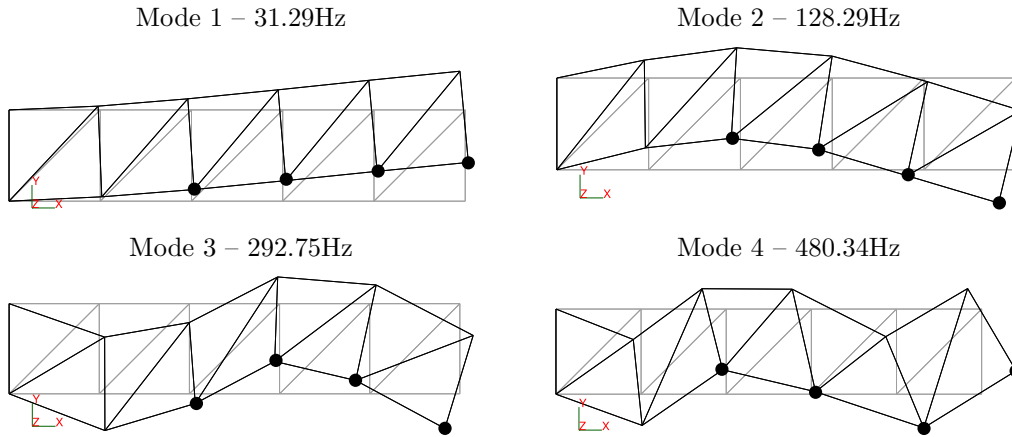


Figure 4.16: First four vertical mode shapes of the system related to the nominal mean values of the stiffnesses. Only the vertical modal displacements of the marked positions (●) are assumed to be available for the artificial experiment.

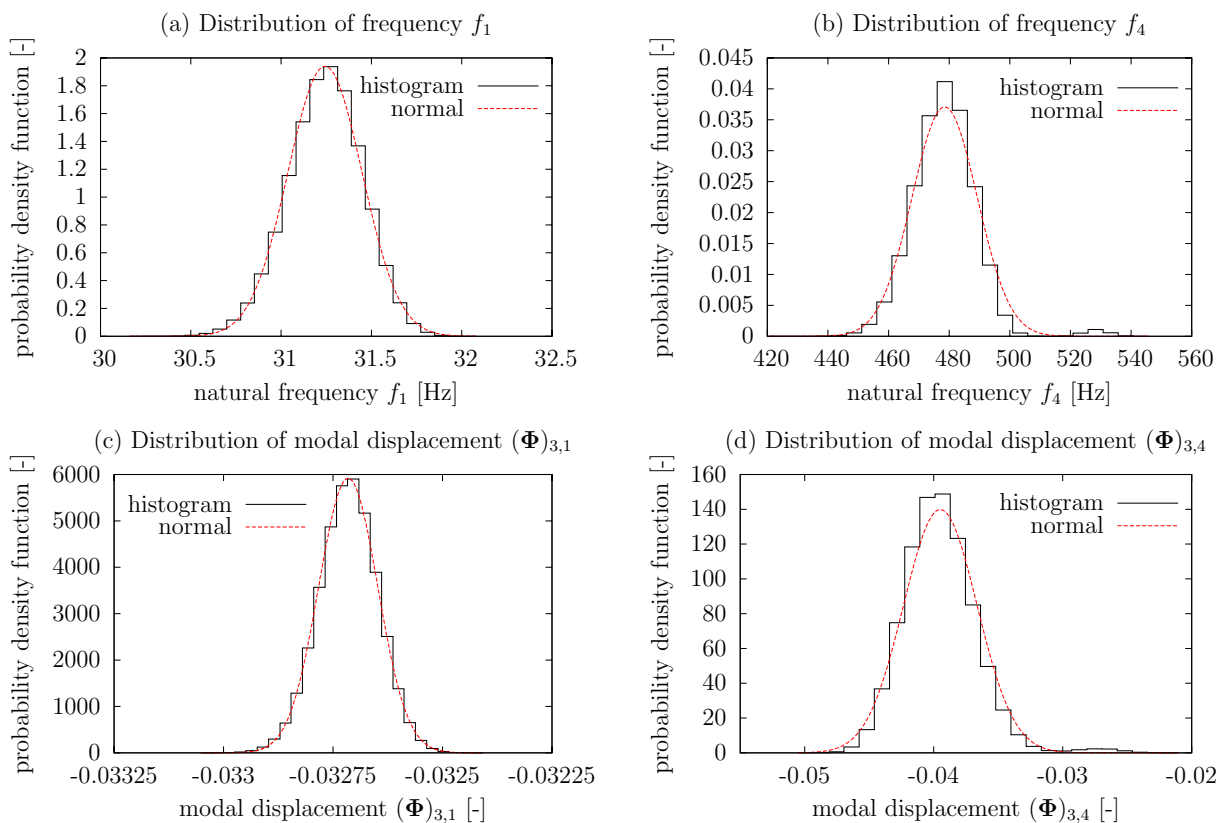


Figure 4.17: Examples of probability density functions of target features. The histogram is a density estimation related to 1,000,000 Latin hypercube samples. The best fit based on a normal distribution is indicated by the red line.

freedom of the structural model. More details about the proposed concept of mode pairing has been presented in Chapter 3. For mode pairing purposes, a set of reference mode shapes has to be defined for both, the artificial experiment and the numerical modal analyses performed to calculate the objective function values. In this benchmark study, both applications use the reference mode shapes of the first four bending modes corresponding to the four measurement points with respect to the nominal mean values of the input parameters. However, if the target feature vector is obtained from real experiments, the mode pairing can be conducted with reference mode shapes of the initial numerical model. For the subsequent model updating, the reference mode shapes should be based on the mean value vector of all experimentally obtained mode shapes.

The suitability of dissimilarity measures that were proposed in Section 4.3 and are intended to be applied as objective functions, is the main emphasis of the current benchmark study. In contrast to the benchmark study of the three degree of freedom system, the number of input and output parameters is higher. Furthermore, the effect of numerical instabilities resulting from ill-conditioned covariance matrices can be demonstrated.

First, the numerical properties are derived for each dissimilarity measure as described in Section 4.4. The boundaries of mean values and standard deviations of the model input parameter vector are set to $[10^{-2}, 5]$ and $[10^{-2}, 0.5]$, respectively. As the accuracy of the derived property indicators depends on the number of samples used for the sample-based stochastic structural analysis, the sample number is varied. Based on this investigation, the most suitable dissimilarity measures are identified and applied in the subsequent stochastic model updating using the nature inspired optimization methods genetic algorithm (GA) and particle swarm optimization (PSO).

4.6.2 Numerically derived properties of the objective functions

The numerical properties for the truss benchmark study are derived as described in Section 4.4. In contrast to the three degree of freedom benchmark study, the investigations are based on a central composite sampling scheme at the boundaries. Each slice contains six assessment points. Hence, the total number of objective function evaluations is 5,216. A variation of 100 and 1,000 Latin hypercube samples applied in the stochastic structural analysis is performed. The indicators obtained from 10 independent objective function assessments are averaged to increase the confidence. Figures 4.18 and 4.19 illustrate the averaged indicators for convexity, monotonicity, and gradients. The acronyms of the dissimilarity measures are explained in Table 4.2. In addition, all slices of a single objective function assessment for several dissimilarity measures are presented in Figures 4.20 and 4.21.

The general observations are similar to those derived within the three degree of freedom benchmark study. With an increasing number of Latin hypercube samples, the

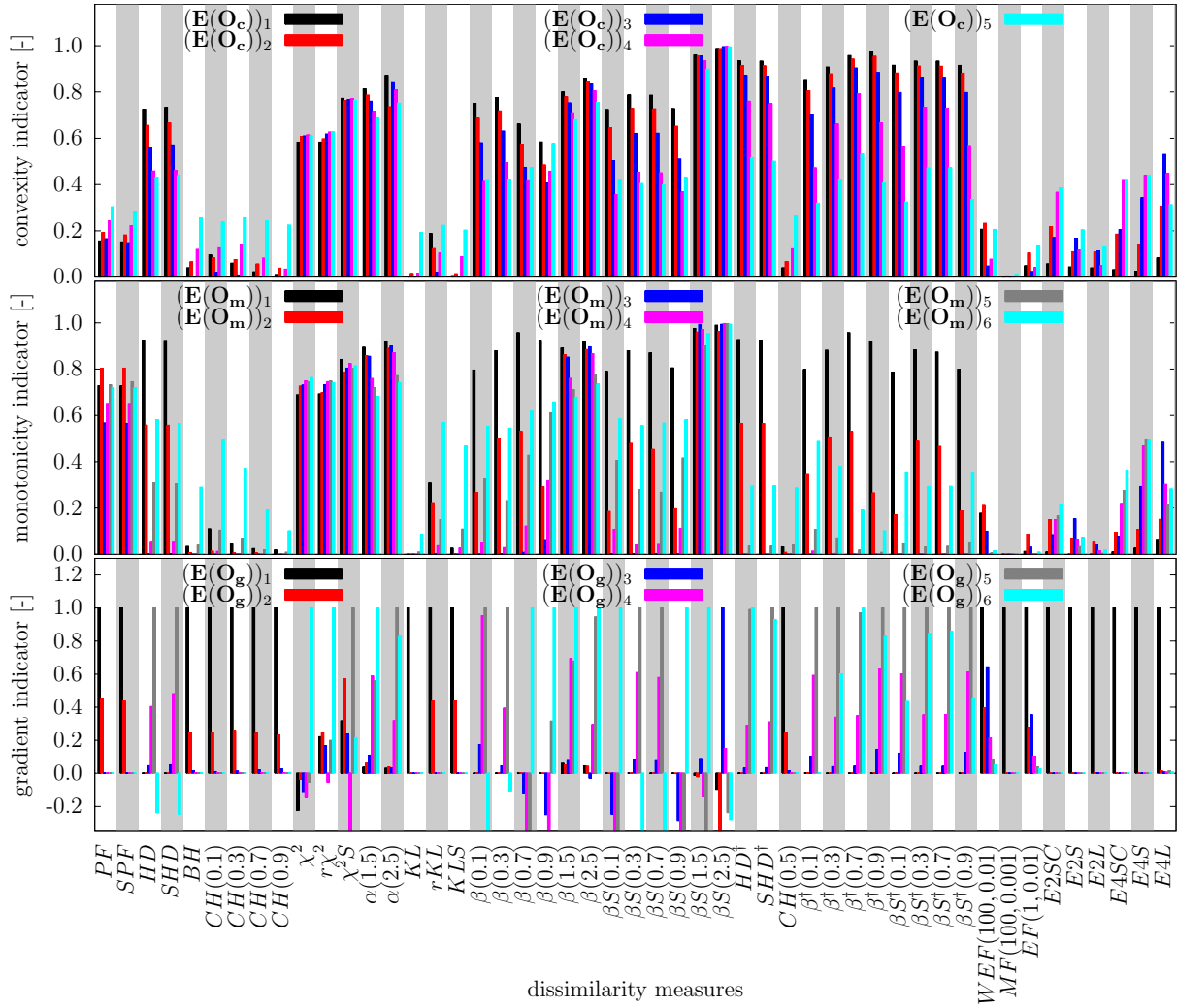


Figure 4.18: Objective function properties for the truss system. The indicators are averaged over 10 identical runs using 100 Latin hypercube samples for each objective function evaluation.

indicators become more accurate, especially in the vicinity of the optima. The monotonicity indicators of the Chernoff distance (CH), the Kullback-Leibler divergence (KL), the β -divergences (β^\dagger), and their deviations are significantly improved. However, the slices in Figures 4.20a and 4.20b indicate that local minima are likely even for 1,000 Latin hypercube samples.

The topology of all bounded measures, like Hellinger distance (HD), squared Hellinger distance (SHD), β -divergence, and symmetrized β -divergence, is very inconvenient for an objective function. The dissimilarity measures have very small gradients in a large area of the design space. Only in the vicinity of the optimum, suitable gradients are observed. Figures 4.20f and 4.20h depict this phenomenon.

By comparing the results of different formulas to calculate the same dissimilarity measure, the deviations are higher than those obtained in the three degree of freedom

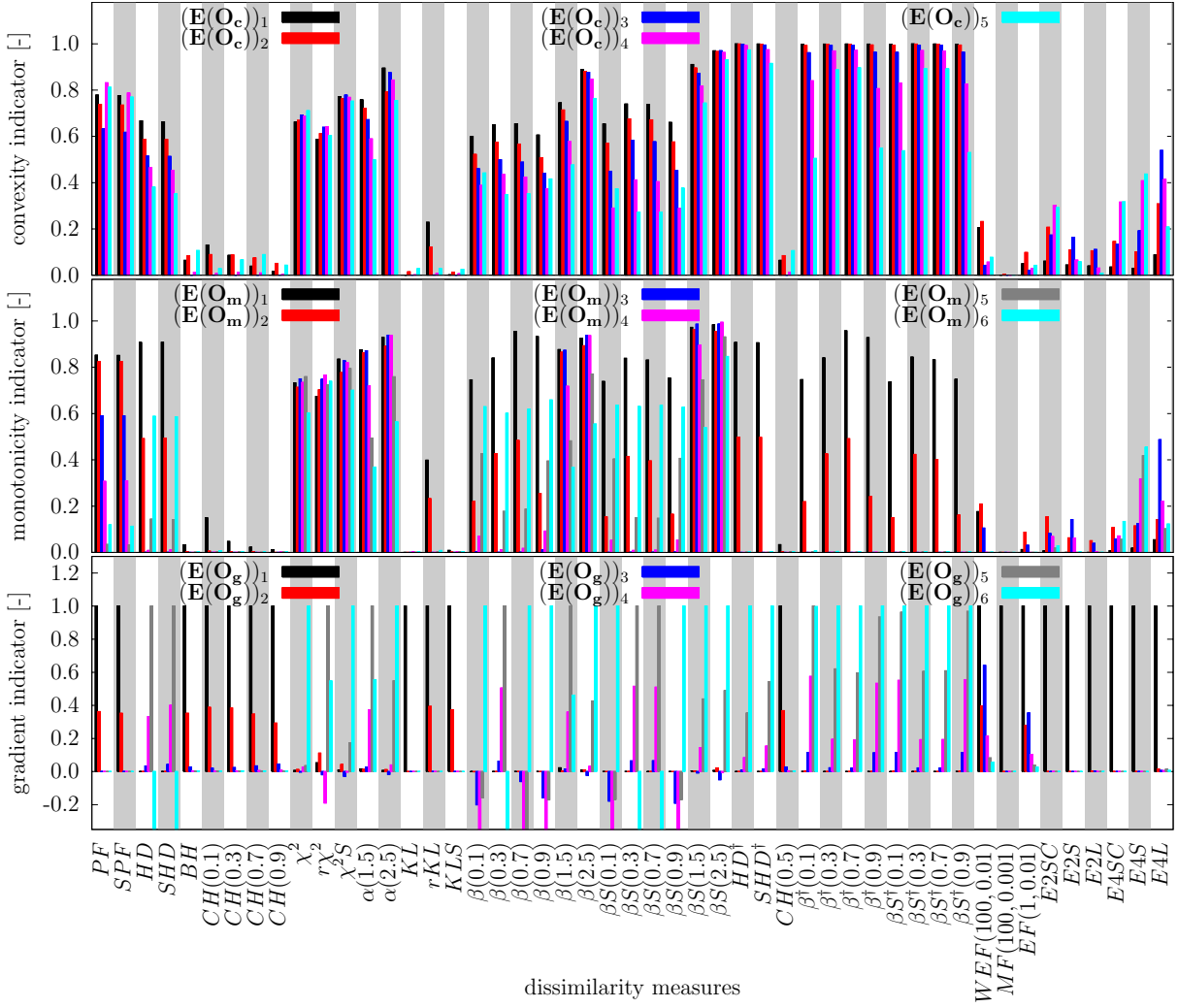


Figure 4.19: Objective function properties for the truss system. The indicators are averaged over 10 identical runs using 1,000 Latin hypercube samples for each objective function evaluation.

Table 4.9: Covariance matrix properties of the random feature vector.

property of $\mathbf{C}_{\mathbf{z}_m}$	benchmark study	
	truss	3DOF
determinant	$5.6788 \cdot 10^{-47}$	$5.6267 \cdot 10^{-14}$
maximal singular value	$7.8520 \cdot 10^1$	$1.8592 \cdot 10^{-4}$
minimal singular value	$1.4676 \cdot 10^{-7}$	$6.8136 \cdot 10^{-6}$
condition number	$5.3503 \cdot 10^8$	$2.7286 \cdot 10^1$

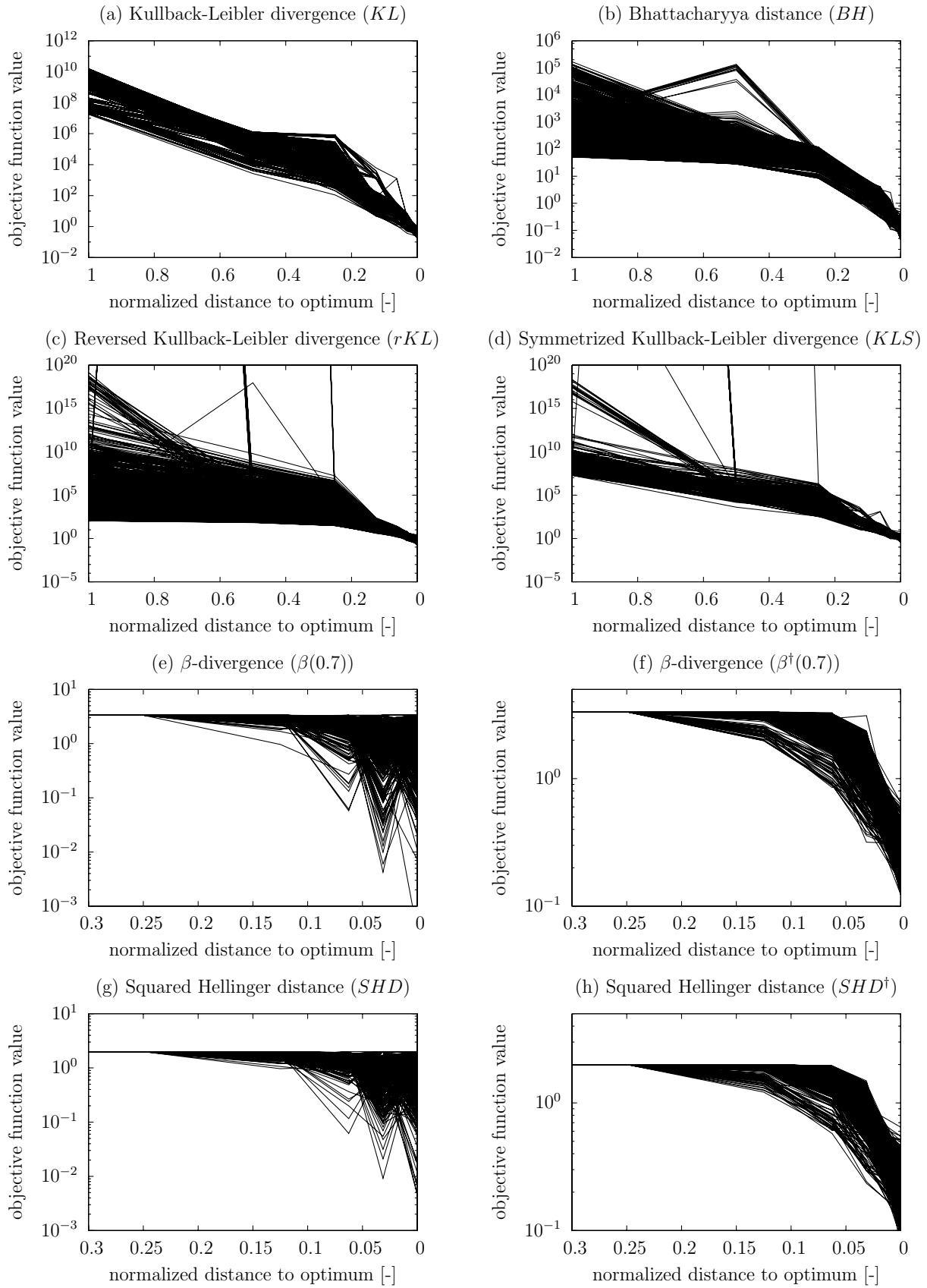


Figure 4.20: Representative slices of objective functions. 1,000 Latin hypercube samples are utilized for the stochastic structural analysis of the truss system.

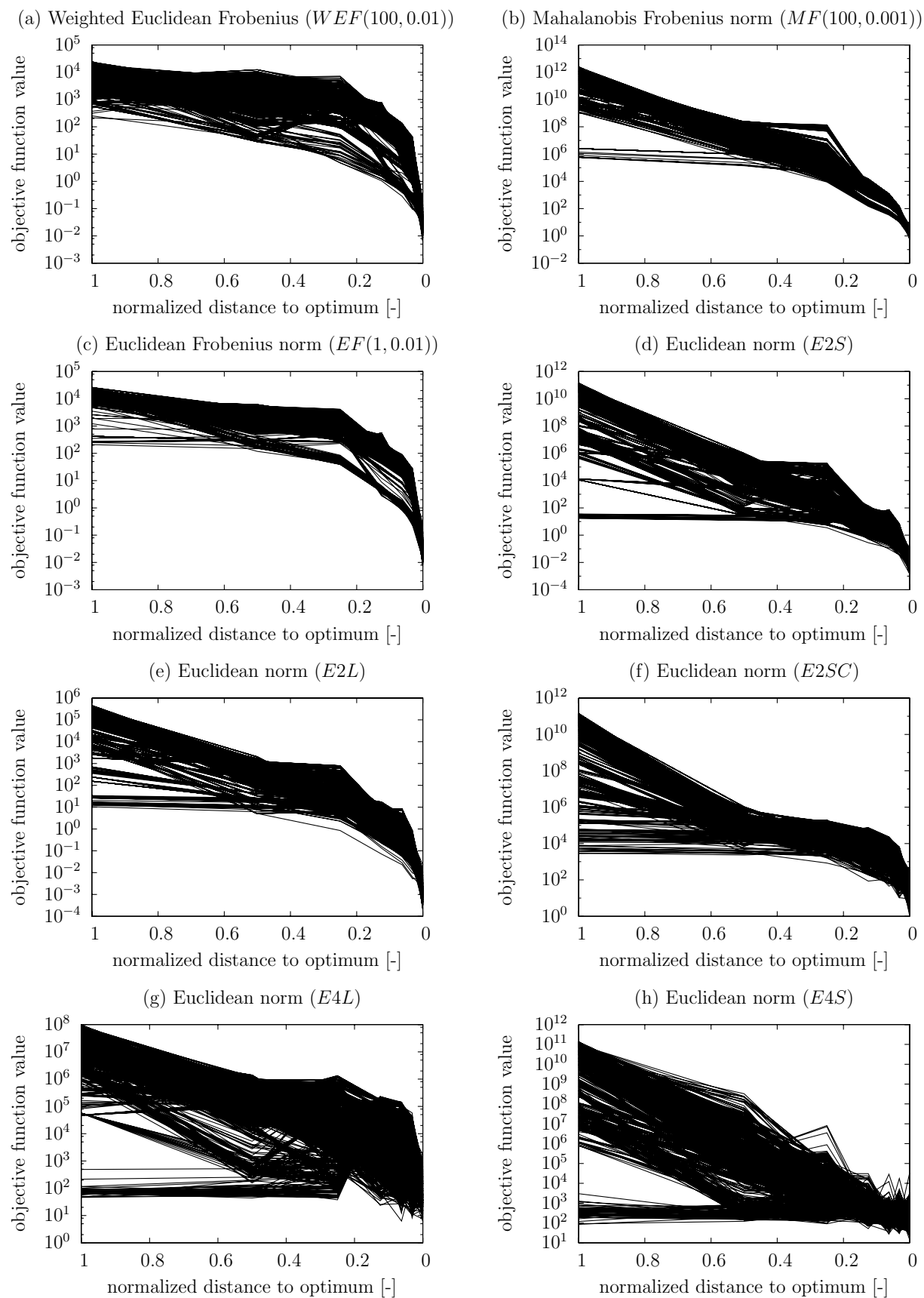


Figure 4.21: Representative slices of objective functions. 1,000 Latin hypercube samples are utilized for the stochastic structural analysis of the truss system. (continued from Figure 4.20)

benchmark study. The alternative formulas are indicated by the superscript \dagger , for example, HD versus HD^\dagger . The original formulas are based on the explicit formula of the Hellinger integral, whereas the alternative formulas are based on the explicit formula of the Chernoff distance. The original formula leads to a negative gradient indicator, which is very undesirable for the objective function. The differences are clearly visible by comparing Figures 4.20e and 4.20g with Figures 4.20f and 4.20h.

The reason for the differences is the unfavorable condition of the covariance matrix of the target output parameters, which leads to numerical instabilities. Some important properties of the covariance matrix of the target output parameters are listed in Table 4.9, which are compared with those corresponding to the covariance matrix of the target output parameters used in the three degree of freedom benchmark study. Consequently, ill-conditioned covariance matrices should be avoided for the equations relying on the Hellinger integral.

Summarizing, the most suitable dissimilarity measures for the truss benchmark study are almost the same as for the three degree of freedom benchmark study. If at least 1,000 Latin hypercube samples are provided, the best performing dissimilarity measures are Bhattacharyya distance, Kullback-Leibler divergence, and Mahalanobis Frobenius norm.

4.6.3 Dissimilarity measures applied as objective functions

The most suitable dissimilarity measures derived from the previous investigation are now applied as objective functions within an optimization-based stochastic model updating of the truss system. In addition, the dissimilarity measures squared Hellinger distance (SHD), β -divergence ($\beta^\dagger(0.7)$), and the Euclidean norm $E2L$ are investigated. Genetic algorithm and particle swarm optimization are combined with 100 and 10,000 Latin hy-

Table 4.10: Most important configuration parameters of the genetic algorithm (GA) applied to the truss system.

parameters	value
number of parents	42
number of individuals	68
number of generations	84

Table 4.11: Most important configuration parameters of the particle swarm optimization (PSO) applied to the truss system.

parameters	value
number of particles	42
number of iterations	84

percube samples utilized for the stochastic structural analysis. The most important configuration parameters of the optimization methods are listed in Tables 4.10 and 4.11. Additional descriptions are presented in Appendix B. The results are summarized in Figures 4.22 and 4.23. The boxplots illustrate the minimum, 25-percent quantile, median, 75-quantile, and maximum of the errors ε_1 . The errors $\varepsilon_1(\mathbf{E}_{\hat{\theta}})$ and $\varepsilon_1(\boldsymbol{\sigma}_{\hat{\theta}})$ are derived with Equation (4.64) regarding the mean values and standard deviations of the identified input parameters. With $m_x = 10$, Equations (4.65) and (4.66) represent the definitions of the deviation measures ε_2 , ε_{3E} , and $\varepsilon_{3\sigma}$ used in this study.

Comparing the results of both benchmark studies, it can be observed that the deviations of the identified input parameters with respect to the nominal values are higher in the case of the truss benchmark study. Especially, the deviations associated with the standard deviations of the model input parameters are high, even if 10,000 Latin hypercube samples are chosen. This can be an indicator for an insufficient number of Latin hypercube samples.

The dissimilarity measure based on the Euclidean norm $E2L$ is the measure with the highest deviation. This observation supports the results derived from the investigation of the objective function properties. In general, the improvement of the identification deduced from an increasing number of Latin hypercube samples from 100 to 10,000 is not significant. However, the results obtained from the genetic algorithm are marginally better than those related to the particle swarm optimization.

A very interesting fact is that the dissimilarity measures Bhattacharyya distance (BH), Kullback-Leibler divergence (KL), β -divergence ($\beta^\dagger(0.7)$), and Mahalanobis Frobenius norm ($MF(100, 0.001)$) behave similar regarding the obtained accuracy of input parameters, when the particle swarm optimization is applied. A totally different behavior is observed, when the genetic algorithm is used as optimization method. Applying the genetic algorithm, the Bhattacharyya distance becomes outstanding in comparison to other investigated dissimilarity measures. Therefore, the Bhattacharyya distance is chosen for a detailed investigation of the identified input parameters.

Table 4.12 illustrates that the averaged errors of the identified input parameters are significantly higher for this benchmark study than for the three degree of freedom benchmark study. The reasons can be manifold and thus need a more detailed investigation. Although it is out of the scope of this study, some discussions and a few recommendations are given. One reason for the high inaccuracy can be an insufficient number of samples used for the stochastic structural analysis. Moreover, the number of iterations, parents, or particles can contribute to the high deviations. Another aspect, which can contribute to high uncertainties, are the ill-conditioned output covariance matrices. This effect could be minimized by an appropriate regularization technique.

A remarkable value is the random variable corresponding to the stiffness of the diagonal truss element T5. The errors are significantly higher for $(\mathbf{E}_{\hat{\theta}})_5$ and $(\boldsymbol{\sigma}_{\hat{\theta}})_5$ than for other

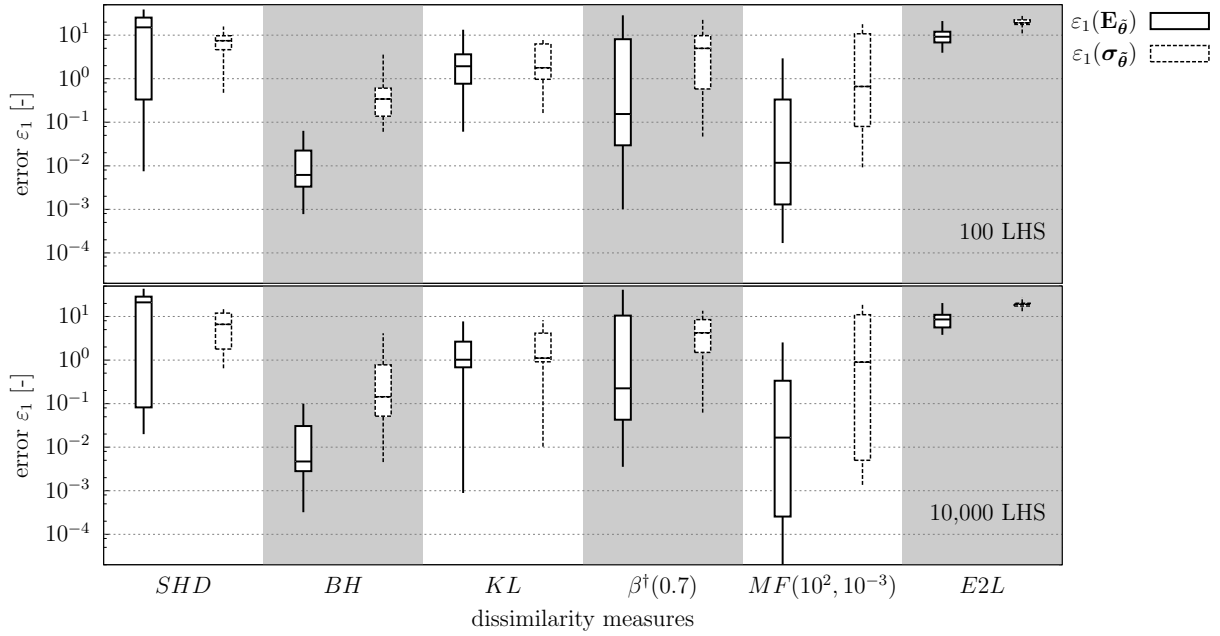


Figure 4.22: Statistics of the error ε_1 according to Equation (4.64) using genetic algorithm (GA) for the truss benchmark study. The statistics are based on 20 independent optimization runs. To evaluate one objective function value, 100 and 10,000 Latin hypercube samples are applied.

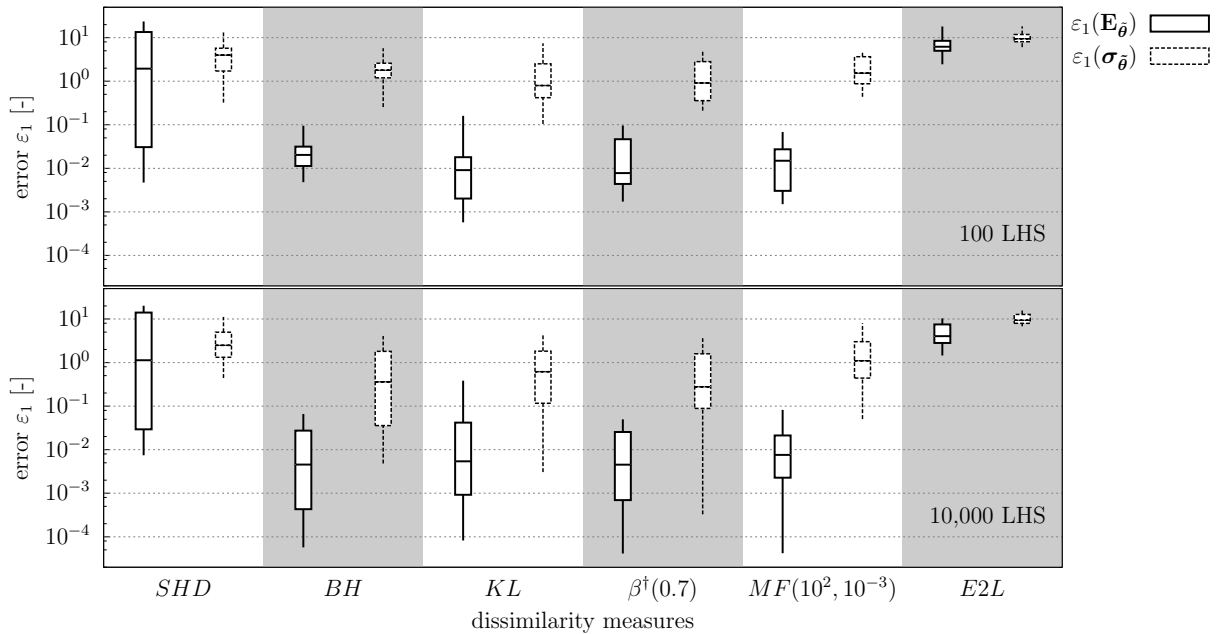


Figure 4.23: Statistics of the error norm ε_1 according to Equation (4.64) using particle swarm optimization (PSO) for the truss benchmark study. The statistics are based on 20 independent optimization runs. To evaluate one objective function value, 100 and 10,000 Latin hypercube samples are applied.

Table 4.12: Comparison of different updating methods for the truss system. The statistical values of identified input parameters are based on 20 independent optimization runs.

method		GA with BH				PSO with BH			
LHS		100		10,000		100		10,000	
total solver runs		$\approx 350,000$		$\approx 35,000,000$		$\approx 350,000$		$\approx 35,000,000$	
		error ε_2 [%]		error ε_2 [%]		error ε_2 [%]		error ε_2 [%]	
i	parameter	$\mathbf{E}(\varepsilon_2(i))$	$\boldsymbol{\sigma}(\varepsilon_2(i))$	$\mathbf{E}(\varepsilon_2(i))$	$\boldsymbol{\sigma}(\varepsilon_2(i))$	$\mathbf{E}(\varepsilon_2(i))$	$\boldsymbol{\sigma}(\varepsilon_2(i))$	$\mathbf{E}(\varepsilon_2(i))$	$\boldsymbol{\sigma}(\varepsilon_2(i))$
1	$(\mathbf{E}_{\hat{\theta}})_1$	0.6206	2.2297	-0.1006	2.2852	3.0713	4.5412	0.3115	2.9638
2	$(\mathbf{E}_{\hat{\theta}})_2$	0.7211	2.6346	1.2616	6.1047	2.1099	5.5362	2.3055	6.7262
3	$(\mathbf{E}_{\hat{\theta}})_3$	3.9979	4.9558	0.9429	2.6634	5.2117	7.5376	2.2303	5.0693
4	$(\mathbf{E}_{\hat{\theta}})_4$	4.2077	5.9552	2.1751	6.8758	2.2068	4.7755	-0.3834	3.0020
5	$(\mathbf{E}_{\hat{\theta}})_5$	3.7668	6.0280	6.8328	8.7265	6.8788	7.4385	4.2290	7.5518
6	$(\boldsymbol{\sigma}_{\hat{\theta}})_1$	6.6807	10.0229	2.0859	10.4507	30.6333	43.9260	4.8326	30.0006
7	$(\boldsymbol{\sigma}_{\hat{\theta}})_2$	9.8041	22.6880	3.4503	30.0115	28.0174	53.0474	16.4557	52.8543
8	$(\boldsymbol{\sigma}_{\hat{\theta}})_3$	27.8289	41.1784	1.6600	10.9736	55.5051	65.7168	21.3374	43.1617
9	$(\boldsymbol{\sigma}_{\hat{\theta}})_4$	29.8348	37.5750	6.6849	40.0135	17.0915	43.9451	-7.7599	17.9164
10	$(\boldsymbol{\sigma}_{\hat{\theta}})_5$	18.5367	33.8419	36.9133	50.2106	50.5774	59.4536	30.3789	57.9866
ε_{3E} resp. $\varepsilon_{3\sigma}$		46.8797	70.5428	38.4734	73.6581	88.0206	121.3027	41.9636	96.8801

identified parameters. It seems to be comprehensible that these values are less sensitive to the global modal behavior than all other input parameters as the respective diagonal is placed in the last segment of the cantilever. Unfortunately, this cannot be confirmed by a correlation analysis using the linear or quadratic Pearson or Spearman correlation coefficient. Other sensitivity analysis methods may be more suitable, which needs to be investigated in further studies.

A direct comparison of the optimization-based stochastic model updating strategies to the sensitivity-based stochastic model updating strategy proposed by [Khodaparast et al. 2008b] is difficult, because in the latter strategy the initial parameters were chosen to be nearby the optimum. The mean values had maximal five percent initial deviations. Of course, with these initial values, the identified input parameters were very close to the nominal values.

In summary, it could be shown that the application of dissimilarity measures as objective functions is in general possible. For the presented benchmark study, the deviations between identified input parameters and nominal input parameters are high. This can be related to other effects, like insensitive input parameters or ill-conditioned matrices.

Conducting optimization methods for the purpose of stochastic model updating, at least an input parameter set, which is close to the nominal input parameters can be identified. This set can be used as the initial parameter set in a subsequently applied sensitivity-based stochastic model updating analysis, which refines the results very fast. Hence, a symbiosis of both approaches can reveal their full potential.

4.7 Discussion

In this chapter, an optimization-based stochastic model updating approach using vibration test data has been proposed. Generally, the statistics of features can be extracted from several measurements of nominal identical structures or under similar, but non-identical experimental conditions. If the source of uncertainty is considered as model input parameter, the identified statistics of the model parameters are associated with real existing variations of model parameters, which were present in the tests.

The proposed optimization-based approach serves as alternative to sensitivity-based algorithms. A special aim was to assess the suitability of several objective functions related to dissimilarity measures that are usually applied in information theory. In total, 49 measures were investigated with respect to their properties of monotonicity and convexity and their first derivatives. Since the objective functions were multi-dimensional and could not be analyzed analytically, a mapping was proposed to extract representable one-dimensional slices from the objective functions. Using these one-dimensional discrete functions, indicators for monotonicity, convexity, and gradients were derived, which were able to rate the properties of a multi-dimensional objective function with low computational effort. Applying this methodology to two representative benchmark studies, the measures Kullback-Leibler divergence, Bhattacharyya distance, β -divergence with parameter $s = 0.7$, and Mahalanobis Frobenius norm could be recommended for vibration-based stochastic model updating using optimization methods.

The 49 dissimilarity measures were applied to an optimization-based stochastic model updating problem. The most suitable measures determined with the indicators for monotonicity, convexity, and gradients were confirmed by the results of the optimization, which justified the proposed methodology to rate the properties of objective functions. By testing several optimization strategies (i.e., genetic algorithm, particle swarm optimization, adaptive response surface method), it was observed that the optimization strategy had only a secondary effect on the results. With similar computational effort, similar accuracies of the identified input parameters were derived for the three degree of freedom benchmark study. A similar quality of identified parameters was obtained from the sensitivity-based perturbation approach.

Nevertheless, all of the investigated approaches showed advantages and disadvantages. Nature inspired optimization strategies, genetic algorithm and particle swarm optimization, did not need an initial input parameter set, but they could only find near-optimal solutions. In contrast, the adaptive response surface method and the sensitivity-based stochastic model updating approaches needed an initial parameter set, which had to be sufficiently close to the optimum. The solutions converged fast, but were often influenced by systematic errors of the algorithms. It was concluded that the combination of optimization-based and sensitivity-based stochastic model updating approaches could be

beneficial.

In the presented benchmark studies, the application of explicit formula to solve the integrals of dissimilarity measures was justified since the feature vectors were almost multivariate normally distributed. This reduced significantly the numerical effort as the mean value vectors and covariance matrices could be estimated with sufficient accuracy by evaluating only a few samples. However, the general definition of dissimilarity measures comprises the potential to apply such measures to non-normal distributed feature vectors. For this purpose, the multi-dimensional probability density functions need to be estimated. To obtain a sufficient accuracy, more samples are needed for the probability density estimation than for the estimation of mean values and covariance matrices.

The high computational effort to perform stochastic model updating limits the application to realistic structures, typically modeled with many degrees of freedom. As the most computational expense is related to derive the solutions of structural analyses, surrogate models are proposed to accelerate the determination of model responses. This is recommended for future research.

Summary and conclusions

In this thesis, a framework for model updating has been proposed, which was integrated into the guideline of verification and validation ([ASME V&V 10 2006]) by the American society of mechanical engineers (ASME) . The model updating framework consists of several independent tasks, which are connected with each other. These tasks are: sensitivity analysis, pretest analysis, execution of experiments, feature extraction, and model updating. Therefore, the success of model updating depends on the success of each task. Meaningful and useful results can only be obtained from a model updating process, if the uncertainties are quantified and reduced for all contributing tasks.

Three specific problems were investigated, which arise frequently in the context of vibration-based model updating: (i) optimal placement of reference sensors within roving setup configurations, (ii) pairing of numerically derived and experimentally obtained mode shapes, and (iii) suitability of objective functions for optimization-based stochastic model updating. Some conclusions could be drawn for each emphasis.

Optimal reference sensor placement: With respect to vibration measurements using roving sensor configurations, a problem was identified, which was hardly addressed in literature. This was the task of determining the optimal positions for reference sensors. Inappropriate positions can introduce a high degree of uncertainty into the measured data.

The innovative approach to define optimal positions for reference sensors was based on the normalized predicted power spectral amplitudes of the responses assuming the statistics of the excitation spectrum are known. The frequency response function was adapted from a finite element model. This enabled the possibility to consider the differences of measured accelerations, velocities, and displacements. To assess predefined reference sensor positions, an objective function could be derived relying on normalized power spectral amplitudes. A genetic algorithm in combination with a novel geometry-based description of the sensor locations lead to a well defined optimization problem of determining the best reference sensor positions. The derived optimal reference sensor positions of a simply supported beam met experience-based expectations. Furthermore, the approach has

been successfully applied to a case study of a test specimen, where the predicted power spectral amplitudes of the responses were validated.

The proposed inventive placement of reference sensors is computationally efficient and can be applied to numerical models of real-sized structures. If the number of sensor set positions is limited to 10^9 possibilities, at least a near-optimal solution can be obtained by applying a nature inspired optimization algorithm with acceptable computational effort.

Of course, the reliability of the obtained optimal reference sensor positions depends strongly on the model and excitation uncertainties. The robust determination of optimal reference sensor positions considers such uncertainties. Consequently, it is proposed for future research.

Pairing of numerically derived and experimentally obtained mode shapes: A suitable mode pairing strategy is essential for automated processes, such as model updating or sensitivity analysis. By means of a numerical benchmark study, it could be demonstrated that the currently available methods were not reliable for certain structures and measurement configurations, especially if the experimentally obtained mode shapes were perturbed by noise.

The derived novel energy-based modal assurance criterion combined the common modal assurance criterion with the physical properties of the instrumented parts of the structure by using modal strain energies. The innovative criterion could be successfully applied to the investigated numerical benchmark study. Furthermore, it was shown that an unsuitable mode pairing strategy affects the results derived from a sensitivity analysis on a finite element model of a railway bridge. This example demonstrated also the application of the energy-based modal assurance criterion to numerical models of realistic structures.

Even if the proposed mode pairing strategy does not replace a carefully conducted pretest analysis and execution of experiments, it contributes to a reduction of uncertainties within the model updating process and preliminary processes, like sensitivity analysis.

Objective functions for optimization-based stochastic model updating: Since stochastic model updating is a new research topic, only few methods are currently available. Most methods are based on sensitivity matrices. Such methods provide a fast convergence of the solution, but are less flexible, for example with respect to the initial parameter set definition. Such stochastic model updating methods stress to identify the statistics of uncertain model parameters using the statistics of experimentally obtained features. The statistics of the features are derived from the execution of several experiments from nominal identical structures or experiments with almost identical test conditions.

In contrast to sensitivity-based stochastic model updating approaches, the optimization-

based stochastic model updating methods are more flexible. The novel contribution was the investigation and determination of suitable objective functions for optimization-based stochastic model updating. Several dissimilarity measures from information theory were tested with respect to their appropriateness to be applied as objective functions. For two representative benchmark studies, the Kullback-Leibler divergence, Bhattacharyya distance, β -divergence with parameter $s = 0.7$, and Mahalanobis Frobenius norm were declared as most suitable with respect to their properties. An inventive approach was developed to rate numerically the properties of a multi-dimensional objective function.

Also the application to a stochastic model updating problem using a genetic algorithm, particle swarm optimization, and adaptive response surface method was successful. Investing same computational effort, the obtained accuracy of identified input parameters was similar. The quality of obtained results derived from optimization-based stochastic model updating and sensitivity-based stochastic model updating was approximately identical. Optimization-based approaches based on nature inspired strategies tended to converge slowly to the nominal solution, but needed no initial parameter set, while sensitivity-based approaches converged fast, if the initial parameter set was close to the optimal values. Hence, a combination of both methods was recommended.

With the investigations on objective functions, a substantial contribution was provided to support the success of optimization-based stochastic model updating methods. They are an important complement to sensitivity-based approaches to determine the uncertainties of vibration-based model updating.

The currently available methods for stochastic model updating are not applicable to real-sized structures as the computational expense is too high. Therefore, the comprehensive numerical model solution needed for the stochastic structural analysis should be replaced by approximations obtained by surrogate models. This is suggested for further research activities.

With this thesis, a milestone has been established to reduce and quantify uncertainties for updated numerical models. Thereby, model updating was considered as a process consisting of several subproblems. The most critical sources of uncertainties, namely the determination of sensor positions and the mode pairing of numerically derived and experimentally obtained modes, were the main emphases of this thesis. As complementation, the uncertainties of model parameters for the special task of investigating nominally identical structures or test conditions were quantified. Consequently, the presented thesis contributes significantly to the quality improvement of updated numerical models. While applying the proposed approaches, vibration-based model updating procedures become cost-effective tools to enhance the predictability of numerical models with the purpose to guarantee all requirements on performance, safety, and reliability of designed and re-designed structures.

Recommendations for future research

6.1 Pretest phase

6.1.1 Robust optimal reference sensor positions

The basic approach to determine optimal reference sensor positions was presented in Chapter 2. As already discussed, the main drawback for its application is the discrepancy between the underlying numerical model and the real test structure, since the definition of reference sensors is typically performed in the pretest phase.

Therefore, the obtained optimal reference sensor positions depend on the numerical model itself. Consequently, uncertainties of model input parameters (e.g., material properties, geometrical measures, and modal damping ratios) need to be taken into account in the optimization process. Since some model input parameters of the structure are uncertain at least in the pretest phase and the excitation is a random stationary process, the spectral response amplitudes will also be obtained as random variables with their respective distribution. The computational expenses to obtain such a random description are very high. Thus, it is proposed to use surrogate models to replace the comprehensive model used for the statistical evaluation. Additional uncertainties arise from the approximations extracted from surrogate models and the statistical evaluation using sampling methods. They need to be considered in the robust optimization of reference sensor positions. A short description, some applications, and recommended references of surrogate modeling are provided in Section 6.2.3.

The aim of this robust design optimization is to determine a set of reference sensor positions that is insensitive to the expected uncertainties of model input parameters. Furthermore, parallel computing in an efficient coding environment is essential for a successful application. As a robust determination of optimal reference sensor positions is required for the design of vibration tests, it should be a major topic for future research.

6.1.2 Optimal roving sensor positions

So far, the determination of roving sensor positions within a multiple setup configuration has not been considered. Of course, not only the positions of reference sensors but also the positions of the remaining sensors assembled in setups can be optimized to reduce uncertainties from measured data.

It is assumed that the number of required sensors and respective positions of the merged configuration can be determined, for instance, by the effective independence method or modal kinetic energy approach (e.g., [Penny et al. 1994]). The position and number of reference sensors can be defined as proposed in Chapter 2. Consequently, the remaining task is to split the total number of sensor positions into setups. For the merging, it is required that each setup is able to identify independently all modes of interest. For example, if the stochastic subspace identification method (e.g., [Peeters et al. 1999], [Peeters et al. 2001], [Reynders et al. 2008] [Reynders 2009]) is applied, stable poles should appear at similar frequencies in each setup. If one mode cannot be detected by a certain setup, it is difficult to merge the modal displacements. This introduces additional uncertainties to the experimentally obtained modal data. Hence, it has to be ensured that sufficient energy of each mode is present in each setup. It is proposed to use power spectral densities of all associated sensor positions as an indicator. Additional requirements can be necessary to separate the modes with similar frequencies.

However, the applied operational modal analysis method suggests possible eigenmodes, for example, by stable poles or by complex mode indicator functions. Therefore, a mathematically derived criterion to optimize the roving sensor positions should be related to the operational modal analysis method intended to apply. Of course, robustness should be considered analogously to the procedure described in Section 6.1.1. The research on optimal placement of roving sensor positions will complement the research on robust optimal reference sensor positions. Both approaches are required to design an optimal vibration test for a roving sensor setup configuration with the purpose to extract modal properties.

6.2 Model updating

6.2.1 Multivariate non-normal distributions

Multivariate normal distributions are assumed in sensitivity-based stochastic model updating schemes, as well as, in the benchmark studies, which are related to the optimization-based stochastic model updating approach presented in this thesis. This assumption is valid for various applications. However, if the random vector of target output parameters cannot be approximated by a multivariate normal distribution, the sensitivity-based stochastic model updating schemes may not be appropriate.

The approach presented in Chapter 4 has the potential to be applied to any type of multivariate distribution. In a general case, the integral defining the dissimilarity measures given in Equation (4.4) needs to be solved analytically or numerically. As already mentioned, rectangle rule, Monte Carlo method, or Metropolis Hastings algorithm [Evans et al. 2005] are suitable numerical integration methods. Typically, the distribution of target output parameters is not available as analytical function. Therefore, the probability density function needs to be estimated. Some methods were proposed in [Scott 1992]. Usually, only few samples are available to estimate the probability density function. The resulting uncertainty and their reduction should be considered in future research.

Also the distribution of model responses is generally derived by sample evaluations of a sample-based stochastic structural analysis of input parameter samples. To obtain similar accuracies, the number of samples to estimate the probability density function is larger than the number to estimate the mean value or covariance matrix. Consequently, it is recommended to reduce the number of function calls needed to evaluate the model input parameter samples, for example, by applying surrogate models. A short description of the surrogate modeling concept is given in Section 6.2.3.

Without implementing this proposed extension to the stochastic model updating methods presented in this thesis, it is not possible to perform a stochastic model updating using strictly non-normal distributed target output parameters.

6.2.2 Sequential parameter optimization

Several optimization methods were successfully applied to problems of optimal sensor placement and stochastic model updating in Chapters 2 and 4, respectively. In these applications, predefined standard sets of parameters to configure the optimization methods are utilized. However, it is expected that a certain set of configuration parameters can be determined that minimizes the total computational expenses with respect to a predefined accuracy of the results. The corresponding research field is termed sequential parameter optimization. [Bartz-Beielstein 2010] and [Bartz-Beielstein et al. 2005] are recommended for a general overview of available methods. A benchmark study was presented in [Nannen et al. 2008] and an application to root identification problems was investigated in [Joan-Arinyo et al. 2011]. [Nguyen et al. 2010] proposed an agent-based approach for robust optimization, which is an extension to the sequential parameter optimization. The application of sequential parameter optimization to model updating problems is hardly addressed in literature, and is therefore recommended for future research.

Obviously, the optimal configuration depends on the structural system and the formulation of the optimization problem. Nevertheless, it should be possible to derive recommended configuration parameters for specific optimization tasks. In case of stochastic model updating, the number of sample evaluations needed for the sample-based stochastic

structural analysis has to be integrated into the determination of optimal configuration parameters.

One group of specific tasks is the model updating of filler beam bridges of the German Railways using measured modal data with the purpose to predict the dynamical behavior for train passages under various speeds. The bridges vary in height and span width, but the construction principle is identical. In the past, large discrepancies between numerically derived and experimentally obtained modal parameters were observed. As several hundred bridges are existing in Germany, a systematic research is justified. In a first step, the application of sequential parameter optimization to deterministic model updating strategies should be sufficient. If measured data from a longterm monitoring are available, stochastic model updating methods may be more appropriate.

6.2.3 Surrogate modeling

In some cases, it may be not sufficient to apply only optimal configuration parameters for the optimization methods to reduce significantly the computational effort. Hence, the additional application of surrogate models is proposed. Surrogate models, also known as meta models or response surface models, try to approximate a comprehensive model of high complexity and high computational expense by simplified models. With this approximation, additional uncertainties are introduced into the model updating process that need to be determined, observed, and reduced. The application of surrogate models to stochastic model updating problems and the investigation of the introduced uncertainties is hardly addressed in literature. Therefore, this application is proposed for future research activities, due to the potential to reduce efficiently the computational expense of stochastic model updating.

A general introduction to surrogate models with several references to theory and applications was given in [Queipo et al. 2005]. Bayesian neural network and support vector machines were investigated by [Unger 2009] with the intention to identify parameters of constitutive laws. Another application of approximating natural frequencies within stochastic modal updating by a Bayesian neural network was documented in [Brehm et al. 2009b]. [Khodaparast et al. 2010] proposed the application of kriging for the purpose of stochastic model updating. A MATLAB toolbox [Suykens et al. 2010] is available, which is based on the theory of [Suykens et al. 2002]. [Queipo et al. 2005] addressed the problem of determining the suitability of a surrogate model and suggests several measures.

Appendices

A

Statistical values

A.1 Statistical measures of distributions

Assuming that n sample sets of the random vector \mathbf{x} are assembled column-wise in a sample matrix \mathbf{X} , the following statistical values can be calculated.

- Mean value [Hogg et al. 2005]

$$(\mathbf{E}(\mathbf{x}))_i = (\mathbf{E}_{\mathbf{x}})_i = \frac{1}{n} \sum_{k=1}^n (\mathbf{X})_{i,k} \quad (\text{A.1})$$

- Covariance (unbiased) [Hogg et al. 2005]

$$(\mathbf{C}_{\mathbf{x}})_{i,j} = \frac{1}{n-1} \sum_{k=1}^n \left((\mathbf{X})_{i,k} - (\mathbf{E}_{\mathbf{x}})_i \right) \left((\mathbf{X})_{j,k} - (\mathbf{E}_{\mathbf{x}})_j \right) \quad (\text{A.2})$$

- Variance (unbiased) [Hogg et al. 2005]

$$(\mathbf{V}(\mathbf{x}))_i = (\mathbf{V}_{\mathbf{x}})_i = (\mathbf{C}_{\mathbf{x}})_{i,i} = \frac{1}{n-1} \sum_{k=1}^n \left((\mathbf{X})_{i,k} - (\mathbf{E}_{\mathbf{x}})_i \right)^2 \quad (\text{A.3})$$

- Standard deviation (unbiased) [Hogg et al. 2005]

$$(\boldsymbol{\sigma}_{\mathbf{x}})_i = \sqrt{(\mathbf{V}_{\mathbf{x}})_i} \quad (\text{A.4})$$

- Skewness (bias-corrected) [MathWorks 2010]

$$(\mathbf{S}_{\mathbf{x}})_i = \frac{\sqrt{n(n-1)}}{n-2} \frac{\frac{1}{n} \sum_{k=1}^n \left((\mathbf{X})_{i,k} - (\mathbf{E}_{\mathbf{x}})_i \right)^3}{\left(\frac{1}{n} \sum_{k=1}^n \left((\mathbf{X})_{i,k} - (\mathbf{E}_{\mathbf{x}})_i \right)^2 \right)^{\frac{3}{2}}} \quad (\text{A.5})$$

- Kurtosis (bias-corrected; assuming zero for normal distributions) [MathWorks 2010]

$$(\mathbf{K}_{\mathbf{x}})_i = \frac{n-1}{(n-2)(n-3)} \left((n+1) \frac{\frac{1}{n} \sum_{k=1}^n \left((\mathbf{X})_{i,k} - (\mathbf{E}_{\mathbf{x}})_i \right)^4}{\left(\frac{1}{n} \sum_{k=1}^n \left((\mathbf{X})_{i,k} - (\mathbf{E}_{\mathbf{x}})_i \right)^2 \right)^2} - 3(n-1) \right) \quad (\text{A.6})$$

- Pearson correlation coefficient (e.g., [Hogg et al. 2005], [Hartung et al. 2007])

$$(\mathbf{r}_{\mathbf{x}})_{i,j} = \frac{\sum_{k=1}^n \left((\mathbf{X})_{i,k} - (\mathbf{E}_{\mathbf{x}})_i \right) \left((\mathbf{X})_{j,k} - (\mathbf{E}_{\mathbf{x}})_j \right)}{\sqrt{\sum_{k=1}^n \left((\mathbf{X})_{i,k} - (\mathbf{E}_{\mathbf{x}})_i \right)^2 \sum_{k=1}^n \left((\mathbf{X})_{j,k} - (\mathbf{E}_{\mathbf{x}})_j \right)^2}} = \frac{(\mathbf{C}_{\mathbf{x}})_{i,j}}{\sqrt{(\mathbf{V}_{\mathbf{x}})_i (\mathbf{V}_{\mathbf{x}})_j}} \quad (\text{A.7})$$

- Spearman correlation coefficient (e.g., [Spearman 1904], [Hogg et al. 2005])

$$\begin{aligned} (\mathbf{r}_{\mathbf{x}}^{\mathbf{S}})_{i,j} &= \frac{\sum_{k=1}^n \left(\left(\overset{\Delta}{\mathbf{X}} \right)_{i,k} - \left(\mathbf{E}_{\overset{\Delta}{\mathbf{x}}} \right)_i \right) \left(\left(\overset{\Delta}{\mathbf{X}} \right)_{j,k} - \left(\mathbf{E}_{\overset{\Delta}{\mathbf{x}}} \right)_j \right)}{\sqrt{\sum_{k=1}^n \left(\left(\overset{\Delta}{\mathbf{X}} \right)_{i,k} - \left(\mathbf{E}_{\overset{\Delta}{\mathbf{x}}} \right)_i \right)^2 \sum_{k=1}^n \left(\left(\overset{\Delta}{\mathbf{X}} \right)_{j,k} - \left(\mathbf{E}_{\overset{\Delta}{\mathbf{x}}} \right)_j \right)^2}} \quad (\text{A.8}) \\ &= 1 - \frac{6}{n(n^2-1)} \sum_{k=1}^n \left(\left(\overset{\Delta}{\mathbf{X}} \right)_{i,k} - \left(\overset{\Delta}{\mathbf{X}} \right)_{j,k} \right)^2 \end{aligned}$$

The rank coefficients $\overset{\Delta}{\mathbf{X}}$ are assigned independently according to the ordering of the matrix entries in each row. The ranking is expressed by values in the interval $[1, n]$.

A.2 L moments of marginal distributions

Assuming n sample sets of the random vector \mathbf{x} are assembled column-wise in a sample matrix \mathbf{X} , the direct estimators for the first four L moments according to [Wang 1996] are

$$(\mathbf{L}_1)_i = \binom{n}{1}^{-1} \sum_{k=1}^n (\mathbf{X})_{i,k}, \quad (\text{A.9})$$

$$(\mathbf{L}_2)_i = \frac{1}{2} \binom{n}{2}^{-1} \sum_{k=1}^n \left(\binom{k-1}{1} - \binom{n-k}{1} \right) (\mathbf{X})_{i,k}, \quad (\text{A.10})$$

$$(\mathbf{L}_3)_i = \frac{1}{3} \binom{n}{3}^{-1} \sum_{k=1}^n \left(\binom{k-1}{2} - 2 \binom{k-1}{1} \binom{n-k}{1} + \binom{n-k}{2} \right) (\mathbf{X})_{i,k}, \text{ and} \quad (\text{A.11})$$

$$(\mathbf{L}_4)_i = \frac{1}{4} \binom{n}{4}^{-1} \sum_{k=1}^n \left(\binom{k-1}{3} - 3 \binom{k-1}{2} \binom{n-k}{1} + 3 \binom{k-1}{1} \binom{n-k}{2} - \binom{n-k}{3} \right) (\mathbf{X})_{i,k}. \quad (\text{A.12})$$

Optimization methods

B.1 Genetic algorithm

A general description of genetic algorithms can be found in [Holland 1992] and [Goldberg 1989]. The initial design sample set is randomly generated and is based on a uniform distribution. The cross over rate, mutation rate, and respective mutation standard deviation need to be defined next to the number of individuals, the number of parents per generation, and the number of generations. The algorithm selects the parents by using a dominance-based ranking. If a design sample violates a boundary, it is set directly to this boundary value. A set of standard configuration parameters is presented in Table B.1.

This form of genetic algorithm is available in the software package *Slang* [Dynardo GmbH and Bauhaus University Weimar 2010].

Table B.1: Standard configuration parameters of the genetic algorithm (GA).

parameters	value
crossover probability	0.5
mutation rate	0.5
mutation standard deviation	0.01

B.2 Particle swarm optimization

The basic concepts of the applied particle swarm implementation are given in [Kennedy et al. 1995], which is enhanced by the passive congregation of [He et al. 2004]. According to [He et al. 2004], the velocity of the i th particle is updated by

$$V_i^{k+1} = \omega V_i^k + c_1 r_1 (P_i^k - X_i^k) + c_2 r_2 (P_g^k - X_i^k) + c_3 r_3 (R_i^k - X_i^k). \quad (\text{B.1})$$

The updated displacement of the i th particle yields

$$X_i^{k+1} = X_i^k + V_i^{k+1}. \quad (\text{B.2})$$

The control factors c_1 , c_2 , and c_3 need to be defined. The factor ω is linearly dependent on the updating step and will be defined for the first and last iteration. To handle the boundary conditions, the fly-back mechanism proposed in [Li et al. 2007b] is applied. This mechanism relies on a harmony search scheme. If a design sample set violates the constraints, the set will be replaced by a randomly chosen set of best previously identified design sample sets. The standard configuration parameters are listed in Table B.2.

The scripting level of the software package *Slang* [Dynardo GmbH and Bauhaus University Weimar 2010] was applied to implement this algorithm.

Table B.2: Standard configuration parameters of the particle swarm optimization (PSO).

parameters	value
c_1	0.5
c_2	0.5
c_3	0.5
ω at first iteration	0.9
ω at last iteration	0.6

B.3 Adaptive response surface method

The proposed adaptive response surface approach uses a combination of the gradient-based method SQP (sequential quadratic programming) and a genetic algorithm (GA) ([Holland 1992][Goldberg 1989]) to perform an optimization at the approximated surfaces. A general description of adaptive response surface methods was presented in [Etman et al. 1996] and [Kurtaran et al. 2002]. The details of the applied optimization algorithm are given as follows.

The adaptive response surface method is based on a panning, an oscillation, and a zooming parameter. The response surface is approximated by linear regression polynoms, whereas the supporting points are defined by a D-optimal quadratic design-of-experiment (DOE) scheme. The response surface is changed adaptively depending on the problem. The optimization on the response surface is performed by a genetic algorithm. As the convergence of the genetic algorithm near the optimum is poor and no unique solution can be found, when using several runs, a subsequent application of the gradient-based algorithm refines the optimum on the response surface obtained by the genetic algorithm. The gradient-based method uses the SQP (NLPQL) approach [Schittkowski 1985], whereas the gradients are calculated using central differences. As the optimization is conducted on a response surface defined by linear polynoms, the criterion of differentiable objectives for the SQP algorithm is guaranteed. If not stated otherwise, the standard configuration parameters according to Table B.3 are applied.

This algorithm is implemented in the software optiSLang [Dynardo GmbH 2009], which has been applied for the calculations.

Table B.3: Standard configuration parameters of the adaptive response surface method (ARSM).

parameters	value
maximal iterations or function calls	50
panning (automatically adapted)	1.0
oscillation	0.6
zooming	0.6
NLPQL maximal iterations	50
NLPQL maximal function calls	50
NLPQL normalization length	20
GA individuals	10
GA generations	15
GA elites	1
GA replace individual	1
GA crossover rate	0.5
GA selection pressure	90%
GA cliff value	20

Bibliography

- Abrahams J. (1982). On the selection of measures of distance between probability distributions. *Information Science* 26(2), 109–113.
- Adhikari S. and Friswell M. I. (2010). Distributed parameter model updating using the Karhunen-Loève expansion. *Mechanical Systems and Signal Processing* 24(2), 326–339.
- Adhikari S., Friswell M. I., Lonkar K., and Sarkar A. (2009). Experimental case studies for uncertainty quantification in structural dynamics. *Probabilistic Engineering Mechanics* 24(4), 473–492.
- Al-Shehabi A. G. and Newmann B. (2002). Optimal blending filter parameters and sensor placement for flight control. In *Proceedings of AIAA Guidance, Navigation, and Control Conference and Exhibit*, AIAA2002-4750, pp. 1120–1128.
- Ali S. M. and Silvey S. D. (1966). A general class of coefficients of divergence of one distribution from another. *Journal of the Royal Statistical Society. Series B* 28(1), 131–142.
- Allemang R. J. (2003). The modal assurance criterion – twenty years of use and abuse. *Sound and Vibration* 37(8), 14–21.
- Allemang R. J. and Brown D. L. (1982). A correlation coefficient for modal vector analysis. In *Proceedings of the 1st International Modal Analysis Conference (IMAC)*, Volume 1, pp. 110–116.
- ANSYS, Inc. (2009). *Ansys Workbench 2.0 Framework - release 12.1.0*. ANSYS, Inc.
- ASME V&V 10 (2006). Guide for verification and validation in computational solid mechanics. American national standard, The American Society of Mechanical Engineers (ASME).
- Avitabile P. and Haselton D. (2002). Application of the test reference identification procedure TRIP. In *Proceedings of LMS Virtual Modeling Conference*, Troy, Michigan, USA.
- Avitabile P., Haselton D., and Moore J. (1996). Modal test reference selection using

- an SVD procedure. In *Proceedings of 14th International Modal Analysis Conference (IMAC)*, pp. 1527–1532.
- Avitabile P., O’Callahan J., and Milani J. (1988). Model correlation and orthogonality criteria. In *Proceedings of 6th International Modal Analysis Conference (IMAC)*, Orlando, Florida, USA, pp. 1039–1047.
- Bakir P. G., Reynders E., and De Roeck G. (2007). Sensitivity-based finite element model updating using constrained optimization with a trust region algorithm. *Journal of Sound and Vibration* 305(1-2), 211–225.
- Bartz-Beielstein T. (2010). Sequential parameter optimization – an annotated bibliography. Technical Report 04/2010, Institute of Computer Science, Faculty of Computer Science and Engineering Science, Cologne University of Applied Sciences, Germany.
- Bartz-Beielstein T., Lasarczyk C., and Preuss M. (2005). Sequential parameter optimization. In *Proceedings of 2005 IEEE Congress on Evolutionary Computation*, Volume 1, Edinburgh, Scotland, UK, pp. 773 – 780.
- Baseville M. (1989). Distance measures for signal processing and pattern recognition. *Signal Processing* 18(4), 349–369.
- Basir O. and Yuan X. (2007). Engine fault diagnosis based on multi-sensor information fusion using Dempster-Shafer evidence theory. *Information Fusion* 8(4), 379–386.
- Bayard D. S., Hadaegh F. Y., and Meldrum D. R. (1988). Optimal experiment design for identification of large space structures. *Automatica* 24(3), 357–364.
- Bedrossian H. (1998). *Optimal placement of sensors and actuators for modal identification*. PhD thesis, Faculty of the Graduate School, University of Southern California, University Park, Los Angeles, California 90007, USA.
- Bhattacharyya A. (1943). On a measure of divergence between two statistical populations defined by probability distributions. *Bulletin of the Calcutta Mathematical Society* 35, 99 –109.
- Bock H.-H. and Diday E. (Eds.) (2000). *Analysis of symbolic data*. Springer-Verlag.
- Brehm M. (2006). Wavelet packet system identification. In *Proceedings of 3rd PhD Workshop Brno-Prague-Weimar, April 28-29*, Weimar, Germany.
- Brehm M., Zabel V., and Bucher C. (2010). An automatic mode pairing strategy using an enhanced modal assurance criterion based on modal strain energies. *Journal of Sound and Vibration* 329(25), 5375–5392.
- Brehm M., Zabel V., and Bucher C. (2011). Optimal reference sensor placement within roving setup configurations. In *Proceedings of 8th International Conference on Structural Dynamics (EURODYN), July 4–6*, Leuven, Belgium.

- Brehm M., Zabel V., and Cantieni R. (2009a). Modellanpassung einer Eisenbahnbrücke für den Hochgeschwindigkeitsverkehr. In *VDI-Berichte Nr. 2063 – Baudynamik*, pp. 403–418. VDI Verlag GmbH.
- Brehm M., Zabel V., and Markwardt K. (2005). Applications of wavelet packets in system identification. In *Proceedings of 76. Jahrestagung der Gesellschaft für Angewandte Mathematik und Mechanik e.V. (GAMM), March 28 – April 1*, Luxemburg.
- Brehm M., Zabel V., and Unger J. F. (2009b). Stochastic model updating using perturbation methods in combination with neural network estimations. In *Proceedings of IMAC XXVII A Conference and Exposition on Structural Dynamics, February 9-12*, Orlando, Florida, USA.
- Brigo D. and Liinev J. (2005). On the distributional distance between the lognormal libor and swap market models. *Quantitative Finance* 5(5), 433–442.
- Brigo D., Mercurio F., Rapisarda F., and Scotti R. (2001). Approximated moment-matching dynamics for basket-options simulation. In *Proceedings of EFMA 2001 Lugano Meetings*.
- Brincker R., Ventura C. E., and Anderson P. (2003). Why output-only testing is a desirable tool for a wide range of practical applications. In *Proceedings of the 21th International Modal Analysis Conference (IMAC)*, Kissimmee, Florida, USA, pp. 1–8.
- Brincker R., Zhang L., and Anderson P. (2000). Modal identification from ambient responses using frequency domain decomposition. In *Proceedings of the 18th International Modal Analysis Conference (IMAC)*, San Antonio, Texas, USA, pp. 625–630.
- Brownjohn J. M. W., Xia P.-Q., Hao H., and Xia Y. (2001). Civil structure condition assessment by FE model updating: methodology and case studies. *Finite Element in Analysis and Design* 37(10), 761–775.
- Bucher C. (2009). *Computational analysis of randomness in structural mechanics*. CRC Press, Taylor & Francis Group.
- Burbea J. and Rao C. R. (1982). On the convexity of some divergence measures based on entropy functions. *IEEE Transactions on Information Theory* 28(3), 489–495.
- Cantieni R. (2009). Application of ambient vibration testing (operational modal analysis) in practice. In *Proceedings of Final Workshop of European Research Project DETAILS, December 9-11*, Lucca, Italy, pp. 118–132.
- Cantieni R., Brehm M., Zabel V., Rauert T., and Hoffmeister B. (2008a). Ambient modal analysis and model updating of a twin composite filler beam railway bridge for high-speed trains with continuous ballast. In *Proceedings of IMAC-XXVI Conference on Structural Dynamics, February 4-7*, Orlando, Florida, USA.

- Cantieni R., Brehm M., Zabel V., Rauert T., and Hoffmeister B. (2008b). Ambient testing and model updating of a filler beam bridge for high-speed trains. In *Proceedings of 7th European Conference on Structural Dynamics (EURODYN)*, July 7–9, Southampton, UK.
- Cauberghe B. (2004). *Applied frequency-domain system identification in the field of experimental and operational modal analysis*. PhD thesis, Vrije Universiteit Brussel.
- Chandler D. and Avitabile P. (2001). Selection of measurement references using the trip procedure. In *Proceedings of the International Society for Optical Engineering (SPIE)*, Volume 4359 (2), pp. 1758–1763.
- Chellini G., De Roeck G., Nardini L., and Salvatore W. (2010). Damage analysis of a steel-concrete composite frame by finite element model updating. *Journal of Constructional Steel Research* 66(3), 398–411.
- Chellini G., Nardini L., and Salvatore W. (2009). Experimental vibration analysis and finite element modelling of sesia viaduct. In *Proceedings of Final Workshop of European Research Project DETAILS, December 9-11*, Lucca, Italy, pp. 133–148.
- Chellini G. and Salvatore W. (2007). Updated models for steel-concrete composite HS railway bridges. In *Proceedings of Experimental Vibration Analysis for Civil Engineering Structures (EVACES)*.
- Chernoff H. (1952). A measure of asymptotic efficiency for test of a hypothesis based on the sum of observations. *Annals of Mathematical Statistics* 23(4), 493–507.
- Chung J. K., Kannappan P., Ng C. T., and Sahoo P. K. (1989). Measures of distance between probability distributions. *Journal of Mathematical Analysis and Applications* 138(1), 280–292.
- Collins J. D., Hart G. C., Haselman T. K., and Kennedy B. (1974). Statistical identification of structures. *AIAA Journal* 12(2), 185–190.
- Cornwell P., Doebling S. W., and Farrar C. R. (1999). Application of the strain energy damage detection method to plate-like structures. *Journal of Sound and Vibration* 224(2), 359–374.
- Cruz A., Vélez W., and Thomson P. (2009). Optimal sensor placement for modal identification of structures using genetic algorithms – a case study: the olympic stadium in cali, colombia. *Annals of Operations Research* DOI 10.1007/s10479-009-0576-6, Link: <http://www.springerlink.com/content/28885L815W3772Q2>.
- Csiszár I. (1967a). Information-type measures of difference of probability distributions and indirect observations. *Studia Scientiarum Mathematicarum Hungarica* 2, 299–318.

- Csiszár I. (1967b). On topological properties of f-divergences. *Studia Scientiarum Mathematicarum Hungarica* 2, 329–339.
- Cunha Á., Caetano E., Magalhães F., and Moutinho C. (2006). From input-output to output-only modal identification of civil engineering structures. Final Report F11 Selected Papers, European thematic network SAMCO, www.samco.org.
- De Maesschalck R., Jouan-Rimbaud D., and Massart D. L. (2000). The Mahalanobis distance. *Chemometrics and Intelligent Laboratory Systems* 50(1), 1–18.
- Doebling S., Hemez F., and Rhee W. (2000). Statistical model updating and validation applied to nonlinear transient structural dynamics. In *European COST F3 Conference on System Identification and Structural Health Monitoring, June 6-9*, Madrid, Spain.
- Doebling S. W., Hemez F., Peterson L. D., and Farhat C. (1997). Improved damage location accuracy using strain energy-based mode selection criteria. *AIAA Journal* 35(4), 693–699.
- Dragomir S. S., Sunde J., and Buse C. (2000). New inequalities for Jeffreys divergence measure. *Tamsui Oxford Journal of Mathematical Sciences* 16(2), 295–309.
- Dynardo GmbH (2009). *optiSLang – the optimizing structural language* (3.1.0 ed.). Weimar, Germany: Dynardo GmbH.
- Dynardo GmbH and Bauhaus University Weimar (2010). *SLang – the structural language* (5.1.0 ed.). Weimar, Germany: Dynardo GmbH and Bauhaus University Weimar.
- Escolano F., Suau P., and Bonev B. (2009). *Information theory in computer vision and pattern recognition*. Springer-Verlag.
- Etman L., Adriaens J., van Slagmaat M., and Schoofs A. (1996). Crashworthiness design optimization using multipoint sequential linear programming. *Structural Optimization* 12, 222–228.
- Evans M. J. and Swartz T. (2005). *Approximating integrals via Monte Carlo and deterministic methods*. Oxford University Press.
- Ewins D. J. (2000a). *Modal testing: theory, practice and application* (2nd ed.). Research Studies Press Ltd.
- Ewins D. J. (2000b). Model validation: correlation for updating. In *Proceedings of Indian Academy Sciences*, Volume 25, Sadhana, pp. 221–246.
- Falk M., Marohn F., and Tewes B. (2002). *Foundations of statistical analyses and applications with SAS*. Birkhäuser.
- Fellin W. and Ostermann A. (2006). Parameter sensitivity in finite element analysis with constitutive models of the rate type. *International Journal for Numerical and Analytical Methods in Geomechanics* 30(2), 91–112.

- Fijany A. and Vatan F. (2005). A new method for sensor placement optimization. In *Proceedings of 41st AIAA/ASME/SAE/ASEE Joint Propulsion Conference and Exhibit, July 11-13*, Tucson, Arizona, USA, pp. 1–8.
- Franchi C. G. and Gallieni D. (1995). Genetic-algorithm-based procedure for pretest analysis. *AIAA Journal* 33(7), 1362–1364.
- Friswell M. I. (1989). The adjustment of structural parameters using a minimum variance estimator. *Mechanical Systems and Signal Processing* 3(2), 143–155.
- Friswell M. I. (2001). Finite element model updating using experimental test data: parameterization and regularization. *Philosophical Transactions of the Royal Society of London A* 359, 169–186.
- Friswell M. I. and Mottershead J. E. (1995). *Finite element model updating in structural dynamics*. Netherlands: Kluwer Academic Publishers.
- Garvey S. D., Friswell M. I., and Penny J. E. T. (1996). Evaluation of a method for automatic selection of measurement locations based on subspace-matching. In *Proceedings of the 14th International Modal Analysis Conference (IMAC)*, Dearborn, MI, USA, pp. 1546–1552.
- Goldberg D. E. (1989). *Genetic algorithms in search, optimization and machine learning*. Boston, MA, USA: Addison-Wesley Longman Publishing Co. Inc.
- Govers Y., Böswald M., Füllekrug U., Göge D., and Link M. (2006). Analysis of sources and quantification of uncertainties in experimental modal data. In *Proceedings of International Conference on Noise and Vibration Engineering (ISMA)*, Leuven, Belgium, pp. 4161–4173.
- Govers Y. and Link M. (2009). Stochastic model updating by covariance matrix adjustment. In *Proceedings of the International Conference on Structural Engineering Dynamics (ICEDyn2009)*, Ericeira, Portugal.
- Govers Y. and Link M. (2010a). Stochastic model updating – covariance matrix adjustment from uncertain experimental modal data. *Mechanical Systems and Signal Processing* 24(3), 696–706.
- Govers Y. and Link M. (2010b). Stochastic model updating of an aircraft like structure by parameter covariance matrix adjustment. In *Proceedings of International Conference on Noise and Vibration Engineering (ISMA)*, Leuven, Belgium, pp. 2639–2656.
- Guyan R. J. (1965). Reduction of stiffness and mass matrices. *AIAA Journal* 3(2), 380.
- Hartung J. and Elpelt B. (2007). *Multivariate statistik* (7th ed.). R. Oldenbourg Verlag.
- Hazewinkel M. (Ed.) (2002). *Encyclopedia of mathematics*. Kluwer Academic Publishers.

- He S., Wu Q. H., Wen J. Y., Saunders J. R., and Paton R. C. (2004). A particle swarm optimizer with passive congregation. *BioSystems* 78, 135–147.
- Hellinger E. (1909). Neue Begründung der Theorie der quadratischen Formen von unendlich vielen Veränderlichen. *Journal für reine und angewandte Mathematik* 136, 210–271.
- Heredia-Zavoni E. and Esteva L. (1998). Optimal instrumentation of uncertain structural systems subject to earthquake ground motions. *Earthquake Engineering and Structural Dynamics* 27, 343–362.
- Hero A. O., Ma B., Michel O., and Gorman J. D. (2001). Alpha-divergence for classification, indexing and retrieval. Technical Report CSPL-328, Communications and Signal Processing Laboratory. The University of Michigan, USA.
- Heylen W., Lammens S., and Sas P. (1999). *Modal analysis theory and testing* (2nd ed.). Leuven, Belgium: Katholieke Universiteit Leuven.
- Hogg R. V., MCKean J. W., and Craig A. T. (2005). *Introduction to mathematical statistics* (6th ed.). Pearson Prentice Hall.
- Holland J. H. (1992). *Adaptation in natural and artificial systems - an introductory analysis with applications to biology, control, and artificial intelligence*. MIT Press.
- Hosking J. R. M. (1990). *L*-moments: Analysis and estimation of distributions using linear combinations of order statistics. *Journal of the Royal Statistical Society. Series B* 52(1), 105–124.
- Hunt D. L. (1992). Application of an enhanced coordinate modal assurance criterion (ECOMAC). In *Proceedings of 10th International Modal Analysis Conference (IMAC)*, pp. 66–71.
- Jain K. C. and Srivastava A. (2007). On symmetric information divergence measures of Csiszar's *f*-divergence class. *Journal of Applied Mathematics, Statistics and Informatics* 3(1), 85–102.
- Jaishi B. and Ren W.-X. (2005). Structural finite element model updating using ambient vibration test results. *Journal of Structural Engineering* 131(4), 617–628.
- Jaishi B. and W.-X. R. (2007). Finite element model updating based on eigenvalue and strain energy residuals using multiobjective optimisation technique. *Mechanical Systems and Signal Processing* 21(5), 2295–2317.
- Jeon B. S., Lee D. J., Song C. K., Lee S. H., and Ryu J. W. (2004). The performance improvement of speech recognition system based on stochastic distance measure. *International Journal of Fuzzy Logic and Intelligent Systems* 4(2), 254–258.

- Joan-Arinyo R., Luzón M., and Yeguas E. (2011). Parameter tuning of PBIL and CHC evolutionary algorithms applied to solve the root identification problem. *Applied Soft Computing* 11(1), 754 – 767.
- Kailath T. (1967). The divergence and Bhattacharyya distance measures in signal selection. *IEEE Transactions on Communication Technology* 15(1), 52–60.
- Kakizawa Y., Shumway R. H., and Taniguchi M. (1998). Discrimination and clustering for multivariate time series. *Journal of the American Statistical Association* 93(441), 328 – 340.
- Kammer D. C. (1991). Sensor placement for on-orbit modal identification and correlation of large space structures. *Journal of Guidance, Control, and Dynamics* 14(2), 251–259.
- Kammer D. C. (1996). Optimal sensor placement for modal identification using system-realization methods. *Journal of Guidance, Control, and Dynamics* 19(3), 729–731.
- Kammer D. C. and Yao L. (1994). Enhancement of on-orbit modal identification of large space structures through sensor placement. *Journal of Sound and Vibration* 171(1), 119–139.
- Kannappan P. (1974). On a generalization of some measures in information theory. *Glasnik Matematički* 9(29), 81–93.
- Keitel H. and Dimmig-Osburg A. (2010). Uncertainty and sensitivity analysis of creep models for uncorrelated and correlated input parameters. *Engineering Structures* 32(11), 3758–3767.
- Kennedy J. and Eberhart R. (1995). Particle swarm optimization. In *Proceedings of IEEE International Conference on Neural Networks*, Volume IV, Perth, Australia, pp. 1942–1948. IEEE Press.
- Keye S. (2003). *Model updating of modal parameters from experimental data and applications in aerospace*. PhD thesis, University of Greenwich.
- Khodaparast H. H. and Mottershead J. E. (2008a). Efficient methods in stochastic model updating. In Sas P. and Bergen B. (Eds.), *Proceedings of International Conference on Noise and Vibration Engineering (ISMA), September 15 - 17*, Leuven, Belgium, pp. 1855 – 1869.
- Khodaparast H. H., Mottershead J. E., and Badrock K. J. (2010). Interval model updating: method and application. In *Proceedings of International Conference on Noise and Vibration Engineering (ISMA)*, Leuven, Belgium, pp. 5277–5289.
- Khodaparast H. H., Mottershead J. E., and Friswell M. I. (2008b). Perturbation methods for the estimation of parameter variability in stochastic model updating. *Mechanical Systems and Signal Processing* 22(8), 1751 – 1773.

- Kim K.-O., Yoo H.-S., and Choi Y.-J. (2001). Optimal sensor placement for dynamic testing of large structures. In *Proceedings of the 42nd AIAA/ASME/ASCE/AHS/ASC Structures, Structural Dynamics and Material Conference and Exhibit*, Seattle, WA, USA, pp. 391–399.
- Kim T. S. and Kim Y. Y. (2000). MAC-based mode-tracking in structural topology optimization. *Computers and Structures* 74(3), 375–383.
- Kincaid R. K. and Padula L. S. (2002). D-optimal designs for sensor and actuator locations. *Computers and Operations Research* 29(6), 701–713.
- Kobayashi H. (1970). Distance measures and asymptotic relative efficiency. *IEEE Transactions on Information Theory* 16(3), 288–291.
- Kobayashi H. and Thomas J. B. (1967). Distance measures and related criteria. In *Proceedings of Fifth Annual Allerton Conference on Circuit and Systems*, University of Illinois, USA, pp. 491–500.
- Krämer C., De Smet C. A. M., and De Roeck G. (1999). Z24 bridge damage detection tests. In *Proceedings of 17th International Modal Analysis Conference (IMAC)*, Kissimmee, Florida, USA, pp. 1023–1029.
- Kuendig C., Sabathy M., and Biro T. (2009). System and sensor for monitoring purposes. In *Proceedings of Final Workshop of European Research Project DETAILS, December 9-11, Lucca, Italy*, pp. 118–132.
- Kulhavý R. (1996). A Kullback-Leibler distance approach to system identification. *Annual Reviews in Control* 20, 119–130.
- Kullback S. (1997). *Information theory and statistics*. New York: Dover Publications.
- Kullback S. and Leibler R. A. (1951). On information and sufficiency. *The Annals of Mathematical Statistics* 22, 79–86.
- Kumar P. and Chhina S. (2005a). A symmetric information divergence measure of the Csiszár’s f-divergence class and its bounds. *Computers and Mathematics with Applications* 49(3), 575–588.
- Kumar P. and Johnson A. (2005b). On a symmetric divergence measure and information inequalities. *Journal of Inequalities in Pure and Applied Mathematics* 6(3), Article 65.
- Kurtaran H., Eskandarın A., Marzougı D., and Bedewi N. (2002). Crashworthiness design optimization using response surface approximations. *Computational Mechanics* 29(4), 409–421.
- Ladevèze P., Puel G., Deraemaeker A., and Romeuf T. (2006). Validation of structural dynamics models containing uncertainties. *Computer Methods in Applied Mechanics and Engineering* 195(4-6), 373–393.

- Lancaster P. and Salkauskas K. (1986). *Curve and surface fitting: an introduction*. London: Academic Press.
- Larson C. B., Zimmermann D. C., and Marek E. L. (1994a). A comparative study of metrics for modal pre-test sensor and actuator selection using the JPL/MPI testbed truss. In *Proceedings of AIAA Dynamics Specialist Conference*, pp. 150–162.
- Larson C. B., Zimmermann D. C., and Marek E. L. (1994b). A comparison of modal test planning techniques: excitation and sensor placement using the NASA 8-bay truss. In *Proceedings of 12th International Modal Analysis Conference (IMAC)*, USA, pp. 205–211.
- Lee Y.-T. (1991). Information-theoretic distortion measures for speech recognition. *IEEE Transactions on Signal Processing* 39(2), 330–335.
- Levin R. I. and Lieven N. A. J. (1998). Dynamic finite element model updating using simulated annealing and genetic algorithms. *Mechanical Systems and Signal Processing* 12(1), 91–120.
- Li D. S., Li H. N., and Fritzen C. P. (2007a). The connection between effective independence and modal kinetic energy methods for sensor placement. *Journal of Sound and Vibration* 305(4-5), 945–955.
- Li D.-S., Li H.-N., and Fritzen C.-P. (2009). A note on fast computation of effective independence through QR downdating for sensor placement. *Mechanical Systems and Signal Processing* 23(4), 1160–1168.
- Li H., Yang H., and Hu S.-L. J. (2006). Modal strain energy decomposition method for damage localization in 3D frame structures. *Journal of Engineering Mechanics* 132(9), 941–951.
- Li L. J., Huang Z. B., Liu F., and Wu Q. H. (2007b). A heuristic particle swarm optimizer for optimization of pin connected structures. *Computers and Structures* 85(7-8), 340–349.
- Lieven N. A. J. and Ewins D. J. (1988). Spatial correlation of mode shapes, the coordinate modal assurance criterion (COMAC). In *Proceedings of International Modal Analysis Conference (IMAC)*.
- Lieven N. A. J. and Waters T. P. (1994). Error location using normalized orthogonality. In *Proceedings of the 12th International Modal Analysis Conference (IMAC)*, Honolulu, Hawaii, USA, pp. 761–764.
- Lin R. M. and Zhu J. (2006). Model updating of damped structures using FRF data. *Mechanical Systems and Signal Processing* 20(8), 2200–2218.
- Link M., Weiland M., and Hahn T. (2008). Structural health monitoring of the Gaernerterplatz bridge over the Fulda river in Kassel. In *Proceedings of the 2nd international*

UHPC symposium, Kassel, Germany.

- Liu K., Reynders E., de Roeck G., and Lombaert G. (2009). Experimental and numerical analysis of a composite bridge for high-speed trains. *Journal of Sound and Vibration* 320(1-2), 201–220.
- Liu W., Gao W.-C., Sun Y., and Xu M.-j. (2008). Optimal sensor placement for spatial lattice structure based on genetic algorithms. *Journal of Sound and Vibration* 317(1-2), 175–189.
- Lombaert G., Moaveni B., and Conte J. P. (2010a). A probabilistic assessment of the resolution in the vibration-based damage identification of a seven-story reinforced concrete test structure. In Casciati F. and Giordano M. (Eds.), *Proceedings of the Fifth European Workshop on Structural Health Monitoring*, Sorrento, Italy, pp. 1067 – 1072. DEStech Publications, Inc.
- Lombaert G., Moaveni B., and Conte J. P. (2010b). Uncertainty quantification in vibration-based damage assessment of a seven-story reinforced concrete shear wall building. In *Proceedings of IV European Conference on Computational Mechanics (ECCM 2010)*, Paris, France.
- Maeck J. and De Roeck G. (2003). Description of the Z24 benchmark. *Mechanical Systems and Signal Processing* 17(1), 127–131.
- Maghami P. G. and Joshi S. M. (1993). Sensor-actuator placement for flexible structures with actuator dynamics. *Journal of Guidance, Control, and Dynamics* 16(2), 301–307.
- Maia N. M. M. and Silva J. M. M. (Eds.) (1997). *Theoretical and experimental modal analysis*. Baldock, UK: Research Studies Press.
- Mares C., Friswell M. I., and Mottershead J. E. (2002). Model updating using robust estimation. *Mechanical Systems and Signal Processing* 16(1), 169–183.
- Mares C., Mottershead J. E., and Friswell M. I. (2006). Stochastic model updating: Part 1 – theory and simulated example. *Mechanical Systems and Signal Processing* 20(7), 1674 – 1695.
- Marwala T. (Ed.) (2010). *Finite-element-model updating using computational intelligence techniques: applications to structural dynamics*. London: Springer-Verlag.
- MathWorks (2010). *MatLab Documentation – Statistics Toolbox* (R2010a ed.). MathWorks.
- Mekenyan O., Nikolova N., Schmieder P., and Veith G. (2004). COREPA-M: A multi-dimensional formulation of COREPA. *QSAR & Combinatorial Science* 23(1), 5–18.
- Meo M. and Zumpano G. (2005). On the optimal sensor placement techniques for a bridge structure. *Engineering Structures* 27(10), 1488–1497.

- Minka T. (2005). Divergence measures and message passing. Technical Report MSR-TR-2005-173, Microsoft Research Ltd.
- Montgomery D. C. and Runger G. C. (2002). *Applied Statistics and Probability for Engineers* (3rd ed.). Netherlands: Wiley & Sons.
- Morales C. (2005). Comments on the MAC and the NCO, and a linear modal correlation coefficient. *Journal of Sound and Vibration* 282(1-2), 529–537.
- Most T. and Bucher C. (2005). A moving least squares weighting function for the element-free galerkin method which almost fulfills essential boundary conditions. *Structural Engineering and Mechanics* 21(3), 315–332.
- Mottershead J. E. and Friswell M. I. (1993). Model updating in structural dynamics: a survey. *Journal of Sound and Vibration* 167(2), 347–375.
- Mottershead J. E., Link M., and Friswell I. M. (2010). The sensitivity method in finite element model updating: a tutorial. *Mechanical Systems and Signal Processing In Press, Corrected Proof*.
- Mottershead J. E., Mares C., James S., and Friswell M. I. (2006). Stochastic model updating: Part 2 – application to a set of physical structures. *Mechanical Systems and Signal Processing* 20(8), 2171–2185.
- Myers R. H., Montgomery D. C., and Anderson-Cook C. M. (2009). *Response surface methodology: Process and product optimization using designed experiments* (third ed.). John Wiley & Sons, Inc.
- Nannen V., Smit S., and Eiben A. (2008). Costs and benefits of tuning parameters of evolutionary algorithms. In Rudolph G., Jansen T., Lucas S., Poloni C., and Beume N. (Eds.), *Parallel Problem Solving from Nature – PPSN X*, Volume 5199 of *Lecture Notes in Computer Science*, pp. 528–538. Springer Berlin / Heidelberg.
- National Instruments (2009). *NI LabVIEW* (9.0 ed.). National Instruments.
- Natke H. G. (1992). *Einführung in die Theorie und Praxis der Zeitreihen- und Modalanalyse* (3. ed.). Vieweg & Sohn.
- Natke H. G. (1998). Problems of model updating procedures: a perspective resumption. *Mechanical Systems and Signal Processing* 12(1), 65–74.
- Nayak S., Sarkar S., and Loeding B. (2009). Distribution-based dimensionality reduction applied to articulated motion recognition. *IEEE Transactions on Pattern Analysis and Machine Intelligence* 31(5), 795 – 810.
- Nguyen V. V., Hartmann D., Baitsch M., and König M. (2010). A distributed agent-based approach for robust optimization. In *Proceedings of 2nd International Conference on Engineering Optimization, September 6-9, Lisbon, Portugal*.

- Nguyen X., Wainwright M. J., and Jordan M. I. (2005). On information divergence measures, surrogate loss functions and decentralized hypothesis testing. In *Proceedings of 43rd Annual Allerton Conference on Communication, Control and Computing*, Allerton, IL, USA.
- Norton M. P. and Karczub D. G. (2003). *Fundamentals of noise and vibration analysis* (2nd ed.). Cambridge, UK: Cambridge University Press.
- Oberguggenberger M., King J., and Schmelzer B. (2009). Classical and imprecise probability methods for sensitivity analysis in engineering: A case study. *International Journal of Approximate Reasoning* 50(4), 680–693.
- O’Callahan J., Avitabile P., and Riemer R. (1989). System equivalent reduction expansion process (SEREP). In *Proceedings of 7th International Modal Analysis Conference (IMAC)*, Las Vegas, Nevada, USA, pp. 29 – 37.
- Papadimitriou C. (2004). Optimal sensor placement methodology for parametric identification of structural systems. *Journal of Sound and Vibration* 278(4-5), 923–947.
- Papadimitriou C. (2005). Pareto optimal sensor locations for structural identification. *Computer Methods in Applied Mechanics and Engineering* 194(12-16), 1655–1673.
- Papadimitriou C. and Beck J. L. (2000). Entropy-based optimal sensor location for structural model updating. *Journal of Vibration and Control* 6(5), 781–800.
- Papadopoulos M. and Garcia E. (1998). Sensor placement methodologies for dynamic testing. *AIAA Journal* 36(2), 256–263.
- Pape D. A. (1994). Selection of measurement locations for experimental modal analysis. In *Proceedings of 12th International Modal Analysis Conference (IMAC)*, USA, pp. 34–41.
- Papoulis A. and Pillai S. U. (2002). *Probability, random variables and stochastic processes* (4th ed.). McGraw-Hill.
- Patrick E. and Fischer F. (1969). Nonparametric feature selection. *IEEE Transactions on Information Theory* 15(5), 577–584.
- Peeters B. and De Roeck G. (1999). Reference-based stochastic subspace identification for output-only modal analysis. *Mechanical Systems and Signal Processing* 13(6), 855–878.
- Peeters B. and De Roeck G. (2001). Stochastic system identification for operational modal analysis: A review. *ASME Journal of Dynamic Systems, Measurement, and Control* 123(4), 659–667.
- Pekalska E. and Duin R. P. W. (2005). *The dissimilarity representation for pattern recognition. Foundations and applications*. World Scientific Publishing.

- Penny J. E. T., Friswell M. I., and Garvey S. D. (1994). Automatic choice of measurement location for dynamic testing. *AIAA Journal* 32(2), 407–414.
- Prasanth R., Cabrera J., Amin J., Mehra R., Purtell R., and Smith R. (2003). Quality of information measures for autonomous decision-making. In *Proceedings of 2nd AIAA Unmanned Unlimited Systems, Technologies, and Operations - Aerospace, 15-18 September, 2003*, AIAA 2003-6671, San Diego, California. AIAA.
- Queipo N. V., Haftka R. T., Shyy W., Goel T., Vaidyanathan R., and Tucker P. K. (2005). Surrogate-based analysis and optimization. *Progress in Aerospace Sciences* 41(1), 1–28.
- Ramakrishnan S. and Selvan S. (2006). A new statistical model based on wavelet domain singular value decomposition for image texture classification. *GVIP Journal* 6(3), 15–22.
- Rao C. R. and Nayak T. K. (1985). Cross entropy, dissimilarity measures, and characterizations of quadratic entropy. *IEEE Transactions on Information Theory* 31(5), 589–593.
- Rauber T., Braun T., and Berns K. (2008a). Probabilistic distance measures of the Dirichlet and Beta distributions. *Pattern Recognition* 41(2), 637–645.
- Rauber T., Conci A., Braun T., and Berns K. (2008b). Bhattacharyya probabilistic distance of the Dirichlet density and its application to Split-and-Merge image segmentation. In *Proceedings of 15th International Conference on Systems, Signals and Image Processing (IWSSIP 2008)*, Bratislava, pp. 145 – 148.
- Rényi A. (1961). On measures of entropy and information. In *Proceedings of 4th Berkeley Symposium on Mathematical Statistics and Probability*, Berkeley, USA, pp. 547–561. University of California Press.
- Reynders E. (2009). *System identification and modal analysis in structural mechanics*. PhD thesis, Katholieke Universiteit Leuven, Belgium.
- Reynders E., de Roeck G., Bakir P. G., and Sauvage C. (2007). Damage identification on the Tilff Bridge by vibration monitoring using optical fibre strain sensors. *Journal of Engineering Mechanics* 133(2), 185–193.
- Reynders E., Pintelon R., and de Roeck G. (2008). Uncertainty bounds on modal parameters obtained from stochastic subspace identification. *Mechanical Systems and Signal Processing* 22(4), 948–969.
- Reynier M. and Abou-Kandil H. (1999). Sensor location for updating problems. *Mechanical Systems and Signal Processing* 13(2), 297–314.
- Ribeiro D., Calçada R., Delgado R., Brehm M., and Zabel V. (2009). Numerical and experimental assessment of the modal parameters of a bowstring arch railway bridge.

- In *Proceedings of Experimental Vibration Analysis for Civil Engineering Structures (EVACES)*, October 14 – 16, Wrocław, Poland.
- Sahoo P. K. (1999). On a functional equation associated with stochastic distance measures. *Bulletin of Korean Mathematical Society* 36(2), 287–303.
- Saltelli A., Ratto M., Andres T., Campolongo F., Cariboni J., Gatelli D., Saisana M., and Tarantola S. (2008). *Global sensitivity analysis. The primer*. John Wileys & Sons, Ltd.
- Saltelli A., Tarantola S., Francesca C., and Ratto M. (2004). *Sensitivity analysis in practice: A guide to assessing scientific models*. John Wileys & Sons, Ltd.
- Schittkowski K. (1985). NLPQL: A fortran subroutine solving constrained nonlinear programming problems. *Annals of Operations Research* 5(1), 485–500.
- Schwarz B., Richardson M., and Avitabile P. (2002). Locating optimal references for modal testing. In *Proceedings of 20th International Modal Analysis Conference (IMAC)*.
- Schwer L. E. (2006). An overview of the ASME guide for verification and validation in computational solid mechanics. In *Proceedings of 5. LS-DYNA Anwenderforum*, Ulm, Germany.
- Scott D. W. (Ed.) (1992). *Multivariate density estimation: Theory, practice, and visualization*. Wiley & Sons.
- Shen J.-L. (1998). Segmental probability distribution model approach for isolated mandarin syllable recognition. *IEE Proceedings Vision, Image and Signal Processing* 145(6), 384–390.
- Shi Z. Y., Law S. S., and Zhang L. M. (1998). Structural damage localization from modal strain energy change. *Journal of Sound and Vibration* 218(5), 825–844.
- Shi Z. Y., Law S. S., and Zhang L. M. (2000). Structural damage detection from modal strain energy change. *Journal of Engineering Mechanics* 126(12), 1216–1223.
- Shibata R. (1997). Bootstrap estimate of Kullback-Leibler information for model selection. *Statistica Sinica* 7, 375–394.
- Sibson R. (1969). Information radius. *Probability Theory and Related Fields* 14(2), 149–160.
- Singh S., Singh M., and Markou M. (2002). Feature selection for face recognition based on data partitioning. In *Proceedings of 16th International Conference on Pattern Recognition*, Volume 1, pp. 680 – 683.
- Spearman C. (1904). The proof and measurement of association between two things. *American Journal of Psychology* 15, 72–101.

- Stabb M. and Blelloch P. (1995). A genetic algorithm for optimally selecting accelerometer locations. In *Proceedings of the 13th International Modal Analysis Conference (IMAC)*, pp. 1530–1534.
- Steenackers G. and Guillaume P. (2006). Finite element model updating taking into account the uncertainty on the model parameters estimates. *Journal of Sound and Vibration* 296(4-5), 919–934.
- Stoll G., Rougemont J., and Naef F. (2006). Few crucial links assure checkpoint efficiency in the yeast cell-cycle network. *Bioinformatics* 22(20), 2539–2546.
- Suykens J. and Alzate C. (2010). Support vector machines and kernel methods: new approaches in unsupervised learning. In *Proceedings of IEEE World Congress on Computational Intelligence WCCI*, Barcelona, Spain.
- Suykens J., Van Gestel T., De Brabanter J., De Moor B., and Vandewalle J. (2002). *Least Squares Support Vector Machines*. Singapore: World Scientific.
- Swann C. and Chattopadhyay A. (2004). Optimal sensor placement for damage characterization using genetic algorithm. In *Proceedings of 45th AIAA/ASME/ASCE/AHS/ASC Structures, Structural Dynamics and Material Conference, April 19-22*, pp. 4718–4730.
- Taneja I. J. (1989). *Advances in electronics and electron physics* (P. W. Hawkes, B. Kazan (eds.)), Volume 76, Chapter On generalized information measures and their applications, pp. 327–413. Academic Press, Inc.
- Teughels A. (2003). *Inverse modelling of civil engineering structures based on operational modal data*. PhD thesis, Katholieke Universiteit to Leuven, Belgium.
- Teughels A., De Roeck G., and Suykens J. (2003). Global optimization by coupled local minimizers and its application to FE model updating. *Computers and Structures* 81(24–25), 2337–2351.
- Thacker N. A., Aherne F. J., and Rockett P. I. (1997). The Bhattacharyya metric as an absolute similarity measure for frequency coded data. *Kybernetika* 34(4), 363–368.
- Tongco E. and Meldrum D. (1994). Optimal sensor placement and active vibration suppression of large flexible space structures. In *Proceedings of AIAA Guidance, Navigation and Control Conference, August 1-3*, Scottsdale, AZ, USA, pp. 857–866.
- Tongco E. and Meldrum D. (1996). Optimal sensor placement of large flexible space structures. *Journal of Guidance, Control, and Dynamics* 19(4), 961–963.
- Topsøe F. (2000). Some inequalities for information divergence and related measures of discrimination. *IEEE Transactions on Information Theory* 46(4), 1602–1609.
- Toussaint G. T. (1974). Some properties of Matusita’s measure of affinity of several distributions. *Annals of the Institute of Statistical Mathematics* 26(1), 389–394.

- Tuttle R., Cole T., and Lollock J. (2005). An automated method for identification of efficient measurement degrees-of-freedom for mode survey testing. In *Proceedings of 46th AIAA/ASME/ASCE/AHS/ASC Structures, Structural Dynamics and Materials Conference, April 18-21*, Austin, Texas, USA.
- Ullah A. (1996). Entropy, divergence and distance measures with econometric applications. *Journal of Statistical Planning and Inference* 49(1), 137–162.
- Unger J. F. (2009). *Neural networks in a multiscale approach for concrete*. PhD thesis, Institute of Structural Mechanics, Bauhaus University Weimar, Germany.
- Vajda I. (1972). On the f-divergence and singularity of probability measures. *Periodica Mathematica Hungarica* 2, 223–234.
- Vajda I. (2009). On metric divergences of probability measures. *Kybernetika* 45(6), 885–900.
- Verma A. K., Ajit S., and Karanki D. R. (2010). *Reliability and safety engineering*. Springer-Verlag.
- Walter-Williams J. and Li Y. (2010). Comparative study of distance functions for nearest neighbors. In *Advanced Techniques in Computing Sciences and Software Engineering*, pp. 79–84. Springer-Verlag.
- Wang J. and Wang H. (2003). The reliability and self-diagnosis of sensors in a multisensor data fusion diagnostic system. *Journal of Testing and Evaluation* 31(5), 370–377.
- Wang Q. J. (1996). Direct sample estimators of L moments. *Water Resources Research* 32(12), 3617–3619.
- Waters T. P. (1995). *Finite element model updating using measured frequency response functions*. PhD thesis, University of Bristol.
- Wenzel H. and Pichler D. (2005). *Ambient vibration monitoring*. England: John Wiley & Sons Ltd.
- Worden K. and Burrows A. P. (2001). Optimal sensor placement for fault detection. *Engineering Structures* 23(8), 885–901.
- Yao L., Sethares W. A., and Kammer D. C. (1993). Sensor placement for on-orbit modal identification via a genetic algorithm. *AIAA Journal* 31(10), 1922–1928.
- Zabel V. (2003). *Applications of wavelet analysis in system identification*. PhD thesis, Institute of Structural Mechanics, Bauhaus University Weimar, Germany.
- Zabel V. and Brehm M. (2008a). Das dynamische Verhalten von Eisenbahnbrücken mit kurzer Spannweite - numerische und experimentelle Untersuchungen. *Bauingenieur. D-A-CH-Mitteilungsblatt* 83, S9–S14.

- Zabel V. and Brehm M. (2008b). Dynamic testing and numerical modelling of a typical short span high-speed railway bridge. In *Proceedings of the Fourth International Conference on Bridge Maintenance, Safety, and Management (IABMAS), July 13-17*, Seoul, Korea. CRC PRESS.
- Zabel V. and Brehm M. (2008c). System identification of high-speed railway bridges. In *Proceedings of Weimar Optimization and Stochastic Days, November 20-21*, Weimar, Germany.
- Zabel V. and Brehm M. (2009a). Stochastic model updating methods – a comparative study. In *Proceedings of IMAC XXVII A Conference and Exposition on Structural Dynamics, February 9-12*, Orlando, Florida, USA.
- Zabel V., Brehm M., De Roeck G., Liu K., and Reynders E. (2009b). Algorithms for structural identification and damage detection. In *Proceedings of Final Workshop of European Research Project DETAILS, December 9-11*, Lucca, Italy, pp. 80–117.
- Zhou S. K. and Chellappa R. (2006). From sample similarity to ensemble similarity: Probabilistic distance measures in reproducing kernel hilbert space. *IEEE Transactions on Pattern Analysis and Machine Intelligence* 28(6), 917–929.

